CHAPTER 4.0 - REACTOR

TABLE OF CONTENTS

TABLE OF CONTENTS (Cont'd)

TABLE OF CONTENTS (Cont'd)

TABLE OF CONTENTS (Cont'd)

TABLE OF CONTENTS (Cont'd)

CHAPTER 4.0 - REACTOR

LIST OF TABLES

CHAPTER 4.0 - REACTOR

LIST OF FIGURES

LIST OF FIGURES (Cont'd)

LIST OF FIGURES (Cont'd)

LIST OF FIGURES (Cont'd)

LIST OF FIGURES (Cont'd)

CHAPTER 4.0 - REACTOR

4.1 SUMMARY DESCRIPTION

This chapter describes (1) the mechanical components of the reactor and reactor core including the fuel rods and fuel assemblies, (2) the nuclear design, and (3) the thermal-hydraulic design.

The reactor core is comprised of an array of 17 x 17 fuel assemblies that are similar in mechanical design and enrichments. The core may consist of any combination of VANTAGE 5 and VANTAGE+ fuel assemblies, as described in Subsection 4.2.2, and arranged in a checkered low-leakage pattern.

The significant new mechanical design features of the VANTAGE 5 design, as defined in References 1 and 2, relative to the previous optimized (OFA) fuel design include the following:

a. Integral Fuel Burnable Absorber (IFBA),

b. Intermediate Flow Mixer (IFM) Grids,

c. Reconstitutable Top Nozzle (RTN),

d. Reconstitutable Debris Filter Bottom Nozzle (DFBN),

e. Extended Burnup Capability, and

f. Axial Blankets.

The VANTAGE+ fuel assembly design (Reference 4) includes the following features: ZIRLO® High Performance Fuel Cladding Material or Optimized ZIRLO™ High Performance Fuel Cladding Material (Reference 7) fuel rods, ZIRLO thimble and instrumentation tubes, and variable pitch plenum spring.

The following features, known as PERFORMANCE+ design features, have been added to the VANTAGE 5 design: ZIRLO mid-grids and IFM grids, an oxide protective coating at the lower end of the fuel rod cladding, and the protective bottom grid.

Beginning with fall 2012 reloads at both Byron and Braidwood, the DBFN was upgraded to the Standard Debris Filter Bottom Nozzle (SDFBN) and the protective bottom grid was upgraded to the Robust Protective Grid (RPG) (Reference 6). These upgraded items are equivalent.

Commencing with Braidwood Unit 1 Cycle 20, Braidwood Unit 2 Cycle 20, Byron Unit 1 Cycle 22 and Byron Unit 2 Cycle 21, the Westinghouse Integral Nozzle (WIN) is implemented as a replacement for the RTN. The WIN design, while similar to the RTN, incorporates design and manufacturing improvements to eliminate the alloy 718 spring screw for attachment of the holddown springs.

The core is cooled and moderated by light water at a pressure of 2250 psia in the reactor coolant system (RCS). The moderator coolant contains boron as a neutron absorber. The concentration of boron in the coolant is varied as required to control relatively slow reactivity changes including the effects of fuel burnup. Additional boron in the form of integral fuel burnable absorbers (IFBA) or discrete burnable absorber rods may be employed to limit the moderator temperature coefficient (MTC) and the local power peaking that can be achieved.

Two hundred and sixty-four fuel rods are mechanically joined in a square array to form a fuel assembly. The fuel rods are supported at intervals along their length by grid assemblies which

---

maintain the lateral spacing between the rods throughout the design life of the assembly. Additionally, intermediate flow mixer (IFM) grids, located between the upper four structural grids, provide flow mixing in the hottest fuel assembly spans. The top and bottom grids are made of Inconel; the intermediate grids and the flow mixer grids are made of Zircaloy/ZIRLO. The grid assemblies consist of an "egg-crate" arrangement of interlocked straps. Structural grid straps contain spring fingers and dimples for fuel rod support as well as coolant mixing vanes. The flow mixer grid straps contain support dimples and coolant mixing vanes only. A protective grid has been added, located just above the bottom nozzle. The grid straps intersect the nozzle flow holes, thus further reducing the possibility of fuel rod damage due to debris-induced fuel rod fretting.

The fuel rods consist of slightly enriched uranium dioxide ceramic cylindrical pellets contained in cold worked Zircaloy-4, ZIRLO, or Optimized ZIRLO clad tubing which is plugged and seal welded at the ends to encapsulate the fuel. An axial blanket of natural or slightly enriched fuel pellets are placed at each end of the enriched pellet column to reduce neutron leakage and improve fuel utilization. The axial blanket may be annular providing added plenum space to reduce the rod internal pressure. A second fuel rod type is utilized to varying degrees within some assemblies. These rods use zirconium diboride (ZrB_2) coated pellets in the central portion of the fuel column described above to control assembly burnup. All fuel rods are pressurized with helium during fabrication to reduce stresses and strains, and to increase fatigue life. In addition, the ZIRLO and Optimized ZIRLO clad fuel rods are oxide coated at the lower end for additional protection against fretting.

The center position in the assembly is reserved for use by the incore instrumentation, while 24 positions in the array are equipped with guide thimbles joined to the grids and the top and bottom nozzles. Depending upon the position of the assembly in the core, the guide thimbles are used as core locations for rod cluster control assemblies (RCCAs), neutron source assemblies, and burnable absorber assemblies. Otherwise, the guide thimbles may be fitted with plugging devices to limit bypass flow.

The conventional bottom nozzle and the debris filter bottom nozzles (DFBN) are box-like structures which serve as the bottom structural element of the fuel assembly and direct the coolant flow distribution to the assembly. A pattern of small flow holes in the DFBN reduce the possibility of fuel rod damage due to debris-induced rod fretting.

The top nozzle functions as the upper structural element of the fuel assembly and provides a partial protective housing of the RCCA or other components. The reconstitutable top nozzle (RTN) may be removed between operating cycles to provide access for fuel rod examination or replacement.

The RCCAs each consist of a group of individual absorber rods fastened at the top end to a common hub or spider assembly, containing full length absorber material to control the reactivity of the core under operating conditions.

The nuclear design analyses and evaluations establish physical locations for control rods, burnable absorber rods, and physical parameters such as fuel enrichments and boron concentration in the coolant. The nuclear design evaluation established that the reactor core has inherent characteristics which together with corrective actions of the reactor control and protective systems provide adequate reactivity control even if the highest reactivity worth RCCA is stuck in the fully withdrawn position.

The design also provides for inherent stability against diametral and azimuthal power oscillations and for control of induced axial power oscillation through the use of control rods.

The thermal-hydraulic design analyses and evaluations establish coolant flow parameters which assure that adequate heat transfer is provided between the fuel cladding and the reactor coolant. The thermal design takes into account local variations in dimensions, power generation, flow distribution, and mixing. The mixing vanes incorporated in the fuel assembly spacer grid design and the flow mixer grid design induce additional flow mixing between the various flow channels within a fuel assembly as well as between adjacent assemblies. Instrumentation is provided in and out of the core to monitor the nuclear, thermal-hydraulic, and mechanical performance of the reactor and to provide inputs to automatic control functions.

Table 4.1-1 presents a list of the principal nuclear, thermal hydraulic, and mechanical design parameters using 17 x 17 VANTAGE 5/VANTAGE+ fuel assemblies. The analytical techniques employed in the core design are tabulated in Table 4.1-2. The loading conditions considered in general for the core internals and components are tabulated in Table 4.1-3. Specific or limiting loads considered for design purposes of the various components are listed as follows: fuel assemblies in Subsection 4.2.1.5, neutron absorber rods, burnable absorber rods, neutron source rods and thimble plug assemblies in Subsection 4.2.1.6.

4.1.1 REFERENCES

1. Davidson, S. L. (Ed.), "Reference Core Report - Vantage 5 Fuel Assembly," WCAP-10444-P-A, September 1985.

2. Letter from R. A. Chrzanowski (CECo) to T. E. Murley (NRC), "Byron Station Units 1 and 2 Application for Amendment to Facility Operating Licenses NPF-37 and NPF-66," July 31, 1989.

3. Letter from S. C. Hunsader (CECo) to T. E. Murley (NRC), "Braidwood Station Units 1 and 2 Application for Amendment to Facility Operating Licenses NPF-72 and NPF-77," October 14, 1989.

4. Davidson, S. L., and Ryan, T. L. (Eds.), "VANTAGE+ Fuel Assembly Reference Core Report," WCAP-12610-P-A, April 1995.

5. Akers, J. J., "Evaluation of Thimble Plug Elimination for Byron Units 1 & 2 and Braidwood Units 1 & 2," NSD-SAE-ESI-99-369, September 17, 1999.

6. Engineering Changes 0000388707 (Byron) and 0000389605 (Braidwood), Westinghouse 17x17 OFA Fuel Design Changes Beginning With B1C19/BRW2C17 Robust P-Grid and Standardized Debris Filter Bottom Nozzle.

7. Schueren, P., "Optimized ZIRLO™, "WCAP-12610-P-A & CENPD-404-P-A Addendum 1-A, July 2006.

TABLE 4.1-1

REACTOR DESIGN TABLE

	THERMAL AND HYDRAULIC DESIGN PARAMETERS	
1.	Reactor Core Heat Output, (100%), MWt	3648
2.	Reactor Core Heat Output, 10^6 BTU/Hr	12450
3.	Heat Generated in Fuel,	97.4%
4.	Core Pressure, Nominal psia	2270
5.	Pressurizer Pressure, Nominal, psia	2250
6.	Minimum DNBR at Nominal Conditions	
	Typical Flow Channel	>2.0
	Thimble (Cold Wall) Flow Channel	>2.0
7.	Minimum DNBR for Design Transients	
	Typical Flow Channel	≥1.25
	Thimble Flow Channel	≥1.24
8.	DNB Correlation(c)	WRB-2
	COOLANT FLOW (d)	
9.	Total Vessel Flow Rate, 10^6 lbm/hr	
	(based on Minimum Measured Flow)	143.8(b)
	(based on Thermal Design Flow)	137.3
10.	Effective Flow Rate for Heat Transfer, 10^6 lbm/hr (based on TDF)	125.9
11.	Effective Flow Area for Heat Transfer, ft^2	54.1
12.	Average Velocity along Fuel Rods, ft/sec (based on TDF)	14.8

TABLE 4.1-1 (Cont'd)

REACTOR DESIGN TABLE

	THERMAL AND HYDRAULIC DESIGN PARAMETERS	
	COOLANT TEMPERATURE °F	
13.	Average Mass Velocity, 10^6 lbm/hr-ft^2 (based on TDF)	2.33
14.	Nominal Inlet	555.2
15.	Average Rise in Vessel	65.6
16.	Average Rise in Core	70.8
17.	Average in Core	592.8
18.	Average in Vessel	588.0
	HEAT TRANSFER	
19.	Active Heat Transfer Surface Area, ft^2	57505
20.	Average Heat Flux [e], BTU/hr-ft^2	210883
21.	Maximum Heat Flux for Normal Operation, [e, f] BTU/hr-ft^2	548296
22.	Average Linear Power [e], kw/ft	5.82
23.	Peak Linear Power for Normal Operation, [e, f] kw/ft	15.14 (not including 0.345% calorimetric uncertainty)
24.	Peak Linear Power Resulting from[g] Overpower Transients/Operator Errors (assuming a maximum overpower of 119%), kw/ft (Centerline melt will not be exceeded)	<22.5
25.	Peak Linear Power for Prevention of Centerline Melt,[h] kw/ft	22.5
26.	Power Density, kw per kg Uranium	108.7 (hot)
27.	Specific Power, kw per kg Uranium	44.1

TABLE 4.1-1 (Cont'd)

REACTOR DESIGN TABLE

	THERMAL AND HYDRAULIC DESIGN PARAMETERS	
28.	Temperature at Peak Linear Power for Prevention of Centerline Melt, °F	4700
29.	Pressure Drop Across Core, psi[(i)]	28.1 ± 2.8
	Across Vessel, including nozzle, psi	see Table 5.1-1
	CORE MECHANICAL DESIGN PARAMETERS	
30.	Design	RCC Canless 17 x 17
31.	Number of Fuel Assemblies	193
32.	UO_2 Rods per Assembly	264
33.	Rod Pitch, in.	0.496
34.	Overall Dimensions, in.	8.426 x 8.426
35.	Fuel Weight (as UO_2), lb	204,236
36.	Clad Weight, lb	43,376
37.	Number of Grids per Assembly	11/12*
38.	Composition of Grids	2 End Grids - Inconel 718 6 Intermediate and 3 flow mixer grids Zircaloy 4/ ZIRLO*
39.	Loading Technique	3 Region Nonuniform

*VANTAGE+ includes one Inconel protective bottom grid.

TABLE 4.1-1 (Cont'd)

REACTOR DESIGN TABLE

	CORE MECHANICAL DESIGN PARAMETERS	
	FUEL RODS	
40.	Number	50,952
41.	Outside Diameter, in.	0.360
42.	Diametral Gap, in.	0.0062
43.	Cladding Thickness, in.	0.0225
44.	Cladding Material	Zircaloy-4/ ZIRLO/Optimized ZIRLO
	FUEL PELLETS	
45.	Material	UO_2 Sintered
46.	Density (% of Theoretical)	95
47.	Diameter, in.	0.3088
48.	Length, in. - Midzone Enriched Fuel - Blanket Fuel	0.370 0.462/0.500
	ROD CLUSTER CONTROL ASSEMBLIES	
49.	Neutron Absorber	Ag-In-Cd or Hafnium
50.	Cladding Material	Type 304 SS-Cold Worked
51.	Cladding Thickness, in.	0.0185
52.	Number of Clusters	53
53.	Number of Absorber Rods per Cluster	24

TABLE 4.1-1 (Cont'd)

REACTOR DESIGN TABLE

	CORE STRUCTURE	
54.	Core Barrel, ID/OD, in.	148.0/152.5
55.	Thermal Shield	Neutron Pad Design
	STRUCTURE CHARACTERISTICS	
56.	Core Diameter, in. (Equivalent)	132.7
57.	Core Height, in. (Active Fuel, Cold Dimensions)	144
	REFLECTOR THICKNESS AND COMPOSITION	
58.	Top - Water plus Steel, in.	-10
59.	Bottom - Water plus Steel, in.	-10
60.	Side - Water plus Steel, in.	-15
61.	H_2O/U Molecular Ratio, Cell (Cold)	2.73
62.	H_2O/U Molecular Ratio, Core Average, Cold (first core)	3.16
	FEED ENRICHMENT, W/O	
63.	Typical Split Batch Enriched Zone	Typical 4.40 to 4.95
	Axial Blanket Range	0.74 to 3.20

(a) Deleted.

(b) Inlet temperature = 556.6°F

(c) The W-3 Alternative correlations (ABB-NV and WLOP) are used for analysis of some accidents outside the range of application for the WRB-2 DNB correlation.

TABLE 4.1-1 (Cont'd)

REACTOR DESIGN TABLE

(d) The design bypass flow (including uncertainties) is 8.3 percent.

(e) Based on densified active fuel length of 143.7 inches.

(f) This limit is associated with the value of F^{T}_{Q} = 2.60.

(g) See Subsection 4.3.2.2.6.

(h) See Subsection 4.4.2.11.6.

(i) Based on best estimate reactor flow rate of 408000 gpm.

TABLE 4.1-2

ANALYTICAL TECHNIQUES IN CORE DESIGN

ANALYSIS	TECHNIQUE	COMPUTER CODE	SECTION REFERENCED
Fuel Rod Design			
Fuel Performance Characteristics (temperature, internal pressure cladding stress, etc.)	Semiempirical thermal Model Model of fuel rod with consideration of fuel density changes, heat transfer, fission gas release, etc.	Westinghouse fuel rod design model	4.2.1.1 4.2.3.1 4.2.3.2 4.2.3.3 4.3.3.1 4.4.2.11
Nuclear Design			
1. Cross Sections and Group Constants	Microscopic data Macroscopic constants for homogenized core regions Group constants for control rods with self-shielding	Modified ENDF/B library LEOPARD/CINDER type PHOENIX - P* HAMMER-AIM*	4.3.3.2 4.3.3.2 4.3.4 4.3.3.2
2. X-Y Power Distributions, Fuel Depletion	2-D and 3-D, 2-Group Diffusion Theory	TURTLE*	4.3.3.3 4.3.4
Critical Boron Concentrations, X-Y Xenon Distributions, Reactivity Coefficients, and Control Rod Worths	Nodal Code	PALADON* ANC*	4.3.3.3 4.3.4

TABLE 4.1-2 (Cont'd)

ANALYSIS	TECHNIQUE	COMPUTER CODE	SECTION REFERENCED
3. Axial Power Distributions Control Rod Worths, and Axial Xenon Distribution	1-D, 2-Group Diffusion Theory	APOLLO*	4.3.4
	2-D and 3-D 2-Group Nodal Analysis Code	PALADON*	4.3.3.3
4. Fuel Rod Power	Integral Transport Theory	LASER*	4.3.3.1
Effective Resonance Temperature	Monte Carlo Weighting Function	REPAD*	
5. Criticality of Reactor and Fuel Assemblies	1-D, Multi-group Transport Theory	AMPX SYSTEM* of Codes	4.3.2.6 4.3.4
	3-D Monte Carlo	KENO-IV	
Thermal Hydraulic Design			
1. Steady-state	Subchannel analysis of local fluid conditions in rod bundles including inertial and crossflow resistance terms. The solution is based on a one-pass model which simulates the core and hot channels.	VIPRE-01*	4.4.4.5

TABLE 4.1-2 (Cont'd)

ANALYSIS	TECHNIQUE	COMPUTER CODE	SECTION REFERENCED
2. Transient Departure from Nucleate Boiling Analysis	Subchannel analysis of local fluid conditions in rod bundles during transients by including accumulation terms in conservation equations. The solution is based on a one-pass model which simulates the core and hot channels.	VIPRE-01*	4.4.4.5.4

*Commonwealth Edison internally applies an in-house naming convention for some or all of these code packages.

TABLE 4.1-3

DESIGN LOADING CONDITIONS CONSIDERED FOR REACTOR CORE COMPONENTS

1. Fuel Assembly Weight
2. Fuel Assembly Spring Forces
3. Internals Weight
4. Control Rod Trip (equivalent static load)
5. Differential Pressure
6. Spring Preloads
7. Coolant Flow Forces (static)
8. Temperature Gradients
9. Differences in Thermal Expansion
   a. Due to temperature differences
   b. Due to expansion of different materials
10. Interference Between Components
11. Vibration (mechanically or hydraulically induced)
12. One or More Loops Out of Service
13. All Operational Transients Listed in Table 5.2-1
14. Pump Overspeed
15. Seismic Loads (operation basis earthquake and safe shutdown earthquake)
16. Blowdown Forces (due to cold and hot leg break)

4.2 FUEL SYSTEM DESIGN

The plant design conditions are divided into four categories in accordance with their anticipated frequency of occurrence and risk to the public: Condition I - normal operation; Condition II - incidents of moderate frequency; Condition III - infrequent incidents; Condition IV - limiting faults. The bases and description of plant operation and events involving each condition are given in Chapter 15.0.

The reactor is designed so that its components meet the following performance and safety criteria:

a. The mechanical design of the reactor core components and their physical arrangement, together with corrective actions of the reactor control, protection, and emergency cooling systems (when applicable) assure that:

   1. Fuel damage (Note: Fuel damage as used here is defined as penetration of the fission product barrier, i.e., the fuel rod clad) is not expected during Condition I and Condition II events. It is not possible, however, to preclude a very small number of rod failures. These are within the capability of the plant cleanup system and are consistent with plant design bases. The number of rod failures is small enough such that the dose limits given in 10 CFR 100 and 10 CFR 50.67 will not be exceeded.

   2. The reactor can be brought to a safe state following a Condition III event with only a small fraction of fuel rods damaged. (Note: Fuel damage as used here is defined as penetration of the fission product barrier, i.e., the fuel rod clad). The extent of fuel damage might preclude immediate resumption of operation.

   3. The reactor can be brought to a safe state and the core can be kept subcritical with acceptable heat transfer geometry following transients arising from Condition IV events.

b. The fuel assemblies are designed to withstand loads induced during shipping, handling, and core loading without exceeding the criteria of Subsection 4.2.1.5.

c. The fuel assemblies are designed to accept control rod insertions in order to provide the required reactivity control for power operations and

reactivity shutdown conditions (if in such core locations).

d. All fuel assemblies have provisions for the insertion of incore instrumentation necessary for plant operation (if in such core locations).

e. The reactor internals, in conjunction with the fuel assemblies and incore control components, direct coolant through the core. This achieves acceptable flow distribution and restricts bypass flow so that the heat transfer performance requirements can be met for all modes of operation.

4.2.1 Design Bases

For both the VANTAGE+ and the VANTAGE 5 fuel assemblies, the fuel rod and fuel assembly design bases are established to satisfy the general performance and safety criteria presented in this section.

Design values for the properties of the materials which comprise the fuel rod, fuel assembly and incore control components are given in Reference 2 for Zircaloy clad fuel, in Reference 24 for ZIRLO clad fuel, and in Reference 30 for Optimized ZIRLO clad fuel. Other supplementary fuel design criteria/limits are given in References 4, 25, 28, and 29. Reference 5 is applicable for new fuel reloads after September 2014.

4.2.1.1 Cladding

a. Material and Mechanical Properties

Zircaloy-4, ZIRLO, and Optimized ZIRLO cladding combine low absorption cross section, high corrosion resistance to coolant, fuel and fission products, high strength and ductility at operating temperatures, and high reliability. Reference 1 documents the operating experience with Zircaloy-4 and ZIRLO as clad material, and References 2 and 4 provide their mechanical properties with due consideration of temperature and irradiation effects. Reference 30 documents the material and mechanical properties for Optimized ZIRLO cladding.

b. Stress-Strain Limits

Cladding stress - The von Mises criterion is used to calculate the effective stresses. The cladding stresses under Condition I and II events are less than the Zircaloy 0.2% offset yield stress with due consideration of temperature and irradiation effects. While the cladding has some capability for accommodating plastic strain, the yield stress has been accepted as a conservative design basis.

Cladding tensile strain - The total tensile creep strain is less than 1% from the unirradiated condition. The elastic tensile strain during a transient is less than 1% from the pretransient value. This limit is consistent with proven practice.

c. Vibration and Fatigue

Strain fatigue - The cumulative strain fatigue cycles are less than the design strain fatigue life. This basis is consistent with proven practice.

Vibration - Potential for fretting wear of the clad surface exists due to flow induced vibrations. This condition is taken into account in the design of the fuel rod support system. The clad wear depth is limited to acceptable values by the grid support dimple and spring design.

d. Chemical Properties of the Cladding

This is discussed in Reference 2 for Zircaloy, Reference 24 for ZIRLO, and Reference 30 for Optimized ZIRLO cladding.

4.2.1.2 Fuel Material

a. Thermal Physical Properties

The thermal-physical properties of UO_2 are described in Reference 2 with due consideration of temperature and irradiation effects.

Fuel pellet temperatures - The center temperature of the hottest pellet is below the melting temperature of the UO_2 melting point of 2805°C (Reference 2) unirradiated and decreasing by 32°C per 10,000 MWD/MTU. While a limited amount of center melting can be tolerated, the design conservatively precludes center melting. A calculated fuel centerline temperature of 4700°F has been selected as an overpower limit to assure no fuel melting. This provides sufficient margin for uncertainties as described in Subsection 4.4.2.9.

Fuel pellet density - The nominal design density of the fuel is 95% of theoretical.

b. Fuel Densification and Fission Product Swelling

The design bases and models used for fuel densification and swelling are provided in References 3 and 4.

c. Chemical Properties

Reference 2 provides the basis for justifying that no adverse chemical interactions occur between the fuel and its adjacent material.

4.2.1.3 Fuel Rod Performance

The detailed fuel rod design establishes such parameters as pellet size and density, cladding-pellet diametral gap, gas plenum size, and helium prepressurization level. The design also considers effects such as fuel density changes, fission gas release, cladding creep, and other physical properties which vary with burnup. The integrity of the fuel rods is ensured by designing to prevent excessive fuel temperatures, excessive internal rod gas pressures due to fission gas releases, and excessive cladding stresses and strains. This is achieved by designing the fuel rods to satisfy the conservative design bases in the following subsections during Condition I and Condition II events over the fuel lifetime. For each design basis, the performance of the limiting fuel rod must not exceed the limits specified.

a. Fuel Rod Models

The basic fuel rod models and the ability to predict operating characteristics are given in Reference 4 and Subsection 4.2.3.

b. Mechanical Design Limits

Fuel rod design methodology has been introduced (Reference 26) that reduces the densification power spike factor to 1.0 and demonstrates that clad flattening will not occur in Westinghouse fuel designs.

The rod internal gas pressure shall remain below the value which causes the fuel-cladding diametral gap to increase due to outward cladding creep during steady-state operation.

Rod pressure is also limited such that extensive DNB propagation shall not occur during normal operation and accident events (Reference 12). A mechanistic approach (Reference 29) has been used to evaluate this criteria and it was confirmed that rod strains are not significant enough to cause channel blockage or burst.

4.2.1.4 Spacer Grids

a. Material Properties and Mechanical Design Limits

Two types of spacer (structural) grids are used in each fuel assembly. The top, bottom, and protective bottom grids are made of Inconel 718. The others are made of Zircaloy-4 or ZIRLO.

Lateral loads resulting from a seismic or LOCA event will not cause unacceptably high plastic grid deformation. Each fuel assembly's geometry will be maintained such that the fuel rods remain in an array amenable to cooling. The behavior of the grids under loading has been studied experimentally to establish strength criteria. For the Zircaloy, ZIRLO, and Inconel grids, the limit is the 95% confidence level of the true mean as taken from the distribution of measurements of buckling loads at operating temperature.

b. Vibration and Fatigue

The grids provide sufficient fuel rod support to limit fuel rod vibration and maintain cladding fretting wear to within acceptable limits.

4.2.1.5 Fuel Assembly

a. Structural Design

As previously discussed in Subsection 4.2.1, the structural integrity of the fuel assemblies is assured by setting design limits on stresses and deformations due to various nonoperational, operational and accident loads. These limits are applied to the design and evaluation of the top and bottom nozzles, guide thimbles, grids, and the thimble joints.

The design bases for evaluating the structural integrity of the fuel assemblies are:

1. Nonoperational - 6g lateral and traverse and 4g longitudinal loading with dimensional stability (Reference 17).

2. Normal and abnormal loads for Conditions I and II - the fuel assembly component structural design criteria are established for the two primary material categories, namely austenitic steels, Zircaloy, and ZIRLO. The stress categories and strength theory presented in the ASME Boiler and Pressure Vessel Code, Section III, are used as a general guide.

   For austenitic steel structural components, the Tresca criterion is used to determine the stress intensities. The design stress intensity value, S_m, is given by the lowest of the following:

   One-third of the specified minimum tensile strength or two-thirds of the specified minimum yield strength at room temperature.

   One-third of the tensile strength or 90% of the yield strength at operating temperature, but not to exceed two-thirds of the specified minimum yield strength at room temperature.

The stress intensity limits are given below. All stress nomenclature is per the ASME Boiler and Pressure Vessel Code, Section III.

Stress Intensity Limits

Categories	Limits
General Primary Membrane Stress Intensity	S_m
Local Primary Membrane Stress Intensity	1.5 S_m
Primary Membrane plus Primary Bending Stress Intensity	1.5 S_m
Total Primary plus Secondary Stress Intensity Range	3.0 S_m

The Zircaloy and ZIRLO structural components, which consist of guide thimbles, inner six grids and fuel rods are in turn subdivided into two categories because of material differences and functional requirements. The fuel rod and grid design criteria are covered separately in Subsections 4.2.1.1 and 4.2.1.4, respectively. For the guide thimble design, the stress intensities, the design stress intensities, and the stress intensity limits are calculated using the same methods as for the austenitic steel structural components. For conservative purposes, the unirradiated properties of Zircaloy and ZIRLO are used.

3. Abnormal loads during Conditions III or IV - worst case represented by seismic loads, or blowdown loads during a LOCA event.

   Deflections or failures of components cannot interfere with the reactor shutdown or emergency cooling of the fuel rods.

   The fuel assembly structural component stresses under faulted conditions are evaluated using primarily the methods outlined in Appendix F of the ASME Boiler and Pressure Vessel Code, Section III.

   For the austenitic steel fuel assembly components, the stress intensity and the design stress intensity value, S_m, are defined in accordance with the rules described in the previous section for normal operating conditions. Since the current analytical methods utilize elastic analysis, the stress intensity limits are defined as the smaller value of 2.4 S_m or 0.70 S_u for primary membrane and 3.6 S_m or 1.05 S_u for primary membrane plus primary bending.

   For the Zircaloy and ZIRLO components, the stress intensities are defined in accordance with the rules described in the previous section for normal operating conditions, and the design stress intensity values, S_m, are set at two-thirds of the material yield strength, S_y, at reactor operating temperature. This results in Zircaloy and ZIRLO stress intensity limits

being the smaller of 1.6 S_y or 0.70 S_u for primary membrane and 2.4 S_y or 1.05 S_u for primary membrane plus bending. For conservative purposes, the Zircaloy and ZIRLO unirradiated properties are used to define the stress limits.

b. Thermal-hydraulic Design

This topic is covered in Section 4.4

4.2.1.6 Core Components

The core components consists of the rod cluster control assemblies (RCCAs), the primary and secondary source assemblies, the thimble plug assemblies and the burnable absorber assemblies. A description of these components is provided in Section 4.2.2.

a. Thermal-Physical Properties of the Absorber Material

The absorber material for the RCCA is either Ag-In-Cd, or Hafnium. The thermal-physical properties of Ag-In-Cd are described in Reference 2, and Hafnium properties are described in Reference 16. The absorber material temperature shall not exceed its minimum melting temperature (1454°F for Ag-In-Cd and 3913°F for Hafnium).

The burnable absorber material is either borosilicate glass in burnable absorber rods, or aluminum oxide boron carbide pellets for the wet annular burnable absorber (WABA) rods. The thermal-physical properties of the borosilicate glass are described in Reference 2, and those of the WABA in Reference 15. The burnable absorber rods are designed so that the borosilicate glass temperature is below its minimum softening temperature of 1492°F (for reference 12.5 weight percent boron). The softening temperature is defined in accordance with ASTM C 338. In addition, the structural elements are designed to prevent excessive slumping.

The WABA rods are designed so that the maximum temperature is less than 1200°F. This ensures that the helium gas release will not exceed 30% for the WABA rod mechanical design life. This also assures that the Zircaloy clad strain limit is satisfied.

b. Compatibility of the Absorber and Cladding Materials

The control rod and borosilicate burnable absorber rod cladding is cold drawn type 304 stainless steel tubing, and the WABA rod cladding is Zircaloy-4. Extensive in-reactor experience and available quantitative information show that reaction rates between 304 stainless steel and water or any contacting metals are negligible at operational temperatures (References 2 and 16).

c. Cladding Stress-Strain Limits

For Conditions I and II, the stress categories and strength theory presented in the ASME Boiler and Pressure Vessel Code, Section III, Subsection NG-3000, are used as a general guide. The code methodology is applied, as with fuel assembly structural design, where possible. For Conditions III and IV, code stresses are not limiting. Failures of the burnable absorber rods during these conditions must not interfere with reactor shutdown or cooling of the fuel rods.

The deformation or failure of the control rod cladding must not prevent reactor shutdown or cooling of the fuel rods. A breach in the cladding does not result in serious consequences because either the Ag-In-Cd or Hafnium material is relatively inert.

The mechanical design bases for the control rods are consistent with the loading conditions of the ASME Boiler and Pressure Vessel Code, Section III:

1. External pressure equal to the reactor coolant system operating pressure with appropriate allowance for overpressure transients.

2. Wear allowance equivalent to 1000 full power reactor trips.

3. Bending of the rod due to a misalignment in the guide tube.

4. Forces imposed on the rods during rod drop.

5. Loads imposed by the accelerations of the control rod drive mechanism.

6. Radiation exposure during maximum core life.

7. Temperature effects from room to operating conditions.

   The burnable absorber assemblies, thimble plug assemblies, and source assemblies are static core components. The mechanical design of these components satisfies the following:

   a. Accommodate the differential thermal expansion between the fuel assembly and the core internals.

   b. Maintain positive contact with the fuel assembly and the core internals.

   The design evaluation of the core components is discussed in Subsection 4.2.3.6.

d. Irradiated Behavior of Absorber Material

   Operating experience and/or testing evaluation of the effects of irradiation upon the properties of Ag-In-Cd and Hafnium have shown that in-pile corrosion behavior is similar to out-of-pile behavior and that, for low oxygen content water, corrosion rates are low (References 2 and 16).

4.2.1.7 Testing, Irradiation Demonstration and Surveillance

An extensive testing program was conducted to verify the adequacy of the predicted fuel performance and the design bases. Reference 19 provides a description of the tests performed and a summary of the results.

In addition, in-plant irradiation demonstration programs have been completed on VANTAGE 5 and VANTAGE+ fuel designs. The objectives of the demonstration programs were to confirm the adequacy of the design and to obtain early performance information. The VANTAGE 5 demonstration assemblies operated for 3 cycles (including 2- to 18-month cycles). Examinations performed at the refueling outages confirmed excellent performance of the demonstration assemblies. The improved corrosion resistance of ZIRLO cladding has been shown with high burnups in the BR-3 and North Anna demonstration assemblies. Cladding corrosion measurements showed that the reduced corrosion exhibited by the ZIRLO clad rods was better than anticipated. The corrosion properties of Optimized ZIRLO cladding are described in Reference 30. The rate of oxidation for Optimized ZIRLO material is approximately 60% that of standard ZIRLO material.

Full production regions of the VANTAGE+ design have been placed in operation.

This page was intentionally deleted.

4.2.2 Description and Design Drawings

The fuel assembly, fuel rod, and core component design data are given in Tables 4.1-1 and 4.3-1. NRC approval of the VANTAGE 5 design is given in Reference 19 and in Reference 24 for the VANTAGE+ design.

Each fuel assembly consists of 264 fuel rods, 24 guide thimble tubes, and 1 instrumentation thimble tube arranged within a supporting structure. The instrumentation thimble is located in the center position and provides a channel for insertion of an incore neutron detector, if the fuel assembly is located in an instrumented core position. The guide thimbles provide channels for insertion of either a rod cluster control assembly, a neutron source assembly, a burnable absorber assembly, or a thimble plug assembly, depending on the position of the particular fuel assembly in the core. Figure 4.2-1 shows a crosssection of the fuel assembly array; Figures 4.2-2a and 4.2-2b show fuel assembly full length outlines. The fuel rods are loaded into the fuel assembly structure so that there is clearance between the fuel rod ends and the top and bottom nozzles. The fuel rod also has an oxide coating at the bottom of the rod to provide additional rod fretting wear protection.

Figures 4.2-2a and 4.2-2b show the VANTAGE 5 and VANTAGE+ assembly designs with their respective overall height and grid elevation dimensions. The design changes between the VANTAGE 5 and VANTAGE+ designs include a slightly shorter fuel rod for the VANTAGE 5 fuel rod design to accommodate extended burnup growth. The VANTAGE 5 and VANTAGE+ designs also incorporate three Zircaloy or ZIRLO intermediate flow mixing (IFM) grids. The DFBN is similar to the OFA design used in first core Cycle 1 fuel except it is lower in height and has a new pattern of smaller flow holes in its thinner top plate. This design minimizes passage of debris particles which could cause fretting damage to fuel rod cladding. Additional debris protection is provided by the protective grid assembly and an elongated fuel rod bottom end plug, which is described in Subsection 4.2.2.2.4.

The VANTAGE+ assembly skeleton is identical to that previously described for VANTAGE 5, except for those modifications necessary to accommodate the intended fuel operation to higher burnups. The modifications consist of the use of ZIRLO guide thimbles and small skeleton dimensional alterations to provide additional fuel assembly and rod growth space at the extended burnup levels. The VANTAGE+ fuel assembly is shorter than the VANTAGE 5 fuel assembly. The grid centerline elevations of the VANTAGE+ are identical to those of the VANTAGE 5 fuel assembly, except for the top grid. The VANTAGE+ top grid has been lowered. Because the VANTAGE+ fuel is intended to replace the VANTAGE 5 fuel, the VANTAGE+ exterior assembly envelope is equivalent in design dimensions, and the functional interface with the reactor internals is also equivalent to those of previous Westinghouse

fuel designs. Also, the VANTAGE+ fuel assembly is designed to be mechanically and hydraulically compatible with the VANTAGE 5 fuel assembly. The same functional requirements and design criteria previously established for the Westinghouse VANTAGE 5 fuel assembly remain valid for the VANTAGE+ fuel assembly. The VANTAGE 5 and VANTAGE+ fuel assembly designs are provided in Figures 4.2-2a and 4.2-2b, respectively.

Each fuel assembly is installed vertically in the reactor vessel and stands upright on the lower core plate, which is fitted with alignment pins to locate and orient the assembly. After all fuel assemblies are set in place, the upper support structure is installed. Alignment pins, built into the upper core plate, engage and locate the upper ends of the fuel assemblies. The upper core plate then bears downward against the holddown springs on the top nozzle of each fuel assembly to hold the fuel assemblies in place.

Visual confirmation of the orientation of the fuel assemblies within the core is provided by an engraved identification number on a corner clamp on the top nozzle and an indexing hole in the opposite corner clamp.

4.2.2.1 Fuel Rods

The VANTAGE 5 and VANTAGE+ fuel rods consist of uranium dioxide ceramic pellets contained in slightly cold worked Zircaloy-4, ZIRLO, and Optimized ZIRLO cladding tubing, which is plugged and seal welded at the ends to encapsulate the fuel. Schematics of the fuel rods are shown in Figure 4.2-3a. The VANTAGE+ fuel rod represents a modification to the VANTAGE 5 fuel rod intended to support operation for fuel clad in place of the Zircaloy-4 clad. The ZIRLO and Optimized ZIRLO alloys are zirconium alloys similar to Zircaloy-4, which have been specifically developed to enhance corrosion resistance. The VANTAGE+ fuel rods contain, as in VANTAGE 5, enriched uranium dioxide fuel pellets, and an integral fuel burnable absorber (IFBA) coating on some of the enriched fuel pellets.

The VANTAGE+ fuel rod has the same clad wall thickness as the VANTAGE 5 design. The VANTAGE 5 fuel rod length is shorter to provide room for the required fuel rod growth. To offset the reduction in the plenum length, the VANTAGE+ fuel rod has a variable pitch plenum spring. The variable pitch plenum spring provides the same support as the regular plenum spring, but with fewer spring turns, which translates to less spring volume. The bottom end plug has an internal grip feature to facilitate fuel rod loading on both designs (VANTAGE+ and VANTAGE 5) and provides appropriate lead-in for the removable top nozzle reconstitution feature. The VANTAGE+ fuel rod also has an oxide coating at the bottom end of the fuel rod. The extra layer of oxide coating provides additional debris-induced, rod-fretting wear protection.

The axial blankets are typically a nominal 6 inches or 8 inches of natural or slightly enriched fuel pellets at each end of the fuel rod pellet stack. Axial blankets reduce neutron leakage and improve fuel utilization. The axial blankets utilize chamfered pellets which are physically different (length) than the enriched pellets to help prevent accidental mixing during manufacturing. The axial blanket may contain an annulus providing additional plenum space to reduce the rod internal pressure.

The IFBA coated fuel pellets are identical to the enriched uranium dioxide pellets except for the addition of a thin zirconium diboride (ZrB_2) coating on the pellet cylindrical surface. This coating may be applied with a linear boron-10 loading (mg/in) that is greater than the original IFBA design for added flexibility in the core design. Coated pellets occupy the central portion of the fuel column (up to 132 inches). The number and pattern of IFBA rods within an assembly may vary depending on the specific application. The ends of the IFBA enriched coated pellets, like the enriched uncoated pellets, are also dished to allow for greater axial expansion at the pellet centerline and void volume for fission gas release. An evaluation and test program for the IFBA design features is given in Section 2.5 of Reference 19. New standard IFBA patterns have been incorporated in the core designs.

As a result of reconstitution activities (Reference 31) performed during unit outages, fuel rods may be replaced with either solid filler rods fabricated from stainless steel, Zircaloy-4, or ZIRLO in accordance with cycle-specific reload analyses.

Void volume and clearances are provided within the rods to accommodate fission gases released from the fuel, differential thermal expansion between the cladding and the fuel, and fuel density changes during irradiation, thus, avoiding overstressing of the cladding or seal welds. Shifting of the fuel within the cladding during handling or shipping prior to core loading is prevented by a stainless steel helical spring which bears on top of the fuel. During assembly, the pellets are stacked in the cladding to the required fuel height, the spring is then inserted into the top end of the fuel tube and the end plugs pressed into the ends of the tube and welded. All fuel rods are internally pressurized with helium during the welding process in order to minimize compressive cladding stresses and prevent cladding flattening due to coolant operating pressures.

4.2.2.2 Fuel Assembly Structure

The fuel assembly structure consists of a bottom nozzle, top nozzle, guide and instrument thimbles, and grids as shown in Figure 4.2-2a.

4.2.2.2.1 Bottom Nozzle

The bottom nozzle serves as the bottom structural element of the fuel assembly and directs the coolant flow distribution to the assembly. The square nozzle is fabricated from Type 304 equivalent stainless steel and consists of a perforated plate and four angle legs with bearing plates as shown in Figure 4.2-2a. The legs form a plenum for the inlet coolant flow to the fuel assembly. The plate also prevents accidental downward ejection of the fuel rods from the fuel assembly. The bottom nozzle is fastened to the fuel assembly guide thimbles by locked screws which penetrate through the nozzle and mate with a threaded plug in each guide thimble. The bottom nozzle may be removed, as necessary to support fuel reconstitution, by the removal of the locking screws. Upon completion of reconstitution activities, a circular locking cap, located around the thimble screw head, will be crimped into mating lobes on the nozzle, thus securing the locking screws in place.

Coolant flows from the plenum in the bottom nozzle upward through the penetrations in the plate to the channels between the fuel rods. The penetrations in the plate are positioned between the rows of the fuel rods.

The VANTAGE 5 and VANTAGE+ designs include use of the DFBN to reduce the possibility of fuel rod damage due to debris-induced fretting. The relatively large flow holes in a conventional bottom nozzle are replaced with a new pattern of smaller flow holes for the DFBN. The holes are sized to minimize passage of debris particles large enough to cause damage while providing sufficient flow area, comparable pressure drop, and continued structural integrity of the nozzle. Tests to measure pressure drop and demonstrate structural integrity verified that the low cobalt 304 stainless steel DFBN is totally compatible with the VANTAGE 5 and VANTAGE+ designs.

Changes in design compared to the 17x17 OFA bottom nozzle design for the Cycle 1 fuel involve: 1) a modified flow hole size and pattern as described above, 2) a decreased nozzle height and thinner top plate to accommodate the extended burnup fuel rod, and 3) increased lead-in chamfers for the core pin interface to improve handling. The DFBN also has a reconstitution design feature which facilitates easy removal of the nozzle from the fuel assembly in the same manner as all previous Byron/Braidwood Stations fuel designs.

Axial loads (holddown) imposed on the fuel assembly and the weight of the fuel assembly are transmitted through the bottom nozzle to the lower core plate. Indexing and positioning of the fuel assembly are controlled by alignment holes in two diagonally opposite bearing plates which mate with locating

pins in the lower core plate. Lateral loads on the fuel assembly are transmitted to the lower core plate through the locating pins.

4.2.2.2.2 Top Nozzle

The top nozzle assembly functions as the upper structural element of the fuel assembly and provides a partial protective housing for the rod cluster control assembly or other core components. It consists of an adapter plate, enclosure, top plate, and pads. Holddown springs are mounted on the top nozzle, as shown in Figures 4.2-2 and 4.2-2a. The springs are made of Inconel-718, the screws are made of Inconel-718 or Inconel-600, and the top nozzle is made of Type 304 stainless steel. The VANTAGE+ fuel assembly uses the same top nozzle design as the VANTAGE 5. The design bases and evaluation of the reconstituted top nozzle are given in Subsection 2.3.2 of Reference 19.

The reconstitutable top nozzle for the VANTAGE 5 and VANTAGE+ fuel assembly differs from the conventional OFA design in two ways: a groove is provided in each thimble throughhole in the nozzle plate to facilitate attachment and removal; and the nozzle plate thickness is reduced to provide additional axial space for fuel rod growth.

In the VANTAGE 5 and VANTAGE+ reconstitutable top nozzle design, a stainless steel nozzle insert is mechanically connected to the top nozzle adapter plate by means of a preformed circumferential bulge near the top of the insert. The insert engages a mating groove in the wall of the adapter plate thimble tube throughhole. The insert has four equally spaced axial slots which allow the insert to deflect inwardly at the elevation of the bulge, thus permitting the installation or removal of the nozzle. The insert bulge is positively held in the adapter plate mating groove by placing a lock tube with a uniform ID identical to that of the thimble tube into the insert.

To remove the top nozzle, a tool is first inserted through the lock tube and expanded radially to engage the bottom edge of the tube. An axial force is then exerted on the tool which overrides the local lock tube deformations and withdraws the lock tube from the insert. After the lock tubes have been withdrawn, the nozzle is removed by raising it off the upper slotted ends of the nozzle inserts which deflect inwardly under the axial lift load. With the top nozzle removed, direct access is provided for fuel rod examination or replacement. Reconstitution is completed by the remounting of the nozzle and the insertion of new lock tubes. The design bases and evaluation of the reconstitutable top nozzle are given in Section 2.3.2 in Reference 19.

The square adapter plate in both the conventional and VANTAGE 5 RTN designs is provided with round penetrations and semicircular ended slots to permit the flow of coolant upward through the top nozzle. The ligaments in

the plate cover the tops of the fuel rods and prevent their upward ejection from the fuel assembly. The enclosure is a box-like structure which sets the distance between the adapter plate and the top plate. The top plate has a large square hole in the center to permit access for the control rods and the control rod spiders and static core component assemblies.

Holddown springs are mounted on the top plate and are fastened in place by bolts and clamps located at two diagonally opposite corners. On the other two corners, integral pads are positioned which contain alignment holes for locating the upper end of the fuel assembly.

Westinghouse Integral Nozzle

Commencing with Braidwood Unit 1 Cycle 20, Braidwood Unit 2 Cycle 20, Byron Unit 1 Cycle 22 and Byron Unit 1 Cycle 21, the Westinghouse Integral Nozzle (WIN) will be implemented as a replacement for the RTN. The WIN top nozzle functions as the upper structural element of the fuel assembly in addition to providing a partial protective housing for the RCCA or other components. The top nozzle consists of an adapter plate, enclosure, top plate, and pads. Holddown springs are mounted on the assembly, as shown in Figure 4.2-3. For the WIN, the springs are made of Alloy 718 and the main nozzle body and the pins are made of Type 304 stainless steel.

The WIN design, while similar to the RTN, incorporates design and manufacturing improvements to eliminate the Alloy 718 spring screw for attachment of the holddown springs. In the WIN nozzle, the springs are assembled into the nozzle pad and pinned in place, as shown in Figure 4.2-3. The WIN design provides a wedged rather than a clamped (bolted) joint for transfer of the fuel assembly holddown forces into the top nozzle structure. Integral pads which contain alignment holes for locating the upper end of the fuel assembly are positioned on the other two corners for the WIN. The flow plate, thermal characteristics, method of attachment of the top nozzle, and handling of the fuel assembly are all unchanged from the RTN top nozzle design.

4.2.2.2.3 Guide and Instrument Thimbles

The guide thimbles are structural members which also provide channels for the neutron absorber rods, burnable absorber rods, neutron source, or thimble plug assemblies. Each thimble is fabricated from Zircaloy-4 or ZIRLO tubing having two different diameters. The tube diameter at the top section provides the annular area necessary to permit rapid control rod insertion during a reactor trip. The lower portion of the guide thimble is swaged to a smaller diameter to reduce diametral clearances and produce a dashpot action near the end of the control rod travel during normal trip operation. Holes are provided on the thimble tube above the dashpot to reduce the rod drop time. The dashpot is closed at the bottom by means of an end plug which is provided with a small flow port to avoid fluid stagnation in the dashpot volume during normal operation.

The top end of the guide thimble is fastened to a tubular nozzle insert by three expansion swages. The insert engages into the top nozzle and is secured into position by a lock tube, as shown in Figures 4.2-6 and 4.2-6a. The lower end of the guide thimble is fitted with an end plug, which is then fastened into the bottom nozzle by a locked screw.

Each grid is fastened to the guide thimble assemblies to create an integrated structure. The fastening method depicted in Figures 4.2-4 and 4.2-5 is used for all but the top and bottom grids in a fuel assembly.

An expanding tool is inserted into the inner diameter of the Zircaloy or ZIRLO thimble tube to the elevation of the Zircaloy sleeves that have been welded into the nine Zircaloy grid assemblies (six structural and three flow mixer). The four-lobed tool forces the thimble and sleeve outward to a predetermined diameter, thus joining the two components.

VANTAGE 5 and VANTAGE+ fuel assembly top grid-to-thimble attachments are identical and are shown on Figure 4.2-6. Starting with Byron Unit 2 Cycle 21 and Braidwood Unit 1 Cycle 21, the attachment method is shown on Figure 4.2-6a. The Zircaloy or ZIRLO thimbles are fastened to the top nozzle inserts by expanding the members as shown in Figures 4.2-6 and 4.2-6a. The inserts then engage the top nozzle and are secured into position by the insertion of lock tubes.

The bottom grid assembly is joined to the assembly as shown in Figure 4.2-7. The stainless steel insert is spotwelded to the bottom grid and later captured between the guide thimble end plug and the bottom nozzle by means of a stainless steel thimble screw.

The described methods of grid and nozzle insert fastening have been mechanically tested and found to meet all applicable design criteria.

The VANTAGE 5/VANTAGE+ guide thimbles are identical. Both the VANTAGE 5 and VANTAGE+ guide thimble tube ID provide an adequate nominal diametral clearance for the control rods. The thimble tube ID also provides sufficient diametral clearance for burnable absorber rods, source rods, and thimble plugs.

The VANTAGE 5 and VANTAGE+ instrumentation tubes are identical in design and both allow sufficient diametral clearance for the flux thimble to traverse the tube without binding.

The central instrumentation tube of each fuel assembly is constrained by seating in counterbores in each nozzle. This tube is a constant diameter and guides the incore neutron detector thimbles. This tube is expanded at the top and mid-grids in the same manner as the previously discussed expansion of the guide thimbles to the grids.

4.2.2.2.4 Grid Assemblies

The fuel rods, as shown in Figure 4.2-2a, are supported at intervals along their length by structural grid assemblies which maintain the lateral spacing between the rods. Each fuel rod is supported within each grid cell by a combination of support dimples and springs. The magnitude of grid spring force on the fuel rods is set high enough to minimize possible fretting,

without overstressing the cladding at the contact points. All grid assemblies allow axial thermal expansion of the fuel rods without imposing restraint sufficient to develop buckling or distortion.

The top and bottom grids are made of Inconel-718 strap material, chosen for its strength and high corrosion resistance. These nonmixing vane grids are identical in the VANTAGE 5 and VANTAGE+ designs.

The six intermediate (mixing vane) grids are made of Zircaloy straps or ZIRLO, chosen for low neutron absorption properties and corrosion resistance, and are identical in the VANTAGE 5 and VANTAGE+ designs. Inner straps include mixing vanes which project into the coolant stream and promote mixing of the coolant. In addition to the anti-snag feature, the intermediate grids incorporate the same grid cell support configuration as the top and bottom Inconel grids (six support locations per cell: four dimples and two springs). The Zircaloy and ZIRLO grid interlocking strap joints and grid/sleeve joints are fabricated by laser welding, whereas the Inconel grid joints are brazed.

The intermediate flow mixer (IFM) grids are located in the three uppermost spans between the Zircaloy or ZIRLO mixing vane structural grids and incorporate a similar mixing vane array. Their prime function is mid-span flow mixing in the hottest fuel assembly spans. Each IFM grid cell contains four dimples which are designed to prevent mid-span channel closure in the spans containing IFMs and fuel rod contact with the mixing vanes. This simplified cell arrangement allows short grid cells so that the IFM grid can accomplish its flow mixing objective with minimal pressure drop.

The IFM grids are fabricated from Zircaloy or ZIRLO and assembled in the same manner as the six intermediate (mixing vane) grids. These grids are not intended to be structural members. The outer strap was designed similar to the other grids to preclude grid hang-up and damage during fuel handling. Impact tests have been performed to show that a coolable geometry is assured at the IFM and structural grid elevation during assured at the IFM and structural grid elevation during seismic/LOCA events. The VANTAGE 5 grid assembly design bases and elevations are given in Section 2.3.5 of Reference 19, and the VANTAGE+ in Section 2.3 of Reference 24.

Reload fuel assemblies incorporate a bottom protective grid and modifications to the top and bottom fuel rod end plug. The protective grid illustrated in Figure 4.2-2b is a partial height grid, similar in configuration to the intermediate flow mixing grid, fabricated of Inconel without mixing vanes, and positioned on the top plate of the bottom nozzle. In conjunction with the protective grid, both the bottom and the top fuel rod end plugs were elongated. The protective grid and elongated bottom end plug provide a zone below the active fuel in which debris can be trapped.

4.2.2.3 Core Components

4.2.2.3.1 Rod Cluster Control Assembly

The rod cluster control assemblies are used for shutdown and control purposes to offset fast reactivity changes. Figure 4.2-8 illustrates the rod cluster control assembly location in the reactor relative to the interfacing fuel assemblies and guide tube assemblies.

A rod cluster control assembly is comprised of a group of individual neutron absorber rods fastened at the top end to a common spider assembly, as illustrated in Figure 4.2-9.

The absorber materials used in the control rod design are either: (1) Ag-In-Cd alloy extruded rods or (2) a solid hafnium bar. The absorber materials are essentially "black" to thermal neutrons and have sufficient additional resonance absorption to significantly increase their worth. For both the Ag-In-Cd alloy and the hafnium design, the material is sealed in cold-worked type 304 stainless steel tubes to prevent the absorber material from coming in direct contact with the coolant (Figure 4.2-10). Sufficient diametral and end clearances are provided to accommodate relative thermal expansions and material swelling, as shown in Subsection 4.2.3.6.

Enhanced Performance Rod Cluster Control Assemblies (EP-RCCA's) which use silver-indium-cadmium (Ag-In-Cd) will be utilized. These have a thin chrome electroplate applied over the length of absorber rodlet cladding in contact with the reactor internal guides to provide increased resistance to cladding wear. In addition, the absorber diameter is reduced slightly at the lower extremity of the rodlets in order to accommodate absorber swelling and minimize cladding interaction. The absorber rod cladding material is a very high purity 10% cold worked type 304 stainless steel tubing.

Because of its relatively high yield strength (minimum of 62,000 psi at 600°F), use of this material results in a design with practical wall thickness that meets ASME Section III type stress criteria for stresses induced by operating conditions.

The high purity stainless steel has a significant reduction in cobalt content as compared to earlier design. The chrome plate further reduces the effluence of cobalt into the coolant, thereby benefiting the ALARA conditions. This high purity cladding is also very resistant to irradiation assisted stress corrosion cracking.

As the bottom 12 inches of the silver absorber material sees a much higher fluence than the rest of the absorber material, an additional 5 mil diametral gap has been introduced in that area to allow for more irradiation induced swelling without imposing

significant hoop stresses in the cladding. This modification was made based on extensive examination of irradiated material which indicated that clad cracking could occur as a result of absorber/clad interference. The gap size is small enough so that heat transfer from the absorber to the coolant is sufficient to maintain a substantial margin against absorber rod melting.

The bottom end plugs are bullet-nosed to reduce the hydraulic drag during reactor trip and to guide the absorber rods smoothly into the dashpot section of the fuel assembly guide thimbles.

The spider assembly is in the form of a central hub with radial vanes supporting fingers from which the absorber rods are suspended. Handling detents and detents for connection to the drive rod assembly are machined into the upper end of the hub. A coil spring inside the spider body absorbs the impact energy at the end of a trip insertion. The radial vanes are joined to the hub by welding and brazing, and the fingers are joined to the vanes by brazing. A centerpost, which holds the spring and

its retainer, is threaded into the hub within the skirt and welded to prevent loosening in service. All components of the spider assembly are made from Types 304 and 308 stainless steel, except for the retainer which is of 17-4 pH material and the springs which are Inconel-718 alloy.

The absorber rods are fastened securely to the spider. The rods are first threaded into the spider fingers and then pinned to maintain joint tightness, after which the pins are welded in place. The end plug below the pin position is designed with a reduced section to permit flexing of the rods to correct for small misalignments.

The overall length is such that when the assembly is withdrawn through its full travel, the tips of the absorber rods remain engaged in the guide thimbles so that alignment between rods and thimbles is always maintained. Since the rods are long and slender, they are relatively free to conform to any small misalignments with the guide thimble.

4.2.2.3.2 Burnable Absorber Assembly

Each burnable absorber assembly consists of borosilicate or WABA burnable absorber rods attached to a holddown assembly. Conventional burnable absorber assemblies (containing borosilicate absorber) are shown in Figure 4.2-11. WABA rods may be used in place of the borosilicate absorber rods.

The borosilicate absorber rods consist of borosilicate glass tubes contained within Type 304 stainless steel tubular cladding which is plugged and seal welded at the ends to encapsulate the glass. The glass is also supported along the length of its inside diameter by a thin wall tubular inner liner. The top end of the liner is open to permit the diffused helium to pass into the void volume and the liner overhangs the glass. The liner has an outward flange at the bottom end to maintain the position of the liner with the glass. A typical borosilicate burnable absorber rod is shown in longitudinal and transverse cross-sections in Figure 4.2-13.

A WABA rod (Figure 4.2-12) consists of annular pellets of alumina-boron carbide (Al_2O_3-B_4C) burnable absorber material contained within two concentric Zircaloy tubes. These Zircaloy tubes which form the inner and outer clad for the WABA rod, are plugged and welded at each end to encapsulate the annular stack of absorber material. The assembled rod is then internally pressurized to 650 psig and seal welded. The absorber stack lengths are positioned axially within the WABA rods by the use of Zircaloy bottom-end spacers. The spacer in the lower portion of the WABA rod was lengthened to account for the ZIRLO guide thimbles. The burnable absorber centerline is aligned with the fuel centerline at hot full power conditions at the BOL. An annular plenum is provided within the rod to accommodate the helium gas released from absorber material depletion during irradiation. The reactor coolant flows inside the inner tube and outside the outer tube of the annular rod. Further design details are given in Section 3.0 of Reference 15.

The burnable absorber rods are statically suspended and positioned in selected guide thimbles within the fuel assemblies. The absorber rods in each assembly are attached together at the top end of the rods to a hold down assembly by a flat, perforated retaining plate which fits within the fuel assembly top nozzle and rests on the adapter plate. The absorber rod assembly is held down and restrained against vertical motion through a spring pack which is attached to the plate and is compressed by the upper core plate when the reactor upper internals assembly is lowered into the reactor. This arrangement ensures that the absorber rods cannot be ejected from the core by flow forces. Each rod is permanently attached to the base plate by a nut which is crimped in place.

The borosilicated rod cladding is slightly cold worked Type 304 stainless steel, and the WABA rod cladding is Zircaloy-4. All other structural materials are Types 304 or 308 stainless steel except for the springs which are Inconel-718. The borosilicate glass tube provides sufficient boron content to meet the criteria discussed in Subsection 4.3.1.

4.2.2.3.3 Neutron Source Assembly

The purpose of the neutron source assembly is to provide a base neutron level to ensure that the neutron detectors are operational and responding to core multiplication neutrons.

Both primary and secondary neutron source rods are used. The primary source rod, containing a radioactive material (californium-252), spontaneously emits neutrons during initial core loading and reactor startup. After the primary source rod decays beyond the desired neutron flux level, neutrons are then supplied by the secondary source rod. The secondary source rod contains a stable material (Sb-Be), which is activated by neutron bombardment during reactor operation. This becomes a source of neutrons during periods of low neutron flux, such as during refueling and subsequent startups.

Four source assemblies are installed in reactor core for the initial fuel cycle: two primary source assemblies and two secondary source assemblies. Each primary source assembly contains one primary source rod and a number of burnable absorber rods. Each secondary source assembly contains a grouping of four or six secondary source rods. In both types of assemblies locations not filled with source or burnable absorber rods contain a thimble plug. The source assemblies are shown in Figures 4.2-14, 4.2-15, and 4.2-15a. After the initial fuel cycle, only the secondary sources are used.

The source assemblies contain a holddown assembly identical to that of the burnable absorber assembly. The primary and secondary source rods have the same cladding material as the absorber rods. The secondary source rods contain pellets stacked to a height of approximately 88 inches. The primary source rods contain capsules of californium source material and alumina spacer pellets to position the source material within the cladding. The rods in each assembly are permanently fastened at the top end to a holddown assembly.

The structural members are constructed of Type 304 stainless steel except for the springs. The springs exposed to the reactor coolant are Inconel-718.

4.2.2.3.4 Thimble Plug Assembly

Thimble plug assemblies may be used if desired to limit bypass flow through the guide thimbles in fuel assemblies which do not contain either control rods, source rods, or burnable absorber rods.

The thimble plug assembly, as shown in Figure 4.2-16, consists of a flat base plate with short rods suspended from the bottom surface and a spring pack assembly. The 24 short rods, called thimble plugs, project into the upper ends of the guide thimbles to reduce the bypass flow. Similar short rods are also used on the source assemblies and burnable absorber assemblies to plug the ends of all vacant fuel assembly guide thimbles. When in the core, the thimble plug assemblies interface with both the upper core plate and with the fuel assembly top nozzles by resting on the adapter plate. The spring pack is compressed by the upper core plate when the upper internals assembly is lowered into place.

All components in the thimble plug assembly, except for the springs, are constructed from Series 300 stainless steel. The springs are Inconel-718. A representative additively manufactured thimble plug assembly (AM-TPA) is shown in Figure 4.2-16A.

4.2.3 Design Evaluation

The fuel assemblies, fuel rods, and incore control components are designed to satisfy the performance and safety criteria of Section 4.2, the mechanical design bases of Subsection 4.2.1, and other interfacing nuclear and thermal-hydraulic design bases specified in Sections 4.3 and 4.4. Effects of accident Conditions II, III, IV, or anticipated transients without trip on fuel integrity are presented in Chapter 15.0 or supporting topical reports.

4.2.3.1 Cladding

a. Vibration and Wear

Fuel rod vibrations are flow induced. The effect of the vibration on the fuel assembly and individual fuel rods is minimal. The cyclic stress range associated with deflections of such small magnitude is insignificant and has no effect on the structural integrity of the fuel rod. No significant wear of the cladding or grid supports is expected during the life of the fuel assembly. Fuel vibration has been experimentally investigated as shown in Reference 7.

b. Fuel Rod Internal Pressure and Cladding Stresses

The burnup dependent fission gas release model (Reference 4) is used in determining the internal gas pressures as a function of irradiation time. The fuel rod has been designed to ensure that the maximum internal pressure of the fuel rod will not exceed the value which would cause an increase in the fuel cladding diametral gap and extensive DNB propagation during normal operation.

The cladding stresses at a constant local fuel rod power are low. Compressive stresses are created by the pressure differential between the coolant pressure and the rod internal gas pressure. Because of the prepressurization with helium, the volume average effective stresses are always less than approximately 10,000 psi at the pressurization level used in this fuel rod design. Stresses due to the temperature gradient are not included in this average effective stress because thermal stresses are, in general, negative at the cladding inside diameter and positive at the cladding outside diameter and their contribution to the cladding volume average stress is small. Furthermore, the thermal stress decreases with time during steady-state operation due to stress relaxation. The stress due to pressure differential is highest in the minimum power rod at the beginning-of-life due to low internal gas pressure, and the thermal stress is highest in the maximum power rod due to the steep temperature gradient.

Tensile stresses could be created once the cladding has come in contact with the pellet. These

stresses would be induced by the fuel pellet swelling during irradiation. Fuel swelling can result in small cladding strains (<1% for expected discharge burnups), but the associated cladding stresses are very low because of cladding creep (thermal and irradiation-induced creep). The 1% strain criterion is extremely conservative for fuel-swelling driven cladding strain because the strain rate associated with solid fission products swelling is very slow.

c. Materials and Chemical Evaluation

Zircaloy-4, ZIRLO, and Optimized ZIRLO cladding have high corrosion resistance to the coolant, fuel, and fission products. As shown in Reference 1, there is PWR operating experience on the capability of Zircaloy-4, ZIRLO, and Optimized ZIRLO as a cladding material. Controls on fuel fabrication specify maximum moisture levels to preclude cladding hydriding.

Metallographic examinations of irradiated commercial fuel rods have shown occurrences of fuel-clad chemical interaction. Reaction layers of <1 mil in thickness have been observed between fuel and clad at limited points around the circumference. Metallographic data indicate that this interface layer remains very thin even at high burnup. Thus, there is no indication of propagation of the layer and eventual cladding penetration.

d. Fretting

Cladding fretting has been experimentally investigated as shown in Reference 7. No significant fretting of the cladding is expected during the life of the fuel assembly.

e. Stress Corrosion

Stress corrosion cracking is another postulated phenomenon related to fuel/clad chemical interaction. Out-of-pile tests have shown that in the presence of high cladding tensile stresses, large concentrations of selected fission products (such as iodine) can chemically attack the Zircaloy-4, ZIRLO, and Optimized ZIRLO tubing and can lead to eventual cladding cracking. Extensive postirradiation examination has produced no in-pile evidence that this mechanism is operative in commercial fuel.

f. Cycling and Fatigue

A comprehensive review of the available strain fatigue models was conducted by Westinghouse as early as 1968. This review included the Langer-O'Donnell model (Reference 8,) the Yao-Munse model and the Manson-Halford model. Upon completion of this review and using the results of the Westinghouse experimental programs discussed below, it was concluded that the approach defined by Langer-O'Donnell would be retained and the empirical factors of their correlation modified in order to conservatively bound the results of the Westinghouse testing program.

The Westinghouse testing program was subdivided into the following subprograms:

1. A rotating bend fatigue experiment on unirradiated Zircaloy-4 specimens at room temperature and at 725°F. Both hydrided and nonhydrided Zircaloy-4 cladding were tested.

2. A biaxial fatigue experiment in gas autoclave on unirradiated Zircaloy-4 cladding, both hydrided and nonhydrided.

3. A fatigue test program on irradiated cladding from the CVS and Yankee Core V conducted at Battelle Memorial Institute.

The results of these test programs provided information on different cladding conditions including the effects of irradiation, of hydrogen levels and of temperature.

The design equations followed the concept for the fatigue design criterion according to the ASME Boiler and Pressure Vessel Code, Section III.

It is recognized that a possible limitation to the satisfactory behavior of the fuel rods in a reactor which is subjected to daily load follow is the failure of the cladding by low cycle strain fatigue. During their normal residence time in reactor, the fuel rods may be subjected to approximately 1000 cycles with typical changes in power level from 50% to 100% of their steady-state values.

The assessment of the fatigue life of the fuel rod cladding is subject to a considerable uncertainty due to the difficulty of evaluating the strain range which results from the cyclic interaction of the fuel pellets and cladding. This difficulty

arises, for example, from such highly unpredictable phenomena as pellet cracking, fragmentation, and relocation. Nevertheless, since early 1968, this particular phenomenon has been investigated analytically and experimentally. Strain fatigue tests on irradiated and nonirradiated hydrided Zr-4 claddings were performed, which permitted a definition of a conservative fatigue life limit and recommendation on a methodology to treat the strain fatigue evaluation of the Westinghouse reference fuel rod designs.

It is believed that the final proof of the adequacy of a given fuel rod design to meet the load follow requirements can only come from incore experiments performed on actual reactors. Experience in load follow operation dates back to early 1970 with the load follow operation of the Saxton reactor. Successful load follow operation has been performed on reactor A (>400 load follow cycles) and reactor B (>500 load follow cycles). In both cases, there was no significant coolant activity increase that could be associated with the load follow mode of operation.

g. Rod Bowing

For Zircaloy-4 grid fuel assemblies, the largest contributors to significant rod bow are high end grid forces (Inconel grids) and low stiffness Zircaloy-4 grid springs. The VANTAGE 5 and VANTAGE+ fuel assembly designs have low spring forces on the top Inconel grids. This reduces the end loadings on the fuel rod brought about by fuel rod growth. The Zircaloy-4 or ZIRLO mid-grid design has a very high spring stiffness. This design offers high resistance to fuel rod rotation within a grid and still has low spring force to allow the rods to slip freely thru the grids. This design reduces the rod bow of the VANTAGE 5 and VANTAGE+ (or any Zircaloy grid design) to values as good or better than all Inconel gridded assemblies.

The current conservative NRC approved methodology for comparing the magnitude of rod bow between two different fuel assembly designs is given in Reference 14. Based on this approved methodology, a comparison of L^2/I (where I = the fuel rod bending moment of inertia and L = span length) and the initial rod-to-rod gap for both the 17x17 VANTAGE 5 and VANTAGE+ fuel assembly designs, shows that the amount of rod bow at any given burnup is essentially the same for both 17x17 VANTAGE 5 and VANTAGE+ fuel assemblies.

The effects of rod bow on DNBR are described in Subsection 4.4.2.2.5.

Thus, for a given burnup, the rod bow effects to be applied to the VANTAGE+ fuel assemblies are the same as those applied to the VANTAGE 5 17x17 fuel.

h. Consequences of Power-Coolant Mismatch

This subject is discussed in Chapter 15.0.

i. Irradiation Stability of the Cladding

As shown in Reference 1, there is considerable PWR operating experience on the capability of Zircaloy as a cladding material and for ZIRLO to date. Extensive experience with irradiated Zircaloy-4 is summarized in Reference 2, in Appendixes A through E in Reference 24 for ZIRLO, and in Reference 30 for Optimized ZIRLO cladding.

j. Creep Collapse and Creepdown

This subject and the associated irradiation stability of cladding have been evaluated using the model described in Reference 26. It has been established that clad collapse has been eliminated from the design basis.

4.2.3.2 Fuel Material Consideration

a. Dimensional Stability of the Fuel

The mechanical design of the fuel rods accounts for the differential thermal expansion of the fuel and the cladding, and for the pellets densification effect.

b. Potential for Chemical Interaction

Sintered, high density uranium dioxide fuel reacts only slightly with the cladding at core operating temperatures and pressures. In the event of cladding defects, the high resistance of uranium dioxide to attack by water protects against fuel deterioration, although limited fuel erosion can occur. The effects of water-logging on fuel behavior are discussed in Subsection 4.2.3.3.

c. Thermal Stability

As has been shown by operating experience and extensive experimental work, the thermal design parameters conservatively account for changes in the thermal performance of the fuel elements due to

pellet fracture which may occur during power operation. Observations from several operating Westinghouse PWRs (Reference 6) have shown that fuel pellets can densify under irradiation to a density higher than the manufactured values. Fuel densification and subsequent settling of the fuel pellets can result in local and distributed gaps in the fuel rods. Fuel densification has been minimized by improvements in the fuel manufacturing process and by specifying a nominal 95% initial fuel density.

The evaluation of fuel densification effects and their consideration in fuel design are described in References 3 and 4.

d. Irradiation Stability

The treatment of fuel swelling and fission gas release is described in Reference 4.

4.2.3.3 Fuel Rod Performance

The initial step in fuel rod design evaluation for a region of fuel is to determine the limiting rod(s). Limiting rods are defined as those rods whose predicted performance provides the minimum margin to each of the design criteria. For a number of design criteria, the limiting rod is the lead burnup rod of a fuel region. In other instances, it may be the maximum power or the minimum burnup rod. For the most part, no single rod will be limiting with respect to all design criteria.

After identifying the limiting rod(s), a worst-case evaluation is made which utilizes the limiting rod design basis power history and considers the effects of model uncertainties and dimensional variations. Furthermore, to verify adherence to the design criteria, the conservative case evaluation also considers the effects of postulated transient power increases, which are achievable during operation consistent with Conditions I and II. These transient power increases can affect both rod average and local power levels. The analytical methods used in the evaluation result in performance parameters which demonstrate the fuel rod behavior. Examples of parameters considered include rod internal pressure, fuel temperature, cladding stress, and cladding strain. In fuel rod design analyses, these performance parameters provide the basis for comparison between expected fuel rod behavior and the corresponding design criteria limits.

In calculating the steady-state performance of a nuclear fuel rod, the following interacting factors are considered:

a. Cladding creep and elastic deflection;

b. Pellet density changes, thermal expansion, gas release, and thermal properties as a function of temperature and fuel burnup;

c. Internal pressure as a function of fission gas release, rod geometry, and temperature distribution; and

d. Cladding corrosion and hydrogen pickup.

These effects are evaluated using fuel rod design models and criteria (References 4, 18, 24, 25, 26, 28, 29 and 30). Reference 5 is applicable for new fuel reloads after September 2014. The model modifications for time dependent fuel densification are given in Reference 4. With these interacting factors considered, the model determines the fuel rod performance characteristics for a given rod geometry, power history, and axial power shape. In particular, internal gas pressure, fuel and cladding temperature, and cladding deflections are calculated. The fuel rod is divided into several axial sections and radially into a number of annular zones. Fuel density changes are calculated separately for each segment. The effects are integrated to obtain the internal rod pressure.

The initial rod internal pressure is selected to delay fuel-clad mechanical interaction and to avoid the potential for flattened rod formation. It is limited, however, by the design criteria for the rod internal pressure given in Subsections 4.2.1.3 and 4.2.3.1.b.

The gap conductance between the pellet surface and the cladding inner diameter is calculated as a function of the composition, temperature, and pressure of the gas mixture, and the gap size or contact pressure between cladding and pellet. After computing the fuel temperature for each pellet annular zone, the fractional fission gas release is assessed using an empirical model derived from experimental data (Reference 4). The total amount of gas released is based on the average fractional release within each axial and radial zone and the gas generation rate, which in turn is a function of burnup. Finally, the gas released is summed over all zones and the pressure is calculated.

The code shows good agreement and fit for a variety of published and proprietary data on fission gas release, fuel temperatures, and cladding deflections (Reference 4). Included in this spectrum are variations in power, time, fuel density, and geometry. In-pile fuel temperature measurement comparisons are shown in Reference 4.

a. Fuel-Cladding Mechanical Interaction

One factor in fuel element duty is potential mechanical interaction of fuel and cladding. This fuel-clad interaction produces cyclic stresses and strains in the cladding, and these in turn consume

clad fatigue life. The reduction of fuel-clad interaction is, therefore, a goal of design. In order to achieve this goal and to enhance the cyclic operational capability of the fuel rod, the technology for using prepressurized fuel rods in Westinghouse PWRs has been developed.

Initially, the gap between the fuel and cladding is sufficient to prevent hard contact between the two. However, during power operation, a gradual compressive creep of the cladding onto the fuel pellet occurs due to the external pressure exerted on the rod by the coolant. Cladding compressive creep eventually results in the fuel-clad contact. During this period of fuel-clad contact, changes in power level could result in changes in cladding stresses and strains. By using prepressurized fuel rods to partially offset the effect of the coolant external pressure, the rate of cladding creep toward the surface of the fuel is reduced. Fuel rod prepressurization delays the time at which fuel-clad contact occurs and hence, significantly reduces the number and extent of cyclic stresses and strains experienced by the cladding both before and after fuel-clad contact. These factors result in an increase in the fatigue life margin of the cladding and lead to greater cladding reliability. If gaps should form in the fuel stacks, cladding flattening will be prevented by the rod prepressurization so that the flattening time will be greater than the fuel core life.

A two dimensional (r, θ) finite element model has been developed to investigate the effects of radial pellet cracks on stress concentrations in the cladding. Stress concentration, herein, is defined as the difference between the maximum cladding stress in the θ-direction and the mean cladding stress. The first case has the fuel and cladding in mechanical equilibrium, and as a result the stress in the cladding is close to zero. In subsequent cases, the pellet power is increased in steps and the resultant fuel thermal expansion imposes tensile stress in the cladding. In addition to uniform cladding stresses, stress concentrations develop in the cladding adjacent to radial cracks in the pellet. These radial cracks have a tendency to open during a power increase but the frictional forces between fuel and cladding oppose the opening of these cracks and result in localized increases in cladding stress. As the power is further increased and large tensile stresses exceed the ultimate tensile strength of UO_2, additional cracks

in the fuel are created which limit the magnitude of the stress concentration in the cladding.

As part of the standard fuel rod design analysis, the maximum stress concentration evaluated from finite element calculations is added to the volume average effective stress in the cladding as determined from one dimensional stress/strain calculations. The resultant cladding stress is then compared to the temperature dependent Zircaloy/ZIRLO yield stress in order to assure that the stress/strain criteria are satisfied.

Pellet thermal expansion due to power increases is considered the only mechanism by which significant stresses and strains can be imposed on the cladding. Power increases in commercial reactors can result from fuel shuffling, reactor power escalation following extended reduced power operation, and control rod movement. In the mechanical design model, lead rods are depleted using best estimate power histories as determined by core physics calculations. During the depletion, the amount of diametral gap closure is evaluated based upon the pellet expansion-cracking model, cladding creep model, and fuel swelling model. At various times during depletion, the power is increased locally on the rod to the burnup dependent attainable power density, as determined by core physics calculations. The radial, tangential, and axial cladding stresses resulting from the power increase are combined into a volume average effective cladding stress.

The von Mises criterion is used to evaluate whether the cladding yield stress has been exceeded. The yield stress correlation is that for irradiated cladding since fuel-clad interaction occurs at high burnup. Furthermore, the effective stress is increased by an allowance, which accounts for stress concentrations in the cladding adjacent to radial cracks in the pellet, prior to the comparison with the yield stress. This allowance was evaluated using a two-dimensional (r,θ) finite element model.

Slow transient power increases can result in large cladding strains without exceeding the cladding yield stress because of cladding creep and stress relaxation. Therefore, in addition to the yield stress criterion, a criterion on allowable cladding strain is necessary. Based upon high strain rate burst and tensile test data on irradiated tubing, 1% strain was determined to be a conservative lower

limit for irradiated cladding ductiblity and thus adopted as a design criterion.

b. Irradiation Experience

Westinghouse fuel operational experience is presented in References 1 and 30. Additional test assembly and test rod experiences are given in Sections 8 and 23 of Reference 6.

c. Fuel and Cladding Temperature

The methods used for evaluation of fuel rod temperatures are presented in Subsection 4.4.2.11.

d. Water-logging

Water-logging damage of a defective fuel rod has occasionally been postulated as a mechanism for subsequent rupture of the cladding. Such damage has been postulated as a consequence of a power increase on a rod after water has entered such a rod through a cladding defect of appropriate size. Rupture is postulated upon power increase if the rod internal pressure increase is excessive due to insufficient venting of water to the reactor coolant. Local cladding deformations typical of water-logging bursts have never been observed in commercial Westinghouse fuel. Experience has shown that the small number of rods which have acquired cladding defects, regardless of primary mechanism, remain intact and do not progressively distort or restrict coolant flow. In fact, such small defects are normally observed through reductions in coolant activity to be progressively closed upon further operation due to the buildup of zirconium oxide and other substances. Secondary failures which have been observed in defected rods are attributed to hydrogen embrittlement of the cladding. Postirradiation examinations point to the hydriding failure mechanism rather than a waterlogging mechanism; the secondary failure occurs as axial cracks in the cladding and are similar regardless of the primary failure mechanism. Such cracks do not result in flow blockage. Hence, the presence of such fuel, the quantity of which must be maintained below Technical Specification limits, does not in any way exacerbate the effects of any postulated transients.

Zircaloy clad fuel rods which have failed due to water-logging (Reference 9) indicate that very rapid power transients are required for fuel failure. Normal operational transients are limited

to about 40 cal/gm-min. (peak rod), while the Spert tests (Reference 10) indicate that 120 cal/gm to 150 cal/gm are required to rupture the cladding even with very short transients (5.5 msec period).

e. Potentially Damaging Temperature Effects During Transients

The fuel rod experiences many operational transients (intentional maneuvers) during its residence in the core. A number of thermal effects must be considered when analyzing the fuel rod performance.

The cladding can be in contact with the fuel pellet at some time in the fuel lifetime. Clad-pellet interaction occurs if the fuel pellet temperature is increased after the cladding is in contact with the pellet. Clad-pellet interaction is discussed in Subsection 4.2.3.3.a.

The potential effects of operation with waterlogged fuel are discussed in Subsection 4.2.3.3.d in which it is concluded that waterlogging is not a concern during operational transients.

Clad flattening has been observed in some operating power reactors. Thermal expansion (axial) of the fuel pellet stack against a flattened section of cladding could cause failure of the cladding. This is no longer a concern because cladding flattening is precluded during the fuel residence in the core (see Subsection 4.2.3.1).

Potential differential thermal expansion between the fuel rods and the guide thimbles during a transient is considered in the design. Excessive bowing of the fuel rods is precluded because the grid assemblies allow axial movement of the fuel rods relative to the grids. Specifically, thermal expansion of the fuel rods is considered in the grid design so that axial loads imposed on the fuel rods during a thermal transient will not result in excessively bowed fuel rods.

f. Fuel Element Burnout and Potential Energy Release

As discussed in Subsection 4.4.2.2, the core is protected from DNB over the full range of possible operating conditions. In the extremely unlikely event that DNB should occur, the cladding temperature will rise due to the steam blanketing at the rod surface and the consequent degradation in heat transfer. During this time, there is potential for chemical reaction between the cladding and the

coolant. However, because of the relatively good film boiling heat transfer following DNB, the energy release resulting from this reaction is insignificant compared to the power produced by the fuel.

g. Coolant Flow Blockage Effects on Fuel Rods

This evaluation is presented in Subsection 4.4.4.7.

4.2.3.4 Spacer Grids

The coolant flow channels are established and maintained by the structure composed of grids and guide thimbles. The lateral spacing between fuel rods is provided and controlled by the support dimples of adjacent grid cells. Contact of the fuel rods on the dimples is maintained through the clamping force of the grid springs. Lateral motion of the fuel rods is opposed by the spring force and the internal moments generated between the spring and the support dimples. Grid testing is discussed in Reference 7.

The fuel assembly component stress levels are limited by the grid design. For example, stresses in the fuel rod due to thermal expansion and Zircaloy, ZIRLO, and Optimized ZIRLO material irradiation growth are limited by the relative motion of the rod as it slips over the grid spring and dimple surfaces.

4.2.3.5 Fuel Assembly

a. Loads Applied by Core Restrain System

The upper core plate bears downward against the fuel assembly top nozzle springs. The springs are designed to accommodate the differential thermal expansion and irradiation growth between the fuel assembly and the core internals.

b. Analysis of Accident Loads

As shown in Reference 7 and in Appendix A of Reference 19, grid crushing tests and seismic and LOCA evaluations show that the fuel assembly will maintain a geometry that is capable of being cooled under the worst-case accident Condition IV event. References 22 and 23 document the acceptability of fuel assemblies in the two Byron Unit 1 locations that have only a single upper core plate fuel locating pin. Reference 21 documents the acceptability of fuel assemblies in the six Byron Unit 2 locations which have only a single upper core plate fuel locating pin.

A prototype fuel assembly has been subjected to column loads in excess of those expected in normal service and faulted conditions (Reference 7). The VANTAGE 5 test program description is given in Appendix A of Reference 19.

No interference between control rod insertion and thimble tubes will occur during a safe shutdown earthquake (SSE).

Stresses in the fuel assembly caused by tripping of the rod cluster control assembly have little influence on fatigue because of the small number of events during the life of an assembly. Assembly components and prototype fuel assemblies made from production parts have been subjected to structural tests to verify that the design bases requirements are met (Reference 7).

c. Loads Applied in Fuel Handling

The fuel assembly design loads for shipping have been established at 6g lateral and traverse and 4g longitudinal. Accelerometers are permanently placed into the shipping containers to monitor and detect fuel assembly accelerations that would exceed the criteria. Past history and experience have indicated that loads which exceed the allowable limits rarely occur. Exceeding the limits requires reinspection of the fuel assembly for damage. Tests on various fuel assembly components such as the grid assembly, sleeves, inserts and structure joints have been performed to assure that the shipping design limits do not result in impairment of fuel assembly function.

4.2.3.6 Reactivity Control Assembly and Burnable Absorber Rods

a. Internal Pressure and Cladding Stresses During Normal, Transient and Accident Conditions

The designs of the burnable absorber and source rods provide a sufficient cold void volume to accommodate the internal pressure increase during operation. This is not a concern for the Ag-In-Cd or hafnium absorber rod because no gas is released by the absorber material.

For the borosilicate burnable absorber rod, the use of glass in tubular form provides a central void volume along the length of the rods. For the wet annular burnable absorber (WABA) rod, the use of annular aluminum oxide-boron carbide pellets provides two concentric void volumes surrounding the pellets. For the source rods a void volume is provided in the cladding in order to limit the internal pressure increase until end-of-life (see Figures 4.2-14 and 4.2-15).

The stress analysis of the burnable absorber and source rods assumes 100 percent gas release to the rod void volume in addition to the initial pressure within the rod. The stress analysis of the WABA rod assumes a conservative 30 percent helium gas

release to the void volume in addition to the initial pressure within the rod.

During normal transient and accident conditions the void volume limits the internal pressures to values which satisfy the criteria in Subsection 4.2.1.6.

These limits are established not only to assure that peak stresses do not reach unacceptable values, but also to limit the amplitude of the oscillatory stress component in consideration of the fatigue characteristics of the materials.

Rod, guide thimble, and dashpot flow analyses indicate that the flow is sufficient to prevent coolant boiling. Therefore, clad temperatures at which the clad material has adequate strength to resist coolant operating pressures and rod internal pressures are maintained.

b. Thermal Stability of the Absorber Material, Including Phase Changes and Thermal Expansion

The radial and axial temperature profiles have been determined by considering gap conductance, thermal expansion, and neutron or gamma heating of the contained material as well as gamma heating of the clad.

The maximum temperature of the absorber material (whether Ag-In-Cd or Hafnium) was calculated to be substantially less than the material's melting point, and occurs axially at only the highest flux region. The thermal expansion properties of the absorber material and the phase changes are discussed in References 2 and 16.

The maximum temperature of the borosilicate glass was calculated to be about 1300°F and takes place following the initial rise to power. As the operating cycle proceeds, the glass temperature decreases for the following reasons: (1) reduction in power generation due to boron 10 depletion, (2) better gap conductance as the helium produced diffuses to the gap, and (3) external gap reduction due to borosilicate glass creep. The maximum absorber temperature for the WABA rod is less than 1200°F and takes place following the initial rise to power. As the operating cycle proceeds, the absorber temperature rapidly decreases below 1000°F.

Sufficient diametral and end clearances have been provided in the neutron absorber, borosilicate

burnable poison, WABA, and source rods to accommodate the relative thermal expansions between the enclosed material and the surrounding clad and end plug.

c. Irradiation Stability of the Absorber Material, Taking into Consideration Gas Release and Swelling

The irradiation stability of the absorber material is discussed in References 2 and 16. Irradiation produces no deleterious effects in the absorber material.

Gas release is not a concern for the absorber rod because no gas is released by the absorber material. Sufficient diametral and end clearances are provided to accommodate swelling of the absorber material.

Based on experience with borosilicate glass, and on nuclear and thermal calculations, gross swelling or cracking of the glass tubing is not expected during operation. Some minor creep of the glass at the spot, on the inner surface of the tube, could occur but would continue only until the glass came in contact with the inner liner. The wall thickness of the inner liner is sized to provide adequate support in the event of slumping, and to collapse locally before rupture of the exterior cladding if unexpected large volume changes, due to swelling or cracking, should occur. The ends of the inner liner are open to allow helium, which diffuses out of the glass, to occupy the central void.

The WABA rod cladding and rod initial internal pressure have been designed so that the clad will not rely upon the pellets for support under all Condition I and II events. The WABA rod design precludes irradiation-induced matrix damage and B_4C particle swelling which may lead to gross pellet disintegration or creep. Rodlet prepressurization will support the outer clad against irradiation-induced creep collapse in the event of 0% gas release (worst case) from the absorber for the design life. Calculations also verify the clad integrity under Condition I and II circumstances with a conservative maximum gas release of 30%. The maximum outer clad strain due to creep has been demonstrated to be less than the allowable strain limit.

d. Potential for Chemical Interaction

The structural materials selected have good resistance to irradiation damage and are compatible with the reactor environment.

Corrosion of the materials exposed to the coolant is quite low and proper control of chloride and oxygen in the coolant will prevent the occurrence of stress corrosion. The potential for interference with rod cluster control movement due to possible corrosion phenomena is very low.

4.2.4 Testing and Inspection Plan

4.2.4.1 Quality Assurance Plan

The Quality Assurance Program Plan of the Westinghouse Nuclear Fuel Division, as summarized in Reference 11, has been developed to serve the division in planning and monitoring its activities for the design and manufacture of nuclear fuel assemblies and associated components.

The program provides for control over all activities affecting product quality, commencing with design and development and continuing through procurement, materials handling, fabrication, testing and inspection, storage, and transportation. The program also provides for the indoctrination and training of personnel and for the auditing of activities affecting product quality through a formal auditing program.

Westinghouse drawings and product, process, and material specifications identify the inspections to be performed.

4.2.4.2 Quality Control

Quality control philosophy is generally based on the following inspections being performed to a 95% confidence that at least 95% of the product meets specification, unless otherwise noted.

a. Fuel System Components and Parts

The characteristics inspected depend upon the component parts and include dimensions, visual appearance, audits of test reports, material certification, and nondestructive examination such as X-ray and ultrasonic tests.

All material used is accepted and released by Quality Control.

b. Pellets

Inspections are performed for dimensional characteristics such as diameter, density, length, and squareness of ends. Additional visual inspections are performed for cracks, chips, and surface conditions according to approved standards.

Density is determined in terms of weight per unit length and is plotted on zone charts used in controlling the process. Chemical analyses are taken on a specified sample basis throughout pellet production.

c. Rod Inspection

Fuel rod, control rod, borosilicate burnable poison, WABA, and source rod inspection consists of the following nondestructive examination techniques and methods, as applicable.

1. Leak Testing

Each rod is tested using a calibrated mass spectrometer with helium being the detectable gas.

2. Enclosure Welds

Rod welds are inspected by ultrasonic or x-ray in accordance with Westinghouse specifications.

3. Dimensional

All fuel rods are dimensionally inspected prior to final release. The requirements include such items as length, camber, weld diameter, and visual appearance.

4. Plenum Dimensions

All fuel rods are inspected by gamma scanning, or other approved methods as discussed in Subsection 4.2.4.4 to ensure proper plenum dimensions.

5. Pellet-to-Pellet Gaps

All fuel rods are inspected by gamma scanning or other methods as discussed in Subsection 4.2.4.4 to ensure that no significant gaps exist between pellets.

6. All fuel rods are active gamma scanned to verify enrichment control prior to acceptance for assembly loading.

7. Traceability

   Traceability of rods and associated rod components is established by Quality Control.

d. Assemblies

Each fuel, control, borosilicate burnable absorber, WABA, and source rod assembly is inspected for compliance with drawing and/or specification requirements. Other core component inspection and specification requirements are given in Subsection 4.2.4.3.

e. Other Inspections

The following inspections are performed as part of the routine inspection operation:

1. Tool and gauge inspection and control including standardization to primary and/or secondary working standards. Tool inspection is performed at prescribed intervals on all serialized tools.

   Complete records are kept of calibration and conditions of tools.

2. Audits are performed of inspection activities and records to assure that prescribed methods are followed and that records are correct and properly maintained.

3. Surveillance inspection where appropriate, and audits of outside contractors are performed to ensure conformance with specified requirements.

f. Process Control

To prevent the possibility of mixing enrichments during fuel manufacture and assembly, strict enrichment segregation and other process controls are exercised.

The UO_2 powder is kept in sealed containers or is processed in a closed system. The containers are either fully identified both by descriptive tagging and preselected color coding or, for the closed system, the material is monitored by a computer data management information system. For the sealed

container system, a Westinghouse identification tag completely describing the contents is affixed to the containers before transfer to powder storage. Isotopic content is confirmed by analysis.

Powder withdrawal from storage can be made by only one authorized group, which directs the powder to the correct pellet production line. All pellet production lines are physically separated from each other and pellets of only a single nominal enrichment and density are produced in a given production line at any given time.

Finished pellets are placed on trays and transferred to segregated storage racks within the confines of the pelleting area. Samples from each pellet lot are tested for physical and chemical properties including isotopic content and impurity levels prior to acceptance by Quality Control. Physical barriers prevent mixing of pellets of different nominal designs and enrichment in this storage area. Unused powder and substandard pellets are returned to storage for disposition.

Loading of pellets into the cladding is performed in isolated production lines and again only one density and enrichment is loaded on a line at a time.

A serialized traceability code is placed on each fuel tube which identifies the enrichment. The end plugs are inserted and then welded to seal the tube. The fuel tube remains coded and traceability identified until just prior to installation in the fuel assembly.

At the time of installation into an assembly, a matrix is generated to identify each rod in its position within a given assembly. The top nozzle is inscribed with a permanent identification number providing traceability to the fuel contained in the assembly.

Similar traceability is provided for burnable poison, source and control rods as required.

4.2.4.3 Core Component Testing and Inspection

Tests and inspections were performed on each core component to verify the mechanical characteristics. In the case of the rod cluster control assembly, prototype testing had been conducted and both manufacturing test/inspections and functional testing at the plant site were performed.

During the component manufacturing phase, the following requirements applied to the core components to assure the proper functioning during reactor operation:

a. All materials were procured to specifications to attain the desired standard of quality.

b. Each spider was proof tested by applying an axial force of 315 +/- 10 lbs. for 30 to 60 seconds to the outmost finger of each vane. This proof load provided a bending moment at the spider body approximately equivalent to 1.4 times the load caused by the acceleration imposed by the control rod drive mechanism.

c. All rods were checked for integrity by the methods described in Subsection 4.2.4.2.c.

d. To assure proper fitup with the fuel assembly, the rod cluster control, borosilicate burnable absorber, WABA, and source assemblies were installed in the fuel assembly and checked for restriction or binding in the dry condition. Also a straightness of 0.01 in/ft was required on the entire inserted length of each rod assembly.

The rod cluster control assemblies were functionally tested, following core loading but prior to initial criticality to demonstrate reliable operation of the assemblies. Each assembly was operated at no flow/cold conditions. In addition, each assembly was operated (and tripped) at full flow/operating temperature conditions. Those control rods whose drop times fell outside the two-sigma limit of the drop time data for all control rods were tested a sufficient number of times (≥3 times) to reasonably ensure proper performance during subsequent plant operations.

In order to demonstrate continuous free movement of the rod cluster control assemblies and to ensure acceptable core power distributions during operation, partial movement checks are performed on the rod cluster control assemblies as required by the Technical Specifications. In addition, periodic drop tests of the rod cluster control assemblies are performed after each refueling shutdown to demonstrate continued ability to meet trip time requirements, to ensure core subcriticality after reactor trip, and to limit potential reactivity insertions from a hypothetical rod cluster control assembly ejection.

If a rod cluster control assembly cannot be moved by its mechanism, adjustments in the boron concentration ensure that adequate shutdown margin would be achieved following a trip. Thus, inability to move one rod cluster control assembly can be tolerated. More than one inoperable rod cluster control

assembly could be tolerated, but would impose additional demands on the plant operator. Therefore, the allowable number of inoperable rod cluster control assemblies has been limited to one.

4.2.4.4 Tests and Inspections by Others

If any tests and inspections are to be performed on behalf of Westinghouse, Westinghouse will review and approve the quality control procedures, inspection plans, etc. to be utilized to ensure that they are equivalent to the description provided above and are performed properly to meet all Westinghouse requirements.

4.2.4.5 Onsite Inspection

Detailed written procedures are used by the station staff for the postshipment inspection of all new fuel and associated components such as control rods and other inserts. The procedures are specific and have been field tested. This process is subject to QA audit and inspection under the applicable portions of the approved QA program to ensure proper implementation and compliance with commitments. This is discussed in the QA Topical Report, NO-AA-10. A master fuel handling procedure specifies the sequence in which handling and inspection takes place.

4.2.5 References

1. Slagle, W. H., "Operational Experience with Westinghouse Cores," WCAP-8183, Revision 23, January 1996.

2. Beaumont, M. D., et al., (Ed.), "Properties of Fuel and Core Component Materials," WCAP-9179, Revision 1 (Proprietary) and WCAP-9224, July, 1978.

3. Hellman, J. M., (Ed.), "Fuel Densification Experimental Results and Model for Reactor Operation," WCAP-8218-P-A, March 1975 (Proprietary) and WCAP-8219-A, March 1975.

4. Foster, J. P., et al., “Westinghouse Improved Performance Analysis and Design Model (PAD 4.0),” WCAP-15063-P-A, Revision 1 with Errata, July 2000.

5. Garde, A., et al., “Westinghouse Clad Corrosion Model for ZIRLO and Optimized ZIRLO,” WCAP-12610-P-A & CENPD-404-P-A, Addendum 2-A, October 2013.

6. Eggleston, F., "Safety Related Research and Development for Westinghouse Pressurized Water Reactors - Program Summaries, WCAP-8768, Revision 2, October 1978.

7. Davidson, S.L., et al., (Ed.), "Verification Testing and Analyses of the 17x17 Optimized Fuel Assembly," WCAP-9401 (Proprietary) and WCAP-9402-A, August 1981.

8. O'Donnell, W. J. and Langer, B. F., "Fatigue Design Basis for Zircaloy Components," Nuclear Science and Engineering, 20, 1-12, 1964.

9. Western New York Nuclear Research Center Correspondence with the AEC on February 11 and August 27, 1971, Docket 50-57.

10. Stephan, L. A., "The Effects of Cladding Material and Heat Treatment on the Response of Waterlogged UO_2 Fuel Rods to Power Bursts," IN-ITR-111, January 1970.

11. Dollard, W. J., "Nuclear Fuel Division Quality Assurance Program Plan," WCAP-7800, Revision 4-A, April 1975.

12. Risher, D. et al., "Safety Analysis for the Revised Fuel Rod Internal Pressure Design Basis," WCAP-8963 (Proprietary), November 1976, WCAP-8964, August 1977.

13. Davidson, S. L., Iorii, J. A., "Reference Core Report 17 x 17 Optimized Fuel Assembly," WCAP-9500-A, May 1982.

14. Skaritka, J., (Ed.), "Fuel Rod Bow Evaluation," WCAP-8691, Rev. 1, July 1979.

15. Skaritka, J., "Westinghouse Wet Annular Burnable Absorber Evaluation Report," WCAP-10021, February 1982.

16. Beaumont, M.D, et al., (Ed.), "Hafnium," Appendix A to WCAP-9179, Revision 1 (Proprietary) and WCAP-9224, February 1981.

17. Letter from E.P.Rahe, Jr. (Westinghouse) to L.E. Phillips (NRC) dated April 12, 1984 (NS-EPR-2893). Subject: Fuel Handling Load Criteria (6g vs. 4g).

18. Davidson, S. L., (Ed.), et al., "Extended Burnup Evaluation of Westinghouse Fuel," WCAP-10125-P-A, December 1985.

19. Davidson, S. L., (Ed.), "Reference Core Report-VANTAGE 5 Fuel Assembly," WCAP-10444-P-A, September 1985.

20. Letter from R. A Chrzanowski (CECo) to T. E. Murley (NRC) dated July 31, 1989. Subject: Byron Station Units 1 and 2 application for Amendment to Facility Operating Licenses NPF-37 and NPF-66.

21. Rarig, B.E., "Fuel Assembly Alignment Pin Removal," Westinghouse SECL 90-561, Revision 1, November 7, 1990.

22. Rarig, B. E., "Removal of Six Fuel Assembly Alignment Pins," Westinghouse SECL 93-054, Revision 1, March 22, 1993.

23. Humphries, B. S., "Fuel Assembly Alignment Pin Damage - Final Configuration," Westinghouse CAE-93-149, March 30, 1993.

24. Davidson, S. L., and Ryan, T. L, (Eds.), "VANTAGE+ Fuel Assembly Reference Core Report," WCAP-12610-P-A, April 1995.

25. Davidson, S. L., "Westinghouse Fuel Criteria Evaluation Process," WCAP-12488-A, October 1994.

26. Kersting, P. J., et al., "Assessment of Clad Flattening and Densification Power Spike Factor Elimination in Westinghouse Nuclear Fuel," WCAP-13589-A, March 1995.

27. Swogger, J. W., "Extended Life Wet Annular Burnable Absorber," Westinghouse 99CB-G-0162, October 1, 1999.

28. Sepp, H. A., "Revision to Design Criteria," WCAP-12488-A, Addendum 1-A, Revision 1, January 2002.

29. Sidener, S., et. al., "Safety Analysis for Revised Fuel Rod Internal Pressure Design Basis (Departure from Nucleate Boiling Mechanistic Propagation Methodology)," WCAP-8963-P-A Addendum 1-A (Westinghouse Propriety), Revision 1-A, June 2006.

30. Schueren, P., "Optimized ZIRLO™, "WCAP-12610-P-A & CENPD-404-P-A Addendum 1-A, July 2006.

31. Slagle, W. H., "Westinghouse Fuel Assembly Reconstitution Evaluation Methodology," WCAP-13060-P-A, July 1993.

4.3 NUCLEAR DESIGN

4.3.1 Design Bases

This section describes the design bases and functional requirements used in the nuclear design of the fuel and reactivity control system and relates these design bases to the General Design Criteria (GDC) in 10 CFR 50, Appendix A. Where appropriate, supplemental criteria such as the final acceptance criteria for emergency core cooling systems (ECCS) are addressed. Before discussing the nuclear design bases, it is appropriate to briefly review the four major categories ascribed to conditions of plant operation.

The full spectrum of plant conditions is divided into four categories, in accordance with the anticipated frequency of occurrence and risk to the public:

a. Condition I - Normal Operation
b. Condition II - Incidents of Moderate Frequency
c. Condition III - Infrequent Faults
d. Condition IV - Limiting Faults

In general, the Condition I occurrences are accommodated with margin between any plant parameter and the value of that parameter which would require either automatic or manual protective action. Condition II incidents are accommodated with, at most, a shutdown of the reactor with the plant capable of returning to operation after corrective action. Fuel damage (fuel damage as used here is defined as penetration of the fission product barrier, i.e., the fuel rod clad) is not expected during Condition I and Condition II events. It is not possible, however, to preclude a small number of rod failures. These are within the capability of the plant cleanup system and are consistent with the plant design basis.

Condition III incidents shall not cause more than a small fraction of the fuel elements in the reactor to be damaged, although sufficient fuel element damage might occur to preclude immediate resumption of operation. The release of radioactive material due to Condition III incidents should not be sufficient to interrupt or restrict public use of these areas beyond their exclusion radius. Furthermore, a Condition III incident shall not, by itself, generate a Condition IV fault or result in a consequential loss of function of the reactor coolant or reactor containment barriers.

Condition IV occurrences are faults that are not expected to occur but are defined as limiting faults which must be designed against. Condition IV faults shall not cause a release of radioactive material that results in an undue risk to public health and safety.

The core design power distribution limits related to fuel integrity are met for Condition I occurrences through conservative design and maintained by the action of the control system. The requirements for Condition II occurrences are met by providing an adequate protection system which monitors reactor parameters. The control and protection systems are described in Chapter 7.0, and the consequences of Condition II, III and IV occurrences are given in Chapter 15.0.

4.3.1.1 Fuel Burnup

Basis

The fuel rod design basis is described in Section 4.2. The nuclear design basis is to install sufficient reactivity in the fuel to attain a desired region average discharge burnup. The above, along with the design basis in Section 4.3.1.3, Control of Power Distribution, satisfies GDC-10.

Discussion

Fuel burnup is a measure of fuel depletion which represents the integrated energy output of the fuel (MWd/Mtu) and is a convenient means for quantifying fuel exposure criteria.

The core design lifetime or design discharge burnup is achieved by installing sufficient initial excess reactivity in each fuel region and by following a fuel replacement program (such as that described in Section 4.3.2) that meets all safety related criteria in each cycle of operation.

Initial excess reactivity installed in the fuel, although not a design basis, must be sufficient to maintain core criticality at full power operating conditions throughout cycle life with equilibrium xenon, samarium, and other fission products present. The end of design cycle life is defined to occur when the chemical shim concentration is essentially zero with control rods present to the degree necessary for operational requirements (e.g., the controlling bank at the "bite" position). In terms of chemical shim boron concentration, this represents approximately 10 ppm with no control rod insertion.

A limitation on initial installed excess reactivity is not required other than as is quantified in terms of other design bases such as core negative reactivity feedback and shutdown margin discussed below.

4.3.1.2 Negative Reactivity Feedbacks (Reactivity Coefficient)

Basis

The fuel temperature coefficient combined with the moderator temperature coefficient of reactivity is negative for

power operating conditions, thereby providing negative reactivity feedback characteristics. The design basis meets GDC-11. Subsequent fuel cycles may have a slightly positive moderator temperature coefficient, as discussed below, but the reactivity feedback will remain negative at full power.

Discussion

When compensation for a rapid increase in reactivity is considered, there are two major effects. These are the resonance absorption effects (Doppler) associated with changing fuel temperature and the spectrum effect resulting from changing moderator density. These basic physics characteristics are often identified by reactivity coefficients. The use of slightly enriched uranium ensures that the Doppler coefficient of reactivity is negative. This coefficient provides the most rapid reactivity compensation. The core is also designed to have an overall negative moderator temperature coefficient (MTC) of reactivity at hot full power so that average coolant temperature or void content provides another slower compensatory effect. Full power operation is permitted only in a range of overall negative moderator temperature coefficient. Below hot full power, a positive MTC is allowed by the Technical Specifications. The allowed moderator temperature coefficient limit can be achieved through use of fixed burnable absorbers, ZrB_2 coated fuel pellets and/or control rods by limiting the reactivity held down by soluble boron.

The core reloads may also be designated to have an overall moderator temperature coefficient of reactivity that is nonpositive at 100 percent power and less than or equal to +7.0 pcm/°F below 70 percent power. From 70 percent power to 100 percent power, the maximum allowed moderator temperature coefficient for reload cores decreases linearly from +7.0 pcm/°F to 0.0 pcm/°F. At full power, void content provides another slower, compensatory effect. The moderator temperature coefficient is maintained at or below the previously stated limit through the use of fixed burnable absorber rods, and/or integral fuel burnable absorbers in the form of a zirconium diboride (ZrB_2) coating on the enriched fuel pellets, and/or control rods, by limiting the reactivity held down by soluble boron.

Burnable absorber content (quantity and distribution) is not stated as a design basis. However, for some reloads, the use of burnable absorbers may be necessary for peaking factor limit control and for the accomplishment of a moderator temperature coefficient that is nonpositive at 100 percent power, less than or equal to +7.0 pcm/°F at 70 percent power, and below a linearly decreasing limit of +7.0 pcm/°F to 0.0 pcm/°F between 70 percent power and 100 percent power, as discussed above.

4.3.1.3 Control of Power Distribution

Basis

The nuclear design basis is that, with at least a 95% confidence level:

a. The fuel will not be operated at greater than 15.2 kW/ft under normal operating conditions, including a 0.345% calorimetric uncertainty.

b. Under abnormal conditions, including the maximum overpower condition, the fuel peak power will not cause melting as defined in Subsection 4.4.1.2.

c. The fuel will not operate with a power distribution that violates the departure from nucleate boiling (DNB) design basis (discussed in Subsection 4.4.1) under Condition I and II events including the maximum overpower condition.

d. Fuel management is such as to produce rod powers and burnups consistent with the assumptions in the fuel rod mechanical integrity analysis of Section 4.2.

The above basis meets GDC-10.

Discussion

Calculation of extreme power shapes which affect fuel design limits is performed with proven methods and verified frequently with measurements from operating reactors. The conditions under which limiting power shapes are assumed to occur are chosen conservatively with regard to any permissible operating state.

Even though there is good agreement between peak power calculations and measurements, a nuclear uncertainty margin (Subsection 4.3.2.2) is applied to calculated peak local power. Such a margin is provided both for the analysis for normal operating states and for anticipated transients.

4.3.1.4 Maximum Controlled Reactivity Insertion Rate

Basis

The maximum reactivity insertion rate due to withdrawal of rod cluster control assemblies at power or by boron dilution is limited. During normal at power operation, the maximum controlled reactivity rate change is less than 45 pcm/sec.* A maximum reactivity insertion rate for accidental withdrawal of control banks is set such that the applicable Condition II acceptance criteria are not exceeded at overpower conditions. This satisfies GDC-25.

The maximum reactivity worth of control rods and the maximum rates of reactivity insertion employing control rods are limited so as to preclude a break of the coolant pressure boundary or disruption of the core internals to a degree which would impair core cooling capacity due to a rod withdrawal or ejection accident (see Chapter 15.0).

Following any Condition IV event (rod ejection, steamline break, etc.) the reactor can be brought to the shutdown condition and the core will maintain acceptable heat transfer geometry. This satisfies GDC-28.

Discussion

Reactivity addition associated with an accidental withdrawal of a control bank (or banks) is limited by the maximum rod speed (or travel rate) and by the worth of the bank(s). The maximum control rod speed is 45 inches per minute and the maximum rate of reactivity change considering two control banks moving is less than 70 pcm/sec. During normal operation at power and with normal control rod overlap, the maximum reactivity change rate is less than 45 pcm/sec.

* 1 pcm = 10^{-5} $\Delta\rho$ (see footnote to Table 4.3-1).

The reactivity change rates are conservatively calculated assuming unfavorable axial power and xenon distributions. The peak xenon burnout rate is 25 pcm/min, significantly lower than the maximum reactivity addition rate of 45 pcm/sec for normal operation and 70 pcm/sec for accidental withdrawal of two banks.

4.3.1.5 Shutdown Margins

Basis

Minimum shutdown margin as specified in the Core Operating Limits Report (COLR) is required at any power operating condition, in the hot standby and hot shutdown conditions and in the cold shutdown condition.

In all analysis involving reactor trip, the single, highest worth rod cluster control assembly is postulated to remain untripped in its full-out position (stuck rod criterion). This satisfies GDC-26.

Discussion

Two independent reactivity control systems are provided, namely control rods and soluble boron in the coolant. The control rod system can compensate for the reactivity effects of the fuel and water temperature changes accompanying power level changes over the range from full-load to no-load. In addition, the control rod system provides the minimum shutdown margin under Condition I events and is capable of making the core subcritical rapidly enough to prevent exceeding acceptable fuel damage limits assuming that the highest worth control rod is stuck out upon trip.

The boron system can compensate for all xenon burnout reactivity changes and will maintain the reactor in the cold shutdown. Thus, backup and emergency shutdown provisions are provided by a mechanical and a chemical shim control system which satisfies GDC-26.

Basis

When fuel assemblies are in the pressure vessel and the vessel head is not in place, k_{eff} will be maintained at or below 0.95 with control rods and soluble boron. Further, the fuel will be maintained sufficiently subcritical that removal of all rod cluster control assemblies will not result in criticality.

Discussion

ANSI Standard N210-1976 specifies a k_{eff} not to exceed 0.95 in spent fuel storage racks and transfer equipment flooded with pure water. No criterion is given for the refueling operation; however, a five percent margin, which is consistent with spent

fuel storage and transfer is adequate for the controlled and continuously monitored operations involved.

The boron concentration required to meet the refueling shutdown criteria is specified in the COLR. Verification that this shutdown criteria is met, including uncertainties, is achieved using standard Westinghouse design codes such as PHOENIX-P (Reference 45), and ANC (Reference 44), a nodal analysis code. The subcriticality of the core is continuously monitored as described in the Technical Specifications.

4.3.1.6 Stability

Basis

The core will be inherently stable to power oscillations at the fundamental mode. This satisfies GDC-12. Spatial power oscillations within the core with a constant core power output, should they occur, can be reliably and readily detected and suppressed.

Discussion

Oscillations of the total power output of the core, from whatever cause, are readily detected by the loop temperature sensors and by the nuclear instrumentation. The core is protected by these systems and a reactor trip would occur if power increased unacceptably, preserving the design margins to fuel design limits. The stability of the turbine/steam generator/core systems and the reactor control system is such that total core power oscillations are not normally possible. The redundancy of the protection circuits ensures an extremely low probability of exceeding design power levels.

The core is designed so that diametral and azimuthal oscillations due to spatial xenon effects are self-damping and no operator action or control action is required to suppress them. The stability to diametral oscillations is so great that this excitation is highly improbable. Convergent azimuthal oscillations can be excited by prohibited motion of individual control rods. Such oscillations are readily observable and alarmed, using the multisection excore ion detectors. Temperature indications are also continuously available from incore thermocouples and loop measurements. Moveable incore detectors can be activated to provide more detailed information. In all presently proposed cores, these horizontal plane oscillations are self-damping by virtue of reactivity feedback effects designed into the core.

However, axial xenon spatial power oscillations may occur late in core life. The control bank and excore detectors are provided for control and monitoring of axial power distributions. Assurance that fuel design limits are not exceeded is provided by the reactor protection system which uses the measured detailed axial power shape as input.

4.3.1.7 Anticipated Transients Without Trip

The effects of anticipated transients with failure to trip are not considered in the design bases of the plant. Analysis has shown that the likelihood of such a hypothetical event is negligibly small. Furthermore, analysis of the consequences of a hypothetical failure to trip following anticipated transients has shown that no significant core damage would result, system peak pressures would be limited to acceptable values and no failure of the reactor coolant system would result (Reference 1).

4.3.2 Description

4.3.2.1 Nuclear Design Description

The reactor core consists of a specified number of fuel rods except that limited substitution of fuel rods by filler rods consisting of Zircaloy, ZIRLO, or stainless steel or by vacancies may be made for a particular design (Reference 52). The rods are held in bundles by spacer grids and top and bottom fittings. The fuel rods are constructed of Zircaloy, ZIRLO, or Optimized ZIRLO tubes containing UO_2 fuel pellets. The bundles, known as fuel assemblies, are arranged in a pattern which approximates a right circular cylinder.

Each fuel assembly contains a 17 x 17 rod array composed of 264 fuel rods, 24 guide thimbles, and an incore instrumentation thimble. Figure 4.2-1 shows a cross sectional view of a 17 x 17 fuel assembly and the related rod cluster control locations. Further details of the fuel assembly are given in Section 4.2.

The fuel rods within a given assembly have the same nominal uranium enrichment in both the radial and axial planes although the top and bottom 6 to 8 inches may contain natural or low enriched uranium. Some assemblies may contain more than one enrichment as a result of reconstitution operations.

Figure 4.3-1 shows a typical equilibrium-cycle core loading of fresh and burned fuel assemblies. The typical reload pattern employs low leakage fuel management in which more highly burned fuel is placed on the core periphery. The core will normally operate approximately 18 months between refueling, accumulating approximately 14,500 MWd/Mtu per year. The exact reloading pattern, initial and final positions of assemblies, number of fresh assemblies and their placement are dependent on the energy requirement for the next cycle and burnup and power histories of the previous cycles.

The feed fuel enrichment is determined by the amount of fissionable material required to provide the desired core lifetime and energy requirements, resulting in the desired region average discharge burnup.

The physics of the burnout process is such that operation of the reactor depletes the amount of fuel available due to the absorption of neutrons by the U-235 atoms and their subsequent fission. The rate of U-235 depletion is directly proportional to the power level at which the reactor is operated. In addition, the fission process results in the formation of fission products, some of which readily absorb neutrons. These effects, depletion and the buildup of fission products, are partially offset by the buildup of plutonium shown in Figure 4.3-2 for the 17 x 17 fuel assembly, which occurs due to the non-fission absorption of neutrons in U-238. Therefore, at the beginning of any cycle, a reactivity reserve equal to the depletion of the fissionable fuel and the buildup of fission product poisons over the specified cycle life must be "built" into the reactor. This excess reactivity is controlled by removable neutron absorbing material in the form of boron dissolved in the primary coolant and burnable absorber rods and/or ZrB_2 coated fuel pellets.

The concentration of boric acid in the primary coolant is varied to provide control and to compensate for long-term reactivity requirements. The concentration of the soluble neutron absorber is varied to compensate for reactivity changes due to fuel burnup, fission product poisoning including xenon and samarium, burnable poison depletion, and the cold-to-operating moderator temperature change. Using its normal makeup path, the chemical and volume control system (CVCS) is capable of inserting negative reactivity at a rate of approximately 30 pcm/min when the reactor coolant boron concentration is 100 ppm. If the emergency boration path is used, the CVCS is capable of inserting 55 gpm of 4 to 4.4 weight percent boric acid solution. Thus emergency boration flow provides a negative reactivity insertion of approximately 45 pcm/min when the reactor coolant concentration is 1000 ppm and approximately 60 pcm/min when the reactor coolant boron concentration is 100 ppm. The peak burnout rate for xenon is 25 pcm/min (Subsection 9.3.4 discusses the capability of the CVCS to counteract xenon decay). Rapid transient reactivity requirements and safe shutdown requirements are met with control rods.

As the boron concentration is increased, the moderator temperature coefficient becomes less negative. The use of a soluble absorber alone would result in a positive moderator coefficient above the limit at beginning-of-life. Therefore, burnable absorber rods and/or ZrB_2 coated fuel pellets are used to reduce the soluble boron concentration sufficiently to ensure that the moderator temperature coefficient is nonpositive at full power, is less than or equal to +7.0 pcm/°F at 70 percent power, and is below a linearly decreasing limit of +7.0 pcm/°F to +0.0 pcm/°F between 70 percent power and 100 percent power. During operation the absorber content in these rods is depleted, thus adding positive reactivity to offset some of the negative reactivity from fuel depletion and fission product buildup. The depletion rate of the burnable absorber material is not critical since chemical shim is always available and flexible enough to

cover any possible deviations in the expected burnable absorber depletion rate. Figure 4.3-3 is a graph of a typical core depletion with burnable absorber rods. The figure also illustrates the anticipated increase in the soluble boron concentration when changing to a positive MTC design.

In addition to reactivity control, the burnable absorbers are strategically located to provide a favorable radial power distribution. Figures 4.3-4 and 4.3-5 show the burnable absorber distribution within a fuel assembly for the several burnable patterns used in a VANTAGE 5 or VANTAGE+ 17 x 17 array. This includes both discrete and integral burnable absorbers. The burnable absorber loading pattern for a typical equilibrium cycle reload core is shown in Figure 4.3-6.

Table 4.3-1 contains a summary of the reactor core design parameters for a typical reload fuel cycle, including reactivity coefficients, delayed neutron fraction, and neutron lifetimes. A positive MTC increases the boron requirements under various core conditions (when compared to a similar design with a negative MTC) as shown in Table 4.3-1.

4.3.2.2 Power Distribution

The accuracy of power distribution calculations has been confirmed through approximately one thousand flux maps during some twenty years of operation under conditions very similar to those expected. Details of this confirmation are given in Reference 2 and in Subsection 4.3.2.2.6.

4.3.2.2.1 Definitions

Power distributions are quantified in terms of hot channel factors. These factors are a measure of the peak pellet power within the reactor core and the total energy produced in a coolant channel and are expressed in terms of quantities related to the nuclear or thermal design namely:

Power density is the thermal power produced per unit volume of the core (kW/liter).

Linear power density is the thermal power produced per unit length of active fuel (kW/ft). Since fuel assembly geometry is standardized, this is the unit of power density most commonly used. For all practical purposes, it differs from kW/liter by a constant factor which includes geometry and the fraction of the total thermal power which is generated in the fuel rod.

Average linear power density is the total thermal power produced in the fuel rods divided by the total active fuel length of all rods in the core.

Local heat flux is the heat flux at the surface of the cladding ($Btu/hr-ft^2$). For nominal rod parameters, this differs from linear power density by a constant factor.

Rod power or rod integral power is the length integrated linear power density in one rod (kW).

Average rod power is the total thermal power produced in the fuel rods divided by the number of fuel rods (assuming all rods have equal length).

The hot channel factors used in the discussion of power distributions in this section are defined as follows:

$F^N_{\Delta H}$, Nuclear Enthalpy Rise Hot Channel Factor, is defined as the ratio of the integral of linear power along the rod with the highest integrated power to the average rod power.

Manufacturing tolerances, hot channel power distribution and surrounding channel power distributions are treated explicitly in the calculation of the DNB ratio described in Section 4.4.

F_Q, Heat Flux Hot Channel Factor, is defined as the maximum local heat flux on the surface of a fuel rod divided by the average fuel rod heat flux, allowing for manufacturing tolerances on fuel pellets and rods.

It is convenient for the purposes of discussion to define subfactors of F_Q, however, design limits are set in terms of the total peaking factor.

F_Q = Total peaking factor or heat flux hot-channel factor

$$= \frac{\text{Maximum kW / ft}}{\text{Average kW / ft}}$$

The measurement of $F_Q(z)$, Heat flux Hot Channel factor, via an incore fluxmap allows for manufacturing tolerances on fuel pellets and rods and uncertainties for fluxmap measurement and engineering. The engineering uncertainties allow for local variations in enrichment, pellet density and diameter, surface area of the fuel rod and eccentricity of the gap between pellet and clad. Combined statistically, the net uncertainty is a factor of 1.03 to be applied to fuel rod surface heat flux and 1.05 for measurement and engineering uncertainties.

So, the corrected $F_Q(z)$ is:
$F^C_Q(z) = F^M_Q(z) \times 1.03 \times 1.05$,

where $F^M_Q(z)$ is the measured value of $F_Q(z)$ from an incore fluxmap.

$F^W_Q(z)$, Transient Heat Flux Hot Channel Factor, is the $F^C_Q(z)$, corrected Heat Flux Hot Channel factor, multiplied by the factor $W(z)$:

$F^W_Q(z) = F^C_Q(z) \times W(z)$

$F^{W}_{Q}(z)$, is then compared to the $F_{Q}(z)$ Limit to ensure $F_{Q}(z)$, is acceptable during non-steady state operation. The W(z) factor accounts for power distribution transients encountered during plant maneuvers within the restriction axial flux difference and rod insertion. W(z) is determined analytically either for Constant Axial Offset Control (CAOC) or Relaxed Axial Offset Control (RAOC) plants.

W(z) is defined as:

$$W(z) = \frac{(F_{Q}(Z)*P) \text{ maximum, simulated transient}}{(F_{Q}(Z)*P) \text{ equilibrium}}$$

The Heat Flux Hot Channel Factor, FQ(Z), shall be limited by the following relationships:

$$F_{Q}(Z) \leq \frac{F^{RTP}_{Q}K(Z)}{P} \quad \text{for } P > 0.5$$

$$F_{Q}(Z) \leq \frac{F^{RTP}_{Q}K(Z)}{0.5} \quad \text{for } P \leq 0.5$$

$$P = \frac{\text{THERMAL POWER}}{\text{RTP}}$$

F^{RTP}_{Q} is the $F_{Q}(Z)$ limit at RTP provided in the Core Operating Limits Report (COLR). K(Z) is the normalized $F_{Q}(Z)$ as a function of core height provided in the COLR.

$F_{Q}(Z)$ is approximated by $F^{C}_{Q}(Z)$ and $F^{W}_{Q}(Z)$. Thus, both $F^{C}_{Q}(Z)$ and $F^{W}_{Q}(Z)$ must meet the preceding limits on $F_{Q}(Z)$.

When Power Distribution Monitoring System (PDMS) is OPERABLE, $F_{Q}(Z)$ is determined continuously.

Then,

$$F^{C}_{Q}(z) = F^{M}_{Q}(z) \times U_{FQ}$$

where U_{FQ} is a factor that accounts for measurement and engineering uncertainty defined in the COLR.

4.3.2.2.2 Radial Power Distributions

The power shape in horizontal sections of the core at full power is a function of the fuel and burnable absorber loading patterns and the presence or absence of a single bank of full length control rods. Thus, at any time in the cycle, a horizontal section of the core can be characterized as unrodded or with group D control rods. These two situations combined with burnup effects determine the radial power shapes which can exist in the core at full power.

The effect on radial power shapes of power level, xenon, samarium and moderator density are considered also but these are small. The effect of nonuniform flow distribution is negligible. While radial power distributions in various planes of the core are often illustrated, the core radial enthalpy rise distribution as determined by the integral of power up each channel is of greater interest. Figures 4.3-7 through 4.3-11 show representative radial power distributions for one eighth of the core for representative operating conditions. These conditions are: (1) hot full power (HFP) near beginning-of-life (BOL) - unrodded - equilibrium xenon; (2) HFP near BOL - Bank D in to the HFP insertion limit - equilibrium xenon; (3) HFP near middle-of-life (MOL) - unrodded - equilibrium xenon; (4) HFP near end-of-life (EOL) - unrodded - equilibrium xenon, and; (5) HFP near end-of-life (EOL) - Bank D in to the HFP insertion limit - equilibrium xenon.

Since the location of the hot channel varies from time to time, a single reference radial design power distribution is selected for DNB calculations. This reference power distribution is chosen conservatively to concentrate power in one area of the core, minimizing the benefits of flow redistribution. Assembly power values are normalized to core average power. The radial power distribution within a fuel rod and its variation with burnup is utilized in thermal calculations and fuel rod design as discussed in Section 4.2.

4.3.2.2.3 Assembly Power Distributions

For the purpose of illustration, assembly power distributions from the BOL and EOL conditions corresponding to Figures 4.3-7 and 4.3-10, respectively, are given for the same assembly in Figures 4.3-12 and 4.3-13, respectively.

Since the detailed power distribution surrounding the hot channel varies from time to time, a conservatively flat assembly power distribution is assumed in the DNB analysis, described in Section 4.4, with the rod of maximum integrated power artificially raised to the design value of $F^N_{\Delta H}$. Care is taken in the nuclear design of all fuel cycles and all operating conditions to ensure that a flatter assembly power distribution does not occur with limiting values of $F^N_{\Delta H}$.

4.3.2.2.4 Axial Power Distributions

The shape of the power profile in the axial or vertical direction is largely under the control of the operator through either the manual operation of the full length control rods or automatic motion of full length rods responding to manual operation of the CVCS. Nuclear effects which cause variations in the axial power shape include burnable absorber length, fuel axial blankets, moderator density, Doppler effect on resonance absorption, spatial xenon and burnup. Automatically controlled variations in total power output and full length rod motion are also important in determining the axial power shape at any time.

Signals are available to the operator from the excore ion chambers which are long ion chambers outside the reactor vessel running parallel to the axis of the core. Separate signals are taken from the top and bottom halves of the chambers. The difference between top and bottom signals from each of four pairs of detectors is displayed on the control panel and called the flux difference, ΔI. Calculations of core average peaking factor for many plants and measurements from operating plants under many operating situations are associated with either ΔI or axial offset in such a way that an upper bound can be placed on the peaking factor. For these correlations, axial offset is defined as:

$$\text{axial offset} = \frac{\phi_t - \phi_b}{\phi_t + \phi_b}$$

and ϕ_t and ϕ_b are the top and bottom detector readings.

Representative axial power shapes for BOL, MOL, and EOL conditions are shown in Figures 4.3-14 through 4.3-16. These figures cover a wide range of axial offset including values not permitted at full power. Reference 3 also illustrates representative axial power shapes for other reactor conditions.

4.3.2.2.5 Deleted

4.3.2.2.6 Limiting Power Distributions

According to the ANSI classification of plant conditions (See Chapter 15.0). Condition I occurrences are those which are expected frequently or regularly in the course of power operation, maintenance, or maneuvering of the plant. As such, Condition I occurrences are accommodated with margin between any plant parameter and the value of that parameter which would require either automatic or manual protective action. Inasmuch as Condition I occurrences occur frequently or regularly, they must be considered from the point of view of affecting the consequences of fault conditions (Conditions II, III and IV). In

this regard, analysis of each fault condition described is generally based on a conservative set of initial conditions corresponding to the most adverse set of conditions which can occur during Condition I operation.

The list of steady state and shutdown conditions, permissible deviations and operational transients is given in Section 15.0. Implicit in the definition of normal operation is proper and timely action by the reactor operator. That is, the operator follows recommended operating procedures for maintaining appropriate power distributions and takes any necessary remedial actions when alerted to do so by the plant instrumentation. Thus, as stated above, the worst or limiting power distribution which can occur during normal operation is to be considered as the starting point for analysis of ANSI Conditions II, III and IV events.

Improper procedural actions or errors by the operator are assumed in the design as occurrences of moderate frequency (ANSI Condition II). Some of the consequences which might result are discussed in Section 15.0. Therefore, the limiting power shapes which result from such Condition II events, are those power shapes which deviate from the normal operating condition at the recommended axial offset bank, e.g., due to lack of proper action by the operator during a xenon transient following a change in power level brought about by control rod motion. Power shapes which fall in this category are used for determination of the reactor protection system setpoints so as to maintain margin to overpower or DNB limits.

The means for maintaining power distributions within the required hot channel factor limits are described in the Technical Specifications. A complete discussion of power distribution control in Westinghouse PWRs is included in Reference 6. Detailed background information on the design constraints on local power density in a Westinghouse PWR, on the defined operating procedures and on the measures taken to preclude exceeding design limits is presented in the Westinghouse topical report on power distribution control and load following procedures (Reference 7). The following paragraphs summarize these reports and describe the calculations used to establish the upper bound on peaking factors.

The calculations used to establish the upper bound on peaking factors, F_Q and $F^N_{\Delta H}$, include all of the nuclear effects which influence the radial and/or axial power distributions throughout core life for various modes of operation including load follow, reduced power operation, and axial xenon transients.

Radial power distributions are calculated for the full power condition and fuel and moderator temperature feedback effects are included for the average enthalpy plane of the reactor. The steady state nuclear design calculations are done for normal flow

with the same mass flow in each channel and flow redistribution is calculated explicitly where it is important in the DNB analysis of accidents. The effect of xenon on radial power distribution is small but is included as part of the normal design process.

The core average axial profile can experience significant changes which can occur rapidly as a result of rod motion and load changes and more slowly due to xenon distribution. For the study of points of closest approach to axial power distribution limits, several thousand cases are examined. Since the properties of the nuclear design dictate what axial shapes can occur, boundaries on the limits of interest can be set in terms of the parameters which are readily observed on the plant. Specifically, the nuclear design parameters which are significant to the axial power distribution analysis are:

a. Core power level,

b. Core height,

c. Coolant temperature and flow,

d. Coolant temperature program as a function of reactor power,

e. Fuel cycle lifetimes,

f. Rod bank worths, and

g. Rod bank overlaps.

Normal operation of the plant assumes compliance with the following conditions:

a. Control rods in a single bank move together with no individual rod insertion differing by more than 13 steps (indicated) from the bank demand position;

b. Control banks are sequenced with overlapping banks;

c. The control full length bank insertion limits are not violated;

d. Axial power distribution procedures, which are given in terms of flux difference control and control bank position, are observed.

The axial power distribution procedures referred to above are part of the required operating procedures which are followed in normal operation. Briefly, they require control of the axial offset (flux difference divided by fractional power) at all power

levels within a permissible operating band, Relaxed Axial Offset Control (Reference 49).

Calculations are performed for normal operation of the reactor including load following maneuvers. Beginning, middle and end of cycle conditions are included in the calculations. Different histories of operation are assumed prior to calculating the effect of load follow transients on the axial power distribution. These different histories cover both base loaded operation and extensive load following. For a given plant and fuel cycle, a finite number of maneuvers are studied to determine the general behavior of the local power density as a function of core elevation.

These cases represent many possible reactor states in the life of one fuel cycle, and they have been chosen as sufficiently definitive of the cycle by comparison with much more exhaustive studies performed on some 20 or 30 different, but typical, plant and fuel cycle combinations. The cases are described in detail in Reference 7, and they are considered to be necessary and sufficient to generate a local power density limit which, when increased by 5% for conservatism, will not be exceeded with a 95% confidence level. Many of the points do not approach the limiting envelope; however, they are part of the time histories which lead to the shapes which define the envelope.

Thus it is not possible to single out any transient or steady state condition which defines the most limiting case. It is not even possible to separate out a small number which form an adequate analysis. The process of generating a myriad of shapes is essential to the philosophy that leads to the required level of confidence. A maneuver which provides a limiting case for one reactor fuel cycle (defined as approaching the line of Figure 4.3-20) is not necessarily a limiting case for another reactor or fuel cycle with different control bank worths, insertion limits, enrichments, burnup, reactivity coefficients, etc. Each shape depends on the detailed history of operation up to that time and on the manner in which the operator conditioned xenon in the days immediately prior to the time at which the power distribution is calculated.

The calculated points are synthesized from axial calculations combined with radial factors appropriate for rodded and unrodded planes. In these calculations, the effects on the radial peak of xenon redistribution that occurs following the withdrawal of a control bank (or banks) from a rodded region is obtained from three-dimensional calculations. The multiplying factor to be applied to the radial peak is obtained from calculations in which xenon distribution is

preconditioned by the presence of control rods and then allowed to redistribute for several hours. A detailed discussion of this effect may be found in Reference 7. The calculated values are increased by a factor of 1.05 for conservatism and a factor of 1.03 for the engineering factor.

The envelope drawn over the calculated (max F_Q x Power) points in Figure 4.3-20 represents an upper bound envelope on local power density versus elevation in the core. It should be emphasized that this envelope is a conservative representation of the bounding values of local power density. Expected values are considerably smaller and, in fact, less conservative bounding values may be justified with additional analysis or surveillance requirements. For example, Figure 4.3-20 bounds both BOL and EOL conditions.

Finally, as previously discussed, this upper bound envelope is based on procedures of load follow which require operation within an allowed operating band of axial flux difference.

Allowing for fuel densification effects, the average linear power at 3648 MWt is 5.82 kW/ft. From Figure 4.3-20, the conservative upper bound value of normalized local power density, including uncertainty allowances, is 2.60 corresponding to a peak linear power of 15.2 kW/ft at 100.345% power.

To determine reactor protection system setpoints, with respect to power distributions, three categories of events are considered, namely rod control equipment malfunctions, operator errors of commission and operator errors of omission. In evaluating these three categories of events, the core is assumed to be operating within four constraints described above.

The first category comprises uncontrolled rod withdrawal (with rods moving in the normal bank sequence) for full length banks. Also included are motions of the full length banks below their insertion limits, which could be caused, for example, by uncontrolled dilution or primary coolant cooldown. Power distributions were calculated throughout these occurrences assuming short term corrective action, that is, no transient xenon effects were considered to result from the malfunction. The event was assumed

to occur from typical normal operating situations which include normal xenon transients. It was further assumed in determining the power distributions that total core power level would be limited by reactor trip to below 119%. Representative results are given in Figure 4.3-21 in units of kW/ft. The peak power density which can occur in such events, assuming reactor trip at or below 119%, is less than that required for centerline melt including uncertainties and densification effects.

The second category, also appearing in Figure 4.3-21, assumes that the operator mispositions the full length rod bank in violation of the insertion limits and creates short term conditions not included in normal operating conditions.

The third category assumes that the operator fails to take action to correct a flux difference violation. The results shown on Figure 4.3-22 are F_Q multiplied by 100.345% power including an allowance for calorimetric error. The figure shows that provided the assumed error in operation does not continue for a period which is long compared to the xenon time constant, the peak linear power does not exceed that required for centerline melt.

Analyses of possible operating power shapes show that the appropriate hot channel factors F_Q and $F^N_{\Delta H}$ for peak local power density and for DNB analysis at full power are the values given and addressed in the Technical Specifications.

The revised thermal design procedure (RTDP) used in the thermal and hydraulic evaluations for Byron/Braidwood requires the use of a nominal $F^N_{\Delta H}$ value. The value is 1.635 for VANTAGE 5 and VANTAGE+ fuel. The difference between the nominal $F^N_{\Delta H}$ values

and the design $F^N_{\Delta H}$ values reported in Table 4.3-1 are statistically accounted for in the design DNBR values as explained in Reference 89 of Section 4.4.

Increasing allowable $F^N_{\Delta H}$ with decreasing power is permitted by all previously approved Westinghouse designs. The increase is permitted by the DNB protection setpoints and allows radial power shape changes with rod insertion to the insertion limit.

The maximum calculated value of the operating nuclear enthalpy rise factor as a function of power level, including uncertainty allowance, does not exceed the design limit at any power level.

The design limit of the nuclear enthalpy rise hot channel factor ($F^N_{\Delta H}$) is given by:

$$F^N_{\Delta H} = 1.70\ [1 + 0.3\ (1 - P)]$$ for VANTAGE 5 and VANTAGE+ fuel,

where P is the fraction of full power.

The 0.3 multiplier has been approved for the Reference Core Report for the 17x17 optimized fuel assembly (Reference 40). In addition, justification for the 0.3 was provided to the NRC in NS-TMA-2323 from T. Anderson to J. Miller, dated October 24, 1980, in which the justification is discussed in Response 2 of the nonproprietary section. The 0.3 multiplier is also applicable for the VANTAGE+ fuel.

F_Q can be increased with decreasing power as shown in the Technical Specifications. Increasing $F^N_{\Delta H}$ with decreasing power is permitted by the DNB protection setpoints and allows radial power shape changes with rod insertion to the insertion limits as described in Subsection 4.4.4.3. The allowance for increased $F^N_{\Delta H}$ permitted is $F^N_{\Delta H} = 1.70\ (1 + 0.3\ (1-P))$*. This becomes a design basis criterion which is used for establishing acceptable control rod patterns and control bank sequencing. Likewise, fuel loading patterns for each cycle are selected with consideration of this design criterion. The worst values of $F^N_{\Delta H}$ for possible rod configurations occurring in normal operation are used in verifying that this criterion is met. Typical radial power distributions are shown in Figures 4.3-6 through 4.3-11.

*See Table 4.3-1.

The worst values generally occur when the rods are at their insertion limits. Maintenance of constant axial offset control establishes rod positions which are above the allowed rod insertion limits, thus providing increased margin to the $F^N_{\Delta H}$ criterion. As discussed in Section 3.2 of Reference 9, it has been determined that provided the above conditions a through d are observed, the Technical Specifications limits, are met. These limits are taken as input to the thermal-hydraulic design basis as described in Subsection 4.4.4.3.1.

When a situation is possible in normal operation which could result in local power densities in excess of those assumed as the precondition for a subsequent hypothetical accident, but which would not itself cause fuel failure, administrative controls and alarms are provided for returning the core to a safe condition. These alarms are described in Chapter 7.0 and the Technical Specifications.

4.3.2.2.7 Experimental Verification of Power Distribution Analysis

This subject is discussed in depth in Reference 2. A summary of this report is given below. It should be noted that power distribution related measurements are incorporated into the evaluation of calculated power distribution using the INCORE code described in Reference 8 or the BEACON code as described in Reference 48. A detailed description of this code's input and output is included in this reference. The measured vs. calculational comparison is normally performed periodically throughout the cycle lifetime of the reactor as required by Technical Specifications.

In a measurement of the heat flux hot channel factor, F_Q, with the movable detector system described in Subsections 7.7.1 and 4.4.6, the following uncertainties have to be considered:

a. Reproducibility of the measured signal

b. Errors in the calculated relationship between detector current and local flux

c. Errors in the calculated relationship between detector flux and peak rod power some distance from the measurement thimble.

The appropriate allowance for Category I above has been quantified by repetitive measurements made with several inter-calibrated detectors by using the common thimble features of the incore detector system. This system allows more than one detector to access any thimble. Errors in Category 2 above are quantified to the extent possible, by using the fluxes measured at one thimble location to predict fluxes at another location which is also measured. Local power distribution predictions are verified in critical experiments on arrays of rods with simulated guide thimbles, control rods, burnable poisons, etc. These critical experiments provide quantification of errors of types 2 and 3 above.

Reference 2 describes critical experiments performed at the Westinghouse Reactor Evaluation Center and measurements taken on two Westinghouse plants with incore systems of the same type as used in this plant described herein. The report concludes that the uncertainty associated with F_Q (heat flux) is 4.58% at the 95% confidence level with only 5% of the measurements greater

than the inferred value. This is the equivalent of a 1.645σ limit on a normal distribution and is the uncertainty to be associated with a full core flux map with movable detectors reduced with a reasonable set of input data incorporating the influence of burnup on the radial power distribution. The uncertainty is usually rounded up to 5%.

In comparing measured power distributions (or detector currents) against the calculations for the same situation, it is not possible to subtract out the detector reproducibility. Thus a comparison between measured and predicted power distributions has to include some measurement error. Such a comparison is given in Figure 4.3-23 for one of the maps used in Reference 2. Since the first publication of the report, hundreds of maps have been taken on these and other reactors. The results confirm the adequacy of the 5% uncertainty allowance on the calculated F_Q.

A similar analysis for the measurement uncertainty in $F^N_{\Delta H}$ (rod integral power) results in an allowance of 3.65% at the equivalent of a 1.645σ confidence level. A detailed analysis (Reference 2) of the $F^N_{\Delta H}$ calculational uncertainty results in an allowance of 3.9% at the equivalent of a 1.645σ confidence level. An 8% uncertainty factor is allowed in the nuclear design calculational basis; that is, the predicted rod integrals at full power must not exceed the design $F^N_{\Delta H}$ less 8%. By maintaining the 8% calculational uncertainty, several design allowances such as quadrant power tilt ratio (QPTR), rod misalignment, and transient radial xenon and their effect on $F^N_{\Delta H}$ can be covered without explicit detailed calculations each cycle.

A recent measurement in the second cycle of a 121 assembly, 12 foot, core is compared with a simplified one-dimensional core average axial calculation in Figure 4.3-24. This calculation does not give explicit representation to the fuel grids.

The accumulated data on power distributions in actual operation is basically of three types:

a. Much of the data is obtained in steady state operation at constant power in the normal operating configuration;

b. Data with unusual values of axial offset are obtained as part of the incore/excore detector calibration exercise which is performed quarterly.

c. Special tests have been performed in load follow and other transient xenon conditions which have yielded useful information on power distributions.

These data are presented in detail in References 9 and 39. Figure 4.3-25 contains a summary of measured values of F_Q as a function of core height for several plants from these reports.

Determination of the Core Power Distribution

The primary function of the BEACON core monitoring system is the

determination of the three-dimensional core power distribution. In BEACON, this calculation is performed with the NRC approved Westinghouse SPNOVA nodal method or the ANC Nodal Expansion Method (NEM). The SPNOVA Method employs a single Effective Fast Group (EFG) calculation to determine the global flux solution, and then uses a local correlation to determine the thermal flux and power distribution. The minimum running time required for the BEACON on-line calculation is achieved in SPNOVA by constructing the core-wide Green's function for the fast diffusion equation. The required time-consuming inversions of an EFG equation are avoided by using the precalculated Green's function (Reference 48). The ANC Nodal Expansion Method is slower than the SPNOVA Nodal Method, however is a more rigorous NEM for the spatial flux solution. NEM is based on basic neutron physics and avoids (as much as possible) the use of empirical correlations and data. Utilizing the NEM eliminates the normalization step and automatically assures identical results between SPNOVA and ANC. The Beacon detailed intra-nodal power is calculated by using peaking data tabulated as a function of fuel type and burnup.

Calibration of the Core Power Distribution

BEACON uses the incore flux detector measurements, core-exit thermocouples and excore detectors to perform the local calibration of the SPNOVA three dimensional power distributions. The SPNOVA predicted detector reaction rates are normalized to the incore measurements at the incore radial locations and over an axial mesh. The thermocouple adjustment is two-dimensional and is made by normalizing the SPNOVA radial power distribution to the assembly power inferred from the core-exit thermocouples. The thermocouple assembly power measurement is periodically calibrated to the incore-measured assembly power. The incore detectors and core-exit thermocouples do not provide complete coverage of the core and BEACON employs a two-dimensional spline fit to interpolate/extrapolate these measurements to the unmonitored assemblies. The spline fit includes a tolerance factor, which controls the degree to which the fit is forced to match the individual measurements. If, for example, the measurements are believed to be extremely accurate (inaccurate), then a low (high) tolerance factor is used and the SPNOVA solution is (not) forced to be in close agreement with the measurements.

The BEACON axial power shape is adjusted to ensure agreement with the axial offset measured by the excore detectors. Adding a sinusoidal component to the SPNOVA calculated axial power shape makes this adjustment. The SPNOVA excore axial offset is determined by an appropriate weighting of the peripheral assembly powers. The excore detector axial offset is periodically calibrated to the incore detector measurement.

BEACON Core Monitoring Methodology

The BEACON core monitoring process is carried out in three steps. In the first step, the SPNOVA model, individual thermocouples and the excore axial offset are calibrated to the full-core incore flux measurement. In the second step, the SPNOVA model is updated based on the most recent operating history, and adjusted using

thermocouple and excore measurements. Using thermocouple and excore measurements performs the continuous monitoring by updating the BEACON model in the third step.

The continuous core monitoring of the current reactor statepoint (fuel burnup, xenon distribution, soluble boron concentration, etc.) provided by the BEACON system allows a more precise determination of the parameters used in transient analysis, and therefore relaxes the requirement to limit the transient initial conditions via power distribution control. As part of the continuous monitoring, the fuel and DNBR limits are calculated using standard Westinghouse methods.

The accuracy of the BEACON analysis decreases as the calibration intervals increase and the power distribution diverges from the reference power shape. In order to minimize the BEACON uncertainty the reference power distribution is updated every 15 minutes, when the axial flux difference (AFD) changes greater than 2%, or when power changes by more than 5%.

The BEACON nuclear/thermal-hydraulic data sets and models are determined using Westinghouse reload design codes and methods. Before BEACON is used for core monitoring, the BEACON model and reference uncertainties are validated prior to use. The online DNBR and limits evaluation is performed with NRC approved DNBR methodologies.

4.3.2.2.8 Testing

A very extensive series of physics tests is performed on the first core, even though this core is not a prototype design. These tests and the criteria for satisfactory results are described in Chapter 14.0. Since not all limiting situations can be created at beginning-of-life, the main purpose of the tests is to provide a check on the calculational methods used in the predictions for the conditions of the test. Physics tests are performed at the beginning of each reload cycle to determine if the operating characteristics of the core are consistent with the design predications and to provide assurance that the core can be operated as designed, on the assumptions that the reload fuel is supplied by the first core designer.

4.3.2.2.9 Monitoring Instrumentation

The adequacy of instrument numbers, spatial deployment, required correlations between readings and peaking factors, calibration and errors are described in References 2, 6, and 9. The relevant conclusions are summarized in Subsections 4.3.2.2.7 and 4.4.6.

Provided the limitations given in Subsection 4.3.2.2.6 on control rods moving together in a single bank and control banks sequenced with design overlap, the multisection excore detector based surveillance system provides adequate online monitoring of power distributions. Further details of specific limits on the observed rod positions and power distributions are given in the Technical Specifications. Descriptions of the systems provided are given in Section 7.7.

Core Power Distribution Instrumentation

BEACON uses the incore flux detector measurements, core-exit thermocouples and excore detectors to perform the local calibration of the SPNOVA three dimensional power distributions. The SPNOVA predicted detector reaction rates are normalized to the incore measurements at the incore radial locations and over an axial mesh. The thermocouple adjustment is two-dimensional and is made by normalizing the SPNOVA radial power distribution to the assembly power inferred from the core-exit thermocouples. The thermocouple assembly power measurement is periodically calibrated to the incore-measured assembly power. The incore detectors and core-exit thermocouples do not provide complete coverage of the core and BEACON employs a two-dimensional spline fit to interpolate/extrapolate these measurements to the unmonitored assemblies. The spline fit includes a tolerance factor, which controls the degree to which the fit is forced to match the individual measurements. If, for example, the measurements are believed to be extremely accurate (inaccurate), then a low (high) tolerance factor is used and the SPNOVA solution is (not) forced to be in close agreement with the measurements.

The BEACON axial power shape is adjusted to ensure agreement with the axial offset measured by the excore detectors. Adding a sinusoidal component to the SPNOVA calculated axial power shape

makes this adjustment. The SPNOVA excore axial offset is determined by an appropriate weighting of the peripheral assembly powers. The excore detector axial offset is periodically calibrated to the incore detector measurement.

Beside incore fluxmap data, thermocouple data and excore data, BEACON online continuous monitoring power distribution system also uses inputs from Reactor coolant system cold leg temperature, control rod position, and power.

4.3.2.3 Reactivity Coefficients

The kinetic characteristics of the reactor core determine the response of the core to changing plant conditions or to operator adjustments made during normal operation, as well as the core response during abnormal or accidental transients. The reactivity coefficients reflect the changes in the neutron multiplication due to varying plant conditions such as power, moderator or fuel temperatures, or less significantly due to a change in pressure or void conditions. Since reactivity coefficients change during the life of the core, ranges of coefficients are employed in transient analysis to determine the response of the plant throughout life. The results of such simulations and the reactivity coefficients used are presented in Chapter 15.0. The reactivity coefficients are calculated on a corewise basis by radial and axial diffusion theory methods and with nodal analysis methods. The effect of radial and axial power distribution on core average reactivity coefficients is implicit in those calculations and is not significant under normal operating conditions. For example, a skewed xenon distribution which results in changing axial offset by 5% changes the moderator and Doppler temperature coefficients by less than 0.01 pcm/°F and 0.03 pcm/°F respectively. An artificially skewed xenon distribution which results in changing the radial $F_{\Delta H}$ by 3%

changes the moderator and Doppler temperature coefficients by less than 0.03 pcm/°F and 0.001 pcm/°F respectively. The spatial effects are accentuated in some transient conditions and are included for example, in the postulated main steamline break and rupture of the RCCA mechanism housing described in Subsections 15.1.5 and 15.4.8.

The analytical methods and calculational models used in calculating the reactivity coefficients are given in Subsection 4.3.3. These models have been confirmed through extensive testing of more than thirty cores similar to the plant described herein; results of these tests are discussed in Subsection 4.3.3.

Quantitative information for calculated reactivity coefficients, including fuel-Doppler coefficient, moderator coefficients (density, temperature, pressure, void) and power coefficient is given in the following sections.

4.3.2.3.1 Fuel Temperature (Doppler) Coefficient

The fuel temperature (Doppler) coefficient is defined as the change in reactivity per degree change in effective fuel temperature and is primarily a measure of the Doppler broadening of U-238 and Pu-240 resonance absorption peaks. Doppler broadening of other isotopes such as U-236, Np-237 etc. are also considered but their contribution to the Doppler effect is small. An increase in fuel temperature increases the effective resonance absorption cross sections of the fuel and produces a corresponding reduction in reactivity.

The fuel temperature coefficient is calculated by performing two-group either two or three dimensional calculations. Moderator temperature is held constant and the power level is varied. Spatial variation of fuel temperature is taken into account by calculating the effective fuel temperature as a function of power density as discussed in Subsection 4.3.3.1.

The Doppler temperature coefficient is shown in Figure 4.3-26 as a function of the effective fuel temperature (at beginning-of-life and end-of-life conditions). The effective fuel temperature is lower than the volume averaged fuel temperature since the neutron flux distribution is non-uniform through the pellet and gives preferential weight to the surface temperature. The Doppler-only contribution to the power coefficient, defined later, is shown in Figure 4.3-27 as a function of relative core power. The integral of the differential curve on Figure 4.3-27 is the Doppler contribution to the power defect and is shown in Figure 4.3-28 as a function of relative power. The Doppler coefficient becomes more negative as a function of life as the Pu-240 content increases, thus increasing the Pu-240 resonance absorption, but overall becomes less negative since the fuel temperature changes with burnup as described in Subsection

4.3.3.1. The upper and lower limits of Doppler coefficient used in accident analyses are given in Chapter 15.0.

4.3.2.3.2 Moderator Coefficients

The moderator coefficient is a measure of the change in reactivity due to a change in specific coolant parameters such as density, temperature, pressure or void. The coefficients so obtained are moderator density, temperature, pressure and void coefficients.

Moderator Density and Temperature Coefficients

The moderator temperature (density) coefficient is defined as the change in reactivity per unit change in the moderator temperature (density). Generally, the effect of the changes in moderator density as well as the temperature are considered together. A decrease in moderator density results in less moderation and hence a decrease in reactivity. Therefore, the moderator density coefficient is positive. As temperature increases, density decreases (for a constant pressure) and hence the moderator temperature coefficient becomes more negative. An increase in coolant temperature, keeping the density constant, leads to a hardened neutron spectrum and results in an increase in resonance absorption in U-238, Pu-240 and other isotopes. The hardened spectrum also causes a decrease in the fission to capture ratio in U-235 and Pu-239. Both of these effects make the moderator temperature coefficient more negative. Since water density changes more rapidly with temperature as temperature increases, the moderator temperature (density) coefficient becomes more negative (positive) with increasing temperature.

The soluble boron used in the reactor as a means of reactivity control also has an effect on moderator temperature coefficient, since the soluble boron density as well as the water density is decreased when the coolant temperature rises. An increase in the soluble boron concentration introduces a positive component in the moderator temperature coefficient.

Thus, if the concentration of soluble boron is large enough, the net value of the coefficient may be positive. With the burnable absorber rods present, however, the initial hot boron concentration is sufficiently low that the moderator temperature coefficient is more negative than the Technical Specifications limit at operating temperatures. The effect of inserting control rods is to make the moderator temperature coefficient more negative by reducing the required soluble boron concentration and by increasing the "leakage" of the core.

With burnup, the moderator temperature coefficient becomes more negative primarily as a result of boric acid dilution but also to an extent from the effects of the buildup of plutonium and fission products. With the presence of burnable absorber rods and integral burnable absorbers, the moderator temperature

coefficient may increase slightly near the middle of life as a result of the depletion of the absorber material. This effect will depend on the number of absorber rods and type (discrete or integral).

The moderator coefficient is calculated for the various plant conditions discussed above by performing two-group two or three dimensional calculations, varying the moderator temperature (and density) by about ± 5°F about each of the mean temperatures. The moderator temperature coefficient is shown as a function of core temperature and boron concentration for the unrodded core in Figures 4.3-29 through 4.3-31. The temperature range covered is from cold (68°F) to about 600°F. The contribution due to Doppler coefficient (because of change in moderator temperature) has been subtracted from these results. Figure 4.3-32 shows the hot, full power moderator temperature coefficient plotted as a function of cycle lifetime for the critical boron concentration condition based on the design boron letdown condition for a typical reload cycle for both a positive and negative MTC design.

The moderator coefficients presented here are calculated on a corewise basis, since they are used to describe the core behavior in normal and accident situations when the moderator temperature changes can be considered to affect the entire core.

Moderator Pressure Coefficient

The moderator pressure coefficient relates the change in moderator density, resulting from a reactor coolant pressure change, to the corresponding effect on neutron production. This coefficient is of much less significance in comparison with the moderator temperature coefficient. A change of 50 psi in pressure has approximately the same effect on reactivity as a half-degree change in moderator temperature. This coefficient can be determined from the moderator temperature coefficient by relating change in pressure to the corresponding change in density. The moderator pressure coefficient may be negative over a portion of the moderator temperature range at beginning-of-life (-0.004 pcm/psi, BOL) but is always positive at operating conditions and becomes more positive during life (+0.3 pcm/psi, EOL).

Moderator Void Coefficient

The moderator void coefficient relates the change in neutron multiplication to the presence of voids in the moderator. In a PWR this coefficient is not very significant because of the low void content in the coolant. The core void content is less than one-half of 1% and is due to local or statistical boiling. The void coefficient varies from 50 pcm/% void at BOL and at low temperatures to -250 pcm/% void at EOL and at operating temperatures. The negative void coefficient at operating temperature becomes more negative with fuel burnup.

4.3.2.3.3 Power Coefficient

The combined effect of moderator temperature and fuel temperature change as the core power level changes is called the total power coefficient and is expressed in terms of reactivity change per percent power change. The power coefficient at BOL and EOL conditions is given in Figure 4.3-33.

It becomes more negative with burnup reflecting the combined effect of moderator and fuel temperature coefficients with burnup. The power defect (integral reactivity effect) at BOL and EOL which includes three dimensional flux redistribution is given in Figure 4.3-34.

4.3.2.3.4 Comparison of Calculated and Experimental Reactivity Coefficients

Subsection 4.3.3 describes the comparison of calculated and experimental reactivity coefficients in detail. Based on the data presented there, the accuracy of the current analytical model is:

$\pm 0.2\%\ \Delta\rho$ for Doppler and power defect
± 2 pcm/°F for the moderator coefficient.

Experimental evaluation of the calculated coefficients will be done during the physics startup tests described in Chapter 14.0.

4.3.2.3.5 Reactivity Coefficients Used in Transient Analysis

Table 4.3-1 gives the limiting values as well as the best estimate values for the reactivity coefficients. The limiting values are used as design limits in the transient analysis. The exact values of the coefficient used in the analysis depend on whether the transient of interest is examined at the BOL or EOL, whether the most negative or the most positive (least negative) coefficients are appropriate, and whether spatial nonuniformity must be considered in the analysis. Conservative values of coefficients, considering various aspects of analysis are used in the transient analysis. This is described in Chapter 15.0.

The reactivity coefficients shown in Figures 4.3-26 through 4.3-34 are best estimate values calculated for a typical reload cycle and apply to the core described in Table 4.3-1. The limiting values shown in Table 4.3-1 are chosen to encompass the best estimate reactivity coefficients, including the uncertainties given in Subsection 4.3.3.3 over appropriate operating conditions. The most positive as well as the most negative values are selected to form the design basis range used in the transient analysis. A direct comparison of the best estimate and design limit values shown in Table 4.3-1 can be misleading since in many instances, the most conservative combination of reactivity coefficients is used in the transient analysis even though the extreme coefficients assumed may not simultaneously occur at the conditions of lifetime, power level, temperature and boron concentration assumed in the analysis. The need for a reevaluation of any accident in a subsequent cycle is contingent upon whether or not the coefficients for that cycle fall within the identified range used in the analysis presented in Chapter 15.0 with due allowance for the calculational uncertainties given in Subsection 4.3.3.3. Control rod requirements are given in Table 4.3-2 for

a typical equilibrium cycle. These latter numbers are provided for information only. Their validity is verified for a particular reload cycle.

4.3.2.4 Control Requirements

To ensure the shutdown margin stated in the COLR under conditions where a cooldown to ambient temperature is required, concentrated soluble boron is added to the coolant. Typical boron concentrations for several core conditions are listed in Table 4.3-1. For all core conditions including refueling, the boron concentration is well below the solubility limit. The rod cluster control assemblies are employed to bring the reactor to the hot shutdown condition. The minimum required shutdown margin is given in the COLR.

The ability to accomplish the shutdown for hot conditions is demonstrated in Table 4.3-2 by comparing the difference between the rod cluster control assembly reactivity available with an allowance for the worst stuck rod with that required for control and protection purposes. The shutdown margin includes an allowance of 7% for analytic uncertainties (see Subsection 4.3.2.4.9). The largest reactivity control requirement appears at the EOL when the moderator temperature coefficient reaches its peak negative value as reflected in the larger power defect.

The control rods are required to provide sufficient reactivity to account for the power defect from full power to zero power and to provide the required shutdown margin. The reactivity addition resulting from power reduction consists of contributions from Doppler, variable average moderator temperature, flux redistribution, and reduction in void content as discussed below.

4.3.2.4.1 Doppler

The Doppler effect arises from the broadening of U-238 and Pu-240 resonance peaks with an increase in effective pellet temperature. This effect is calculated over the range of zero power to full power.

4.3.2.4.2 Variable Average Moderator Temperature

When the core is shutdown to the hot, zero power condition, the average moderator temperature changes from the equilibrium full load value determined by the steam generator and turbine characteristics (steam pressure, heat transfer, tube fouling, etc.) to the equilibrium no load value, which is based on the steam generator shell side design pressure. The design change in temperature is conservatively increased by 4°F to account for the control dead band and measurement errors.

Since the density contribution to the moderator coefficient is negative, there is a reactivity addition with power reduction. The moderator coefficient becomes more negative as the fuel depletes because the boron concentration is reduced. This effect is the major contributor to the increased requirement at end-of-life.

4.3.2.4.3 Redistribution

During full power operation, the coolant density decreases with core height, and this, together with partial insertion of control rods, results in less fuel depletion near the top of the core. Under steady state conditions, the relative power distribution will be slightly asymmetric towards the bottom of the core. On the other hand, at hot zero power conditions, the coolant density is uniform up the core, and there is no flattening due to Doppler. The result will be a flux distribution which at zero power can be skewed toward the top of the core. The reactivity insertion due to the skewed distribution is calculated with an allowance for effects of xenon distribution.

4.3.2.4.4 Void Content

A small void content in the core is due to nucleate boiling at full power. The void collapse coincident with power reduction makes a small reactivity contribution.

4.3.2.4.5 Rod Insertion Allowance

At full power, the control bank is operated within a prescribed band of travel to compensate for small periodic changes in boron concentration, changes in temperature and very small changes in the xenon concentration not compensated for by a change in boron concentration. When the control bank reaches either limit of this band, a change in boron concentration is required to compensate for additional reactivity changes. Since the insertion limit is set by a rod travel limit, a conservatively high calculation of the inserted worth is made which exceeds the normally inserted reactivity.

4.3.2.4.6 Burnup

Excess reactivity of 10% $\Delta\rho$ to 25% $\Delta\rho$ (hot) is installed at the beginning of each cycle to provide sufficient reactivity to compensate for fuel depletion and fission products throughout the cycle. This reactivity is controlled by the addition of soluble boron to the coolant and by burnable absorbers. The soluble boron concentration for several core configurations and the unit boron worth are given in Table 4.3-1. Since the excess reactivity for burnup is controlled by soluble boron and/or burnable absorbers, it is not included in control rod requirements.

4.3.2.4.7 Xenon and Samarium Poisoning

Changes in xenon and samarium concentrations in the core occur at a sufficiently slow rate, even following rapid power level changes, that the resulting reactivity change is controlled by changing the soluble boron concentration.

4.3.2.4.8 pH Effects

Changes in reactivity due to a change in coolant pH, if any, are sufficiently small in magnitude and occur slowly enough to be controlled by the boron system. Further details are provided in Reference 11.

4.3.2.4.9 Experimental Confirmation

Following a normal shutdown, the total core reactivity change during cooldown with a stuck rod has been measured on a 121 assembly, 10 foot high core and 121 assembly, 12 foot high core. In each case, the core was allowed to cool down until it reached criticality simulating the steamline break accident. For the 10 foot core, the total reactivity change associated with the cooldown is overpredicted by about 0.3% $\Delta\rho$ with respect to the measured result. This represents an error of about 5% in the total reactivity change and is about half the uncertainty allowance for this quantity. For the 12 foot core, the difference between the measured and predicted reactivity change was an even smaller 0.2% $\Delta\rho$. These measurements and others demonstrate the ability of the methods described in Subsection 4.3.3.

4.3.2.4.10 Control

Core reactivity is controlled by means of a chemical poison dissolved in the coolant, rod cluster control assemblies, and burnable absorber rods as described below.

4.3.2.4.11 Chemical Poisoning

Boron in solution as boric acid is used to control relatively slow reactivity changes associated with:

a. The moderator temperature defect in going from cold shutdown at ambient temperature to the hot operating temperature at zero power,

b. The transient xenon and samarium poisoning, such as that following power changes or changes in rod cluster control position,

c. The excess reactivity required to compensate for the effects of fissile inventory depletion and buildup of long-life fission products.

d. The burnable absorber depletion.

The boron concentrations for various core conditions are presented in Table 4.3-1.

4.3.2.4.12 Rod Cluster Control Assemblies

Full length rod cluster control assemblies (RCCAs) exclusively are employed in this reactor. The number of RCCAs is 53. The full length rod cluster control assemblies are used for shutdown and control purposes to offset fast reactivity changes associated with:

a. The required shutdown margin in the hot zero power, stuck rod condition,

b. The reactivity compensation as a result of an increase in power above hot zero power (power defect including Doppler, and moderator reactivity changes),

c. Unprogrammed fluctuations in boron concentration, coolant temperature, or xenon concentration (with rods not exceeding the allowable rod insertion limits),

d. Reactivity ramp rates resulting from load changes.

The allowed full length control bank reactivity insertion is limited at full power to maintain shutdown capability. As the power level is reduced, control rod reactivity requirements are also reduced and more rod insertion is allowed. The control bank position is monitored and the operator is notified by an alarm if the limit is approached. The determination of the insertion limit uses conservative xenon distributions and axial power shapes. In addition, the rod cluster control assembly withdrawal pattern determined from these analyses is used in determining power distribution factors and in determining the maximum worth of an inserted rod cluster control assembly ejection accident. For further discussion, refer to the Technical Specifications on rod insertion limits.

Power distribution, rod ejection and rod misalignment analyses are based on the arrangement of the shutdown and control groups of the rod cluster control assemblies shown in Figure 4.3-35. All shutdown rod cluster control assemblies are withdrawn before withdrawal of the control banks is initiated. In going from zero to 100% power, control banks A, B, C and D are withdrawn sequentially. The limits of rod positions and further discussion on the basis for rod insertion limits are provided in the Technical Specifications.

4.3.2.4.13 Reactor Coolant Temperature

Reactor coolant (or moderator) temperature control has added flexibility in reactivity control of the Westinghouse PWR.

Maintaining the moderator temperature coefficient less than the Technical Specifications limit allows for the following:

a. Maximize return to power capabilities.

b. Provide ±5% power load regulation capabilities without requiring control rod compensation.

Reactor coolant temperature control supplements the dilution capability of the plant by lowering the reactor coolant temperature to supply positive reactivity through the negative moderator coefficient of the reactor, particularly at hot full power conditions. After the transient is over, the system automatically recovers the reactor coolant temperature to the programmed value.

Moderator temperature control of reactivity, like soluble boron control, has the advantage of not significantly affecting the core power distribution. However, unlike boron control, temperature control can be rapid enough to achieve reactor power change rates of 5%/minute.

4.3.2.4.14 Burnable Absorber Rods

The burnable absorbers (discrete and/or integral type) provide partial control of the excess reactivity available during the fuel cycle. In doing so, these burnable absorbers along with rod withdrawal limits, as necessary, prevent the moderator temperature coefficient from exceeding the Technical Specifications limits at normal operating conditions. They perform this function by reducing the requirement for soluble boron in the moderator at the beginning of the fuel cycle as described previously. For purposes of illustration, a typical burnable absorber rod pattern in the core together with the number of rods per assembly is shown in Figure 4.3-6 for a typical cycle using both discrete and integral absorbers. The arrangements within an assembly are displayed in Figures 4.3-4 and 4.3-5. The boron in the rods is depleted with burnup but at a sufficiently slow rate so that the resulting critical concentration of soluble boron is such that the moderator temperature coefficient remains less than the Technical Specifications limits at all times for full power operating conditions.

4.3.2.4.15 Peak Xenon Startup

Compensation for the peak xenon buildup is accomplished using the boron control system. Startup from the peak xenon condition is accomplished with a combination of rod motion and boron dilution. The boron dilution may be made at any time, including during the shutdown period, provided the shutdown margin is maintained.

4.3.2.4.16 Load Follow Control and Xenon Control

During load follow maneuvers, power changes are accomplished using control rod motion and dilution or boration by the boron system as required. Control rod motion is limited by the control rod insertion limits on full length rods as provided in the

Technical Specifications and discussed in Subsections 4.3.2.4.12 and 4.3.2.4.13. The power distribution is maintained within acceptable limits through the location of the full length rod bank. Reactivity changes due to the changing xenon concentration can be controlled by rod motion and/or changes in the soluble boron concentration.

Rapid power increases (5%/min) from part power during load follow operation are accomplished with a combination of rod motion, moderator temperature reduction, and boron dilution. Compensation for the rapid power increase is accomplished initially by a combination of rod withdrawal and moderator temperature reduction. As the slower boron dilution takes affect after the initial rapid power increase, the moderator temperature returns to the programmed value.

4.3.2.4.17 Burnup

Control of the excess reactivity for burnup is accomplished using soluble boron and/or burnable absorbers. The boron concentration must be limited during operating conditions to ensure the moderator temperature coefficient is more negative than the Technical Specifications limit. A sufficient number of burnable absorbers are installed at the beginning of a cycle to give the desired cycle lifetime without exceeding the boron concentration limit. The practical minimum boron concentration is 10 ppm.

4.3.2.5 Control Rod Patterns and Reactivity Worths

The full length rod cluster control assemblies are designated by function as the control groups and the shutdown groups. The terms "group" and "bank" are used synonymously throughout this report to describe a particular grouping of control assemblies. The rod cluster assembly pattern is displayed in Figure 4.3-35 which is not expected to change during the life of the plant. The control banks are labeled A, B, C, and D and the shutdown banks are labeled SA, SB, etc., as applicable. Each bank, although operated and controlled as a unit, is comprised of two subgroups. The axial position of the full length rod cluster control assemblies may be controlled manually or automatically. The rod cluster control assemblies are all dropped into the core following actuation of reactor trip signals.

Two criteria have been employed for selection of the control groups. First the total reactivity worth must be adequate to meet the requirements specified in Table 4.3-2. Second, in view of the fact that these rods may be partially inserted at power operation, the total power peaking factor should be low enough to ensure that the power capability requirements are met. Analyses indicate that the first requirement can be met either by a single group or by two or more banks whose total worth equals at least the required amount. The axial power shape would be more peaked following movement of a single group of rods worth 3% to 4% $\Delta\rho$;

therefore, four banks (described as A, B, C, and D in Figure 4.3-35) with average worth approximately one percent Δρ have been selected.

The position of control banks for criticality under any reactor condition is determined by the concentration of boron in the coolant. On an approach to criticality boron is adjusted to ensure that criticality will be achieved with control rods above the insertion limit set by shutdown and other considerations (see the Technical Specifications). Early in the cycle there may also be a withdrawal limit at low power to maintain a more negative moderator temperature coefficient than the Technical Specifications limits.

Ejected rod worths are given in Subsection 15.4.8 for several different conditions.

Allowable deviations due to misaligned control rods are discussed in the Technical Specifications.

A representative calculation for two banks of control rods withdrawn simultaneously (rod withdrawal accident) is given in Figure 4.3-36.

Calculation of control rod reactivity worth versus time following reactor trip involves both control rod velocity and differential reactivity worth. The rod position versus time of travel after rod release normalized to "Distance to Top of Dashpot" and "Drop Time to Top of Dashpot" is given in Figure 15.0-4 for Ag-In-Cd. For the Hafnium control rod material, the rod drop times are within the bounds shown in this figure. For nuclear design purposes, the reactivity worth versus rod position is calculated by a series of steady state calculations at various control rod positions assuming all rods out of the core as the initial position in order to minimize the initial reactivity insertion rate. Also to be conservative, the rod of highest worth is assumed stuck out of the core and the flux distribution (and thus reactivity importance) is assumed to be skewed to the bottom of the core. The result of these calculations is shown in Figure 15.0-5.

The shutdown groups provide additional negative reactivity to assure an adequate shutdown margin. Shutdown margin is defined as the amount by which the core would be subcritical at hot shutdown if all rod cluster control assemblies are tripped, but assuming that the highest worth assembly remains fully withdrawn and no changes in xenon or boron take place. The loss of control rod worth due to the material irradiation is negligible since only bank D and bank C may be in the core under normal operating conditions.

The values given in Table 4.3-2 show that the available reactivity in withdrawn rod cluster control assemblies provides

the design bases minimum shutdown margin allowing for the highest worth cluster to be at its fully withdrawn position. An allowance for the uncertainty in the calculated worth of N-1 rods is made before determination of the shutdown margin.

Measured worth of control and shutdown banks is determined during Low Power Physics Testing by use of Dynamic Rod Worth Measurement WCAP-13360-P-A (DRWM) or rod swap WCAP-9863-P-A.

4.3.2.6 Criticality of the Reactor During Refueling and Criticality of Fuel Assemblies

Criticality of fuel assemblies outside the reactor is precluded by adequate design of fuel transfer, shipping and storage facilities and by administrative control procedures. The two principal methods of preventing criticality are limiting the fuel assembly array size and limiting assembly interaction by fixing the minimum separation between assemblies and/or inserting neutron poisons between assemblies.

The design basis for preventing criticality outside the reactor is that, considering possible variations, there is a 95% probability at a 95% confidence level that the effective multiplication factor (K_{eff}) of the fuel assembly array will be less than 0.95 as recommended in ANSI N57.2-1983. The following are the conditions that are assumed in meeting this design basis:

a. The fuel assembly contains the highest enrichment authorized without any control rods or any noncontained burnable poison and is at its most reactive point in life.

b. For flooded conditions, the moderator is water borated to 550 ppm at the temperature within the design limits which yields the largest reactivity.

c. The array is either infinite in lateral extent or is surrounded by a conservatively chosen reflector, whichever is appropriate for the design.

d. Mechanical uncertainties are treated by either using "worst case" conditions or by performing sensitivity studies and obtaining appropriate uncertainties.

e. Credit is taken for the neutron absorption in structural materials and in Boral, added specifically for neutron absorption.

For spent fuel rack storage application, water is present. However, the design methodology also prevents accidental criticality when new fuel assemblies are stored in the dry

condition. For this case possible sources of moderation such as those that could arise during fire-fighting operations are included in the analysis. The design basis K_{eff} is 0.98 as recommended in ANSI N57.2-1983.

The design method which ensures the criticality safety of fuel assemblies outside the reactor uses the AMPX system of codes (References 32 and 33) for cross-section generation and KENO Va (Reference 34) for reactivity determination.

The 227 energy group cross-section library (Reference 32) that is the common starting point for all cross-sections has been generated from ENDF/B-V data. The NITAWL program (Reference 33) includes in this library the self-shielded resonance cross-sections that are appropriate for a particular geometry. The Nordheim Integral Treatment is used. Energy and spatial weighting of cross-sections is performed by the XSDRNPM program (Reference 33) which is a one dimensional S_N transport theory code. These multigroup cross-section sets are then used as input to KENO Va (Reference 34) which is a three-dimensional Monte Carlo theory program designed for reactivity calculations.

A set of 32 critical experiments has been analyzed using the above method to demonstrate its applicability to criticality analysis and to establish the method bias and variability. The experiments range from water moderated oxide fuel arrays separated by various materials that simulate LWR fuel shipping and storage conditions (References 35) to dry, harder spectrum uranium metal cylinder arrays with various interspersed materials (Reference 37) that demonstrate the wide range of applicability of the method.

Some descriptive facts about each of the 32 benchmark critical experiments are given in Table 4.3-3. The average K_{eff} of the benchmarks is 0.993, which, when compared to the average measured K_{eff} (1.0007), gives a bias of 0.0077. The standard deviation of the K_{eff} values is 0.00136 Δk. The 95/95 one-sided tolerance limit factor for 32 values is 2.20. There is thus a 95% probability with a 95% confidence level that the uncertainty in reactivity due to the method is not greater than 0.0030 Δk.

The transport theory computer code, PHOENIX-P (Reference 45), is used to determine the reactivity changes caused by the fuel assembly, spent fuel racks (tolerance), and the spent fuel pool conditions (temperature and soluble boron). PHOENIX-P is a depletable, two-dimensional, multigroup, discrete ordinate, transport theory code that uses a 70-energy group, nuclear data library.

The PHOENIX-P code has been validated by comparisons with experiments where the isotopic fuel composition has been examined following discharge from a reactor. In addition, an extensive set of benchmark critical experiments has been analyzed with PHOENIX-P.

The soluble boron credit methodology contained in WCAP-14416-NP-A (Reference 47) requires that the calculation for 95/95 K_{eff} without soluble boron in the fuel pool water, performed for the spent fuel pool racks show that K_{eff} is less than 1.0 with a reactivity allowance for the uncertainty due to fuel assembly and fuel storage rack tolerances. This ensures that criticality does not occur in the spent fuel pool racks at a 0 ppm boron concentration in the spent fuel pool water.

The storage configuration for fuel assemblies in the spent fuel storage racks is derived from the calculation of 95/95 K_{eff} with no soluble boron, such that K_{eff} will be less than 1.0 at a 95-percent probability at a 95-percent confidence level. The calculation is performed at cold conditions (68 °F) with no soluble boron in the spent fuel pool water.

The final equation for determining the 95/95 K_{eff} with no soluble boron is shown below:

$$K_{eff} = K_{nominal} + B_{method} + B_{temp} + B_{self} + B_{uncert}$$

where:

$K_{nominal}$ = nominal conditions KENO-Va K_{eff}

B_{method} = method bias determined from benchmark critical comparisons

B_{temp} = temperature bias

B_{self} = B-10 self-shielding bias, if applicable

B_{uncert} = statistical summation of uncertainty components

$$= \left[\sum_{i=1}^{n} (\text{tolerance}_i)^2\right]^{1/2} \text{ for n tolerances, and/or}$$

$$= \left[\sum_{i=1}^{n} (\text{uncertainty}_i)^2\right]^{1/2} \text{ for n uncertainties.}$$

Using the above equations, the storage configuration derived for the assemblies must show a K_{eff} of less than 1.0 with no soluble boron. This storage configuration is the basis for fuel assembly storage in the spent fuel pool with credit for soluble boron.

To maintain adequate safety margin for criticality in the spent fuel storage racks, the K_{eff} of the spent fuel storage racks is less than or equal to 0.95 with allowances for tolerances and uncertainties in the presence of spent fuel pool soluble boron. A spent fuel pool soluble boron concentration is chosen that provides a K_{eff} that is less than or equal to 0.95 when biases, tolerances, and uncertainties are included. The tolerance calculations are performed assuming the presence of this spent fuel pool soluble boron. The final 95/95 K_{eff} is less than or equal to 0.95 with allowances for biases, tolerances, and uncertainties, including the presence of the determined concentration of spent fuel pool soluble boron.

4.3.2.7 Stability

4.3.2.7.1 Introduction

The stability of the PWR cores against xenon-induced spatial oscillations and the control of such transients are discussed extensively in References 6, 14, 15, and 16. The stability of OFA and VANTAGE 5 fuels is discussed in References 40 and 41, respectively. A summary of these reports is given in the following discussion and the design bases are given in Subsection 4.3.1.6.

In a large reactor core, xenon-induced oscillations can take place with no corresponding change in the total power of the core. The oscillation may be caused by a power shift in the core which occurs rapidly by comparison with the xenon-iodine time constants. Such a power shift occurs in the axial direction when a plant load change is made by control rod motion and results in a change in the moderator density and fuel temperature distributions. Such a power shift could occur in the diametral plane of the core as a result of abnormal control action.

Due to the negative power coefficient of reactivity, PWR cores are inherently stable to oscillations in total power. Protection against total power instabilities is provided by the control and protection system as described in Section 7.7. Hence, the discussion on the core stability will be limited here to xenon-induced spatial oscillations.

4.3.2.7.2 Stability Index

Power distributions, either in the axial direction or in the X-Y plane, can undergo oscillations due to perturbations introduced in the equilibrium distributions without changing the total core power. The overtones in the current PWRs, and the stability of the core against xenon-induced oscillations can be determined in terms of the eigenvalues of the first flux overtones. Writing, either in the axial direction or in the X-Y plane, the eigenvalue ξ of the first flux harmonic as:

$$\xi = b + ic, \qquad (4.3\text{-}1)$$

then b is defined as the stability index and $T = 2\pi/c$ as the oscillation period of the first harmonic. The time-dependence of the first harmonic $\delta\phi$ in the power distribution can now be represented as:

$$\delta\phi\ (t) = A\ e\xi t - ae^{bt} \cos ct, \qquad (4.3\text{-}2)$$

where A and a are constants. The stability index can also be obtained approximately by:

$$b = \frac{1}{T} \ln \frac{A_{n+1}}{A_n} \qquad (4.3\text{-}3)$$

where A_n, A_{n+1} are the successive peak amplitudes of the oscillation and T is the time period between the successive peaks.

4.3.2.7.3 Prediction of the Core Stability

The stability of the core described herein (i.e., with 17 x 17 fuel assemblies) against xenon-induced spatial oscillations is expected to be equal to or better than that of earlier designs for cores of similar size. The prediction is based on a comparison of the parameters which are significant in determining the stability of the core against the xenon-induced oscillations, namely (1) the overall core size is unchanged and spatial power distributions will be similar, (2) the moderator temperature coefficient is expected to be similar, and (3) the Doppler coefficient of reactivity is expected to be similar at full power.

Analysis of both the axial and X-Y xenon transient tests, discussed in Subsection 4.3.2.7.5, shows that the calculational model is adequate for the prediction of core stability.

4.3.2.7.4 Stability Measurements

a. Axial Measurements

Two axial xenon transient tests conducted in a PWR with a core height of 12 feet and 121 fuel assemblies are reported in Reference 17, and will be briefly discussed here. The tests were performed at approximately 10% and 50% of cycle life.

Both a free-running oscillation test and a controlled test were performed during the first test. The second test at mid-cycle consisted of a free-running oscillation test only. In each of the free-running oscillation tests, a perturbation was introduced to

the equilibrium power distribution through an impulse motion of the control Bank D and the subsequent oscillation period. In the controlled test conducted early in the cycle, the part length rods were used to follow the oscillations to maintain an axial offset within the prescribed limits. The axial offset of power was obtained from the excore ion chamber readings (which had been calibrated against the incore flux maps) as a function of time for both free-running tests as shown in Figure 4.3-39.

The total core power was maintained constant during these spatial xenon tests, and the stability index and the oscillation period were obtained from a least-square fit of the axial offset data in the form of Equation (4.3-3). The axial offset of power is the quantity that properly represents the axial stability in the sense that it essentially eliminates any contribution from even order harmonics including the fundamental mode. The conclusions of the tests are:

1. The core was stable against induced axial xenon transients both at the core average burnups of 1550 MWd/Mtu and 7700 MWd/Mtu. The measured stability indices are $-0.041\ hr^{-1}$ for the first test (Curve 1 of Figure 4.3-39) and $-0.014\ hr^{-1}$ for the second test (Curve 2 of Figure 4.3-39). The corresponding oscillation periods are 32.4 hrs. and 27.2 hrs, respectively.

2. The reactor core becomes less stable as fuel burnup progresses and the axial stability index was essentially zero at 12,000 MWd/Mtu.

b. Measurements in the X-Y Plane

Two X-Y xenon oscillation tests were performed at a PWR plant with a core height of 12 feet and 157 fuel assemblies. The first test was conducted at a core average burnup of 1540 MWd/Mtu and the second at a core average burnup of 12900 MWd/Mtu. Both of the X-Y xenon tests show that the core was stable in the X-Y plane at both burnups. The second test shows that the core became more stable as the fuel burnup increased and all Westinghouse PWRs with 121 and 157 assemblies are expected to be stable throughout their burnup cycles.

In each of the two X-Y tests, a perturbation was introduced to the equilibrium power distribution through an impulse motion of one rod cluster control unit located along the diagonal axis. Following the

perturbation, the uncontrolled oscillation was monitored using the moveable detector and thermocouple system and the excore power range detectors. The quadrant tilt difference (QTD) is the quantity that properly represents the diametral oscillation in the X-Y plane of the reactor core in that the differences of the quadrant average powers over two symmetrically opposite quadrants essentially eliminates the contribution to the oscillation from the azimuthal mode. The QTD data were fitted in the form of Equation (4.3-3) through a least-square method. A stability index of $-0.076\ hr^{-1}$ with a period of 29.6 hours was obtained from the thermocouple data shown in Figure 4.3-40.

It was observed in the second X-Y xenon test that the PWR core with 157 fuel assemblies had become more stable due to an increased fuel depletion and the stability index was not determined.

4.3.2.7.5 Comparison of Calculations with Measurements

The analysis of the axial xenon transient tests was performed in an axial slab geometry using a flux synthesis technique. The direct simulation of the axial offset data was carried out using the PANDA Code (Reference 18). The analysis of the X-Y xenon transient tests was performed in an X-Y geometry using a modified TURTLE (Reference 10) Code. Both the PANDA and TURTLE codes solve the two-group time-dependent neutron diffusion equation with time-dependent xenon and iodine concentrations. The fuel temperature and moderator density feed back is limited to a steady-state model. All the X-Y calculations were performed in an average enthalpy plane.

The basic nuclear cross-sections used in this study were generated from a unit cell depletion program which has evolved from the codes LEOPARD (Reference 19) and CINDER (Reference 20). The detailed experimental data during the tests including the reactor power level, enthalpy rise, and the impulse motion of the control rod assembly, as well as the plant follow burnup data were closely simulated in the study.

The results of the stability calculation for the axial tests are compared with the experimental data in Table 4.3-4. The calculations show conservative results for both of the axial tests with a margin of approximately $-0.01\ hr^{-1}$ in the stability index.

An analytical simulation of the first X-Y xenon oscillation test shows a calculated stability index of $-0.081\ hr^{-1}$, in good agreement with the measured value of $-0.076\ hr^{-1}$. As indicated earlier, the second X-Y xenon test showed that the core had become more stable compared to the first test and no evaluation of the stability index was attempted. This increase in the core stability in the X-Y plane due to increased fuel burnup is due

mainly to the increased magnitude of the negative moderator temperature coefficient.

Previous studies of the physics of xenon oscillations, including three-dimensional analysis, are reported in the series of topical reports, References 14, 15 and 16. A more detailed description of the experimental results and analysis of the axial and X-Y xenon transient tests is presented in Reference 17 and Section 1 of Reference 21.

4.3.2.7.6 Stability Control and Protection

The excore detector system is utilized to provide indications of xenon-induced spatial oscillations. The readings from the multi-section excore detectors are available to the operator in the form of axial offset, quadrant power tilt, and a detailed relative core average axial power shape which is required input to the automatic control and protection systems.

a. Axial Power Distribution

For maintenance of proper axial power distributions, the operator is instructed to maintain an axial offset within a prescribed operating band, based on the excore detector readings. Should the axial offset be permitted to move far enough outside this band, the protection limit will be reached and the power will be automatically reduced.

Twelve-foot PWR cores become less stable to axial xenon oscillations as fuel burnup progresses. However, free xenon oscillations are not allowed to occur except for special tests. The full length control rod banks present in all modern Westinghouse PWRs are sufficient to dampen and control any axial xenon oscillations present.

Should the axial offset be inadvertently permitted to move far enough outside the control band due to an axial xenon oscillation, or any other reason, the protection limit on axial offset will be reached and the power will be automatically reduced.

b. Radial Power Distribution

The core described herein is calculated to be stable against X-Y xenon induced oscillations at all times in life.

The X-Y stability of large PWRs has been further verified as part of the startup physics test program for PWR cores with 193 fuel assemblies. The measured X-Y stability of the cores with 157 and 193 assemblies was in good agreement with the calculated

stability as discussed in Subsections 4.3.2.7.4 and 4.3.2.7.5. In the unlikely event that X-Y oscillations occur, back-up actions are possible and would be implemented, if necessary, to increase the natural stability of the core. This is based on the fact that several actions could be taken to make the moderator temperature coefficient more negative, which will increase the stability of the core in the X-Y plane.

Provisions for protection against non-symmetric perturbations in the X-Y power distribution that could result from equipment malfunctions are made in the protection system design. This includes control rod drop, rod misalignment and asymmetric loss of coolant flow.

A more detailed discussion of the power distribution control in PWR cores is presented in References 6 and 7.

4.3.2.8 Vessel Irradiation

A brief review of the methods and analyses used in the determination of neutron and gamma ray flux attenuation between the core and the pressure vessel is given below. A more complete discussion on the pressure vessel irradiation and surveillance program is given in Section 5.3.

The materials that serve to attenuate neutrons originating in the core and gamma rays from both the core and structural components consist of the core baffle, core barrel, neutron pads and associated water annuli all of which are within the region between the core and the pressure vessel.

In general, few group neutron diffusion theory and nodal analysis codes are used to determine fission power density distribution within the active core and the accuracy of these analyses is verified by incore measurements on operating reactors. Region and rodwise power sharing information from the core calculations is then used as source information in two-dimensional S_n transport calculations which compute the flux distributions throughout the reactor.

The neutron flux distribution and spectrum in the various structural components varies significantly from the core to the pressure vessel. Representative values of the neutron flux distribution and spectrum are presented in Table 4.3-5. The values listed are based on time averaged equilibrium cycle reactor core parameters and power distributions; and, thus, are suitable for long term net projections and for correlation with radiation damage estimates.

As discussed in Section 5.3, the irradiation surveillance program utilizes actual test samples to verify the accuracy of the calculated fluxes at the vessel.

4.3.3 Analytical Methods

Calculations required in nuclear design consist of three distinct types, which are performed in sequence:

a. Determination of effective fuel temperatures

b. Generation of macroscopic few-group parameters

c. Space-dependent, few-group diffusion calculations

These calculations are carried out by computer codes which can be executed individually. At Westinghouse, however, most of the codes required have been linked to form an automated design sequence which minimizes design time, avoids errors in transcription of data, and standardizes the design methods.

4.3.3.1 Fuel Temperature (Doppler) Calculations

Temperatures vary radially within the fuel rod, depending on the heat generation rate in the pellet, the conductivity of the materials in the pellet, gap, and clad; and the temperature of the coolant.

The fuel temperatures for use in most nuclear design Doppler calculations are obtained from a simplified version of the Westinghouse fuel rod design model described in Subsection 4.2.1.3 which considers the effect of radial variation of pellet conductivity, expansion-coefficient and heat generation rate, elastic deflection of the clad, and a gap conductance which depends on the initial fill gap, the hot open gap dimension, and the fraction of the pellet over which the gap is closed. The fraction of the gap assumed closed represents an empirical adjustment used to produce good agreement with observed reactivity data at beginning-of-life. Further gap closure occurs with burnup and accounts for the decrease in Doppler defect with burnup which has been observed in operating plants. For detailed calculations of the Doppler coefficient, such as for use in xenon stability calculations, a more sophisticated temperature model is used which accounts for the effects of fuel swelling, fission gas release, and plastic clad deformation.

Radial power distributions in the pellet as a function of burnup are obtained from LASER Reference 22 calculations.

The effective U-238 temperature for resonance absorption is obtained from the radial temperature distribution by applying a radially dependent weighting function. The weighting function was determined from REPAD Reference 23 Monte Carlo calculations of resonance escape probabilities in several steady-state and

transient temperature distributions. In each case a flat pellet temperature was determined which produced the same resonance escape probability as the actual distribution. The weighting function was empirically determined from these results.

The effective Pu-240 temperature for resonance absorption is determined by a convolution of the radial distribution of Pu-240 densities from LASER burnup calculations and the radial weighting function. The resulting temperature is burnup dependent, but the difference between U-238 and Pu-240 temperatures, in terms of reactivity effects, is small.

The effective pellet temperature for pellet dimensional change is that value which produces the same outer pellet radius in a virgin pellet as that obtained from the temperature model. The effective clad temperature for dimensional change is its average value.

The temperature calculational model has been validated by plant Doppler defect data as shown in Table 4.3-6 and Doppler coefficient data as shown in Figure 4.3-41. Stability index measurements also provide a sensitive measure of the Doppler coefficient near full power (See Subsection 4.3.2.7). It can be seen that Doppler defect data is typically within 0.2% $\Delta\rho$ of prediction.

4.3.3.2 Macroscopic Group Constants

Macroscopic few-group constants and analogous microscopic cross sections (needed for feedback and microscopic depletion calculations) are generated for fuel cells by the LEOPARD (Reference 19) and CINDER (Reference 20) codes, which are linked internally and provide burnup dependent cross sections. Normally a simplified approximation of the main fuel chains is used; however, where needed, a complete solution for all the significant isotopes in the fuel chains from Th-232 to Cm-244 is available (Reference 24). Fast and thermal cross section library tapes contain microscopic cross sections taken for the most part from the ENDF/B (Reference 25) library, with a few exceptions where other data provided better agreement with critical experiments, isotopic measurements, and plant critical boron values. The effect on the unit fuel cell of non-lattice components in the fuel assembly is obtained by supplying an appropriate volume fraction of these materials in an extra region which is homogenized with the unit cell in the fast (MUFT) and thermal (SOFOCATE) flux calculations. In the thermal calculation, the fuel rod, clad, and moderator are homogenized by energy-dependent disadvantage factors derived from an analytical fit to integral transport theory results.

Group constants for burnable absorber cells, guide thimbles, instrument thimbles and interassembly gaps are generated in a manner analogous to the fuel cell calculation. Reflector group constants are taken from infinite medium LEOPARD calculations.

Baffle group constants are calculated from an average of core and radial reflector microscopic group constants for stainless steel.

Group constants for control rods are calculated in a linked version of the HAMMER (Reference 26) and AIM (Reference 27) codes. The Doppler broadened cross sections of the control rod materials are represented as smooth cross sections in the 54 group LEOPARD fast group structure and in 30 thermal groups. The four group constants in the rod cell and appropriate extra region are generated in the coupled space-energy transport HAMMER calculation. A corresponding AIM calculation of the homogenized rod cell with extra region is used to adjust the absorption cross sections of the rod cell to match the reaction rates in HAMMER. These transport-equivalent group constants are reduced to two-group constants for use in space-dependent diffusion calculations. In discrete X-Y calculations only one mesh interval per cell is used, and the rod group constants are further adjusted for use in this standard mesh by reaction rate matching the standard mesh unit assembly to a fine-mesh unit assembly calculation.

Nodal group constants are obtained by a flux-volume homogenization of the fuel cells, burnable poison cells, guide thimbles, instrumentation thimbles, interassembly gap, and control rod cells from one mesh interval per cell X-Y unit fuel assembly diffusion calculations.

Validation of the cross section method is based on analysis of critical experiments as shown in Table 4.3-3, isotopic data as shown in Table 4.3-7, plant critical boron (CB) values at HZP, BOL, as shown in Table 4.3-8 and at HFP as a function of burnup as shown in Figures 4.3-42 through 4.3-44. Control rod worth measurements shown in Table 4.3-9. Confirmatory critical experiments on burnable absorbers are described in Reference 28.

4.3.3.3 Spatial Few-Group Diffusion Calculations

Spatial few-group calculations consist primarily of two-group diffusion X-Y calculations using an updated version of the TURTLE Code, and two-group X-Y nodal calculations using PALADON (Reference 38), and two-group axial calculations using an updated version of the PANDA Code.

Discrete X-Y calculations (1 mesh per cell) are carried out to determine critical boron concentrations and power distributions in the X-Y plane. An axial average in the X-Y plane is obtained by synthesis from unrodded and rodded planes. Axial effects in unrodded depletion calculations are accounted for by the axial buckling, which varies with burnup and is determined by radial depletion calculations which are matched in reactivity to the analogous R-Z depletion calculation. The moderator coefficient is evaluated by varying the inlet temperature in the same X-Y calculations used for power distribution and reactivity predictions.

Validation of TURTLE reactivity calculations is associated with the validation of the group constants themselves, as discussed in Subsection 4.3.3.2. Validation of the Doppler calculations is associated with the fuel temperature validation discussed in Subsection 4.3.3.1. Validation of the moderator coefficient calculations is obtained by comparison with plant measurements at hot zero power conditions as shown in Table 4.3-10.

PALADON is used in two-dimensional and three-dimensional calculations. PALADON can be used in safety analysis calculations, critical boron concentrations, control rod worths, reactivity coefficients, etc.

Axial calculations are used to determine differential control rod worth curves (reactivity versus rod insertion) and axial power shapes during steady state and transient xenon conditions (flyspeck curve). Group constants and the radial buckling used in the axial calculation are obtained from the three dimensional TURTLE calculation from which group constants are homogenized by flux-volume weighting.

Validation of the spatial codes for calculating power distributions involves the use of incore and excore detectors and is discussed in Subsection 4.3.2.2.7.

Based on comparison with measured data it is estimated that the accuracy of current analytical methods is:

± 0.2% $\Delta\rho$ for Doppler defect
± 2 x 10^{-5} $\Delta\rho$/°F for moderator coefficient
± 50 ppm for critical boron concentration with depletion
± 3% for power distributions
± 0.2% $\Delta\rho$ for rod bank worth
± 4 pcm/step for differential rod worth
± 0.5 pcm/ppm for boron worth
± 0.1% $\Delta\rho$ for moderator defect

4.3.4 Changes

The design methods for the criticality of fuel assemblies outside the reactor now uses the AMPX/KENO ORNL system of codes as described in Section 4.3.2.6.

The design methods now use upgraded versions of the computer codes for the multi-dimensional analysis.

Three principal computer codes are used in the nuclear design: PHOENIX-P (two-dimensional), APOLLO (one-dimensional), and ANC (two-dimensional and three-dimensional). Descriptions and uses for these codes are given below.

APOLLO, an advanced version of PANDA (Reference 18), is a two-group, onedimensional diffusion-depletion code. APOLLO utilizes the burnup-dependent macroscopic cross-sections generated by PHOENIX-P. Thermal feedback is included in the calculations. The APOLLO model is used as an axial model. APOLLO is utilized to determine axial power and burnup distributions, differential rod worths, and control rod operational limits (insertion limits and return-to-power limits), etc.

ANC (Reference 44) is an advanced nodal analysis theory code capable of two-dimensional and three-dimensional calculations. In this design, ANC is employed as the reference model for all safety analysis calculations, critical boron concentrations, control rod worths, reactivity coefficients, etc. In addition, 3D ANC is used to validate one and two-dimensional results and to provide information about radial (x-y) peaking factors as a function of axial position. It has the capability of calculating discrete pin powers from the nodal information as well.

PHOENIX-P (Reference 45) is a two-dimensional multigroup transport code for lattice physics calculations for all reactivity calculations, depletion rates, and reactivity feedback models. The 70-group nuclear cross-section library in PHOENIX-P is derived from ENDF/B-VI (Reference 46) files.

BEACON (Reference 48) provides both a, full three-dimensional nodal power distribution calculation as well as a simplified more approximate one-dimensional calculation. The BEACON online limits evaluation is performed in three dimensions and the one-dimensional calculation will only be used as a scoping tool in predictive analysis. The BEACON nuclear/thermal-hydraulic data sets and models are determined using the Westinghouse reload design codes and methods. In addition, before BEACON is used for core monitoring, the BEACON model and reference uncertainties are validated during prior cycle operation. The on-line DNBR and limits evaluation is performed with the NRC approved DNBR methodologies.

Hafnium can be used as an alternative to Ag-In-Cd in rod control cluster assemblies. Nuclear calculations show that hafnium and Ag-In-Cd worths differ by less than 1%. Consequently, the rodded data provided in the Tables and Figures of Section 4.3 are applicable regardless of whether Ag-In-Cd or hafnium is used.

4.3.5 References

1. "Westinghouse Anticipated Transients Without Reactor Trip Analysis," WCAP-8330, August, 1974.

2. Langford, F. L., and Nath, R. J., "Evaluation of Nuclear Hot Channel Factor Uncertainties," WCAP-7308-L (Proprietary) and WCAP-7810, December 1971, and WCAP-7308-L-P-A, June 1988.

3. McFarlane, A. F., "Core Power Capability in Westinghouse PWRs," WCAP-7267-L (Proprietary), October, 1969 and WCAP-7809, December, 1971.

4. Hellman, J. M., (Ed), "Fuel Densification Experimental Results and Model for Reactor Application," WCAP-8218-P-A (Proprietary) and WCAP-8219-A, March, 1975.

5. Hellman, J. M., and Yang, J. W., "Effects of Fuel Densification Power Spikes on Clad Thermal Transients," WCAP-8359, July, 1974.

6. Moore, J. S., "Power Distribution Control of Westinghouse Pressurized Water Reactors," WCAP-7208 (Proprietary), September, 1968 and WCAP-7811, December, 1971.

7. Morita, T., et al., "Topical Report, Power Distribution Control and Load Following Procedures," WCAP-8385 (Proprietary) and WCAP-8403, September, 1974.

8. Meyer, C. E., and Stover, R. L., "Incore Power Distribution Determination in Westinghouse Pressurized Water Reactors," WCAP-8498, July, 1975.

9. McFarlane, A. F., "Power Peaking Factors," WCAP-7912-P-A (Proprietary) and WCAP-7912-A, January, 1975.

10. Altomare, S., and Barry, R. F., "The TURTLE 24.0 Diffusion Depletion Code," WCAP-7213-P-A (Proprietary) and WCAP-7758-A, January, 1975.

11. Cermak, J. O., et al., "Pressurized Water Reactor pH - Reactivity Effect Final Report," WCAP-3696-8 (EURAEC-2074), October, 1968.

12. Strawbridge, L. E. and Barry, R. F., "Criticality Calculation for Uniform Water-Moderated Lattices," Nucl. Sci. and Eng. 23, 58-73 (1965).

13. Dominick, I. E. and Orr, W. L., "Experimental Verification of Wet Fuel Storage Criticality Analyses," WCAP-8682 (Proprietary) and WCAP-8683, December, 1975.

14. Poncelet, C. G. and Christie, A. M., "Xenon-Induced Spatial Instabilities in Large PWRs," WCAP-3680-20, (EURAEC-1974) March, 1968.

15. Skogen, F. B. and McFarlane, A. F., "Control Procedures for Xenon Induced X-Y Instabilities in Large PWRs," WCAP-3680-21, (EURAEC2111), February, 1969.

16. Skogen, F. B. and McFarlane, A. F., "Xenon-Induced Spatial Instabilities in Three-Dimensions," WCAP-3680-22 (EURAEC-2116), September, 1969.

17. Lee, J. C., et al., "Axial Xenon Transient Tests at the Rochester Gas and Electric Reactor," WCAP-7964, June, 1971.

18. Yarbrough, M. B., et al., "APOLLO-A One Dimensional Neutron Theory Program," WCAP-13524, Revision 1, August 1994.

19. R. F. Barry, "The Revised LEOPARD Code - A Spectrum Dependent Non-Spatial Depletion Program," WCAP-2759, Revision 0, March 1965 (Westinghouse Proprietary).

20. England, T. R., "CINDER - A One-Point Depletion and Fission Product Program," WAPD-TM-334, Revision 0, August 1962.

21. Eggleston, F. T., "Safety-Related Research and Development for Westinghouse Pressurized Water Reactors, Program Summaries, Spring 1976," WCAP-8768, June, 1976.

22. Poncelet, C. G., "LASER - A Depletion Program for Lattice Calculations Based on MUFT and THERMOS," WCAP-6073, April, 1966.

23. Olhoeft, J. E., "The Doppler Effect for a Non-Uniform Temperature Distribution in Reactor Fuel Elements," WCAP-2048, July, 1962.

24. Nodvik, R. J., et al., "Supplementary Report on Evaluation of Mass Spectrometric and Radiochemical Analyses of Yankee Core I Spent Fuel, Including Isotopes of Elements Thorium Through Curium," WCAP-6086, August, 1969.

25. Drake, M. K. (Ed), "Data Formats and Procedure for the ENDF/B Neutron Cross Section Library," BNL-50274, ENDF-102, Vol. 1, 1970.

26. Suich, J. E. and Honeck, H. C., "The HAMMER System, Heterogeneous Analysis by Multigroup Methods of Exponentials and Reactors," DP-1064, January, 1967.

27. Flatt, H. P. and Buller, D. C., "AIM-5, A Multigroup, One Dimensional Diffusion Equation Code," NAA-SR-4694, March, 1960.

28. Moore, J. S., "Nuclear Design of Westinghouse Pressurized Water Reactors with Burnable Poison Rods," WCAP-9000-L, Revision 1 (Proprietary), July, 1969 and WCAP-7806, December, 1971.

29. Nodvik, R. J., "Saxton Core II Fuel Performance Evaluation," WCAP-3385-56, Part II, "Evaluation of Mass Spectrometric and Radiochemical Analyses of Irradiated Saxton Plutonium Fuel," July, 1970.

30. Leamer, R. D., et al., "PUO_2-UO_2 Fueled Critical Experiments," WCAP-3726-1, July, 1967.

31. Not used.

32. Ford III, W. E., CSRL-V: Processed ENDIFB-V 227-Neutron-Group and Pointwise Cross-Section Libraries for Criticality Safety, Reactor and Shielding Studies. ORNL/CSD/TM-160, June 1982.

33. Greene, N. M., et al., "AMPX: A Modular Code System for Generating Coupled Multigroup Neutron-Gamma Libraries from ENDF/B," ORNL/TM-3706 (March 1976).

34. Petrie, L. M., and Lander, N. F., "KENO Va--An Improved Monte Carlo Criticality Program with Supergrouping," NUREG/CR-0200, Vol. 2, Section F-11 (Nov. 1993).

35. Baldwin, M. N., Critical Experiments Supporting Close Proximity Water Storage of Power Reactor Fuel, BAW-1484-7, July 1979.

36. Not used.

37. Thomas, J. T., "Critical Three-Dimensional Arrays of U (93.2) -- Metal Cylinders," Nuclear Science and Engineering, Vol. 52, pp 350-359 (1973).

38. Camden, T. M., et. al., "PALADON - Westinghouse Nodal Computer Code," WCAP-9485 (Proprietary) and WCAP-9486 (December 1978).

39. "Augmented Startup and Cycle 1 Physics Program Supplement 1," WCAP-8575 Supplement 1, June 1976 (Westinghouse Proprietary) and WCAP-8576, June 1976 (Nonproprietary).

40. Davidson, S. L.,and Iorii, J. A., "Reference Core Report - 17x17 Optimized Fuel Assembly," WCAP-9500-A, May 1982.

41. Davidson, S. L., and Kramer, W. R. (Eds.), "Reference Core Report VANTAGE 5 Fuel Assembly," WCAP-10444-P-A, September 1985.

42. Bohl, H., Jr., et al., "MUFT-4--Fast Neutron Spectrum Code for the IBM-704," WAPD-TM-72, July 1957.

43. Amster, H., and Suarez, R., "The Calculation of Thermal Constants Averaged Over a Wigner-Wilkins Flux Spectrum/Description of the SOFOCATE Code," WAPD-TM-39, January 1957.

44. Liu, Y. S., et al., "ANC-A Westinghouse Advanced Nodal Computer Code," WCAP-10965-P-A, December 1985 (Westinghouse Proprietary).

45. Nguyen, T. Q., et al., "Qualification of the PHOENIX-P/ANC Nuclear Design System for Pressurized Water Reactor Cores," WCAP-11596-P-A, June, 1988. (Westinghouse Proprietary).

46. Rose, P.F., "ENDF-201 ENDF/B-VI Summary Documentation," BNL-NCB-17541 [ENDF-201] 4th Edition [ENDF-B-VI], October 1999 and Supplements.

47. WCAP-14416-NP-A, "Westinghouse Spent Fuel Rack Criticality Analysis Methodology," Revision 1, November 1996.

48. Beard, C. L., et.al., "BEACON – Core Monitoring and Operations Support System," WCAP-12472-P-A (Proprietary), August 1994.

49. Miller, R.W., et.al., "Relaxation of Constant Axial Offset Control, F_Q Surveillance Technical Specification," WCAP-10216-P-A (Westinghouse Proprietary), February 1994.

50 Morita, T., et. al., "BEACON Core Monitoring and Operations Support System (WCAP-12472-P-A) Addendum 1, "WCAP-12472-P-A Addendum 1A (Westinghouse Proprietary), January 2000.

51. Sidener, S., et. al., "Safety Analysis for Revised Fuel Rod Internal Pressure Design Basis (Departure from Nucleate Boiling Mechanistic Propagation Methodology," WCAP-8963-P-A Addendum 1-A (Westinghouse Propriety), Revision 1-A, June 2006.

52. Slagle, W. H., "Westinghouse Fuel Assembly Reconstitution Evaluation Methodology," WCAP-13060-P-A, July 1993.

TABLE 4.3-1

NUCLEAR DESIGN
KEY SAFETY PARAMETERS

SAFETY PARAMETER	VANTAGE 5
Reactor Core Power (MWt)	3648
Core Average Coolant Temperature FP (°F)	579.5 - 592.8
Coolant System Pressure (psia)	2250
Core Average Linear Heat Rate (kW/ft)	5.82
Most Positive MTC (pcm/°F)**	+7.0 to 0.00
Most Positive MDC(Δk/g/cc)	0.54
Doppler Temperature Coefficient (pcm/°F)	-.91 to -2.9
Doppler Power Coefficient (pcm/% Power) Least Negative	-9.55 to -6.05
Doppler Power Coefficient (pcm/% Power) Most Negative	-19.4 to -12.6
Beta-Effective	.0044 - .0075
Boron Worth (pcm/ppm)	-5 to -16
Shutdown Margin (%delta-rho)	1.3
Nuclear Design $F^N_{\Delta H}$	1.574*
Total Heat Flux Hot Channel Factor, F_Q	2.60

* For VANTAGE 5/VANTAGE+, the values in Subsection 4.3.2.2.6 include the 1.08 uncertainty allowance.

**Control rod withdrawal limits may be required to preclude an MTC more positive than the Technical Specifications limit.

Note: 1 pcm = (% mille rho) = 10^{-5} $\Delta\rho$ where $\Delta\rho$ is calculated from two statepoint values of K_{eff} by ℓn (k1/k2)

TABLE 4.3-1 (Cont'd)

Boron Concentrations (ppm)	Original Negative MTC Design	Positive MTC Design
Zero Power, k_{eff} = 1.00, Cold, Rod Cluster Control Assemblies Out	1258	1890
Design Basis Refueling Boron Concentration	2000	2300
Zero Power, k_{eff} < 0.95, Cold, Rod Cluster Control Assemblies In, 100 ppm allowance included	1351	2011
Zero Power, No Xenon, k_{eff} = 1.00, Hot, Rod Cluster Control Assemblies Out	1259	2056
Full Power, No Xenon, k_{eff} = 1.0, Hot, Rod Cluster Control Assemblies Out	1128	1923
Full Power, Equilibrium Xenon, k_{eff} = 1.0, Hot, Rod Cluster Control Assemblies Out	833	1590
Reduction with Fuel Burnup		
Reload Cycle, ppm/GWd/Mtu***	See Figure 4.3-3	

***Gigawatt, Day (GWd) = 1000 Megawatt Day (1000 MWd). Burnable absorber rods may reduce the boron depletion rate.

TABLE 4.3-2

REACTIVITY REQUIREMENTS FOR ROD CLUSTER CONTROL ASSEMBLIES

		TYPICAL END OF LIFE (EQUILIBRIUM CYCLE)
	REACTIVITY EFFECTS	
1.	Control requirements	
	Fuel temperature (Doppler), %Δρ	0.94
	Moderator temperature, %Δρ	0.75
	Void, %Δρ	0.05
	Redistribution, %Δρ0.90	
	Rod Insertion Allowance, %Δρ	0.50
2.	Total Control Requirements, %Δρ	3.14
3.	Estimated Ag-In-Cd or Hafnium Rod Cluster Control Assembly Worth (53 Rods)	
	a. All full length assemblies inserted, %Δρ	6.50
	b. All but one (highest worth) assemblies inserted, %Δρ	5.57
4.	Estimated Rod Cluster Control Assembly credit with 7 percent adjustment to accommodate uncertainties (3b - 7 percent), %Δρ	5.18
5.	Shutdown margin available (4-2), %Δρ	2.04*

*The design basis minimum shutdown margin is 1.3 %Δρ.

TABLE 4.3-3

BENCHMARK CRITICAL EXPERIMENTS[35, 37]

	GENERAL DESCRIPTION	ENRICHMENT W/O U235	REFLECTOR	SEPARATING MATERIAL	SOLUBLE BORON (ppm)
1.	UO_2 rod lattice	2.46	water	water	0
2.	UO_2 rod lattice	2.46	water	water	1037
3.	UO_2 rod lattice	2.46	water	water	764
4.	UO_2 rod lattice	2.46	water	B4C pins	0
5.	UO_2 rod lattice	2.46	water	B4C pins	0
6.	UO_2 rod lattice	2.46	water	B4C pins	0
7.	UO_2 rod lattice	2.46	water	B4C pins	0
8.	UO_2 rod lattice	2.46	water	B4C pins	0
9.	UO_2 rod lattice	2.46	water	water	0
10.	UO_2 rod lattice	2.46	water	water	143
11.	UO_2 rod lattice	2.46	water	stainless steel	514
12.	UO_2 rod lattice	2.46	water	stainless steel	217
13.	UO_2 rod lattice	2.46	water	borated aluminum	15
14.	UO_2 rod lattice	2.46	water	borated aluminum	92
15.	UO_2 rod lattice	2.46	water	borated aluminum	395
16.	UO_2 rod lattice	2.46	water	borated aluminum	121
17.	UO_2 rod lattice	2.46	water	borated aluminum	487
18.	UO_2 rod lattice	2.46	water	borated aluminum	197
19.	UO_2 rod lattice	2.46	water	borated aluminum	634
20.	UO_2 rod lattice	2.46	water	borated aluminum	320
21.	UO_2 rod lattice	2.46	water	borated aluminum	72
22.	U metal cylinders	93.2	bare	air	0
23.	U metal cylinders	93.2	bare	air	0
24.	U metal cylinders	93.2	bare	air	0
25.	U metal cylinders	93.2	bare	air	0
26.	U metal cylinders	93.2	bare	air	0
27.	U metal cylinders	93.2	bare	air	0
28.	U metal cylinders	93.2	bare	plexiglass	0
29.	U metal cylinders	93.2	paraffin	plexiglass	0
30.	U metal cylinders	93.2	bare	plexiglass	0
31.	U metal cylinders	93.2	paraffin	plexiglass	0
32.	U metal cylinders	93.2	paraffin	plexiglass	0
33.	U metal cylinders	93.2	paraffin	plexiglass	0

TABLE 4.3-4

AXIAL STABILITY INDEX PRESSURIZED WATER REACTOR CORE WITH A 12-FOOT HEIGHT

BURNUP (MWd/Mtu)	F_Z	C_B (ppm)	STABILITY INDEX (hr^{-1}) Exp	Calc
1550	1.34	1065	-0.041	-0.032
7700	1.27	700	-0.014	-0.006
		Difference:	+0.027	+0.026

TABLE 4.3-5

TYPICAL NEUTRON FLUX LEVELS (n/cm^2 -sec) AT FULL POWER

	E > 1.0 Mev	5.53 Kev < E ≤ 1.0 Mev	.625 ev ≤ E < 5.53 Kev	E < .625 ev $(nv)_0$
Core Center	6.51×10^{13}	1.12×10^{14}	8.50×10^{13}	3.00×10^{13}
Core Outer Radius at Midheight	3.23×10^{13}	5.74×10^{13}	4.63×10^{13}	8.60×10^{12}
Core Top, on Axis	1.53×10^{13}	2.42×10^{13}	2.10×10^{13}	1.63×10^{13}
Core Bottom, on Axis	2.36×10^{13}	3.94×10^{13}	3.50×10^{13}	1.46×10^{13}
Pressure Vessel Inner Wall, Azimuthal Peak, Core Midheight	2.77×10^{10}	5.75×10^{10}	6.03×10^{10}	8.38×10^{10}

TABLE 4.3-6

COMPARISON OF MEASURED AND CALCULATED DOPPLER DEFECTS

PLANT	FUEL TYPE	CORE BURNUP (MWd/Mtu)	MEASURED (pcm)	CALCULATED (pcm)
1	Air-filled	1800	1700	1710
2	Air-filled	7700	1300	1440
3	Air and helium-filled	8460	1200	1210

TABLE 4.3-7

SAXTON CORE II ISOTOPICS

ROD MY, AXIAL ZONE 6

ATOM RATIO	MEASURED*	2σ PRECISION (%)	LEOPARD CALCULATION
U-234/U	4.65×10^{-5}	±29	4.60×10^{-5}
U-235/U	5.74×10^{-3}	±0.9	5.73×10^{-3}
U-236/U	3.55×10^{-4}	±5.6	3.74×10^{-4}
U-238/U	0.99386	±0.01	0.99385
Pu-238/Pu	1.32×10^{-3}	±2.3	1.222×10^{-3}
Pu-239/Pu	0.73971	±0.03	0.74497
Pu-240/Pu	0.19302	±0.2	0.19102
Pu-241/Pu	6.014×10^{-2}	±0.3	5.74×10^{-2}
Pu-242/Pu	5.81×10^{-3}	±0.9	5.38×10^{-3}
Pu/U**	5.938×10^{-2}	±0.7	5.970×10^{-2}
Np-237/U-238	1.14×10^{-4}	±15	0.86×10^{-4}
Am-241/Pu-239	1.23×10^{-2}	±15	1.08×10^{-2}
Cm-242/Pu-239	1.05×10^{-4}	±10	1.11×10^{-4}
Cm-244/Pu-239	1.09×10^{-4}	±20	0.98×10^{-4}

*Reported in Reference 29
**Weight ratio

TABLE 4.3-8

CRITICAL BORON CONCENTRATIONS, (ppm) HZP, BOL

PLANT TYPE	MEASURED	CALCULATED
2-Loop, 121 Assemblies 10 foot core	1583	1589
2-Loop, 121 Assemblies 12 foot core	1625	1624
2-Loop, 121 Assemblies 12 foot core	1517	1517
3-Loop, 157 Assemblies 12 foot core	1169	1161
3-Loop, 157 Assemblies 12 foot core	1344	1319
4-Loop, 193 Assemblies 12 foot core	1370	1355
4 Loop, 193 Assemblies 12 foot core	1321	1306

TABLE 4.3-9

BENCHMARK CRITICAL EXPERIMENTS

B_4C CONTROL ROD WORTH

WREC CRITICAL EXPERIMENT	NO. OF FUEL RODS	NO. OF CONTROL RODS (in.)	MEASURED(a) WORTH, %Δρ	CALCULATED WORTH, %Δρ
2A	888	12 .395 OD B_4C	8.20	8.37
3B	888	12 .232 OD B_4C	4.81	4.82
4B	884	16 .232 OD B_4C	6.57	6.35
5B	945	16 .232 OD B_4C	5.98	5.83

(a) The measured worth was derived from the calculated value of ln (k_1/k_2), where k_1 and k_2 were calculated with the measured buckling before and after insertion of the control rods, which replace fuel rods in arrays at the center of the experiment. The standard deviation in the measured worth is about 0.3% Δρ based on the uncertainties in the measured axial bucklings.

AG-IN-CD COMPARISON OF MEASURED AND CALCULATED ROD WORTH

4-LOOP PLANT, 193 ASSEMBLIES, 12-FOOT CORE	MEASURED (pcm)	CALCULATED (pcm)
Bank D	1403	1366
Bank C	1196	1154
All Rods In Less One	6437	6460
ESADA Critical*, 0.69 Inch Pitch, 2 w/o PuO_2, 8% Pu^{240} 9 Control Rods		
6.21 inch rod separation	2250	2250
2.07 inch rod separation	4220	4160
1.38 inch rod separation	4100	4019

*Reported in Reference 30.

TABLE 4.3-9 (Cont'd)

BENCHMARK CRITICAL EXPERIMENT
HAFNIUM CONTROL ROD WORTH

CONTROL ROD CONFIGURATION	NO. OF FUEL RODS	MEASURED (b) WORTH (ΔPPM B-10)	CALCULATED (b) WORTH (ΔPPM B-10)
9 Hafnium Rods, 0.341" OD	1192	138.3	141.0

(b) Calculated and measured worths are given in terms of an equivalent change in B-10 concentration.

TABLE 4.3-10

COMPARISON OF MEASURED AND CALCULATED MODERATOR COEFFICIENTS AT HZP, BOL

PLANT TYPE/ CONTROL BANK CONFIGURATION	MEASURED α_{iso}* (pcm/°F)	CALCULATED α_{iso} (pcm/°F)
2-loop, 121 assemblies,		
12 foot core		
D at 180 steps	+0.85	+1.02
D in, C at 180 steps	-2.40	-1.90
C and D in, B at 165 steps	-4.40	-5.58
B, C, and D in A at 174 steps	-8.70	-8.12
3-loop, 157 assemblies,		
12 foot core		
D at 160 steps	-0.50	-0.50
D in, C at 190 steps	-3.01	-2.75
D in, C at 28 steps	-7.67	-7.02
B, C and D in	-5.16	-4.45
4-loop, 193 assemblies,		
12 foot core		
ARO	-0.52	-1.2
D in	-4.35	-5.7
D + C in	-8.59	-10.0
D + C + B in	-10.14	-10.55
D + C + B + A in	-14.63	-14.45

*Isothermal coefficients, which include the Doppler effect in the fuel.

$$\alpha_{iso} = 10^5 \ln \frac{(k_2)}{k_1} / \Delta T°F$$

4.4 THERMAL AND HYDRAULIC DESIGN

4.4.1 Design Basis

The overall objective of the thermal and hydraulic design of the reactor core is to provide adequate heat transfer which is compatible with the heat generation distribution in the core such that heat removal by the reactor coolant system (RCS) or the emergency core cooling system (ECCS) (when applicable) assures that the following performance and safety criteria requirements are met:

a. Fuel damage (defined as penetration of the fission product barrier, i.e., the fuel rod cladding) is not expected during normal operation and operational transients (Condition I) or any transient conditions arising from faults of moderate frequency (Condition II). It is not possible, however, to preclude a very small number of rod failures. These will be within the capability of the plant cleanup system and are consistent with the plant design bases.

b. The reactor can be brought to a safe state following a Condition III event with only a small fraction of fuel rods damaged (see above definition) although sufficient fuel damage might occur to preclude immediate resumption of operation.

c. The reactor can be brought to a safe state and the core can be kept subcritical with acceptable heat transfer geometry following transients arising from Condition IV events.

In order to satisfy the above requirements, the following design bases have been established for the thermal and hydraulic design of the reactor core.

4.4.1.1 Departure from Nucleate Boiling Design Basis

Basis

There will be at least a 95% probability that departure from nucleate boiling (DNB) will not occur on the limiting fuel rods during normal operation and operational transients and any transient conditions arising from faults of moderate frequency (Condition I and II events) at 95% confidence level.

Discussion

The design method employed to meet the DNB design basis for the VANTAGE 5/VANTAGE+ fuel assemblies is the revised thermal design procedure (RTDP) (Reference 89). With the RTDP methodology, uncertainties in plant operating parameters, nuclear and thermal parameters, fuel fabrication parameters, computer codes and DNB correlation predications are considered statistically to obtain DNB uncertainty factors. Based on the DNB uncertainty factors, RTDP design limit departure from nucleate boiling ratio (DNBR) values are determined such that there is at least a 95 percent probability at a 95% confidence level that DNB will not occur on the most limiting fuel rod during normal operation and operational transients and during transient conditions arising from faults of moderate frequency (Condition I and II events). Since the parameter uncertainties are considered in determining the RTDP design limit DNBR values, the plant safety analyses are performed using input parameters at their nominal values.

The RTDP design limit DNBR values for the WRB-2 correlation are 1.25 (typical cell) and 1.24 (thimble cell) in the mixing vane region of the VANTAGE 5/VANTAGE+ fuel. The RTDP design limit DNBR value for the ABB-NV correlation is 1.19 for the typical and thimble cells below the mixing vane region of the VANTAGE 5/ VANTAGE+ fuel.

The design limit DNBR values are used as a basis for the Technical Specifications and for consideration of the applicability for a regulatory review, as defined in 10 CFR 50.59.

To maintain DNBR margin to offset DNB penalties, such as those due to fuel rod bow, safety analyses were performed to DNBR limits higher than the design limit DNBR values. The difference between the design limit DNBRs and the safety analysis limit DNBRs results in available DNBR margin. The net DNBR margin, after consideration of all penalties, is available for operating and design flexibility.

The standard thermal design procedure (STDP) is used for those analyses where RTDP is not applicable. In the STDP method, the parameters used in the analysis are treated in a conservative way from a DNBR standpoint. The parameter uncertainties are applied directly to the plant safety analyses input values to give the lowest minimum DNBR. The DNBR limit for STDP is the appropriate DNB correlation limit increased by sufficient margin to offset the applicable DNBR penalties.

By preventing DNB, adequate heat transfer is ensured between the fuel cladding and the reactor coolant, thereby preventing cladding damage as a result of inadequate cooling. Maximum fuel rod surface temperature is not a design basis, since it will be within a few degrees of coolant temperature during operation in the nucleate boiling region. Limits provided by the nuclear control and protection systems are such that this design basis will be met for transients associated with Condition II events including overpower transients. There is an additional large DNBR margin at rated power operation and during normal operating transients.

This page was intentionally deleted.

4.4.1.2 Fuel Temperature Design Basis

Basis

During modes of operation associated with Condition I and Condition II events, there is at least a 95% probability at the 95% confidence level that the peak kW/ft fuel rods will not exceed the UO_2 melting temperature. The melting temperature of UO_2 is taken as 5080°F (Reference 4), unirradiated and decreasing 58°F per 10,000 MWD/MTU. By precluding UO_2 melting, the fuel geometry is preserved and possible adverse effects of molten UO_2 on the cladding are eliminated. To preclude center melting and as a basis for overpower protection system setpoints, a calculated centerline fuel temperature of 4700°F has been selected as the overpower limit. This provides sufficient margin for uncertainties in the thermal evaluations as described in Subsection 4.4.2.9.1.

Discussion

Fuel rod thermal evaluations are performed at rated power, maximum overpower and during transients at various burnups. These analyses assure that this design basis as well as the fuel integrity design bases given in Section 4.2 are met. They also provide input for the evaluation of Condition III and IV events given in Chapter 15.0.

4.4.1.3 Core Flow Design Basis

Basis

A minimum of 91.7% of the thermal flow rate will pass through the fuel rod region of the core and be effective for fuel rod cooling. Coolant flow through the thimble tubes as well as the leakage from the core barrel-baffle region into the core are not considered effective for heat removal.

Discussion

Core cooling evaluations are based on the thermal flow rate (minimum flow) entering the reactor vessel. A maximum 8.3% of this value is allotted as bypass flow. This includes rod cluster control guide thimble cooling flow, head cooling flow, baffle leakage, and leakage to the vessel outlet nozzle. Also, the removal of all thimble plugs from the core can be accommodated with this flow basis.

4.4.1.4 Hydrodynamic Stability Design Basis

Basis

Modes of operation associated with Condition I and II events shall not lead to hydrodynamic instability.

4.4.1.5 Other Considerations

The above design bases together with the fuel cladding and fuel assembly design bases given in Subsection 4.2.1 are sufficiently comprehensive so additional limits are not required.

Fuel rod diametral gap characteristics, moderator-coolant flow velocity and distribution, and moderator void are not inherently limiting. Each of these parameters is incorporated into the thermal and hydraulic models used to ensure the above mentioned design criteria are met. For instance, the fuel rod diametral gap characteristics change with time (see Subsection 4.2.3.3) and the fuel rod integrity is evaluated on that basis. The effect of the moderator flow velocity and distribution (see Subsection 4.4.2.2) and moderator void distribution (see Subsection 4.4.2.4) are included in the core thermal evaluation and, thus, affect the design bases.

Meeting the fuel cladding integrity criteria covers possible effects of cladding temperature limitations. As noted in Subsection 4.2.3.3, the fuel rod conditions change with time. A single cladding temperature limit for Condition I or Condition II events is not appropriate since of necessity it would be overly conservative. A cladding temperature limit is applied to the loss-of-coolant accident (Subsection 15.6.5), control rod ejection accident, and locked rotor accident.

4.4.2 Description

4.4.2.1 Summary Comparison

Table 4.4-1 provides design parameters for 17x17 VANTAGE 5/VANTAGE+ fuel.

4.4.2.2 Critical Heat Flux Ratio or Departure from Nucleate Boiling Ratio and Mixing Technology

The minimum DNBRs for the rated power, design overpower, and anticipated transient conditions are given in Table 4.4-1. The minimum DNBR in the limiting flow channel will be downstream of the peak heat flux location (hot spot) due to the increased downstream enthalpy rise.

DNBRs are calculated by using the correlation and definitions described in the following Subsections 4.4.2.2.1 and 4.4.2.2.2. The VIPRE-01 computer code (discussed in Subsection 4.4.4.5 is used to determine the flow distribution in the core and the local conditions in the hot channel for use in the DNB correlation. The use of hot channel factors is discussed in Subsection 4.4.4.3.1 (nuclear enthalpy rise hot channel factor) and in Subsection 4.4.2.2.4 (hot channel factors).

4.4.2.2.1 Departure from Nucleate Boiling Technology

The W-3 correlation, and several modifications of it, were previously used in Westinghouse critical heat flux (CHF) calculations. The W-3 correlation was originally developed from single tube data, (Reference 6) but was subsequently modified to apply to the 0.422 inch O.D. rod R-grid, (Reference 7) and L-grid, (Reference 8) as well as the 0.374 inch O.D., (References 9,10) rod bundle data. These modifications to the W-3 correlation were demonstrated to be adequate for reactor rod bundle design.

The WRB-1 (Reference 1) correlation was developed based exclusively on the large bank of mixing vane grid rod bundle CHF data

(over 1100 points) that Westinghouse has collected. The WRB-1 correlation, based on local fluid conditions, represents the rod bundle data with better accuracy over a wide range of variables than the previous correlation used in design. This correlation accounts directly for both typical and thimble cold wall cell effects, uniform and nonuniform heat flux profiles, and variations in rod heated length and in grid spacing.

The applicable range of parameters for the WRB-1 correlation is:

Pressure	:	$1440 \leq P \leq 2490$ psia
Local Mass Velocity	:	$0.9 \leq G_{loc}/10^6 \leq 3.7$ lb/ft^2-hr
Local Quality	:	$-0.2 \leq X_{loc} \leq 0.3$
Heated Length, Inlet to CHF Location	:	$L_h \leq 14$ feet
Grid Spacing	:	$13 \leq g_{sp} \leq 32$ inches
Equivalent Hydraulic Diameter	:	$0.37 \leq d_e \leq 0.60$ inches
Equivalent Heated Hydraulic Diameter	:	$0.46 \leq d_h \leq 0.59$ inches

Figure 4.4-2 shows measured critical heat flux plotted against predicted critical heat flux using the WRB-1 correlation.

Critical heat flux tests which model the 17x17 optimized fuel assembly (OFA) were performed with the results described in detail in Reference 5. It was concluded that the CHF characteristics of the 17x17 optimized fuel assembly design were not significantly different from those of the 17x17 standard design, and were adequately described by the R-grid form of the WRB-1 CHF correlation. Furthermore, the 17x17 OFA data were incorporated into the R grid data base without changing the DNBR design criterion of 1.17.

The WRB-2 DNB correlation (Reference 84) was developed to take credit for the VANTAGE 5 intermediate flow mixer (IFM) grid design. A limit of 1.17 is also applicable for the WRB-2 correlation. Figure 4.4-2a shows measured critical heat flux plotted against predicted critical heat flux using the WRB-2 correlation.

The applicable range of parameters for the WRB-2 correlation is:

Pressure	:	$1440 \leq P \leq 2490$ psia
Local Mass Velocity	:	$0.9 \leq G_{loc}/10^6 \leq 3.7$ lb/ft^2-hr
Local Quality	:	$-0.1 \leq X_{loc} \leq 0.3$
Heated Length, Inlet to CHF Location	:	$L_h \leq 14$ feet
Grid Spacing	:	$10 \leq g_{sp} \leq 26$ inches
Equivalent Hydraulic Diameter	:	$0.33 \leq d_e \leq 0.51$ inches
Equivalent Heated Hydraulic Diameter	:	$0.45 \leq d_h \leq 0.66$ inches

Prior to the Measurement Uncertainty Recapture Power Uprate (MUR-PU), the W-3 DNB correlation was applied to conditions which were outside the ranges of parameters for the WRB-1 and WRB-2 correlations. For the DNB analyses supporting the MUR-PU, the W-3 Alternative correlations have been implemented. The W-3 Alternative correlations, consisting of ABB-NV and WLOP, are based exclusively on DNB data from rod bundle tests, have a wider applicable range, and are more accurate than the W-3 correlation for prediction of margin to DNB. The two correlations are used for DNBR calculations as an alternative to the W-3 correlation, in supplement to the primary DNB correlation, WRB-2.

The ABB-NV correlation was originally developed for fuel designs in Combustion Engineering designed Pressurized Water Reactors (PWR) based on a linear relationship between CHF and local quality. The correlation includes the following parameters: pressure, local mass velocity, local equilibrium quality, distance from grid to CHF location, heated length from inlet to CHF location, and heated hydraulic diameter of the subchannel. Supplemental rod bundle data evaluation confirms that ABB-NV with the 95/95 correlation limit of 1.13 is applicable to the fuel region below the first mixing vane grid of the fuel designs for Westinghouse designed PWRs (Reference 94). Figure 4.4-2b shows measured critical heat flux plotted against predicted heat flux using the ABB-NV correlation.

The applicable range of the ABB-NV correlation is:

Pressure (psia)	:	1750 to 2415
Local Mass Velocity (10^6 lbm/hr-ft^2)	:	0.8 to 3.16
Local Quality (fraction)	:	<0.22
Heated Length, inlet to CHF location (in.)	:	48 (minimum) to 150
Heated Hydraulic Diameter Ratio	:	0.679 to 1.08
Grid Distance (in.)	:	7.3 to 24

The WLOP correlation is modified ABB-NV correlation specifically developed for low pressure conditions and extended flow range to cover low pressure/low flow conditions. Modifications to ABB-NV were made based on test data from rod bundles containing non-mixing vane grids. The WLOP correlation with a 95/95 DNBR limit of 1.18 has also been validated with test data from rod bundles containing mixing vane grids (Reference 94). Figure 4.4-2c shows measured critical heat flux plotted against predicted heat flux using the WLOP correlation.

The applicable range of the WLOP correlation is:

Pressure (psia)	:	185 to 1800
Local Mass Velocity (10^6 lbm/hr-ft^2)	:	0.23 to 3.07
Local Quality (fraction)	:	<0.75
Heated Length, inlet to CHF location (in.)	:	48 (minimum) to 168
Heated Hydraulic Diameter Ratio	:	0.679 to 1.00
Grid Spacing Term (Reference 94)	:	27 to 115

4.4.2.2.2 Definition of Departure from Nucleate Boiling Ratio

The DNBR as applied to this design for both typical and thimble cold wall cells is:

$$DNBR = \frac{q''_{DNB,N}}{q''_{loc}} \qquad (4.4\text{-}1)$$

Where: q''_{loc} = the actual local heat flux

$$q''_{DNB,N} = \frac{q''_{DNB,EU}}{F} \qquad (4.4\text{-}2)$$

and $q''_{DNB,EU}$ is the uniform critical heat flux as predicted by the appropriate correlation, for example, the WRB-2 correlation (Reference 84).

F is the flux shape factor to account for nonuniform axial heat flux distributions (Reference 11) with the "C" term modified as in Reference 6.

4.4.2.2.3 Mixing Technology

The rate of heat exchange by mixing between flow channels is proportional to the difference in the local mean fluid enthalpy of the respective channels, the local fluid density and flow velocity. The proportionality is expressed by the dimensionless thermal diffusion coefficient (TDC) which is defined as:

$$TDC = \frac{w'}{\rho V a} \qquad (4.4\text{-}3)$$

where:

w'	=	flow exchange rate per unit length, $lb_m/ft\text{-}sec$
ρ	=	fluid density, lb_m/ft^3
V	=	fluid velocity, ft/sec
a	=	lateral flow area between channels per unit length, ft^2/ft

The application of the TDC in the THINC analysis for determining the overall mixing effect or heat exchange rate is presented in Reference 12. The application of the TDC in the VIPRE-01 analysis is presented in Reference 92. The same TDC is applied in both analyses.

Various mixing tests were performed at Columbia University (Reference 13). These series of tests, using the "R" mixing vane grid design on 13-, 26-, and 32-inch grid spacing, were conducted in pressurized water loops at Reynolds numbers similar to that of a PWR core under the following single and two phase (subcooled boiling) flow conditions:

Pressure	1500 to 2400 psia
Inlet temperature	332 to 642°F
Mass velocity	1.0 to 3.5 x 10^6 $lb_m/hr\text{-}ft^3$
Reynolds number	1.34 to 7.45 x 10^5
Bulk outlet quality	-52.1 to -13.5%

TDC was determined by comparing the THINC code predictions with the measured subchannel exit temperatures. Data for 26-inch axial grid spacing are presented in Figure 4.4-3 where the thermal diffusion coefficient is plotted versus the Reynolds number. TDC is found to be independent of Reynolds number, mass velocity, pressure and quality over the ranges tested. The

two-phase data (local, subcooled boiling) fell within the scatter of the single phase data. The effect of two-phase flow on the value of TDC has been demonstrated by Cadek (Reference 13), Rowe and Angle (References 14,15), and Gonzalez-Santalo and Griffith (Reference 16). In the subcooled boiling region, the values of TDC were indistinguishable from the single phase values. In the quality region, Rowe and Angle show that in the case with rod spacing similar to that in PWR reactor core geometry, the value of TDC increased with quality to a point and then decreased, but never below the single phase value. Gonzalez-Santalo and Griffith showed that the mixing coefficient increased as the void fraction increased.

The data from these tests on the R grid showed that a design TDC value of 0.038 (for 26-inch grid spacing) can be used in determining the effect of coolant mixing in the THINC or VIPRE-01 analysis.

A mixing test program similar to the one described above was conducted at Columbia University for the current 17x17 geometry and mixing vane grids on 26-inch spacing (Reference 17). The mean value of TDC obtained from these tests was 0.059 and all data were well above the current design value of 0.038.

The Zircaloy grid employed in the 17x17 optimized fuel assembly design was designed to have the same mixing characteristics as the current 17x17 R-grid design. This is verified by the fact that the DNB performance of the OFA grid design is similar to that of the current R-grid design, as discussed in Subsection 4.4.2.2.1. Thus, the current conservative design value of TDC is applicable to the 17x17 optimized fuel assembly design.

In addition, since the actual optimized fuel grid spacing is approximately 20 inches, additional margin is available for this design, since the value of TDC increases as grid spacing decreases (Reference 13).

The inclusion of three intermediate flow mixer (IFM) grids in the upper span of the VANTAGE 5 fuel assembly results in a grid spacing of approximately 10 inches. Therefore, the TDC value used for optimized fuel is a conservatively low value for use in VANTAGE 5 to determine the effect of coolant mixing in the core thermal performance analysis.

4.4.2.2.4 Hot Channel Factors

The total hot channel factors for heat flux and enthalpy rise are defined as the maximum-to-core average ratios of these quantities. The heat flux hot channel factor considers the local maximum linear heat generation rate at a point (the hot spot), and the enthalpy rise hot channel factor involves the maximum integrated value along a channel (the hot channel).

Each of the total hot channel factors considers a nuclear hot channel factor (see Subsection 4.4.4.3) describing the neutron

power distribution and an engineering hot channel factor, which allows for variations in flow conditions and fabrication tolerances. The engineering hot channel factors are made up of subfactors which account for the influence of the variations of fuel pellet diameter, density, enrichment and eccentricity; inlet flow distribution; flow redistribution; and flow mixing.

kW/ft Hot Channel Factor Engineering Uncertainty

The kW/ft hot channel factor engineering uncertainty is used to evaluate the maximum linear heat generation rate in the core. This subfactor is determined by statistically combining the fabrication variations for fuel pellet diameter, density, and enrichment, and has a value of 1.03 at the 95% probability level with 95% confidence. As shown in Reference 18, no DNB penalty need be taken for the short relatively low intensity heat flux spikes caused by variations in the above parameters, as well as fuel pellet eccentricity and fuel rod diameter variation.

Enthalpy Rise Engineering Uncertainty

The effect of variations in flow conditions and fabrication tolerances on the hot channel enthalpy rise is directly considered in the VIPRE-01 subchannel analysis (see Subsection 4.4.4.5) under any reactor operating condition. The items considered contributing to the enthalpy rise engineering uncertainty are discussed below.

a. Pellet diameter, density and enrichment and fuel rod diameter:

   Variations in pellet diameter, density and enrichment and fuel rod diameter, are considered statistically in establishing the limit DNBRs (see Subsection 4.4.1.1) for the revised thermal design procedure (Reference 89) employed in this application. Uncertainties in these variables are determined from sampling of manufacturing data.

b. Inlet Flow Maldistribution:

   The consideration of inlet flow maldistribution in core thermal performances is discussed in Subsection 4.4.4.2.2. A design basis of 5% reduction in coolant flow to the hot assembly is used in the VIPRE-01 analysis.

c. Flow Redistribution:

   The flow redistribution accounts for the reduction in flow in the hot channel resulting from the high flow resistance in the channel due to the local or bulk boiling. The effect of the nonuniform power distribution is inherently considered in the VIPRE-01 analysis for every operating condition which is evaluated.

d. Flow Mixing:

The subchannel mixing model incorporated in the VIPRE-01 code and used in reactor design is based on experimental data (Reference 19) discussed in Subsection 4.4.4.5. The mixing vanes incorporated in the spacer grid design induce additional flow mixing among the various flow channels in a fuel assembly as well as between adjacent assemblies. This mixing reduces the enthalpy rise in the hot channel resulting from local power peaking or unfavorable mechanical tolerances.

4.4.2.2.5 Effects of Rod Bow on DNBR

The phenomenon of fuel rod bowing, as described in Reference (81), is accounted for in the DNBR safety analysis of Condition I and Condition II events for the Byron/Braidwood plants. Applicable credits for margin resulting from retained conservatism in the evaluation of DNBR and/or margin obtained from measured plant operating parameters (such as $F^N_{\Delta H}$ or core flow) -- which are less limiting than those required by the plant safety analysis -- are used to offset the effect of rod bow.

The safety analysis for Byron/Braidwood cores maintains sufficient margin between the safety analysis DNBR Limits and the design DNBR limits to accommodate full flow and low flow DNBR penalties which are based on the methodology in Reference 83.

The maximum rod bow penalties accounted for in the design safety analysis are based on an assembly average burnup of 24000 MWd/Mtu. At burnups greater than 24000 MWd/Mtu, credit is taken for the effect of $F^N_{\Delta H}$ burndown, due to the decrease in fissionable isotopes and the buildup of fission product inventory, and no additional rod bow penalty is required (Reference 87).

For the upper assembly span of VANTAGE 5 fuel where additional restraint is provided with the intermediate flow mixer (IFM) grids, the grid-to-grid spacing in DNB limiting spans is approximately 10 inches compared to approximately 20 inches in the optimized fuel. Using the NRC approved scaling factor results in predicted channel closure in the limiting spans of less than 50% closure. Therefore, no rod bow DNBR penalty is required in the 10-inch spans in the VANTAGE 5 safety analyses.

4.4.2.2.6 Transition Core

The Westinghouse transition core DNB methodology is given in References 84, 85, and 86. Using this methodology, transition cores are analyzed as if they were full cores of one assembly type (full optimized or full VANTAGE 5), applying the applicable

transition core penalties. The VANTAGE 5 transition core DNBR penalty is based on the fraction of VANTAGE 5 fuel actually in the transition core. This penalty will be included in the safety analysis limit DNBRs such that sufficient margin over the design limit DNBR exists to accommodate the transition core penalty and the appropriate rod bow DNBR penalty.

The optimized and VANTAGE 5 designs have been shown to be hydraulically compatible in Reference 84.

4.4.2.3 Linear Heat Generation Rate

The core average and maximum LHGRs are given in Table 4.4-1. The method of determining the maximum LHGR is given in Subsection 4.3.2.2.

4.4.2.4 Void Fraction Distribution

The VIPRE-01 calculated core average and the hot subchannel maximum and average void fractions are presented in Table 4.4-2 for operation at full power. The void models used in the VIPRE-01

computer code are described in Subsection 4.4.2.7.3.

4.4.2.5 Core Coolant Flow Distribution

Assembly average coolant mass velocity and enthalpy at various radial and axial core locations are given below. Typical coolant enthalpy rise and flow distributions are shown for the 4-foot elevation (1/3 of core height) in Figure 4.4-4, and 8-foot elevation (2/3 of core height) in Figure 4.4-5 and at the core exit in Figure 4.4-6. These distributions are for a representative Westinghouse four-loop plant. The THINC code analysis for this case utilized a uniform core inlet enthalpy and inlet flow distribution. No orificing is employed in the reactor design.

4.4.2.6 Core Pressure Drops and Hydraulic Loads

4.4.2.6.1 Core Pressure Drops

The analytical model and experimental data used to calculate the pressure drops shown in Table 4.4-1 are described in Subsection 4.4.2.7. The core pressure drop includes the fuel assembly, lower core plate, and upper core plate pressure drops. The full power operation pressure drop values shown in Table 4.4-1 are the unrecoverable pressure drops across the vessel, including the inlet and outlet nozzles, and across the core. These pressure drops are based on the best estimate flow for actual plant operating conditions as described in Section 5.1. Section 5.1 also defines and describes the thermal design flow (minimum flow) which is the basis for reactor core thermal performance and the mechanical design flow (maximum flow) which is used in the mechanical design of the reactor vessel internals and fuel assemblies. Since the best estimate flow is that flow which is most likely to exist in an operating plant, the calculated pressure drops in Table 4.4-1 are based on this best estimate flow.

Uncertainties associated with the core pressure drop values are discussed in Subsection 4.4.2.9.2.

4.4.2.6.2 Hydraulic Loads

The fuel assembly hold down springs are designed to keep the fuel assemblies in contact with the lower core plate under all Condition I and II events with the exception of the turbine overspeed transient associated with a loss of external

load. The hold down springs are designed to tolerate the possibility of an over deflection associated with fuel assembly lift off for this case and provide contact between the fuel assembly and the lower core plate following this transient. More adverse flow conditions occur during a loss-of-coolant accident. These conditions presented in Subsection 15.6.5.

Hydraulic loads at normal operating conditions are calculated considering the mechanical design flow which is described in Section 5.1 and accounting for the minimum core bypass flow based on manufacturing tolerances. Core hydraulic loads at cold plant startup conditions are based on the cold mechanical design flow, but are adjusted to account for the coolant density difference. Conservative core hydraulic loads for a pump overspeed transient, which could possibly create flow rates 20% greater than the mechanical design flow, are evaluated to be approximately twice the fuel assembly weight.

The hydraulic verification tests are discussed in References 5 and 84.

4.4.2.7 Correlation and Physical Data

4.4.2.7.1 Surface Heat Transfer Coefficients

Forced convection heat transfer coefficients are obtained from the familiar Dittus-Boelter correlation (Reference 21), with the properties evaluated at bulk fluid conditions:

$$\frac{hD_e}{K} = 0.023 \left[\frac{D_e G}{\mu}\right]^{0.8} \left[\frac{C_p \mu}{K}\right]^{0.4} \qquad (4.4\text{-}4)$$

where:

h = heat transfer coefficient, Btu/hr-ft^2-°F

D_e = equivalent diameter, ft

K = thermal conductivity, Btu/hr-ft°F

G = mass velocity, lb_m/hr-ft^2

μ = dynamic viscosity, lb_m/ft-hr

C_p = heat capacity, Btu/lb_m-°F

This correlation has been shown to be conservative (Reference 22) for rod bundle geometries with pitch to diameter ratios in the range used by PWRs.

The onset of nucleate boiling occurs when the cladding wall temperature reaches the amount of superheat predicted by Thom's (Reference 23) correlation. After this occurrence, the outer cladding wall temperature is determined by:

$$\Delta T_{sat} = (0.072 \exp(-P/1260)) \ (q")^{0.5} \qquad (4.4\text{-}5)$$

where:

ΔT_{sat} = wall superheat, $T_W - T_{sat}$, °F

$q"$ = wall heat flux, Btu/hr-ft^2

P = pressure, psia

T_W = outer cladding wall temperature, °F

T_{sat} = saturation temperature of coolant at P, °F

4.4.2.7.2 Total Core and Vessel Pressure Drop

Unrecoverable pressure losses occur as a result of viscous drag (friction) and/or geometry changes (form) in the fluid flow path. The flow field is assumed to be incompressible, turbulent, single-phase water. These assumptions apply to the core and vessel pressure drop calculations for the purpose of establishing the primary loop flow rate. Two-phase considerations are neglected in the vessel pressure drop evaluation because the core average void is negligible (see Table 4.4-2). Two-phase flow considerations in the core thermal subchannel analyses are considered and the models are discussed in Subsection 4.4.4.2.3.

Core and vessel pressure losses are calculated by equations of the form:

$$\Delta P_L = \left(K + F \frac{L}{D_e}\right) \frac{\rho V^2}{2 \ g_c (144)} \qquad (4.4\text{-}6)$$

where:

ΔP_L = unrecoverable pressure drop, lb_f/in^2

ρ = fluid density, lb_m/ft^3

L = length, ft

De = equivalent diameter, ft

V = fluid velocity, ft/sec

g_c = $32.174 \ \frac{lb_{m-ft}}{lb_f - sec^2}$

K = form loss coefficient, dimensionless

F = friction loss coefficient, dimensionless

Fluid density is assumed to be constant at the appropriate value for each component in the core and vessel. Because of the complex core and vessel flow geometry, precise analytical values for the form and friction loss coefficients are not available. Therefore, experimental values for these coefficients are obtained from geometrically similar models.

Values are quoted in Table 4.4-1 for unrecoverable pressure loss across the reactor vessel, including the inlet and outlet nozzles, and across the core. The results of full scale tests of core components and fuel assemblies were utilized in developing the core pressure loss characteristic. The pressure drop for the vessel was obtained by combining the core loss with correlation of 1/7th scale model hydraulic test data on a number of vessels (References 24, 25) and form loss relationships (Reference 26). Moody (Reference 27) curves were used to obtain the single phase friction factors.

Core pressure drops were confirmed by the verification testing described in References 5 and 84. These hydraulic verification tests include hydraulic head losses and effects of velocity changes as well as unrecoverable pressure losses. The effects of velocity changes are small, since the static pressure taps are located at elevations of approximately equal flow areas (and therefore approximately equal velocities). When wall static pressure taps are used near ambient fluid conditions, it can be shown analytically that the elevation head losses do not contribute to the measured core pressure drops. Therefore, data from the hydraulic verification tests can be directly applied to confirm the pressure drop values quoted in Table 4.4-1 which are based on unrecoverable pressure losses only.

Tests of the primary coolant loop flow rates will be made (see Subsection 4.4.5.1) prior to initial criticality to verify that the flow rates used in the design, which were determined in part from the pressure losses calculated by the method described here, are conservative.

4.4.2.7.3 Void Fraction Correlation

VIPRE-01 considers two-phase flow in two steps. First, a quality model is used to compute the flowing vapor mass fraction (true quality) including the effects of subcooled boiling. Then, given the true quality, a bulk void model is applied to compute the vapor volume fraction (void fraction).

VIPRE-01 uses a profile fit model (Reference 93) for determining subcooled quality. It calculates the local vapor volumetric fraction in forced convection boiling by: 1) predicting the point of bubble departure from the heated surface, and 2) postulating a relationship between the true local vapor fraction and the corresponding thermal equilibrium value.

The void fraction in the bulk boiling region is predicted by using homogeneous flow theory and assuming no slip. The void fraction in this region is therefore a function only of the thermodynamic quality.

4.4.2.8 Thermal Effects of Operational Transients

DNB core safety limits are generated as a function of coolant temperature, pressure, core power, and the axial and radial power distributions. Operation within these DNB safety limits ensures that the DNB design basis is met for both steady-state operation and for anticipated operational transients that are slow with respect to fluid transport delays in the primary system. In addition, for fast transients, e.g., uncontrolled rod bank withdrawal at power incident, specific protection functions are provided as described in Chapter 7 and the use of these protection functions is described in Chapter 15. The thermal response of the fuel is discussed in Subsection 4.2.3.3.

4.4.2.9 Uncertainties in Estimates

4.4.2.9.1 Uncertainties in Fuel and Cladding Temperatures

As discussed in Subsection 4.4.2.11, the fuel temperature is a function of crud, oxide, cladding, gap, and pellet conductances. Uncertainties in the fuel temperature calculation are essentially of two types: fabrication uncertainties such as variations in the pellet and cladding dimensions and the pellet density; and model uncertainties such as variations in the pellet conductivity and the gap conductance. These uncertainties have been quantified by comparison of the thermal model to the in-pile thermocouple measurements (References 31 through 37) by out-of-pile measurements of the fuel and cladding properties (References 38 through 49), and by measurements of the fuel and cladding dimensions during fabrication. The resulting uncertainties are then used in all evaluations involving the fuel temperature. The effect of densification on fuel temperature uncertainties is presented in Reference 50.

In addition to the temperature uncertainty described above, the measurement uncertainty in determining the local power, and the effect of density and enrichment variations on the local power are considered in establishing the heat flux hot channel factor. These uncertainties are described in Subsection 4.3.2.2.1.

Reactor trip setpoints, as specified in Technical Requirements Manual (TRM) 2.0.a include allowance for instrument and measurement uncertainties such as calorimetric error, instrument drift and channel reproducibility, temperature measurement uncertainties, noise, and heat capacity variations.

Uncertainty in determining the cladding temperatures results from uncertainties in the crud and oxide thicknesses. Because of the excellent heat transfer between the surface of the rod and the coolant, the film temperature drop does not appreciably contribute to the uncertainty.

4.4.2.9.2 Uncertainties in Pressure Drops

Core and vessel pressure drops based on the best estimate flow, as described in Section 5.1, are quoted in Table 4.4-1. The uncertainties quoted are based on the uncertainties in both the test results and the analytical extension of these values to the reactor application.

A major use of the core and vessel pressure drops is to determine the primary system coolant flow rates as discussed in Section 5.1. In addition, as discussed in Subsection 4.4.5.1, tests on the primary system prior to initial criticality will be made to verify that a conservative primary system coolant flow rate has been used in the design and analyses of the plant.

4.4.2.9.3 Uncertainties Due to Inlet Flow Maldistribution

The effects of uncertainties in the inlet flow maldistribution criteria used in the core thermal analyses are discussed in Subsection 4.4.4.2.2.

4.4.2.9.4 Uncertainty in DNB Correlation

The uncertainty in the DNB correlation (Subsection 4.4.2.2) can be written as a statement on the probability of not being in DNB based on the statistics of the DNB data. This is discussed in Subsection 4.4.2.2.

4.4.2.9.5 Uncertainties in DNBR Calculations

The uncertainties in the DNBRs calculated by VIPRE-01 analysis (see Subsection 4.4.4.5) due to nuclear peaking factors are accounted for by applying conservatively high values of the nuclear peaking factors and including measurement error allowances in the statistical evaluation of the limit DNBR (See Subsection 4.4.1.1) using the revised thermal design procedure (Reference 89). In addition, engineering hot channel factors are employed as discussed in Subsection 4.4.2.2.4.

The results of a sensitivity study (Reference 20) with THINC-IV show that the minimum DNBR in the hot channel is relatively insensitive to variations in the core-wide radial power distribution (for the same value of $F^N_{\Delta H}$). VIPRE-01 was demonstrated to be equivalent to THINC-IV in Reference 92.

The ability of the VIPRE computer code to accurately predict flow and enthalpy distributions in the rod bundles is discussed in Subsection 4.4.4.5 and in Reference 92. Studies have been performed (References 92 and 93) to determine the sensitivity of the minimum DNBR in the hot channel to void fraction correlation (Subsection 4.4.2.7.3) and the inlet flow distributions. The results of these studies show that the minimum DNBR is relatively insensitive to variation in these parameters. Furthermore, the VIPRE flow field model for predicting conditions in the hot channels is consistent with that used in the derivation of the DNB correlation limits, including void/quality modeling, turbulent mixing and crossflow, and two-phase friction (Reference 92).

As required in Reference 89, an uncertainty of 4% in DNBR is included in the design procedure to account for any VIPRE-01 Code uncertainty.

4.4.2.9.6 Uncertainties in Flow Rates

The uncertainties associated with loop flow rates are discussed in Section 5.1. A thermal design flow is defined for use in core thermal performance evaluations which accounts for both prediction and measurement uncertainties.

In addition, a maximum of 8.3% of the thermal design flow is assumed to be ineffective for core heat removal capability because it bypasses through the various available vessel flow paths described in Subsection 4.4.4.2.1.

The possibility of a significant reduction in the core flow rate over a relatively short period of time as a result of crud depositions on the fuel rods has been evaluated. Operating experience to date has indicated that a flow resistance-allowance for possible crud deposition is not required. There has been no detectable long-term flow reduction reported at any Westinghouse plant. Inspection of the inside surfaces of steam generator tubes removed from operating plants has confirmed that there is no significant surface deposition that would affect system flow. Although all of the coolant piping surfaces have not been inspected, the small piping friction contribution to the total system resistance and the lack of significant deposition on piping near steam generator nozzles support the conclusion that an allowance for piping deposition is not necessary. The effect of crud enters into the calculation of core pressure drop through the fuel rod frictional component by use of a surface roughness factor. Present analyses utilize a surface roughness value which

is a factor of three greater than the best estimate obtained from crud sampling from several operating Westinghouse reactors.

The operator has at his disposal several methods of detecting significant RCS flow reduction, these are:

a. Flow meter on each RCS loop,

b. If operating in an automatic control rod mode (T_c held constant) a reduction in reactor power would be present for significant reductions in RCS flow,

c. If operating in a manual control rod mode (power held constant) an increase in ΔT across the core would be present for significant reductions in flow,

d. Local changes in flow could be indicated by incore flux maps (assuming significant changes in local power), and

e. Core exit thermocouple readings.

The operator will verify flow, perform calorimetric power checks, and generate incore flux maps as required by the Technical Specifications.

4.4.2.9.7 Uncertainties in Hydraulic Loads

As discussed in Subsection 4.4.2.6.2, hydraulic loads on the fuel assembly are evaluated for a pump overspeed transient which creates flow rates 20% greater than the mechanical design flow. The mechanical design flow as stated in Section 5.1 is greater than the best estimate or most likely flow rate value for the actual plant operating condition.

4.4.2.9.8 Uncertainty in Mixing Coefficient

The value of the mixing coefficient, TDC, used in VIPRE-01 analyses for this application is 0.038. The mean value of TDC obtained in the R-grid mixing tests described in Subsection 4.4.2.2.3 was 0.042 (for 26-inch grid spacing). The value 0.038 is one standard deviation below the mean value; and approximately 90% of the data gives values of TDC greater than 0.038 (Reference 13).

The results of the mixing tests done on the current 17x17 geometry, as discussed in Subsection 4.4.2.2.3, had a mean value of TDC of 0.059 and standard deviation $\sigma = 0.007$. Hence, the current design value of TDC is almost 3 standard deviations below the mean for 26-inch grid spacing.

4.4.2.10 Flux Tilt Consideration

Significant quadrant power tilts are not anticipated during normal operation since this phenomenon is caused by some perturbation. For example, a dropped or misaligned RCCA could cause changes in the hot channel factors; however, these events are analyzed separately in Chapter 15.0. Other possible causes for quadrant power tilts include X-Y xenon transients, inlet temperature mismatches, enrichment variations within tolerances and so forth.

In addition to unanticipated quadrant power tilts as described above, other readily explainable asymmetries may be observed during calibration of the excore detector quadrant power tilt alarm. Incore power distributions are evaluated periodically from monthly flux maps or weekly PDMS surveillances. Incore flux maps are also obtained for calibration purposes. Each of these maps is reviewed for deviations from the expected power distributions. Asymmetry in the core, from quadrant to quadrant, is frequently a consequence of the design when assembly and/or component shuffling and rotation requirements do not allow exact symmetry preservation. In each case, the acceptability of an observed asymmetry, planned or otherwise depends solely on meeting the required accident analyses assumptions.

In practice, once acceptability has been established by review of the incore maps or PDMS surveillances, the quadrant power tilt alarms and related instrumentation may be adjusted to indicate zero quadrant power tilt ratio as the final step in the power range excore detector calibration process. This action ensures that the instrumentation is correctly calibrated to alarm in the event an unexplained or unanticipated change occurs in the quadrant to quadrant relationships between calibration intervals. Proper functioning of the quadrant power tilt alarm is significant because no allowances are made in the design for increased hot channel factors due to unexpected developing flux tilts since all likely causes are prevented by design or procedures or specifically analyzed. Finally, in the event that unexplained flux tilts do occur, Technical Specifications 3.2.4 provides appropriate corrective actions to ensure continued safe operation of the reactor.

When PDMS is operable, the core is monitored on a minute by minute basis, essentially 1 minute fluxmaps. The Monitor function of PDMS is calculating peaking factors, margins to limits, quadrant power distribution and core average axial offset. When PDMS is operable and in operation, the quadrant power tilt ratio Technical Specification 3.2.4 is relaxed (References 91 and 95).

4.4.2.11 Fuel and Cladding Temperatures

Consistent with the thermal-hydraulic design bases described in Subsection 4.4.1, the following discussion pertains mainly to

fuel pellet temperature evaluation. A discussion of fuel clad integrity is presented in Subsection 4.2.3.1.

The thermal-hydraulic design assures that the maximum fuel temperature is below the melting point of UO_2 (melting point of 5080°F (Reference 4) unirradiated and decreasing by 58°F per 10,000 MWd/Mtu). To preclude center melting and as a basis for overpower protection system setpoints, a calculated centerline fuel temperature of 4700°F has been selected as the overpower limit. This provides sufficient margin for uncertainties in the thermal evaluations as described in Subsection 4.4.2.9.1. The temperature distribution within the fuel pellet is predominantly a function of the local power density and the UO_2 thermal conductivity. However, the computation of radial fuel temperature distributions combines crud, oxide, cladding gap and pellet conductances. The factors which influence these conductances, such as gap size (or contact pressure), internal gas pressure, gas composition, pellet density, and radial power distribution within the pellet, etc., have been combined into a semi-empirical thermal model (see Subsection 4.2.3.3) with the model modifications for time dependent fuel densification given in Reference 50. This thermal model enables the determination of these factors and their net effects on temperature profiles. The temperature predictions have been compared to in-pile fuel temperature measurements (References 31 through 37), and melt radius data (References 52, 53), with good results.

As described in Reference 50, fuel rod thermal evaluations (fuel centerline, average and surface temperatures) are determined throughout the fuel rod lifetime with consideration of time dependent densification. To determine the maximum fuel temperatures, various burnup rods, including the highest burnup rod, are analyzed over the rod linear power range of interest.

The principal factors which are employed in the determination of the fuel temperature are discussed below.

4.4.2.11.1 UO_2 Thermal Conductivity

The thermal conductivity of uranium dioxide was evaluated from data reported by Howard et al. (Reference 38); Lucks et al. (Reference 39); Danial et al. (Reference 40); Feith (Reference 41); Vogt et al. (Reference 42); Nishijima et al. (Reference 43); Wheeler et al. (Reference 44); Godfrey et al. (Reference 45); Stora et al. (Reference 46); Bush (Reference 47); Asamoto et al. (Reference 48); Kruger (Reference 49); and Gyllander (Reference 54).

At the higher temperatures, thermal conductivity is best obtained by utilizing the integral conductivity to melt which can be determined with more certainty.

From an examination of the data, it has been concluded that the best estimate for the value of Kdt is 93 watts/cm. This conclusion is based on the integral values reported by Gyllander (Reference 54), Lyons, et al. (Reference 55), Coplin, et al. (Reference 56), Duncan (Reference 52), Bain (Reference 57), and Stora (Reference 58).

The design curve for the thermal conductivity is shown in Figure 4.4-8. The section of the curve at temperatures between O°C and 1300°C is in excellent agreement with the recommendation of the IAEA panel (Reference 59). The section of the curve above 1300°C is derived for an integral value of 93 watts/cm (References 52, 54, 58).

Thermal conductivity for UO_2 at 95% theoretical density can be represented best by the following equation:

$$K = \frac{1}{11.8 + 0.0238T} + 8.775 \times 10^{-13} \ T^3 \qquad (4.4\text{-}7)$$

where:

K = watts/cm-°C
T = °C.

4.4.2.11.2 Radial Power Distribution in UO_2 Fuel Rods

An accurate description of the radial power distribution as a function of burnup is needed for determining the power level for incipient fuel melting and other important performance parameters such as pellet thermal expansion, fuel swelling and fission gas release rates.

This information on radial power distributions in UO_2 fuel rods was determined with the neutron transport theory code, LASER. The LASER Code has been validated by comparing the code predictions on radial burnup and isotopic distributions with measured radial microdrill data (References 60, 61). A "radial power depression factor", f, is determined using radial power distributions predicted by LASER. The factor f enters into the determination of the pellet centerline temperature, T_c, relative to the pellet surface temperature, T_s, through the expression:

$$\int_{T_s}^{T_{ck}} (T)\, dT = \frac{q'f}{4\pi} \qquad (4.4\text{-}8)$$

where:

K(T) = the thermal conductivity for UO_2 with a uniform density distribution
q' = the linear power generation rate.

4.4.2.11.3 Gap Conductance

The temperature drop across the pellet-clad gap is a function of the gap size and the thermal conductivity of the gas in the gap. The gap conductance model is selected such that when combined with the UO_2 thermal conductivity model, the calculated fuel centerline temperatures reflect the in-pile temperature measurements.

The temperature drop across the gap is calculated by assuming an annular gap conductance model of the following form:

$$h = \frac{K_{gas}}{\frac{\delta}{2} + \delta_r} \qquad (4.4\text{-}9)$$

where:

h = contact conductance, Btu/hr-ft^2-°F
K_{gas} = thermal conductivity of the gas mixture including a correction factor (Reference 62) for the accommodation coefficient for light gases (e.g. helium), Btu/hr-ft-°F.
δ = effective diametral gap size, ft.
δ_r = effective gap spacing due to surface roughness, ft.

or an empirical correlation derived from thermocouple and melt radius data.

The larger gap conductance value from these two equations is used to calculate the temperature drop across the gap for finite gaps.

For evaluations in which the pellet-clad gap is closed, a contact conductance is calculated. The contact conductance between UO_2 and Zircaloy has been measured and found to be dependent on the contact pressure, composition of the gas at the interface and the surface roughness (References 62, 63). The contact conductance between UO_2 and ZIRLO/Optimized ZIRLO cladding is equivalent. This information together with the surface roughness found in Westinghouse reactors leads to the following correlation:

$$h = 0.6P + \frac{K_{gas}}{\delta_r} \qquad (4.4\text{-}10)$$

where: P = contact pressure, psi

4.4.2.11.4 Surface Heat Transfer Coefficients

The fuel rod surface heat transfer coefficients during subcooled forced convection and nucleate boiling are presented in Subsection 4.4.2.7.1.

4.4.2.11.5 Fuel Clad Temperatures

The outer surface of the fuel rod at the hot spot operates at a temperature of approximately 660°F for steady state operation at rated power throughout core life due to the onset of nucleate boiling. Initially (beginning-of-life), this temperature is that of the clad metal outer surface.

During operation over the life of the core, the buildup of oxides and crud on the fuel rod surface causes the clad surface temperature to increase. Allowance is made in the fuel center melt evaluation for this temperature rise. Since the thermal hydraulic design basis limits DNB, adequate heat transfer is provided between the fuel clad and the reactor coolant so that the core thermal output is not limited by considerations of clad temperature.

4.4.2.11.6 Treatment of Peaking Factors

The total heat flux hot channel factor, F_Q, is defined by the ratio of the maximum to core average heat flux. As presented in Table 4.3-1 and discussed in Subsection 4.3.2.2.6, the design value of F_Q for normal operation is 2.60. This results in a peak linear power of 15.14 kW/ft at full power conditions.

As described in Subsection 4.3.2.2.6, the peak linear power resulting from overpower transients/operator errors (assuming a maximum overpower of 119%) will not exceed that required for fuel centerline melt. The centerline temperature kW/ft must be below the UO_2 melt temperature over the lifetime of the rod, including allowances for uncertainties. The fuel temperature design basis is discussed in Subsection 4.4.1.2 and results in a maximum allowable calculated centerline temperature of 4700°F. The peak linear power for prevention of centerline melt is 22.5 kW/ft. The centerline temperature at the peak linear power resulting from overpower transients/overpower errors (assuming a maximum overpower of 119%) is below that required to produce melting.

4.4.3 Description of the Thermal and Hydraulic Design of the Reactor Coolant System

4.4.3.1 Plant Configuration Data

Plant configuration data for the thermal hydraulic and fluid systems external to the core are provided in the appropriate Chapters 5.0, 6.0, and 9.0. Implementation of the emergency core cooling system (ECCS) is discussed in Chapter 15.0. Some specific areas of interest are the following:

a. Total coolant flow rates for the reactor coolant system (RCS) and each loop are provided in Table 5.1-1. Flow rates employed in the evaluation of the core are presented in Section 4.4.

b. Total RCS volume including pressurizer and surge line, RCS liquid volume including pressurizer water at steady state power conditions are given in Table 5.1-1.

c. The flow path length through each volume may be calculated from physical data provided in the above referenced tables.

d. The height of fluid in each component of the RCS may be determined from the physical data presented in Section 5.4. The components of the RCS are water filled during power operation with the pressurizer being approximately 60% water filled.

e. Components of the ECCS are to be located so as to meet the criteria for net positive suction head described in Section 6.3.

f. Line lengths and sizes for the safety injection system are determined so as to guarantee a total system resistance which will provide, as a minimum, the fluid delivery rates assumed in the safety analyses described in Chapter 15.0.

g. The parameters for components of the RCS are presented in Section 5.4, component and subsystem design.

h. The steady state pressure drops and temperature distributions through the RCS are presented in Table 5.1-1.

4.4.3.2 Operating Restrictions on Pumps

The minimum net positive suction head (NPSH) and minimum seal injection flow rate must be established before operating the reactor coolant pumps. With the minimum labyrinth seal injection

flow rate established, the operator will have to verify that the system pressure satisfies NPSH requirements.

4.4.3.3 Power-Flow Operating Map (BWR)

Not applicable to Pressurized Water Reactors.

4.4.3.4 Temperature-Power Operating Map

The relationship between reactor coolant system temperature and power is shown in Figure 4.4-9.

The effects of reduced core flow, due to inoperative pumps are discussed in Subsections 15.3.1 and 15.3.2. Natural circulation capability of the system is shown in Table 15.2-2.

4.4.3.5 Load-Following Characteristics

The reactor coolant system is designed on the basis of steady state operation at full power heat load. The reactor coolant pumps utilize constant speed drives as described in Section 5.4 and the reactor power is controlled to maintain average coolant temperature at a value which is a linear function of load, as described in Section 7.7.

4.4.3.6 Thermal and Hydraulic Characteristics Summary Table

The thermal and hydraulic characteristics are given in Table 4.4-1.

4.4.4 Evaluation

4.4.4.1 Critical Heat Flux

The critical heat flux correlations utilized in the core thermal analysis are explained in detail in Subsection 4.4.2.

4.4.4.2 Core Hydraulics

4.4.4.2.1 Flow Paths Considered in Core Pressure Drop and Thermal Design

The following flow paths for core bypass flow are considered:

a. Flow through the spray nozzles into the upper head for head cooling purposes.

b. Flow entering into the RCC guide thimbles.

c. Leakage flow from the vessel inlet nozzle directly to the vessel outlet nozzle through the gap between the vessel and the barrel.

d. Flow introduced between the baffle and the barrel for the purpose of cooling these components and which is not considered available for core cooling.

e. Flow in the gaps between the fuel assemblies on the core periphery and the adjacent baffle wall.

The above contributions are evaluated to confirm that the design value of the core bypass flow is met. The design value of the core bypass flow is equal to 8.3% of the total vessel flow.

Calculations have been performed using drawing tolerances in the worst direction and accounting for uncertainties in pressure losses. Based on these calculations, the core bypass is no greater than the design values quoted above.

Flow model test results for the flow path through the reactor are discussed in Subsection 4.4.2.7.2.

4.4.4.2.2 Inlet Flow Distributions

Data have been considered from several 1/7 scale hydraulic reactor model tests (References 24, 25, 64) in arriving at the core inlet flow maldistribution criteria to be used in the VIPRE-01 analyses (see Subsection 4.4.4.5). THINC-I analyses made, using these data, have indicated that a conservative design basis is to consider 5% reduction in the flow to the hot assembly (Reference 65). The same design basis of 5% reduction to the hot assembly inlet is used in VIPRE-01 analyses.

The experimental error estimated in the inlet velocity distribution has been considered as outlined in Reference 20 where the sensitivity of changes in inlet velocity distributions to hot channel thermal performance is shown to be small. Studies (Reference 20) made with THINC-IV show that it is adequate to use the 5% reduction in inlet flow to the hot assembly for a loop out of service based on the experimental data in References 24 and 25. VIPRE-01 was demonstrated to be equivalent to THINC-IV in Reference 92.

The effect of the total flow rate on the inlet velocity distribution was studied in the experiments of Reference 23. As was expected, on the basis of the theoretical analysis, no significant variation could be found in inlet velocity distribution with reduced flow rate.

4.4.4.2.3 Empirical Friction Factor Correlations

Empirical friction factor correlations are used in the VIPRE-01 computer code (described in Subsection 4.4.4.5).

The friction factor in the axial direction, parallel to the fuel rod axis, is evaluated using a correlation for the smooth tube (Reference 92). The effect of two-phase flow on the friction loss is expressed in terms of the single-phase friction pressure drop and a two phase friction multiplier. The multiplier is calculated directly using the homogeneous equilibrium flow model.

The flow in the lateral directions, normal to the fuel rod axis, views the reactor core as a large tube bank. Thus, the lateral friction factor proposed by Idel'chik (Reference 26) is applicable. This correlation is of the form:

$$F_L = A\ Re_L^{-0.2} \qquad (4.4\text{-}11)$$

where:

A is a function of the rod pitch and diameter as given in Reference 26.

Re_L is the lateral Reynolds number based on the rod diameter.

Extensive comparisons of VIPRE-01 predictions using these correlations to THINC-IV predictions are given in Reference 92, and verify the applicability of these correlations in PWR design.

4.4.4.3 Influence of Power Distribution

The core power distribution which is largely established at beginning-of-life by fuel enrichment, loading pattern, and core power level is also a function of variables such as control rod worth and position, and fuel depletion throughout lifetime. Radial power distributions in various planes of the core are often illustrated for general interest, however, the core radial enthalpy rise distribution as determined by the integral of power up each channel is of greater importance for DNB analyses. These radial power distributions, characterized by $F_{\Delta H}^N$ (defined in

Subsection 4.3.2.2.1) as well axial heat flux profiles are discussed in the following two sections.

4.4.4.3.1 Nuclear Enthalpy Rise Hot Channel Factor, $F^N_{\Delta H}$

Given the local power density q' (kW/ft) at a point x, y, z in a core with N fuel rods and height H,

$$F^N_{\Delta H} = \frac{\text{hot rod power}}{\text{average rod power}} = \frac{\text{MAX} \int_o^H q'(x_o, y_o, z)\, dz}{\frac{1}{N} \sum_{\text{all rods}} \int_o^H q'(x, y, z)\, dz} \qquad (4.4\text{-}12)$$

where x_o, y_o are the position coordinates of the hot rod.

The way in which $F^N_{\Delta H}$ is used in the DNB calculation is important. The location of minimum DNBR depends on the axial profile and the value of DNBR depends on the enthalpy rise to that point. Basically, the maximum value of the rod integral is used to identify the most likely rod for minimum DNBR. An axial power profile is obtained which, when normalized to the value of $F^N_{\Delta H}$, recreates the axial heat flux along the limiting rod. The surrounding rods are assumed to have the same axial profile with rod average powers which are typical distributions found in hot assemblies. In this manner, worst case axial profiles can be combined with worst case radial distributions for reference DNB calculations.

It should be noted again that $F^N_{\Delta H}$ is an integral and is used as such in DNB calculations. Local heat fluxes are obtained by using hot channel and adjacent channel explicit power shapes which take into account variations in horizontal power shapes throughout the core. The sensitivity of the DNB calculations to radial power shapes is discussed in Reference 20. The VIPRE-01 analyses were based on the design axial power distributions discussed in Reference 20.

For operation at a fraction P of full power, the design $F^N_{\Delta H}$ used in DNB calculations is given by:

$$F^N_{\Delta H} = 1.635\ (1 + 0.3\ (1\text{-}P)) \quad \text{(VANTAGE 5/VANTAGE+ fuel)}$$

where P is fraction of full power.

The permitted relaxation of $F^N_{\Delta H}$ is included in the DNB protection setpoints and allows radial power shape changes with rod insertion to the insertion limits (Reference 68), thus allowing greater flexibility in the nuclear design.

The Revised Thermal Design Procedure (RTDP) used in the Thermal and Hydraulic evaluations for Byron/Braidwood allows the use of a nominal $F^N_{\Delta H}$ value. This is the 1.635 value for $F^N_{\Delta H}$ given above. The difference between the nominal $F^N_{\Delta H}$ value of 1.635 (VANTAGE 5/VANTAGE+) and the design $F^N_{\Delta H}$ value of 1.70 (VANTAGE 5/VANTAGE+) is statistically accounted for in the design limit DNBR values as explained in Reference 89.

4.4.4.3.2 Axial Heat Flux Distributions

As discussed in Subsection 4.3.2.2, the axial heat flux distribution can vary as a result of rod motion, power change, or due to a spatial xenon transient which may occur in the axial direction. Consequently, it is necessary to measure the axial power imbalance by means of the excore nuclear detectors (as discussed in Subsection 4.3.2.2) and protect the core from excessive axial power imbalance.

The reference axial shape used in establishing core DNB limits (that is overtemperature ΔT protection system setpoints) is a chopped cosine with a peak to average value of 1.70. The reactor trip system provides automatic reduction of the trip setpoints on excessive axial power imbalance. To determine the magnitude of the setpoint reduction, the reference shape is supplemented by other axial shapes skewed to the bottom and top of the core.

The course of those accidents in which DNB is a concern is analyzed in Chapter 15.0 assuming that the protection setpoints have been set on the basis of these shapes. In many cases the axial power distribution in the hot channel changes throughout the course of the accident due to rod motion, coolant temperature and power level changes.

4.4.4.4 Core Thermal Response

A general summary of the steady-state thermal-hydraulic design parameters is provided in Table 4.4-1 for all loops in operation.

As stated in Subsection 4.4.1, the design bases of the application are to prevent DNB and to prevent fuel melting for Condition I and II events. The protective systems described in Chapter 7.0 are designed to meet these bases. The response of the core to Condition II transients is given in Chapter 15.0.

4.4.4.5 Analytical Techniques

4.4.4.5.1 Core Analysis

The objective of reactor core thermal design is to determine the maximum heat removal capability in all flow subchannels and show that the core safety limits, as presented in the Technical Specifications, are not exceeded, including the effects of engineering and nuclear hot channel factors. The thermal design considers local variations in dimensions, power generation, flow redistribution, and mixing.

Prior to the MUR power uprate to 3645 MWt, the THINC-IV code (References 20, 51, and 88) was used for the core thermal design. Commencing with the MUR power uprate, the VIPRE-01 code is used for the core thermal design. VIPRE-01 is a three-dimensional subchannel code that has been developed to account for hydraulic and nuclear effects on the enthalpy rise in the core and hot channels (Reference 93). VIPRE-01 modeling of a PWR core is based on one-pass modeling approach (Reference 92). In the one-pass modeling, hot channels and their adjacent channels are modeled in detail, while the rest of the core is modeled simultaneously on a relatively coarse mesh. The behavior of the hot assembly is determined by superimposing the power distribution upon inlet flow distribution while allowing for flow mixing and flow distribution between flow channels. Local variations in fuel rod power, fuel rod and pellet fabrication, and turbulent mixing are also considered in determining conditions in the hot channels. Conservation equations of mass, axial and lateral momentum, and energy are solved for the fluid enthalpy, axial flow rate, lateral flow, and pressure drop.

4.4.4.5.2 Steady-State Analysis

The VIPRE-01 core model as approved by the NRC, Reference 92, is used with the applicable DNB correlations to determine DNBR distributions along the hot channels of the reactor core under all expected operating conditions. The VIPRE-01 code is described in detail in Reference 93, including discussions on code validation with experimental data. The VIPRE-01 modeling method is described in Reference 92, including empirical models and correlations used.

The use of a uniform pressure gradient in the thermal-hydraulic design of Westinghouse PWRs has been addressed and approved for application in the subchannel analysis.

The effect of crud on the flow and enthalpy distribution in the core is not directly accounted for in the VIPRE-01 evaluations. However, conservative treatment by the VIPRE-01 modeling method has been demonstrated to bound this effect in DNBR calculations (Reference 92). The VIPRE-01 model has been demonstrated in Reference 92 to be equivalent to the THINC-IV code for steady-state analyses.

Estimates of uncertainties are discussed in Subsection 4.4.2.9.

4.4.4.5.3 Experimental Verification

Extensive experimental verification of VIPRE-01 is presented in Reference 93.

The VIPRE-01 analysis is based on a knowledge and understanding of the heat transfer and hydrodynamic behavior of the coolant flow and the mechanical characteristics of the fuel elements.

The use of the VIPRE-01 analysis provides a realistic evaluation of the core performance and is used in the thermal analyses as described above.

4.4.4.5.4 Transient Analysis

VIPRE-01 is capable of transient DNB analysis. The conservation equations in the VIPRE-01 code contain the necessary accumulation terms for transient calculations. The input description can include one or more of the following time dependent arrays:

1. Inlet flow variation,
2. Core heat flux variation,
3. Core pressure variation,
4. Inlet temperature or enthalpy variation.

At the beginning of the transient, the calculation procedure is carried out as in the steady state analysis. The time is incremented by an amount determined either by the user or by the time step control options in the code itself. At each new time step the calculations are carried out with the addition of the accumulation terms which are evaluated using the information from the previous time step. This procedure is continued until a preset maximum time is reached.

At time intervals selected by the user, a complete description of the coolant parameter distributions as well as DNBR is printed out. In this manner the variation of any parameter with time can be readily determined.

The methods for evaluating fuel rod thermal response are described in Section 15.0.11.

Transient conditions are calculated by safety analysis codes, as described in Chapter 15, and presented in terms of a fractional value compared to the steady state core conditions at time zero for the transient. For the DNB analysis of transients for which the effects of fuel stored energy and heat conduction are significant, e.g., loss of flow and locked rotor events, the transient capabilities of VIPRE-01 are used.

For the DNB analysis of slower transients, VIPRE-01 is used to determine the minimum DNBR by means of a steady-state calculation. Appropriate selection criteria are used to determine the limiting statepoint time in the transient for the steady-state calculation. This statepoint is then analyzed using a VIPRE-01 steady-state calculation to assure DNBR values in compliance with the limit for conformance to the design criterion. Several additional statepoints may be investigated before and after the time of this limiting statepoint to assure that the minimum DNBR time as been determined.

4.4.4.6 Hydrodynamic and Flow Power Coupled Instability

Boiling flows may be susceptible to thermohydrodynamic instabilities (Reference 70). These instabilities are undesirable in reactors since they may cause a change in thermohydraulic conditions that may lead to a reduction in the DNB heat flux relative to that observed during a steady flow condition or to undesired forced vibrations of core components. Therefore, a thermohydraulic design criterion was developed which states that modes of operation under Condition I and II events shall not lead to thermohydrodynamic instabilities.

Two specific types of flow instabilities are considered for Westinghouse PWR operation. These are the Ledinegg or flow excursion type of static instability and the density wave type of dynamic instability.

A Ledinegg instability involves a sudden change in flow rate from one steady state to another. This instability occurs (Reference 70) when the slope of the reactor coolant system pressure drop-flow rate curve $(\partial \Delta P/\partial G|_{internal})$ becomes algebraically smaller than the loop supply (pump head) pressure drop-flow rate curve $(\partial \Delta P/\partial G|_{external})$. The criterion for stability is, thus, $(\partial \Delta P/\partial G|_{internal} > \partial \Delta P/\partial G|_{external})$. The Westinghouse pump head curve has a negative slope $(\partial \Delta P/\partial G|_{external} < 0)$ whereas the reactor coolant system pressure drop-flow curve has a positive slope $(\partial \Delta P/\partial G|_{internal} > 0)$ over the Condition I and Condition II operational ranges. Thus, the Ledinegg instability will not occur.

The mechanism of density wave oscillations in a heated channel has been described by Lahey and Moody (Reference 71). Briefly, an inlet flow fluctuation produces an enthalpy perturbation. This perturbs the length and the pressure drop of the single phase region and causes quality or void perturbations in the two-phase regions which travel up the channel with the flow. The quality and length perturbations in the two-phase region create two-phase pressure drop perturbations. However, since the total pressure drop across the core is maintained by the characteristics of the fluid system external to the core, then the two-phase pressure drop perturbation feeds back to the single phase region. These resulting perturbations can be either attenuated or self-sustained.

A simple method has been developed by Ishii (Reference 72) for parallel closed channel systems to evaluate whether a given condition is stable with respect to the density wave type of dynamic instability. This method had been used to assess the stability of typical Westinghouse reactor designs (References 73,74,75), under Condition I and II operation. The results indicate that a large margin to density wave instability exists, e.g., increases on the order of 150% of rated reactor power would be required for the predicted inception of this type of instability.

The application of the method of Ishii (Reference 72) to Westinghouse reactor designs is conservative due to the parallel open channel feature of Westinghouse PWR cores. For such cores, there is little resistance to lateral flow leaving the flow channels of high power density. There is also energy transfer from channels of high power density to lower power density channels. This coupling with cooler channels has led to the opinion that an open channel configuration is more stable than the above closed channel analysis under the same boundary conditions. Flow stability tests (Reference 76) have been conducted where the closed channel systems were shown to be less stable than when the same channels were cross connected at several locations. The cross-connections were such that the resistance to channel to channel cross flow and enthalpy perturbations would be greater than that which would exist in a PWR core which has a relatively low resistance to cross flow.

Flow instabilities which have been observed have occurred almost exclusively in closed channel systems operating at low pressure relative to the Westinghouse PWR operating pressures. Kao, Morgan and Parker (Reference 77) analyzed parallel closed channel stability experiments simulating a reactor core flow. These experiments were conducted at pressures up to 2200 psia. The results showed that for flow and power levels typical of power reactor conditions, no flow oscillations could be induced above 1200 psia.

Additional evidence that flow instabilities do not adversely affect thermal margin is provided by the data from the rod bundle DNB tests. Many Westinghouse rod bundles have been tested over wide ranges of operating conditions with no evidence of premature DNB or of inconsistent data which might be indicative of flow instabilities in the rod bundle.

In summary, it is concluded that thermohydrodynamic instabilities will not occur under Condition I and II modes of operation for Westinghouse PWR reactor designs. A large power margin exists to predicted inception of such instabilities. Analysis has been performed which shows that minor plant to plant differences in Westinghouse reactor designs such as fuel assembly arrays, core power to flow ratios, fuel assembly length, etc. will not result in gross deterioration of the above power margins.

4.4.4.7 Fuel Rod Behavior Effects from Coolant Flow Blockage

Coolant flow blockages can occur within the coolant channels of a fuel assembly or external to the reactor core. The effects of fuel assembly blockage within the assembly on fuel rod behavior are more pronounced than external blockages of the same magnitude. In both cases the flow blockages cause local reductions in coolant flow. The amount of local flow reduction, where it occurs in the reactor, and how far along the flow stream the reduction persists are considerations which will influence the fuel rod behavior. The effects of coolant flow blockages in terms of maintaining rated core performance are determined both by analytical and experimental methods. The experimental data are usually used to augment analytical tools such as computer programs similar to the THINC-IV or VIPRE-01 codes. Inspection of the DNB correlations (Subsection 4.4.2.2) shows that the predicted DNBR is dependent upon the local values of quality and mass velocity.

The VIPRE-01 code is capable of predicting the effects of local flow blockages on DNBR within the fuel assembly on a subchannel basis, regardless of where the flow blockage occurs. In Reference 93, it is shown that for a fuel assembly similar to the Westinghouse design, VIPRE-01 accurately predicts the flow distribution within the fuel assembly when the inlet nozzle is completely blocked. Full recovery of the flow was found to occur about 30 inches downstream of the blockage. With the reactor operating at the nominal full power conditions specified in Table 4.4-1, the effects of an increase in enthalpy and decrease in mass velocity in the lower portion of the fuel assembly would not result in the reactor reaching the design DNBR specified in Subsection 4.4.1.1.

From a review of the open literature, it is concluded that flow blockage in "open lattice cores" similar to the Westinghouse cores cause flow perturbations which are local to the blockage. For instance, A. Ohtsubo et al. (Reference 78) show that the mean bundle velocity is approached asymptotically about 4 inches downstream from a flow blockage in a single flow cell. Similar results were also found for 2 and 3 cells completely blocked. P. Basmer, et al., (Reference 79) tested an open lattice fuel assembly in which 41 percent of the subchannels were completely blocked in the center of the test bundle between spacer grids. Their results show the stagnant zone behind the flow blockage essentially disappears after 1.65 L/De or about 5 inches for their test bundle. They also found that leakage flow through the blockage tended to shorten the stagnant zone or, in essence, the complete recovery length. Thus, local flow blockages within a fuel assembly have little effect on subchannel enthalpy rise. The reduction in local mass velocity is then the main parameter which affects the DNBR. If the plants were operating at full power and nominal steady state conditions as specified in Table 4.4-1, a reduction in local mass velocity greater than 50% (VANTAGE 5/VANTAGE+ fuel) would be required to reduce the DNBR to the design DNBR. The above

mass velocity effect on the DNB correlation was based on the assumption of fully developed flow along the full channel length. In reality, a local flow blockage is expected to promote turbulence and thus would likely not effect DNBR at all.

Coolant flow blockages induce local crossflows as well as promote turbulence. Fuel rod behavior is changed under the influence of a sufficiently high crossflow component. Fuel rod vibration could occur, caused by this crossflow component, through vortex shedding or turbulent mechanisms. If the crossflow velocity exceeds the limit established for fluid elastic stability, large amplitude whirling results. The limits for a controlled vibration mechanism are established from studies of vortex shedding and turbulent pressure fluctuations. The crossflow velocity required to exceed fluid elastic stability limits is dependent on the axial location of the blockage and the characterization of the crossflow (jet flow or not). These limits are greater than those for vibratory fuel rod wear. Crossflow velocity above the established limits can lead to mechanical wear of the fuel rods at the grid support locations. Fuel rod wear due to flow induced vibration is considered in the fuel rod fretting evaluation (Section 4.2).

4.4.5 Testing and Verification

4.4.5.1 Tests Prior to Initial Criticality

A reactor coolant flow test is performed following fuel loading, but prior to initial criticality. Coolant loop pressure drop data are obtained in this test. These data, in conjunction with coolant pump performance information, determine the coolant flow rates at reactor operating conditions. This test verifies that proper coolant flow rates have been used in the core thermal and hydraulic analysis.

4.4.5.2 Initial Power and Plant Operation

Core power distribution measurements are made at several core power levels (see Chapter 14.0). These tests are used to ensure that conservative peaking factors are used in the core thermal and hydraulic analysis.

Additional demonstration of the overall conservatism of the THINC analysis was obtained by comparing THINC predictions to incore thermocouple measurements (Reference 80). These measurements were performed on the Zion reactor. No further in-reactor testing is planned. VIPRE-01 was demonstrated to be equivalent to the THINC code in Reference 92.

4.4.5.3 Component and Fuel Inspections

Inspections performed on the manufactured fuel are delineated in Subsection 4.2.4. Fabrication measurements critical to thermal and hydraulic analysis are obtained to verify that the

hot channel factors engineering uncertainty in the design analyses (Subsection 4.4.2.2.4) are met.

4.4.6 Instrumentation Requirements

4.4.6.1 Incore Instrumentation

Instrumentation is located in the core so that by correlating movable neutron detector information with fixed thermocouple information, radial, axial, and azimuthal core characteristics may be obtained for all core quadrants.

The incore instrumentation system is comprised of thermocouples, positioned to measure fuel assembly coolant outlet temperatures at preselected positions, and fission chamber detectors positioned in guide thimbles which run the length of selected fuel assemblies to measure the neutron flux distribution. Figure 4.4-10 shows the number and location of instrumented assemblies in the core.

The core-exit thermocouples provide a backup to the flux monitoring instrumentation for monitoring power distribution. The routine, systematic, collection of thermocouple readings by the operator provides a data base. From this data base, abnormally high or abnormally low readings, quadrant temperature tilts, or systematic departures from a prior reference map can be deduced.

The movable incore neutron detector system would be used for more detailed mapping if the thermocouple system were to indicate an abnormality. These two complementary systems are more useful when taken together than either system alone would be. The incore instrumentation system is described in more detail in Section 7.7.

The incore instrumentation is provided to obtain data from which fission power density distribution in the core, coolant enthalpy distribution in the core, and fuel burnup distribution may be determined.

BEACON uses the incore flux detector measurements, core-exit thermocouples and excore detectors to perform the local calibration of the SPNOVA three dimensional power distributions. The thermocouple assembly power measurement is periodically calibrated to the incore-measured assembly power. The incore detectors and core-exit thermocouples do not provide complete coverage of the core and BEACON employs a two-dimensional spline fit to interpolate/extrapolate these measurements to the unmonitored assemblies. Adding a sinusoidal component to the SPNOVA calculated axial power shape makes this adjustment. The SPNOVA excore axial offset is determined by an appropriate weighting of the peripheral assembly powers. Beside incore fluxmap data, thermocouple data and excore data, BEACON online continuous monitoring power distribution system also uses inputs from reactor coolant system cold leg temperature, control rod position, and power.

4.4.6.2 Overtemperature and Overpower ΔT Instrumentation

The overtemperature ΔT trip protects the core against low DNBR. The overpower ΔT trip protects against excessive power (fuel rod rating protection).

As discussed in Chapter 7.0, factors included in establishing the overtemperature ΔT and overpower ΔT trip setpoints includes the reactor coolant temperature in each loop and the axial distribution of core power through the use of the two section excore neutron detectors.

4.4.6.3 Instrumentation to Limit Maximum Power Output

The outputs of the three ranges (source, intermediate, and power) of detectors, with the electronics of the nuclear instruments, are used to limit the maximum power output of the reactor within their respective ranges.

At Braidwood, there are six radial locations containing a total of eight neutron flux detectors installed around the reactor in the primary shield, with two proportional counters for the source range installed on opposite "flat" portions of the core containing the primary startup sources at an elevation approximately one quarter of the core height. Two compensated ionization chambers for the intermediate range, located in the same instrument wells and detector assemblies as the source range detectors, are positioned at an elevation corresponding to one half of the core height; four dual section uncompensated ionization chamber assemblies for the power range are installed vertically at the four corners of the core and located equidistant from the reactor vessel at all points and, to minimize neutron flux pattern distortions, within one foot of the reactor vessel. At Byron, there are six radial locations containing a total of six neutron detectors installed around the reactor in the primary shield, with two detector assemblies containing two fission chambers positioned at 90° and 270° for source and intermediate range monitoring, at elevations corresponding to one half the core height. These detectors are also used for post accident monitoring input. Four dual section uncompensated ionization chamber assemblies for the power range are installed vertically at the four corners of the core and located equidistant from the reactor vessel at all points and, to minimize neutron flux pattern distortions, within one foot of the reactor vessel.

Each power range detector provides two signals corresponding to the neutron flux in the upper and in the lower sections of a core quadrant. The three ranges of detectors are used as inputs to monitor neutron flux from a completely shutdown condition up to 120% of full power with the capability of recording overpower excursions up to 200% of full power.

The output of the power range channels is used for:

a. The rod speed control function,

b. To alert the operator to an excessive power unbalance between the quadrants,

c. Protect the core against rod ejection accidents, and

d. Protect the core against power distributions resulting from dropped rods.

e. Input to Power Distribution Monitoring System (PDMS) via process computer.

Details of the neutron detectors and nuclear instrumentation design and the control and trip logic are given in Chapter 7.0. The limits on neutron flux operation are given in the Technical Specifications. Trip setpoints are given in TRM 2.0.a.

4.4.6.4 Loose Parts Monitoring System

The loose parts monitoring system is a monitoring, alarm, and diagnostics system, which provides real-time information to the operator on a variety of mechanical vibration phenomena which may occur in the reactor coolant system. This approach enables operating personnel to be continuously informed of the vibration levels of key portions of the operating nuclear steam system, to be notified if preselected alarm limits have been exceeded, and

to have sufficient data and additional criteria to analyze the data, and make an on-the-spot decision as to the severity of an alarm condition.

The loose parts monitoring system detects and annunciates unusual noises that indicate a metallic loose part. The system is provided with active and passive sensing channels. The active channels include a signal conditioning and alarm module. The passive channels must be patched to a signal conditioning and alarm module in place of an active channel for more precise determination of noise locations. All active and passive sensors and their respective preamplifiers are located inside the containment building, and all signal conditioning and monitoring/alarms for the active channels are located in cabinets in the auxiliary electrical equipment room. Both passive and active channels are wired to the cabinets by individual twisted shielded-pair cables. Each active channel has its own loose parts detector module, which conditions the signal and provides alarm signals when warranted. Each conditioned signal is routed to the data handling system for analysis and recording, and the alarm outputs are routed to a common master module, which annunciates the alarms.

4.4.6.4.1 Containment Building Equipment

Accelerometers are used as sensors and are located on equipment as follows:

a. Two Reactor vessel head studs,

b. Two locations on reactor vessel bottom,

c. Two locations on lower plenum-steam generator A, B, C and D.

d. Cooling line to reactor coolant pump A, B, C and D,

e. Lower tap-narrow range level steam generator A, B, C and D, and

f. Upper tap-narrow range level steam generator A, B, C and D.

The containment normal environmental conditions which apply to the containment building located portions of the loose parts monitoring system are included in Table 3.11-2.

The low-noise coaxial cable is used to connect the output of the accelerometer to the remote charge preamplifier. The cable can withstand temperatures in excess of 500°F under a high radiation environment.

Remote charge preamplifiers are used as impedance converters to convert the high output impedance of the accelerometers, normally more than 10,000 megohms, to less than 2 ohms. The output of the remote charge preamplifier is transmitted to the loose parts monitoring panel by twisted shielded-pair cable of 16 AWG size wire.

4.4.6.4.2 Auxiliary Electrical Equipment Room Equipment

Signal-conditioning amplifiers: Each active channel contains a modular, solid-state, amplifier, which provides the power supply voltage to the remote preamplifier and conditions the voltage output signal from the preamplifier to the higher levels required for monitoring and recording.

The alarm module is a modular, solid-state, logic module designed to accept alarm inputs from signal conditioning amplifiers. The module provides indication of the first channel alarming and a time discriminator to reduce the false alarm rate of high alarms. Visual (LED) and audible alarms are provided to alert the operator to unusual occurrences.

The data handling and recording equipment provides selection, routing, and recording of conditioned signals.

An audio monitor allows audio interpretation of the accelerometer signals. Audio interpretation has proved to be a valuable diagnostic aid for trained personnel since the accelerometers act essentially as very sensitive microphones. Each channel input signal is selected through a switch.

4.4.6.4.3 Basis for Alarm Settings

Metal-to-metal impacts resulting from loose parts excite the preferential ringing modes of the nuclear steam supply (NSS) components. The modes are typically between 1 and 10 kHz and are easily detected by externally mounted accelerometers.

After installation of a strategically located accelerometer array, the overall and individual channel characteristics of the accelerometer system will be determined before operational monitoring. These overall characteristics include the frequency response and resonance modes of the structures, the accelerometer mounting characteristics, and gain normalization of the overall system. In addition, the acoustical transport times (delay times) between each accelerometer pair will be determined. Once operation of the NSS has commenced, each accelerometer channel will exhibit its own particular and unique frequency spectrum. This frequency

signature, or normal background, results from such sources as primary flow turbulence, reactor coolant pump vibrations, feedwater and steam flow turbulence, structural responses of NSS components and secondary plant equipment, and other localized noise sources. In addition, airborne noises from fans and other equipment contribute to the overall background. To achieve more reliable detection of unusual noises indicative of metal-to-metal impact, a careful spectral comparison of the measured local background will be performed.

The anticipated major sources of internal and external noise are as follows:

a. fluidic turbulent flow,

b. control rod motion,

c. two-phase flow in the steam generators,

d. electric motor operation, including reactor coolant pump motors, and

e. fans and ventilation ducts.

Based on the spectral comparison, the broad-band signal is bank-limited to the portion of the spectra that maximizes the signal-to-noise ratio. This bank-limited signal, which in most cases eliminates or minimizes the contributions of normal acoustical background, is then monitored for large amplitude increases. To reduce spurious alarms, the band-limited signal is time integrated before the amplitude detector. This time integration is based on the characteristic that the most damaging loose parts will normally exhibit multiple impacts over a period of less than 1 second. Such multiple impacts are caused by entrapment of the metallic part in the normally encountered turbulent flow. In this fashion, by time integrating the band-limited signal, single events of low amplitude are not annunciated. However, high amplitude single events are annunciated since the structure will continue to ring longer than the integration time of the detector.

4.4.6.4.4 Operability After Operational Basis Earthquake

The loose parts monitoring system is not qualified for a seismic condition, but it is designed and built to industry standard design practices, which usually permits significant vibration effects without damage and it is adequate for the function the system is designed to fulfill. This system is basically the same as loose parts monitoring systems installed and operating at several other nuclear power plants.

A seismic qualification program has been prepared for the Byron/Braidwood Stations LPMS. The qualification demonstrates the capability of the LPMS to meet the seismic requirements of Regulatory Guide 1.133.

4.4.6.4.5 Operating Procedures

The normal operating condition of the loose parts monitoring system is one of real-time continuous surveillance. In the absence of alarms, periodic trending data should be obtained. These data comprise range settings for all charge amplifiers and meter readings for loose parts monitoring.

This page was intentionally deleted.

This page was intentionally deleted.

This page was intentionally deleted.

Channel checks and functional tests are performed automatically to verify channel operability in the automatic mode. An operator alarm is annunciated for abnormal conditions. Audio monitoring is also provided to detect the presence of loose parts. If a signal indicates the presence or possibility of a loose part, station personnel can actuate the data acquisition system to obtain data for further evaluation. For an additional functional test, the operator can simulate a loose part impact into each channel to test its alarm function. On a periodic basis, background noise can be measured to determine if the background noise is too high to descern a valid impact or if the channel may falsely indicate the presence of a loose part. On sensing a valid loose part, the system will annunciate an impact alarm and automatically start recording the event in the automatic mode.

4.4.6.4.6 Testing

Baseline background data for all 24 loose parts monitoring system (LPMS) sensors will be obtained during the heatup, at temperature, and cooldown phases of integrated hot functional testing of the NSSS.

The operating conditions for the LPMS are the normal containment and control room environments. System sensitivity will be measured during the system preoperational test. Alarm settings will be derived from the baseline background data.

The system sensitivity of the type loose parts monitoring system (LPMS) used for Byron/Braidwood Stations has been demonstrated and certified in tests at an operational nuclear power plant. Test results indicate that a sensitivity 0.1 ft-lb within 3 feet of a sensor is within the capability of the monitoring system. At an impact level of 0.5 ft-lb a signal to noise ratio of 6 can be maintained for normal plant operation conditions.

Subsequent to final preoperational tests and calibration, a comprehensive report will be prepared and submitted per Regulatory Guide 1.133.

4.4.6.4.7 Training

The training program for the appropriate plant personnel will include noise and vibration theory, system equipment descriptions, data processing, and diagnostic information. Operator training will be conducted initially by means of a vendor-supplied program. Subsequent training will be accomplished within the normal training program at the stations. A description of the stations' training programs are provided in Section 13.2. Recordkeeping requirements are provided in the company Quality Assurance Topical Report.

4.4.7 Reload Safety Evaluations

The analyses and evaluations presented in Section 4.4 establish the capability of the reactor to perform its safety function throughout its design lifetime under all normal modes of operation.

The methodology employed for the reload safety evaluation assures the above.

The goal of the reload safety evaluation is to confirm the validity of the existing safety analysis.

The existing safety analysis is defined as the reference safety analysis and is

intended to be valid for all plant cycles. Thus, safety analysis input parameter values are selected to bound the values expected in all subsequent cycles. This bounding analysis concept is the key to the Westinghouse reload safety analysis methodology. When all reload safety related parameters for a given accident are bounded, the reference safety analysis is valid. On the other hand, when a reload parameter is not bounded, further evaluation is provided to confirm that the margin of safety as defined in the basis for any Technical Specification is not reduced. This reload safety evaluation methodology is applied whenever the input parameter values for a reference safety analysis are available.

The Westinghouse reload safety evaluation methodology consists of:

a. A systematic evaluation to determine whether the reload parameters are bounded by the values used in the reference safety analysis.

b. A determination of the effects on the reference safety analysis when a reload parameter is not bounded to ensure that specified design bases are met.

If a potential regulatory review or the need for a change to the plant Technical Specifications is identified, the requirements of 10 CFR 50.59 are applied.

4.4.8 References

1. Motley, F. E., Hill, K. W., Cadek, F. F. and Shefcheck, J., "New Westinghouse Correlation WRB-1 for Predicting Critical Heat Flux in Rod Bundles with Mixing Vane Grids," WCAP-8762-P-A (Proprietary) and WCAP-8763-A (Non-Proprietary), July, 1984.

2. Letter from J. F. Stolz (NRC) to C. Eicheldinger (Westinghouse); Subject: Staff Evaluation of WCAP-7956, WCAP-8054, WCAP-8567 and WCAP-8762, April 19, 1978.

3. Chelemer, H., Boman, L. H. and Sharp, D. R., "Improved Thermal Design Procedure," WCAP-8567-P-A, (Proprietary) and WCAP-8568-A, (Non-Proprietary), February 1989.

4. Christensen, J. A., Allio, R. J. and Biancheria, A., "Melting Point of Irradiated UO_2," WCAP-6065, February, 1965.

5. Davidson, S. L., Motley, F. E., Lee, Y. C., Bogard, T., Bryan, W. J., "Verification Testing and Analyses of the 17x17 Optimized Fuel Assembly," WCAP-9401-P-A, (Proprietary) and WCAP-9402-A (Non-Proprietary), August, 1981.

6. L. S. Tong, "Boiling and Critical Heat Flux," TID-25887, 1972.

7. F. E. Motley, F. F. Cadek, "DNB Test Results for New Mixing Vane Grids (R)," WCAP-7695-P-A (Westinghouse Proprietary) and WCAP-7958-A (Non-Proprietary), January, 1975.

8. F. E. Motley, F. F. Cadek, "Application of Modified Spacer Factor to L Grid Typical and Cold Wall Cell DNB," WCAP-7988-P-A (Westinghouse Proprietary), and WCAP-8030-A (Non-Proprietary), January, 1975.

9. F. E. Motley, A. H. Wenzel, F. F. Cadek, "Critical Heat Flux Testing of 17 x 17 Fuel Assembly Geometry with 22-Inch Grid Spacing," WCAP-8536, (Westinghouse Proprietary) and WCAP-8537 (Non-Proprietary), May, 1975.

10. K. W. Hill, F. E. Motley, F. F. Cadek, A. H. Wenzel, "Effect of 17 x 17 Fuel Assembly Geometry on DNB," WCAP-8296-P-A (Westinghouse Proprietary) and WCAP-8297-A (Non-Proprietary), February, 1975.

11. L. S. Tong, "Prediction of Departure from Nucleate Boiling for an Axially Non-Uniform Heat Flux Distribution," J. Nuclear Energy, 21, 241-248, 1967.

12. H. Chelemer, J. Weisman, and L. S. Tong, "Subchannel Thermal Analysis of Rod Bundle Cores," WCAP-7015, Revision 1, January 1969.

13. F. F. Cadek, F. E. Motley, and D. P. Dominicis, "Effect of Axial Spacing on Interchannel Thermal Mixing with the R Mixing Van Grid," WCAP-7941-P-A (Proprietary), January 1975 and WCAP-7959-A, January 1975.

14. D. S. Rowe and C. W. Angle, "Crossflow Mixing Between Parallel Flow Channels During Boiling, Part II Measurements of Flow and Enthalpy in Two Parallel Channels," BNWL-371, Part 2, December 1967.

15. D. S. Rowe and C. W. Angle, "Crossflow Mixing Between Parallel Flow Channels During Boiling, Part III Effect of Spacers on Mixing Between Two Channels," BNWL-371, Part 3, January 1969.

16. J. M. Gonzalez-Santalo and P. Griffith, "Two-Phase Flow Mixing in Rod Bundle Subchannels," ASME Paper 72-WA/NE-19.

17. F. E. Motley, A. H. Wenzel, and F. F. Cadek, "The Effect of 17 x 17 Fuel Assembly Geometry on Interchannel Thermal Mixing," WCAP-8298-P-A (Proprietary), January 1975 and WCAP 8299-A, January 1975.

18. Hill, K. W., Motley, F. E. and Cadek, F. F., "Effect of Local Heat Flux Spikes on DNB in Non-Uniform Heated Rod Bundles," WCAP-8174-P-A (Proprietary) and WCAP-8202-A (Non-Proprietary), February, 1975.

19. F. F. Cadek, "Interchannel Thermal Mixing with Mixing Vane Grids," WCAP-7667-P-A (Proprietary), January 1975 and WCAP-7755-A (Non-Proprietary), January 1975.

20. L. E. Hochreiter, "Application of the THINC IV Program to PWR Design," WCAP-8054-P-A (Proprietary) and WCAP-8195-A (Non-Proprietary), February, 1989.

21. F. W. Dittus and L. M. K. Boelter, "Heat Transfer in Automobile Radiators of the Tubular Type," Calif. Univ. Publication in Eng., 2, No. 13, 443461, 1930.

22. J. Weisman, "Heat Transfer to Water Flowing Parallel to Tube Bundles," Nucl. Sci. Eng., 6, 78-79, 1959.

23. J. R. S. Thom et al., "Boiling in Sub-cooled Water During Flowup Heated Tubes or Annuli," Prc. Instn. Mech. Engrs., 180, Pt. C 226- 46, 1955-66.

24. G. Hetsroni, "Hydraulic Tests of the San Onofre Reactor Model," WCAP-3269-8, June 1964.

25. G. Hetsroni, "Studies of the Connecticut-Yankee Hydraulic Model," NYO-3250-2, June 1965.

26. I. E. Idel'chik, "Handbook of Hydraulic Resistance," AEC-TR-6630, 1960.

27. L. F. Moody, "Friction Factors for Pipe Flow," Transaction of the American Society of Mechanical Engineers, 66, 671-684, 1944.

28. Not used.

29. Not used.

30. Not used.

31. G. Kjaerheim and E. Rolstad, "In Pile Determination of UO Thermal Conductivity, Density Effects and Gap Conductance," HPR-80, December 1967.

32. G. Kjaerheim, "In-Pile Measurements of Centre Fuel Temperatures and Thermal Conductivity Determination of Oxide Fuels," paper lFA-175 presented at the European Atomic Energy Society Symposium on Performance Experience of Water-Cooled Power Reactor Fuel, Stockholm, Sweden, October 21-22, 1969.

33. I. Cohen, G. Lustman, and D. Eichenberg, "Measurement of the Thermal Conductivity of Metal-Clad Uranium Oxide Rods During Irradiation," WAPD-228, 1960.

34. D. J. Clough, and J. B. Sayers, "The Measurement of the Thermal Conductivity of UO_2 under Irradiation in the Temperature Range 150°-1600°C," AERE-R24690, UKAEA. Research Group, Harwell, December 1964.

35. J. P. Stora et al., "Thermal Conductivity of Sintered Uranium Oxide under In-Pile Conditions," EURAEC-1095, 1964.

36. I. Devold, "A Study of the Temperature Distribution in UO Reactor Fuel Elements," AE-318, Aktiebolaget Atomenergi, Stockholm, Sweden, 1968.

37. M. G. Balfour, J. A. Christensen, and H. M. Ferrari, "In-Pile Measurement of UO_2 Thermal Conductivity," WCAP-2923, 1966.

38. V. C Howard and T. G. Gulvin, "Thermal Conductivity Determinations on Uranium Dioxide by a Radial Flow Method," UKAEA IG-Report 51, November 1960.

39. C. F. Lucks and H. W. Deem, "Thermal Conductivity and Electrical Conductivity of UO_2," in Progress Reports Relating to Civilian Applications, BMI-1448 (Rev.) for June 1960; BMI-1489 (Rev.) for December 1960 and BMI-1518 (Rev.) for May 1961.

40. J. L. Daniel, J. Matolich, Jr., H. W. Deem, "Thermal Conductivity of UO_2," HW-69945, September 1962.

41. A. D. Feith, "Thermal Conductivity of UO_2 by a Radial Heat Flow Method," TID-21668, 1962.

42. J. Vogt, L. Grandell, and U. Runfors, "Determination of the Thermal Conductivity of Unirradiated Uranium Dioxide," AB Atomenergi Report RMB-527, 1964, Quoted by IAEA Technical Report Series No. 59, "Thermal Conductivity of Uranium Dioxide."

43. T. Nishijima, T. Kawada, and A. Ishihata, "Thermal Conductivity of Sintered UO_2 and $A1_2O_3$ at High Temperature," J. American Ceramic Society, 48, 31, 34, 1965.

44. J. B. Ainscough and M. J. Wheeler, "Thermal Diffusivity and Thermal Conductivity of Sintered Uranium Dioxide," in Proceedings of the Seventh Conference of Thermal Conductivity, p.467, National Bureau of Standards, Washington, 1968.

45. T. G. Godfrey et al., "Thermal Conductivity of Uranium Dioxide and Armco Iron by an Improved Radial Heat Flow Technique," ORNL-3556, June 1964.

46. J. P. Stora et al., "Thermal Conductivity of Sintered Uranium Oxide Under In-Pile Conditions," EURAEC-1095, August 1964.

47. A. J. Bush, "Apparatus of Measuring Thermal Conductivity to 2500°C," Westinghouse Research Laboratories Report 64-lP6-401-43, (Proprietary) February 1965.

48. R. R. Asamoto, F. L. Anselin, and A. E. Conti, "The Effect of Density on the Thermal Conductivity of Uranium Dioxide," GEAP-5493, April 1968.

49. O. L. Kruger, "Heat Transfer Properties of Uranium and Plutonium Dioxide," Paper 11-N-68F presented at the Fall meeting of Nuclear Division of the American Ceramic Society, Pittsburgh, September 1968.

50. J. M. Hellman (Ed.), "Fuel Densification Experimental Results and Model for Reactor Application," WCAP-8218-P-A (Proprietary) March 1975 and WCAP-8219-A, March 1975.

51. L. E. Hochreiter, H. Chelemer, and P. T. Chu, "THINC-IV An Improved Program for Thermal-Hydraulic Analysis of Rod Bundle Cores," WCAP-7956-A (Non-Proprietary), February, 1989.

52. R. N. Duncan, "Rabbit Capsule Irradiation of UO_2," CVTR Project, CVNA-142, June 1962.

53. R. C. Nelson et al., "Fission Gas Release from UO_2 Fuel Rods with Gross Central Melting," GEAP-4571, July 1964.

54. J. A. Gyllander, "In-Pile Determination of the Thermal Conductivity OF $U0_2$ in the Range 500-2500°C," AE-411, January 1971.

55. M. F. Lyons et al., "UO_2 Powder and Pellet Thermal Conductivity During Irradiation," GEAP-5100-1, March 1966.

56. D. H. Coplin et al., "The Thermal Conductivity of UO_2 by Direct In-reactor Measurements," GEAP-5100-6, March 1968.

57. A. S. Bain, "The Heat Rating Required to Produce Center Melting in Various UO_2 Fuels," ASTM Special Technical Publication, No. 306, pp. 30-46, Philadelphia, 1962.

58. J. P. Stora, "In-Reactor Measurements of the Integrated Thermal Conductivity of UO_2 - Effect of Porosity," Trans. ANS, 13, 137-138, 1970.

59. International Atomic Energy Agency, "Thermal Conductivity of Uranium Dioxide," Report of the Panel held in Vienna, April 1965, IAEA Technical Reports Series, No. 59, Vienna, The Agency, 1966.

60. C. G. Poncelet, "Burnup Physics of Heterogeneous Reactor Lattices," WCAP-6069, June 1965.

61. R. J. Nodvick, "Saxton Core II Fuel Performance Evaluation," WCAP-3385-56, Part II, "Evaluation of Mass Spectrometric and Radio-chemical Analyses of Irradiated Saxton Plutonium Fuel," July 1970.

62. R. A. Dean, "Thermal Contact Conductance Between UO_2 and Zircaloy 2, CVNA-127," May 1962.

63. A. M. Ross and R. L. Stoute, "Heat Transfer Coefficient Between UO_2 and Zircaloy-2," AECL-1552, June 1962.

64. F. D. Carter, "Inlet Orificing of Open PWR Cores," WCAP-9004, January 1969 (Proprietary) and WCAP-7836, January 1972 (Non-Proprietary).

65. J. Shefcheck, "Application of the THINC Program to PWR Design," WCAP-7359-L (Proprietary), August 1969 and WCAP-7838, January 1972.

66. Not used.

67. Not used.

68. A. F. McFarlane, "Power Peaking Factors," WCAP-7912-P-A (Proprietary), January 1975 and WCAP-7912-A, January 1975.

69. T. Morita et al., "Topical Report, Power Distribution Control and Load Following Procedures," WCAP-8385 (Proprietary), September 1974 and WCAP-8403, September 1974.

70. J. A. Boure, A. E. Bergles, and L. S. Tong, "Review of Two-Phase Flow Instability," Nucl. Engr. Design 25 (1973) pp. 165-192.

71. R. T. Lahey and F. J. Moody, "The Thermal Hydraulics of a Boiling Water Reactor," American Nuclear Society, 1977.

72. P. Saha, M. Ishii, and N. Zuber, "An Experimental Investigation of the Thermally Induced Flow Oscillations in Two-Phase Systems," J. of Heat Transfer, November 1976, pp. 616-622.

73. Virgil C. Summer FSAR, Docket #50-395.

74. Byron/Braidwood FSAR, Docket #50-456.

75. South Texas FSAR, Docket #50-498.

76. S. Kakac, T. N. Veziroglu, K. Akyuzlu, O. Berkol, "Sustained and Transient Boiling Flow Instabilities in a Cross-Connected Four Parallel-Channel Upflow System," Proc. of 5th International Heat Transfer Conference, Tokyo, Sept. 3-7, 1974.

77. H. S. Kao, C. D. Morgan, and W. B. Parker, "Prediction of Flow Oscillation in Reactor Core Channel," Trans. ANS, Vol. 16, 1973, pp. 212-213.

78. A. Ohtsubo, and S. Uruwashi, "Stagnant Fluid due to Local Flow Blockage," J. Nucl. Sci. Technol., 9, No. 7, 433-434, 1972.

79. P. Basmer, D. Kirsh, and G. F. Schultheiss, "Investigation of the Flow Pattern in the Recirculation Zone Downstream of Local Coolant Blockages in Pin Bundles," Atomwirtschaft, 17, No. 8, 416-417, 1972. (In German).

80. T. M. Burke, C. E. Meyer, and J. Shefcheck, "Analysis of Data from the Zion (Unit 1) THINC Verification Test," WCAP-8453-A (Non-Proprietary), May, 1976.

81. J. Skaritka (Ed.), "Fuel Rod Bow Evaluation," WCAP-8691, Rev. 1, July 1979.4

82. Not Used.

83. "Partial Response to Request Number 1 for Additional Information on WCAP-8691, Revision 1" Letter, E. P. Rahe, Jr., (Westinghouse) to J. R. Miller (NRC), NS-EPR-2515, dated October 9, 1981; "Remaining Response to Request Number 1 for Additional Information on WCAP-8691, Revision 1" Letter, E. P. Rahe, Jr., (Westinghouse) to J. R. Miller (NRC), NS-EPR-2572, dated March 16, 1982.

84. Davidson, S. L., and Kramer, W. R.; (Ed.), "Reference Core Report VANTAGE 5 Fuel Assembly," WCAP-10444-P-A, September 1985.

85. Letter from E. P. Rahe (W) to Miller (NRC) dated March 19, 1982, NS-EPR-2573, “WCAP-9500 and WCAPs 9401/9402 NRC SER Mixed Core Compatibility Items.”

86. Schueren, P., and McAtee, K. R., "Extension of Methodology for Calculating Transition Core DNBR Penalties," WCAP-11837-P-A, January, 1990.

87. Letter from C. Berlinger (NRC) to E. P. Rahe, Jr. (W) dated June 18, 1986, Request for Reduction in Fuel Assembly Burnup Limit for Calculation of Maximum Rod Bow Penalty.

88. Friedland, A. J., and Ray, S., "Improved THINC-IV Modelling for PWR Core Design," WCAP-12330-A (Proprietary), September 1991.

89. Friedland, A. J., and Ray, S., "Revised Thermal Design Procedure," WCAP-11397-P-A, April 1989.

90. Not used.

91. Beard, C. L., et.al., "BEACON – Core Monitoring and Operations Support System," WCAP-12472-P-A (Proprietary), August 1994.

92. Sung, Y. X., et al., "VIPRE-01 Modeling and Qualification for Pressurized Water Reactor Non-LOCA Thermal-Hydraulic Safety Analysis," WCAP-14565-P-A (Proprietary) / WCAP-15306-NP-A (Non-Proprietary), October 1999.

93. Stewart, C. W., et al., "VIPRE-01: A Thermal-Hydraulic Code for Reactor Core," Volume 1-3 (Revision 3, August 1989), Volume 4 (April 1987), NP-2511-CCM-A, Electric Power Research Institute.

94. Joffre, P. F. et al., "Addendum 2 to WCAP-14565-P-A, Extended Application of ABB-NV Correlation and Modified ABB-NV Correlation WLOP for PWR Low Pressure Applications," WCAP-14565-P-A Addendum 2-P-A (Proprietary) / WCAP-15306-NP-A Addendum 2-NP-A (Non-Proprietary), April 2008.

95. Braidwood Station, Units 1 and 2, and Byron Station, Units 1 and 2 – Issuance of Amendments Regarding Axial Flux Difference Technical Specifications (EPID L-2018-LLA-0098), TS Amendment No. 200 for Braidwood Station, Units 1 and 2 and TS Amendment No. 205 for Byron Station, Units 1 and 2, issued December 12, 2018.

TABLE 4.4-1

THERMAL AND HYDRAULIC DATA

THERMAL AND HYDRAULIC DESIGN PARAMETERS	
Reactor Core Heat Output, (100%), MWt	3648
Reactor Core Heat Output, 10^6 Btu/Hr	12450
Heat Generated in Fuel, %	97.4
Core Pressure, Nominal, psia	2270
Pressurizer Pressure, psia	2250
Minimum DNBR at Nominal Conditions	
Typical Flow Channel	>2.0
Thimble (Cold Wall) Flow Channel	>2.0
Minimum DNBR for Design Transients	
Typical Flow Channel	≥1.25
Thimble Flow Channel	≥1.24
DNB Correlation[c]	WRB-2
COOLANT FLOW[d]	
Total Vessel Flow Rate, 10^6 lbm/hr	
(based on Minimum Measured Flow)	143.8[b]
(based on Thermal Design Flow)	137.3
Effective Flow Rate for Heat Transfer, 10^6 lbm/hr (based on TDF)	125.9
Effective Flow Area for Heat Transfer, ft^2	54.1
Average Velocity along Fuel Rods, ft/sec (based on TDF)	14.8
Average Mass Velocity, 10^6 lbm/hr-ft^2 (based on TDF)	2.33

TABLE 4.4-1 (Cont'd)

THERMAL AND HYDRAULIC DESIGN PARAMETERS	
COOLANT TEMPERATURE, °F	
Nominal Inlet	555.2
Average Rise in Vessel	65.6
Average Rise in Core	70.8
Average in Core	592.8
Average in Vessel	588.0
HEAT TRANSFER	
Active Heat Transfer Surface Area, ft^2	57505
Average Heat Flux[e], $BTU/hr\text{-}ft^2$	210883
Maximum Heat Flux for Normal Operation, [e, f] $BTU/hr\text{-}ft^2$	548296
Average Linear Power[e], kW/ft	5.82
Peak Linear Power for Normal Operation,[e, f] kw/ft	15.14
Peak Linear Power Resulting from[g] Overpower Transients/Operator Errors (assuming a maximum overpower of 119%), kW/ft (centerline melt will not be exceeded)	22.5
Peak Linear Power for Prevention of[h] Centerline Melt, kW/ft	22.5
Temperature at Peak Linear Power for Prevention of Centerline Melt, °F	4700
Pressure Drop Across Core, psi[i]	28.1 ± 2.8
Across Vessel, including nozzle, psi	see Table 5.1-1

TABLE 4.4-1 (Cont'd)

(a) Deleted.

(b) Inlet temperature = 556.6 °F.

(c) The W-3 Alternative correlations (ABB-NV and WLOP) are used for analysis of some accidents outside the range of application for the WRB-2 DNB correlation.

(d) The design bypass flow (including uncertainties) is 8.3 percent.

(e) Based on densified active fuel length of 143.7 inches.

(f) This limit is associated with the value of F_Q^T = 2.60.

(g) See Subsection 4.3.2.2.6.

(h) See Subsection 4.4.2.11.6.

(i) Based on best estimate reactor flow rate of 408000 gpm.

TABLE 4.4-2

VOID FRACTIONS AT NOMINAL REACTOR CONDITIONS

		AVERAGE	MAXIMUM
Core	(VANTAGE 5 /VANTAGE +)	<0.01%	
Hot Subchannel	(VANTAGE 5 /VANTAGE +)	5.3%	14.8%

Attachment 4.4A

Additional Information On the Plant Specific Application of the Westinghouse Improved Thermal Design Procedure To Byron/Braidwood

4.4A Additional Information On the Plant Specific Application of the Westinghouse Improved Thermal Design Procedure To Byron/Braidwood

The NRC Safety Evaluation Report on WCAP-9500 entitled Reference Core Report 17x17 Optimized Fuel Assembly noted the specific plants using the Westinghouse Improved Thermal Design Procedure (ITDP) must supply additional information on the plant specific application of the ITDP to perform thermal-hydraulic analyses. Thus, Byron/ Braidwood specific responses to NRC information requests are provided below.

4.4A.1 Request 1

Provide the sensitivity factors (S_i) and their range of applicability.

4.4A.2 Response 1

The sensitivity factors (S_i) and their range of applicability are given in Table 1 of Reference 2 for Byron/Braidwood. Please note that these values are the same as those used in WCAP-9500 with the exception of the range for vessel flow. The range on flow for Byron/ Braidwood has been extended down to 273270 gpm (70% flow) with no change in the corresponding sensitivity factor being required.

4.4A.3 Request 2

If the S_i values used in the Byron/Braidwood analyses are different than those used in WCAP-9500, then the applicant must reevaluate the use of an uncertainty allowance for application of equation 3-2 of WCAP-8567, "Improved Thermal Design Procedure" and the linearity assumption must be validated.

4.4A.4 Response 2

The S_i values used in Byron/Braidwood analyses are the same as those used in WCAP-9500. Therefore, reevaluating the use of an uncertainty allowance for application of equation 302 of WCAP-8567, "Improved Thermal Design Procedure" and the linearity assumption is not required.

4.4A.5 Request 3

Provide and justify the variances and distributions for input parameters.

4.4A.6 Response 3

The distribution assumed for the input parameters such as pressurizer pressure, core average temperature, reactor power, and RCS flow are normal, two-sided 95+% probability distributions.

The variances of these parameters for Byron/Braidwood are consistent with the variances calculated in the generic response. Specifically, the uncertainties for pressurizer pressure and core average temperature are identical to the generic response since the sensors, process racks, and computer and readout devices are standard Westinghouse supplied NSSS equipment.

Variances in reactor power and reactor coolant system flow are calculated based on equation 4 and equation 8 respectively in Reference 1. As can be seen from the equations, both primary and secondary side parameters are measured for power and flow calorimetrics. The error allowances for the parameters measured by Westinghouse supplied equipment are identical to those used in the generic submittal (Reference 1). Two input parameters are measured by non-Westinghouse supplied instruments. These are feedwater temperature and feedwater pressure. As expected, the error allowances for these instruments vary slightly from those used in Reference 1. The error allowances for feedwater temperature and pressure were statistically combined (as described in Reference 1) to get the total channel allowance for each parameter.

The feedwater pressure error allowance was calculated to be less than the error allowance used in Reference 1. Therefore, the error contribution to the reactor power and flow uncertainties from feedwater pressure is less than that used in the generic response.

Similarly, the errors for feedwater temperature were combined to get the total channel allowance. The total allowance was found to be slightly higher than that used to calculate RCS flow uncertainty in Reference 1. However, the error allowance from feedwater temperature is very small relative to the other contributing errors and in fact this small additional error is absorbed in the statistical combination. Therefore, the flow uncertainty calculated in Reference 1 is applicable for Byron/Braidwood.

As stated in Reference 1, the flow calorimetric can be performed one of several ways. Commonwealth Edison plans to do a precision flow calorimetric at the beginning of the cycle and normalize the loop elbow

taps. For monthly surveillance to assure plant operation consistent with the ITDP assumptions, the loop flows will be read off the plant process computer. The total flow uncertainty associated with this method was calculated in Reference 1 and is applicable to the Byron/Braidwood units.

It is to be noted that the total channel allowance for feedwater temperature was calculated to be less than the error assumed for the reactor power uncertainty calculation in Reference 1. Therefore, the power uncertainty for Byron/Braidwood is bounded by the uncertainty calculated in the generic response.

4.4A.7 Request 4

Justify that the normal conditions used in the analyses bound all permitted modes of plant operation.

4.4A.8 Response 4

This item was addressed in Reference 1 and is applicable to the Byron/Braidwood units.

4.4A.9 Request 5

Provide a discussion of what code uncertainties, including their values, are included in the DNBR analyses.

4.4A.10 Response 5

The uncertainties included in the ITDP DNBR analyses for Byron/Braidwood are given in Table 1 of Reference 2. As a result of these values being different from those used in WCAP-9500, the Design DNBR Limits also differ. The calculation of the Design limit DNBRs for the Typical and Thimble cells are given in Reference 2, Tables 2 and 3 respectively. Since the Design DNBR Limits given in Table 2 and 3 are different from those originally given, Section 4.4 has been revised to incorporate the Reference 2 values.

4.4A.11 Request 6

Provide a block diagram depicting sensor, processing equipment, computer and readout devices for each parameter channel used in the uncertainty analysis. Within each element of the block diagram identify the accuracy, drift, range, span, operating limits, and setpoints. Identify the overall accuracy of each channel transmitter to final output and specify the minimum acceptable accuracy for use with the new procedure. Also identify the overall accuracy of the

final output value and maximum accuracy requirements for each input channel for this final output device.

4.4A.12 Response 6

Block diagrams are not provided in this response. However, as in the generic response, a table is provided in Reference 2 giving the error breakdown from sensor to computer and readout devices. This table is abbreviated though, giving only the error breakdowns for instruments that differ from those in Table 4, "Typical Instrument Uncertainties," of Reference 1. As noted earlier, these instruments are those that measure feedwater temperature and pressure.

4.4A.13 Request 7

If there are any changes to the THINC-IV correlation, or parameter values outside of previously demonstrated acceptable ranges, the staff requires a reevaluation of the sensitivity factors and of the use of equation 3-2 of WCAP-8567.

4.4A.14 Response 7

For Byron/Braidwood, the THINC-IV code and WRB-1 DNB Correlation are the same as that used in WCAP-9500. Therefore, reevaluating the sensitivity factors and the use of equation 3-2 of WCAP-8567 is not required.

References

1. Westinghouse letter, NS-EPR-2577, E. P. Rahe to C. H. Berlinger (NRC), March 31, 1982, proprietary.

2. General Electric Company letter transmitting improved thermal design information to the NRC (to be written), proprietary.

4.5 REACTOR MATERIALS

Section 4.5 provides a discussion of the materials employed in the control rod drive system and the reactor internals.

A more detailed evaluation of the reactor materials and reactivity control systems indicating the degree of conformance with the recommendations of the applicable Regulatory Guides is presented in the Final Safety Analysis Report as follows:

a. control rod drive mechanism and reactor internals: Chapter 3.0,

b. control rod drive mechanism testing: Chapters 3.0, 14.0, and the Technical Specifications,

c. control rod drive mechanism and reactor internals materials: Chapter 5.0,

d. safety injection system: Chapter 6.0,

e. instrumentation for reactor control and protection: Chapter 7.0, and

f. failure of the control rod drive mechanism cooling system and chemical and volume control system: Chapter 9.0.

4.5.1 Control Rod System Structural Materials

4.5.1.1 Materials Specifications

All parts exposed to reactor coolant are made of metals which resist the corrosive action of the water. Three types of metals are used exclusively: stainless steels, nickel-chromium-iron, and cobalt based alloys. In the case of stainless steels, only austenitic and martensitic stainless steels are used. For pressure boundary parts, martensitic stainless steels are not used in the heat treated conditions which cause susceptibility to stress corrosion cracking or accelerated corrosion in the Westinghouse pressurized water reactor water chemistry.

a. Pressure Boundary

   All pressure containing materials comply with Section III of the ASME Boiler and Pressure Vessel Code, and are fabricated from austenitic (Type 304) stainless steel.

b. Coil stack assembly

   The coil housings require a magnetic material. Both low carbon cast steel and ductile iron have been successfully tested for this application. On the

basis of cost and performance, ductile iron was selected for the control rod drive mechanism (CRDM). The finished housings are zinc plated or flame sprayed to provide corrosion resistance.

Coils are wound on bobbins of molded Dow Corning 302 material, with double glass insulated copper wire. Coils are then vacuum impregnated with silicon varnish. A wrapping of mica sheet is secured to the coil outside diameter. The result is a well insulated coil capable of sustained operation at 200°C.

c. Latch assembly

Magnetic pole pieces are fabricated from Type 410 stainless steel. All nonmagnetic parts, except pins and springs, are fabricated from Type 304 stainless steel. Haynes 25 is used to fabricate link pins. Springs are made from nickel-chromium-iron alloy (Inconel-750). Latch arm tips are clad with Stellite-6 to provide improved wearability. Hard chrome plate and Stellite-6 are used selectively for bearing and wear surfaces.

d. Drive rod assembly

The drive rod assembly utilizes a Type 410 stainless steel drive rod and disconnect rod assembly. The coupling is machined from type 403 stainless steel. Other parts are Type 304 stainless steel with the exception of the springs, which are nickel-chromium-iron alloy, and the locking button, which is Haynes 25; and the belleville washers which are Inconel 718. Several small parts (screws and pins) are Inconel 600.

Material specifications for Class 1 components of the CRDM are as follows:

CRDM, upper head	SB-166 or SB-167 and SA-182 Grade F304
Latch housing	SA-336, Grade F8 or SA-351 Grade CF8
Rod travel housing	SA-336, Grade F8
Cap	SA-479, Type 304
Welding materials	Stainless Steel Weld Metal Analysis A-8

4.5.1.2 Austenitic Stainless Steel Components

a. All austenitic stainless steel materials used in the fabrication of CRDM components are processed, inspected and tested to avoid sensitization and prevent intergranular stress corrosion cracking.

The rules covering these controls are stipulated in Westinghouse process specifications. As applicable, these process specifications supplement the equipment specifications and purchase order requirements of every individual austenitic stainless steel component regardless of the ASME Code Classification.

Westinghouse practice is that austenitic stainless steel materials of product forms with simple shapes need not be corrosion tested provided that the solution heat treatment is followed by water quenching. Simple shapes are defined as all plates, sheets, bars, pipe and tubes, as well as forgings, fittings and other shaped products which do not have inaccessible cavities or chambers that would preclude rapid cooling when water quenched. When testing is required the tests are performed in accordance with ASTM A 262, Practice A or E, as amended by Westinghouse Process Specification 84201 MW.

If, during the course of fabrication the steel is inadvertently exposed to the sensitization temperature range, 800°F to 1500°F the material may be tested in accordance with ASTM A 262, as amended by Westinghouse Process Specification 84201 MW to verify that it is not susceptible to intergranular attack, except that testing is not required for:

1. Cast metal or weld metal with a ferrite content of 5 percent or more,

2. Material with a carbon content of 0.03% or less that is subjected to temperatures in the range of 800°F to 1,500°F for less than 1 hour.

3. Material exposed to special processing provided the processing is properly controlled to develop a uniform product and provided that adequate documentation exists of service experience and/or test data to demonstrate that the processing will not result in increased susceptibility to intergranular stress corrosion.

   If it is not verified that such material is not susceptible to intergranular attack, the material

will be re-solution annealed and water quenched or rejected.

b. The welding of austenitic stainless steel is controlled to mitigate the occurrence of microfissuring or hot cracking in the weld.

Available data indicates that a minimum delta ferrite level expressed in Ferrite Number (FN), above which the weld metals commonly used by Westinghouse will not be prone to hot cracking, lies somewhere between 0 FN and 3 FN. The undiluted weld deposits of the starting welding materials are required to contain a minimum of 5 FN.

4.5.1.3 Other Materials

The CRDMs are cleaned prior to delivery in accordance with the guidance of ANSI N45.2.1. Westinghouse personnel do conduct surveillance to ensure that manufacturers and installers adhere to appropriate requirements.

Haynes 25 is used in small quantities to fabricate link pins. The material is ordered in the solution treated and cold worked condition. Stress corrosion cracking has not been observed in this application over the last 15 years.

The CRDM springs are made from nickel-chromium-iron alloy (Inconel-750) ordered to MIL-S-23192 or MIL-N-24114 Class A #1 temper drawn wire. Operating experience has shown that springs made of this material are not subject to stress-corrosion cracking.

4.5.1.4 Cleaning and Cleanliness Control

The CRDMs are cleaned prior to delivery in accordance with the guidance of ANSI N45.2.1. Measures are applied, as appropriate, to apply packaging requirements to procurement orders, to review supplier packaging procedures, to apply proper cleaning requirements, marking and identification and to provide protection to equipment from physical or weather damage, to apply special handling precautions and to define storage requirements. Westinghouse quality assurance procedures are described in "Westinghouse Water Reactor Divisions Quality Assurance Plan," WCAP-8370, Revision 8A updated per letter NS-TMA-2039, From T. M. Anderson to W. P. Haass, February 8, 1979.

4.5.2 Reactor Internals Materials

4.5.2.1 Materials Specifications

All the major material for the reactor internals is Type 304 stainless steel. Parts not fabricated from Type 304 stainless steel include bolts and dowel pins, which are fabricated from

Type 316 stainless steel, and radial support key bolts, which are fabricated from Inconel-750.

Material specifications for reactor vessel internals for emergency core cooling systems are listed in Table 5.2-4.

There are no other materials used in the reactor internals or core support structures which are not otherwise included in ASME Code, Section III, Appendix I.

4.5.2.2 Controls on Welding

The discussions provided in Subsection 4.5.1 are applicable to the welding of reactor internals and core support components.

4.5.2.3 Nondestructive Examination of Wrought Seamless Tubular Products and Fittings

The nondestructive examination of wrought seamless tubular products and fittings is in accordance with Section III of the ASME Code.

4.5.2.4 Fabrication and Processing of Austenitic Stainless Steel Components

The discussions provided in Subsection 4.5.1.4 are applicable to the cleaning of reactor internals and core support structures in accordance with ANSI N45.2.1.

4.6 FUNCTIONAL DESIGN OF REACTIVITY CONTROL SYSTEMS

4.6.1 Information for Control Rod Drive System (CRDS)

Figure 4.2-8 provides the layout of the CRDS. The CRDS is a magnetically operated jack with no hydraulic system associated with its functioning. The control rod drive mechanism consists of four separate subassemblies.

a. The pressure vessel which includes the latch housing and rod travel housings.

b. The coil stack assembly which includes three operating coils: stationary gripper coil, movable gripper coil and lift coil.

c. The latch assembly which includes the guide tube, the stationary and the movable pole pieces and the stationary and movable gripper latches.

d. The drive rod assembly which includes the RCC coupling system and the drive rod.

4.6.2 Evaluation of the CRDS

The CRDS has been analyzed in detail in a failure mode and effects analysis (Reference 1). This study, and the analyses presented in Chapter 15.0, demonstrates that the CRDS performs its intended safety function, reactor trip, by putting the reactor in a subcritical condition when a safety system setting is approached, with any assumed credible failure of a single active component. The essential elements of the CRDS (those required to ensure reactor trip) are isolated from nonessential portions of the CRDS (the rod control system).

Despite the extremely low probability of a common mode failure impairing the ability of the reactor trip system to perform its safety function, analyses have been performed in accordance with the requirements of WASH-1270. These analyses, documented in References 2 and 3, have demonstrated that acceptable safety criteria would not be exceeded even if the CRDS were rendered incapable of functioning during a reactor transient for which their function would normally be expected.

The design of the control rod drive mechanism is such that failure of the control rod drive mechanism cooling system will, in the worst case, result in an individual control rod trip or a full reactor trip.

4.6.3 Testing and Verification of the CRDS

The CRDS was extensively tested prior to its operation. These tests may be subdivided into five categories: (1) prototype

tests of components, (2) prototype CRDS tests, (3) production tests of components following manufacture and prior to installation, (4) onsite preoperational tests, and (5) initial startup tests.

In accordance with Table 14.2-65, the reactor trip system operation was verified in a startup test. This test ensured that the system operated in accordance with the safety analysis report, design requirements, and plant installation. A final test was performed in which a manual reactor trip was initiated, (after fuel load but prior to initial criticality) to verify that all rods would fully insert.

The rod cluster control assemblies were dropped and the drops were timed. The time from beginning of decay of stationary gripper coil voltage to dashpot entry shall be less than or equal to 2.7 seconds for each rod, the Technical Specification limit. In compliance with Tables 14.2-66 and 14.2-66a, all rods falling outside the two-sigma limit were retested a minimum of three times each. Rods were dropped into representative flow conditions.

In addition, the CRDS is subject to periodic inservice tests. These tests are conducted to verify the operability of the CRDS when called upon to function.

4.6.4 Information for Combined Performance of Reactivity Systems

As is indicated in Chapter 15.0, the only postulated events which assume credit for reactivity control systems other than a reactor trip to render the plant subcritical are the steam line break, feedwater line break, and loss-of-coolant accident. The reactivity control systems for which credit is taken in these accidents are the reactor trip system and the safety injection system (SIS). Note that no credit is taken for the boration capabilities of the chemical and volume control system (CVCS) as a system in the analysis of transients presented in Chapter 15.0. The adverse boron dilution possibilities due to the operation of the CVCS are investigated in Chapter 15.0. Prior proper operation of the CVCS has been presumed as an initial condition to evaluate transients, and appropriate Technical Specifications have been prepared to ensure the correct operation or remedial action.

4.6.5 Evaluation of Combined Performance

The evaluations of the steam line break, feedwater line break, and the loss-of-coolant accident, which presume the combined actuation of the reactor trip system to the CRDS and the SIS, are presented in Chapter 15.0. Reactor trip signals and safety injection signals for these events are generated from functionally diverse sensors and actuate diverse means of reactivity control, i.e., control rod insertion and injection of soluble poison.

Nondiverse but redundant types of equipment are utilized only in the processing of the incoming sensor signals into appropriate logic, which initiates the protective action. In particular, note that protection from equipment failures is provided by redundant equipment and periodic testing. Effects of failures of this equipment have been extensively investigated as reported in Reference 4. The failure mode and effects analysis described in this reference verifies that any single failure will not have a deleterious effect on the engineered safety features actuation system.

4.6.6 References

1. Shopsky, W. E., "Failure Mode and Effects Analysis (FMEA) of the Solid State Full Length Rod Control System," WCAP 8976, August 1977.

2. "Westinghouse Anticipated Transients Without Trip Analysis," WCAP-8330, August 1974.

3. Gangloff, W. C. and Loftus, W. D., "An Evaluation of Solid State Logic Reactor Protection in Anticipated Transients," WCAP-7706-L (Proprietary) and WCAP-7706 (Nonproprietary), July 1971.

4. Eggleston, F. T., Rawlins, D. H. and Petrow, J. R., "Failure Mode and Effects Analysis (FMEA) of the Engineering Safeguard Features Actuation System," WCAP-8584 (Proprietary) and WCAP-8760 (Nonproprietary), April 1976.

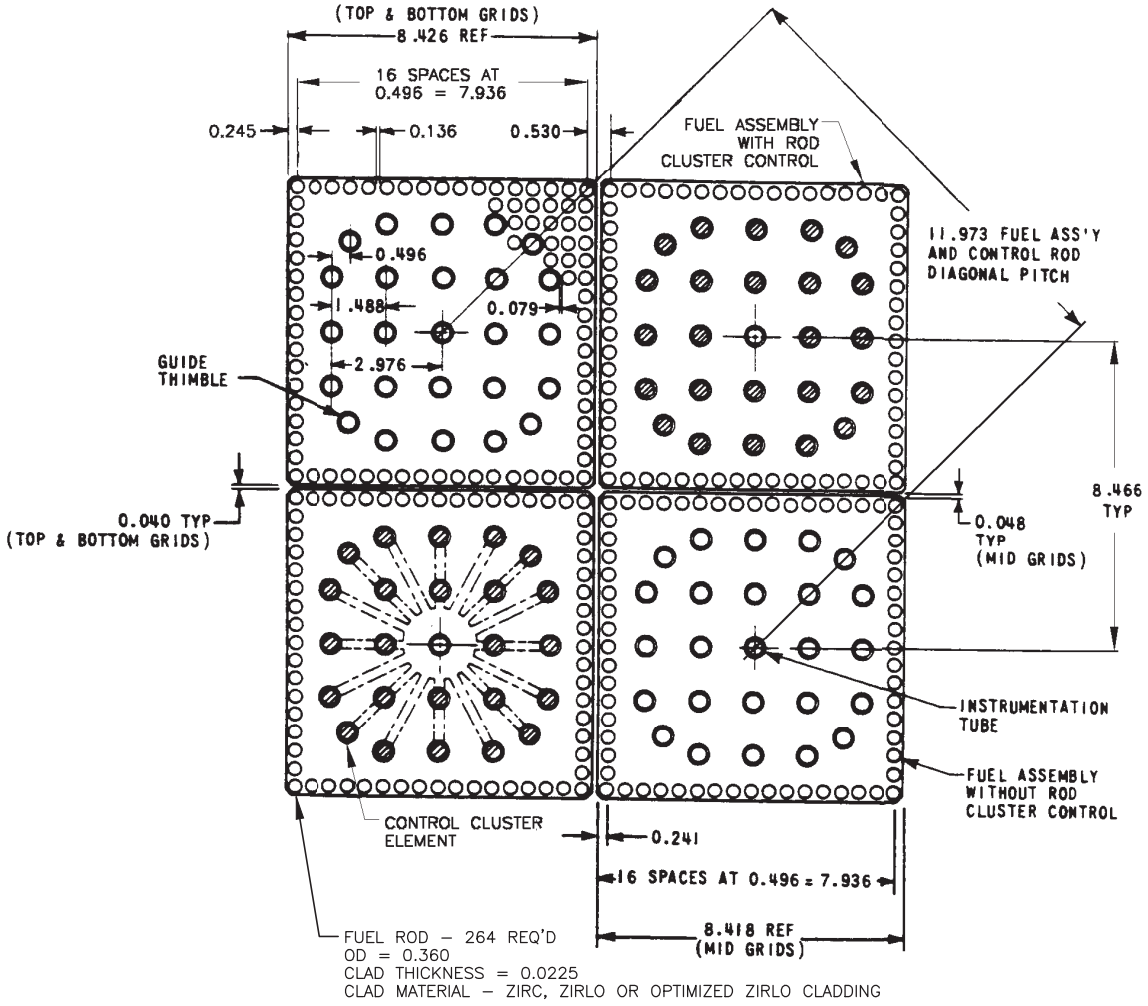

BYRON/BRAIDWOOD STATION
UPDATED FINAL SAFETY ANALYSIS REPORT

FIGURE 4.2–1

17 X 17 VANTAGE 5/VANTAGE + FUEL
ASSEMBLY CROSS SECTION

Figure 4.2-2 has been deleted intentionally.

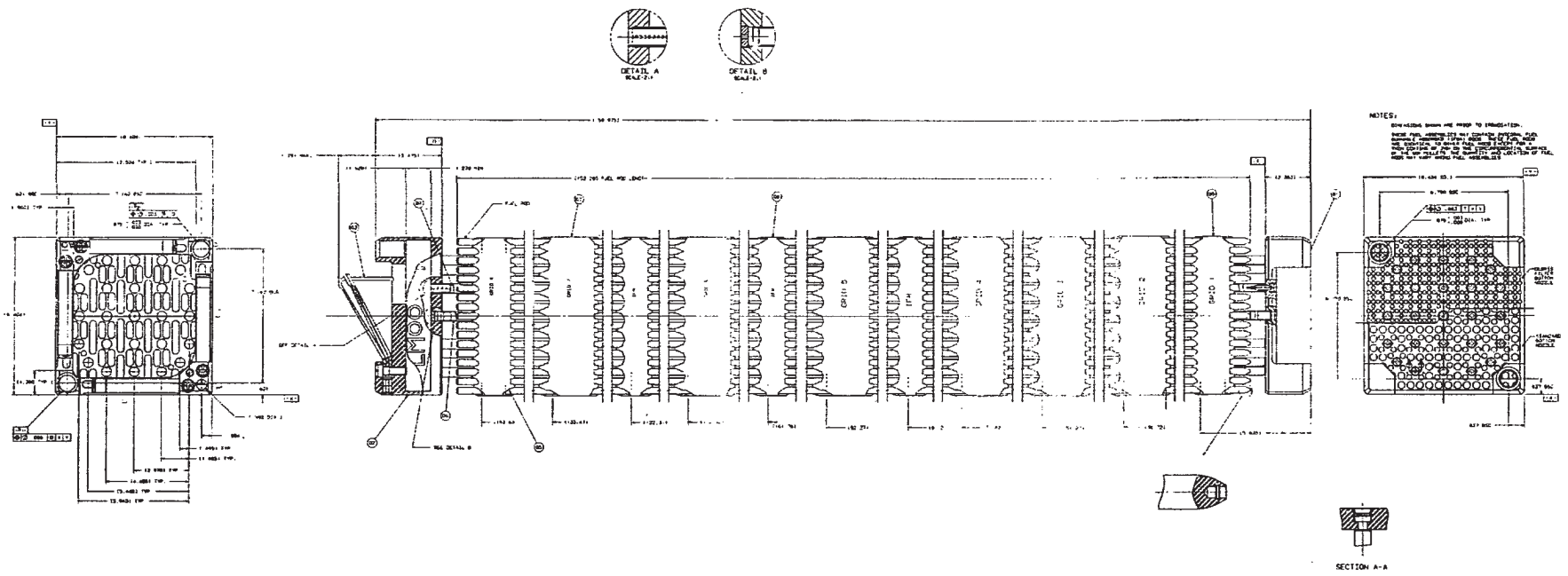

BYRON/BRAIDWOOD STATIONS
UPDATED FINAL SAFETY ANALYSIS REPORT

FIGURE 4.2-2a

17 X 17 VANTAGE 5 FUEL ASSEMBLY OUTLINE

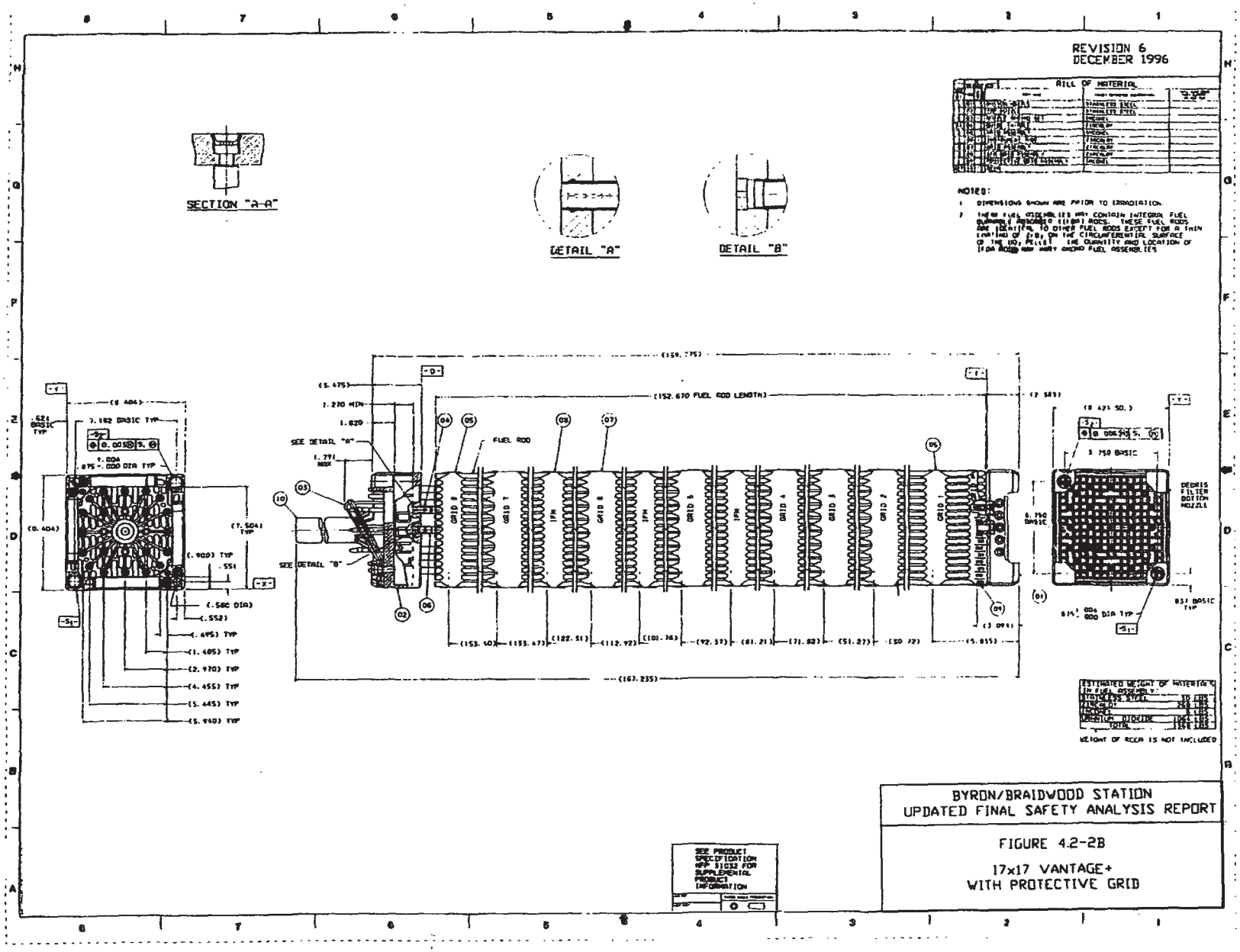

BYRON/BRAIDWOOD STATION
UPDATED FINAL SAFETY ANALYSIS REPORT

FIGURE 4.2-2B

17x17 VANTAGE+
WITH PROTECTIVE GRID

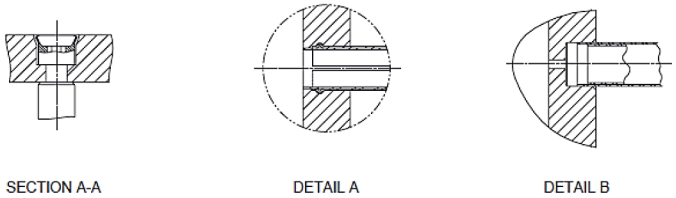

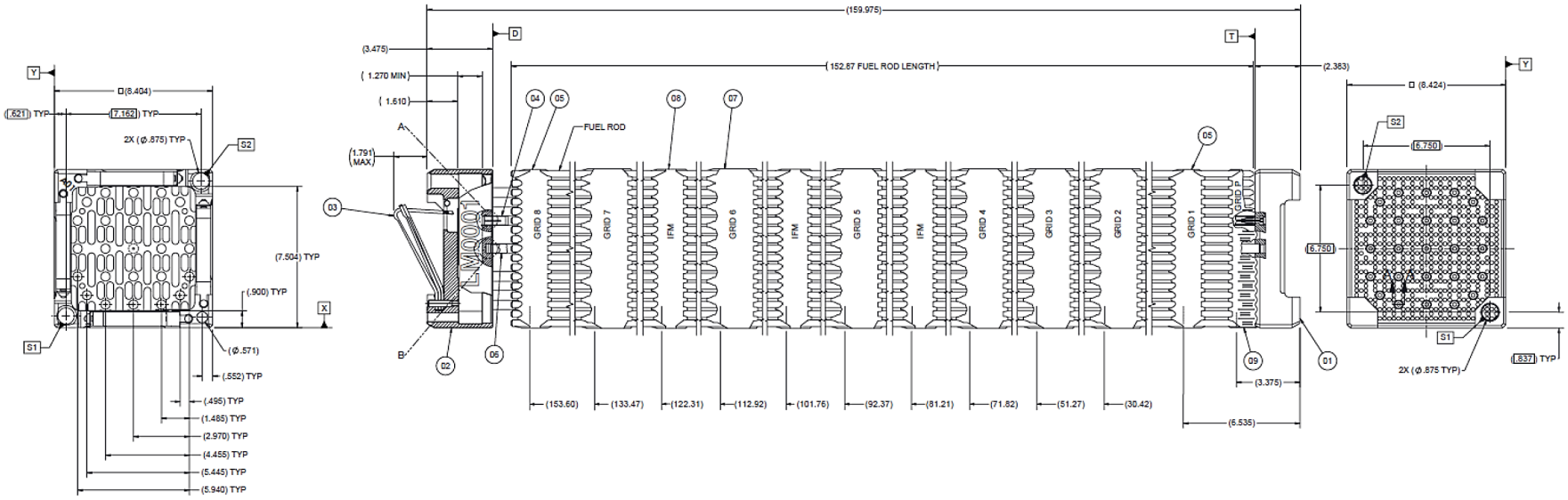

BYRON/BRAIDWOOD STATIONS
UPDATED FINAL SAFETY ANALYSIS REPORT

FIGURE 4.2-2C

17x17 VANTAGE+ FUEL WITH DEBRIS MITIGATING FEATURES (INCLUDING THE RPG, WIN AND SDFBN COMPONENTS)

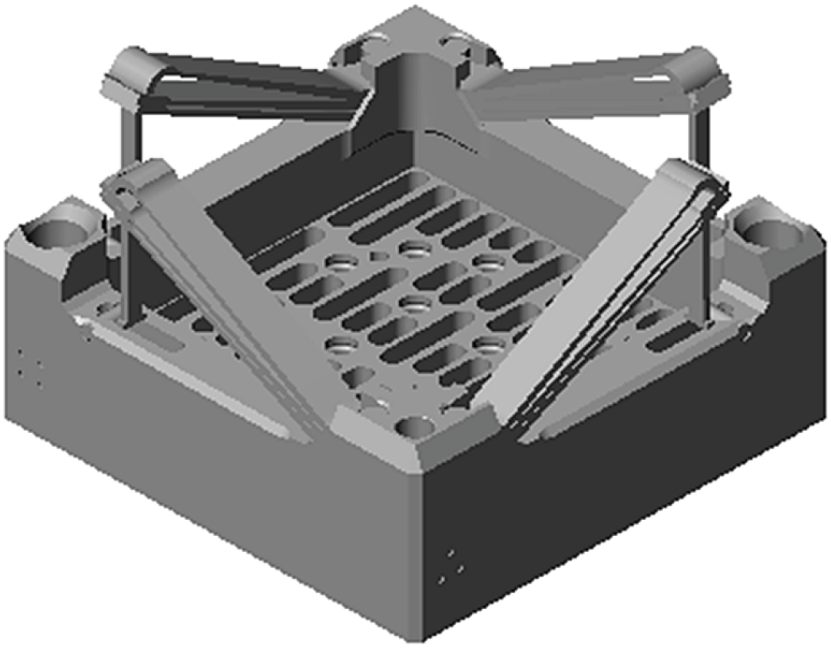

BYRON/BRAIDWOOD STATIONS
UPDATED FINAL SAFETY ANALYSIS REPORT

FIGURE 4.2-3

WESTINGHOUSE INTEGRAL NOZZLE (WIN)

REVISION 6
DECEMBER 1996

DIM	17x17 V-5	17x17 V+ (W/PROTECTIVE GRID)
A	152.285	152.67
B	7.525	7.410
C	144.00	144.00
DIA D	.315	.315
DIA E	.360	.360

DIMENSIONS ARE IN INCHES

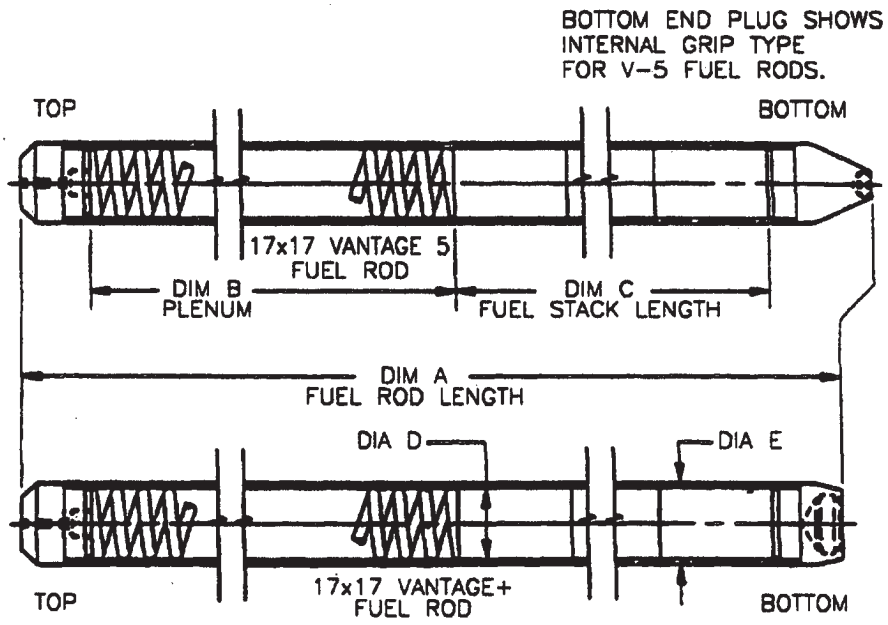

BYRON/BRAIDWOOD STATION
UPDATED FINAL SAFETY ANALYSIS REPORT

FIGURE 4.2-3A

17x17 VANTAGE 5/VANTAGE+
FUEL ROD ASSMBLY COMPARISON

REVISION 6
DECEMBER 1996

MID GRID EXPANSION JOINT DESIGN

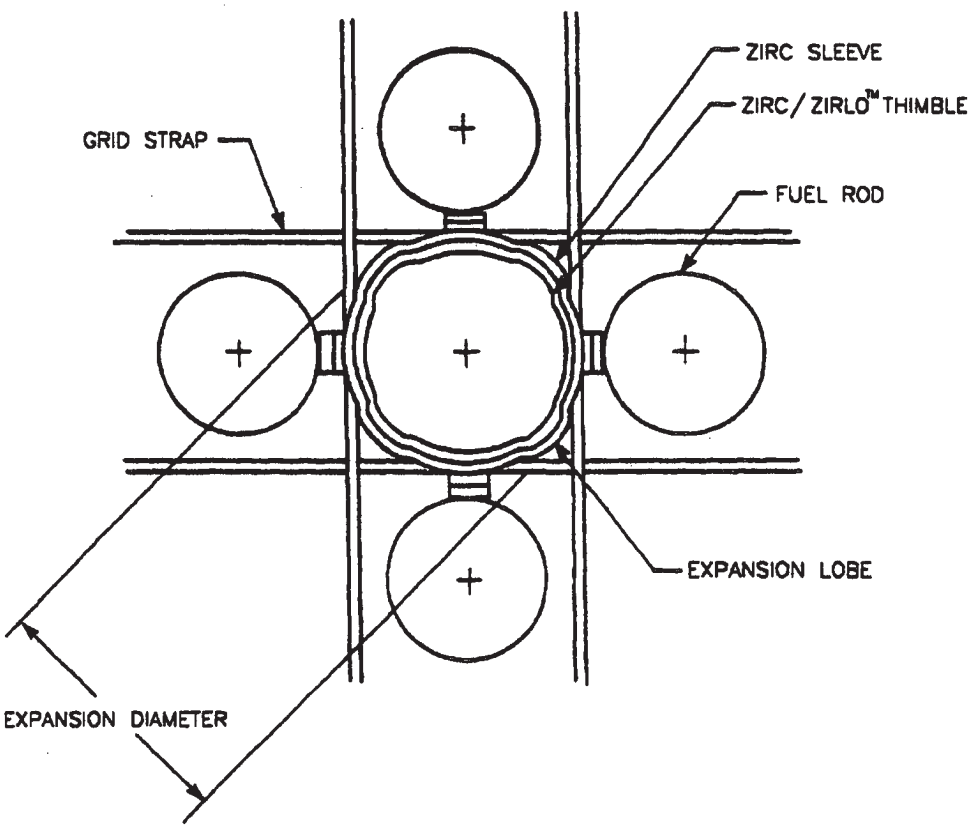

BYRON/BRAIDWOOD STATION UPDATED FINAL SAFETY ANALYSIS REPORT
FIGURE 4.2–4 PLAN VIEW OF MID GRID AND IFM GRID TO GUIDE THIMBLE JOINT (BOTTOM VIEW)

REVISION 6
DECEMBER 1996

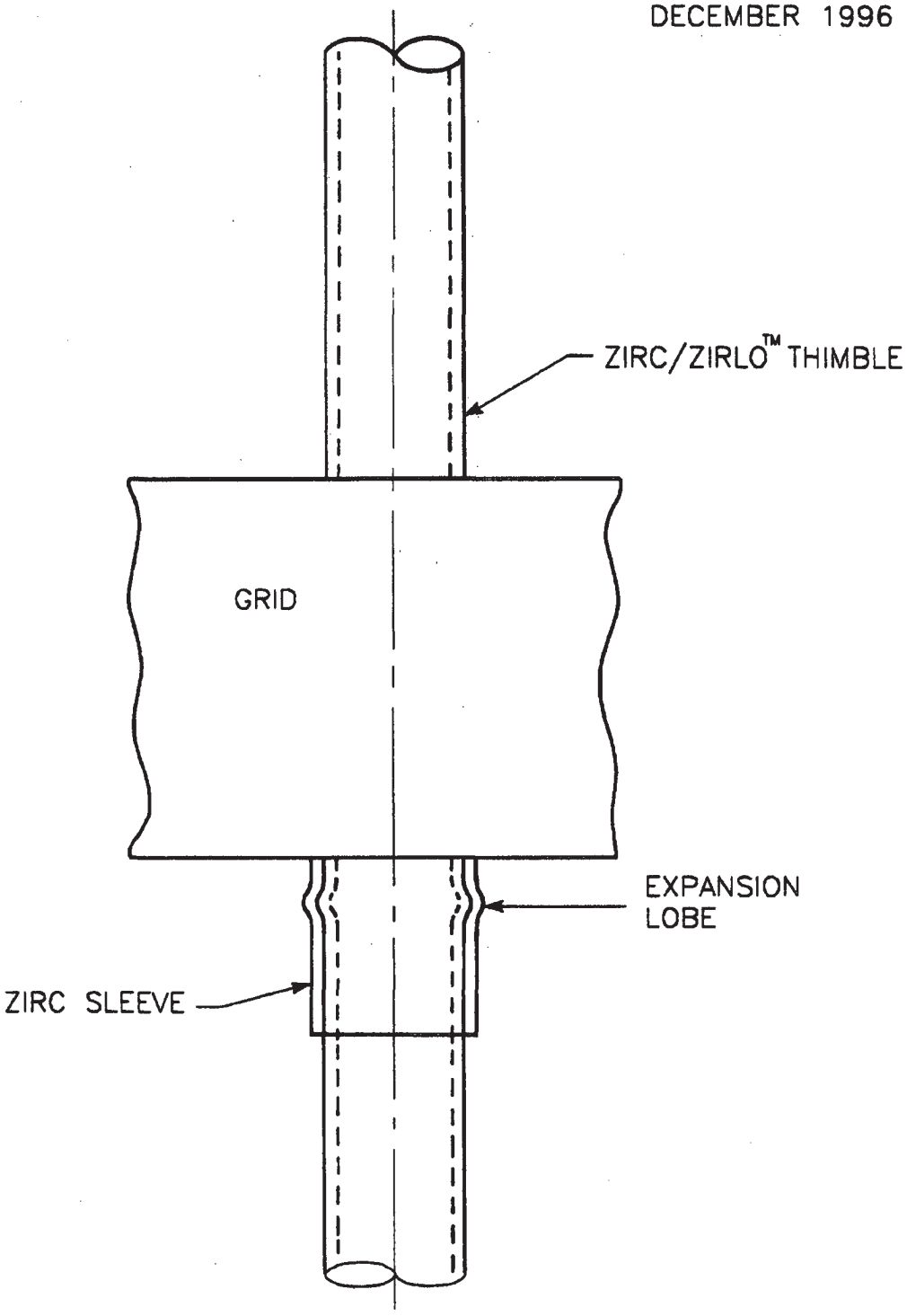

BYRON/BRAIDWOOD STATION
UPDATED FINAL SAFETY ANALYSIS REPORT

FIGURE 4.2-5

ELEVATION VIEW OF MID AND IFM GRID TO GUIDE THIMBLE JOINT

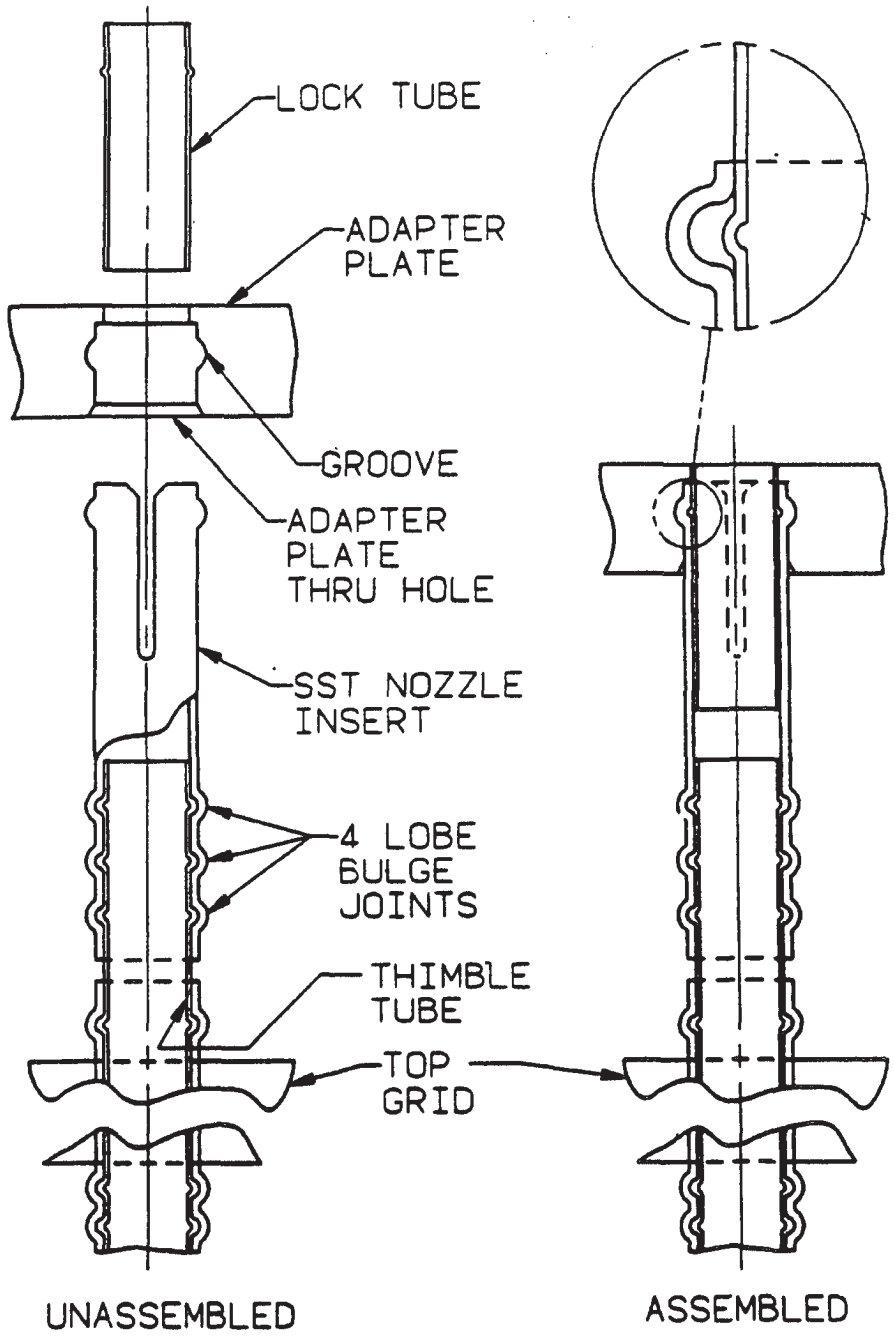

BYRON/BRAIDWOOD STATIONS
UPDATED FINAL SAFETY ANALYSIS REPORT

FIGURE 4.2-6

TOP GRID AND RECONSTITUTABLE TOP NOZZLE ATTACHMENT DETAIL

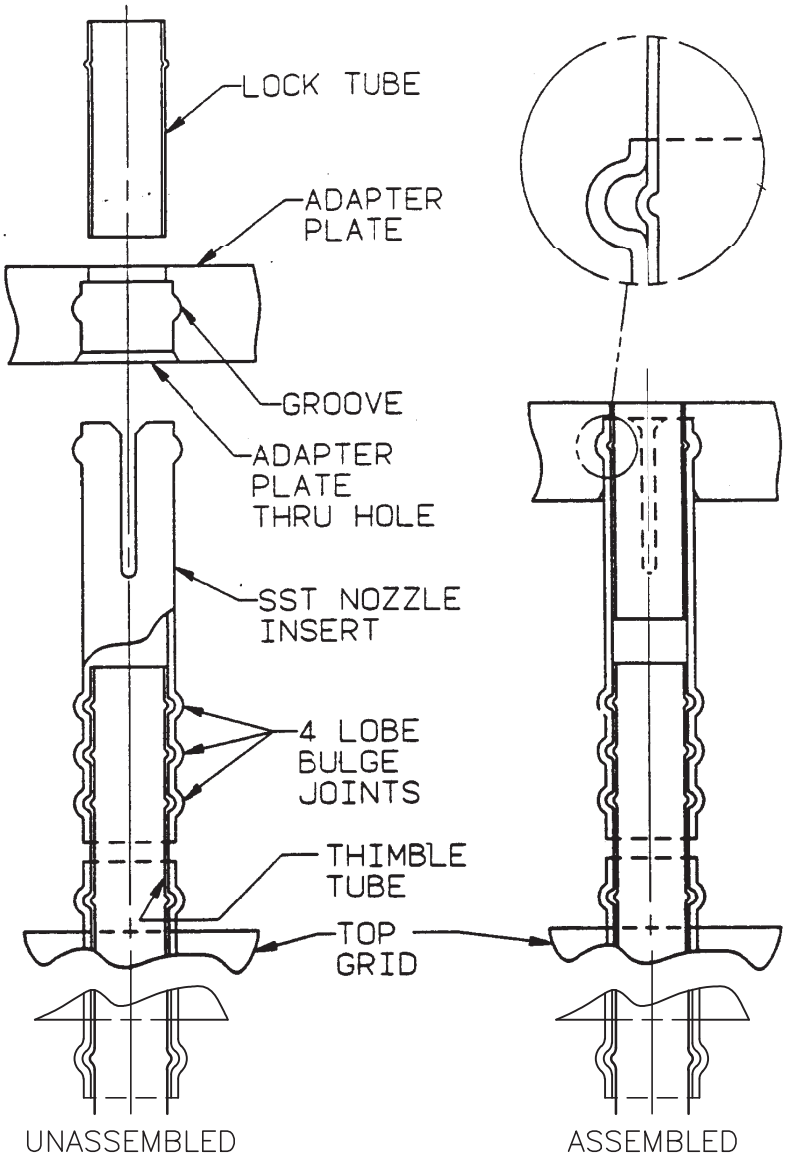

BYRON/BRAIDWOOD STATIONS
UPDATED FINAL SAFETY ANALYSIS REPORT

FIGURE 4.2–6a

TOP GRID TWO BULGE CONNECTION
(STARTING WITH BYRON UNIT 2 CYCLE 21
& BRAIDWOOD UNIT 1 CYCLE 21)
AND TOP NOZZLE ATTACHMENT DETAIL

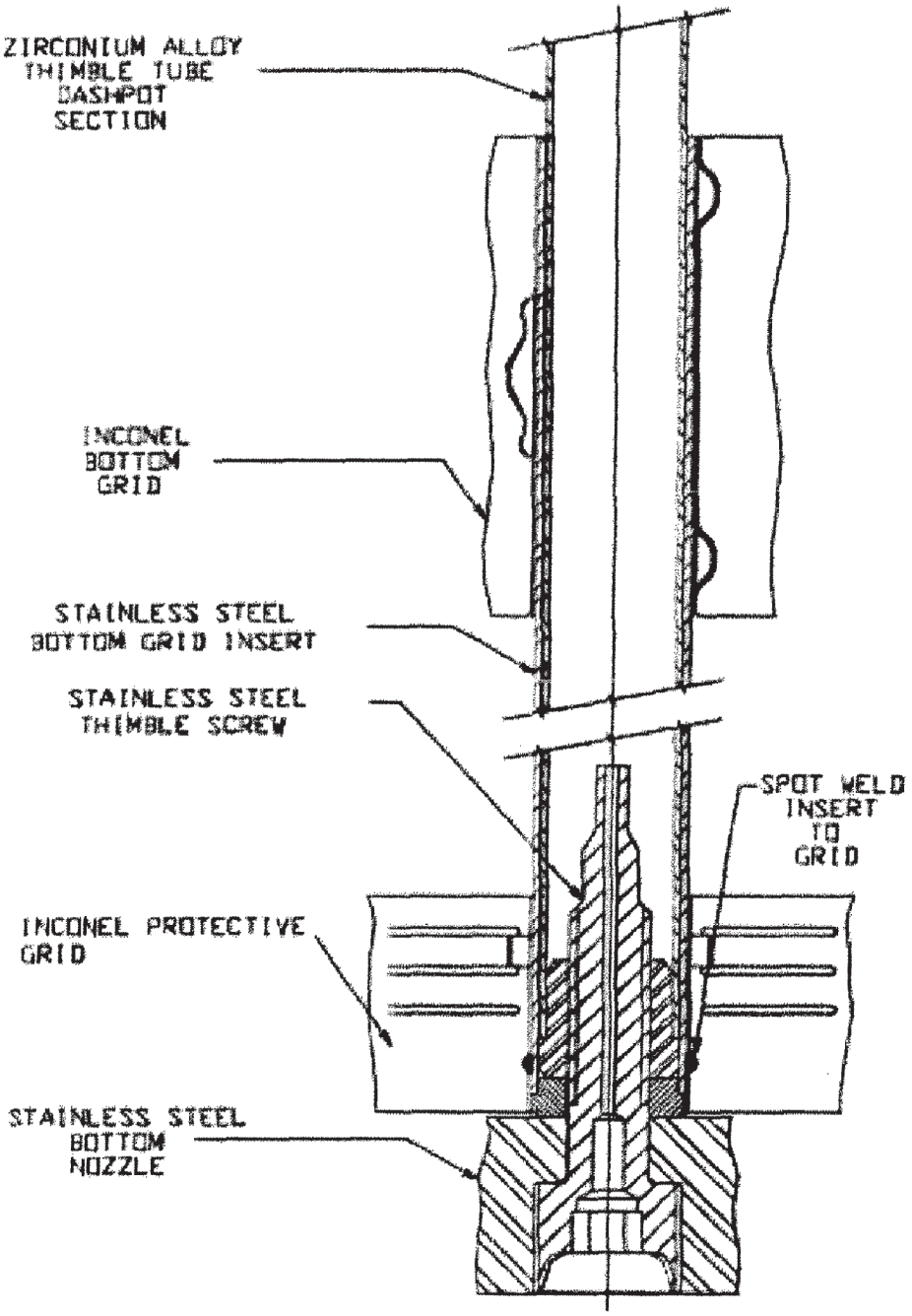

BYRON/BRAIDWOOD STATIONS
UPDATED FINAL SAFETY ANALYSIS REPORT

FIGURE 4.2-7

GUIDE THIMBLE TO BOTTOM GRID
AND NOZZLE JOINT

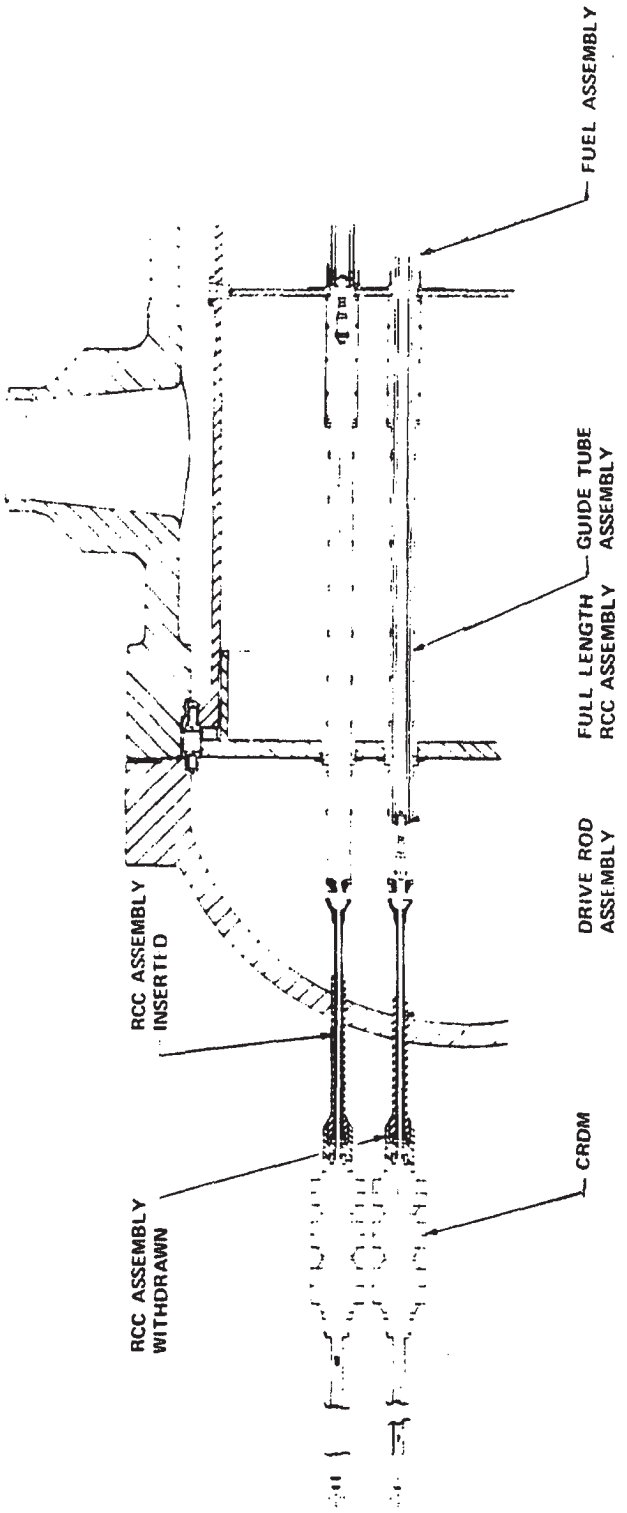

BYRON/BRAIDWOOD STATIONS
UPDATED FINAL SAFETY ANALYSIS REPORT

FIGURE 4.2-8

ROD CLUSTER CONTROL AND DRIVE ROD

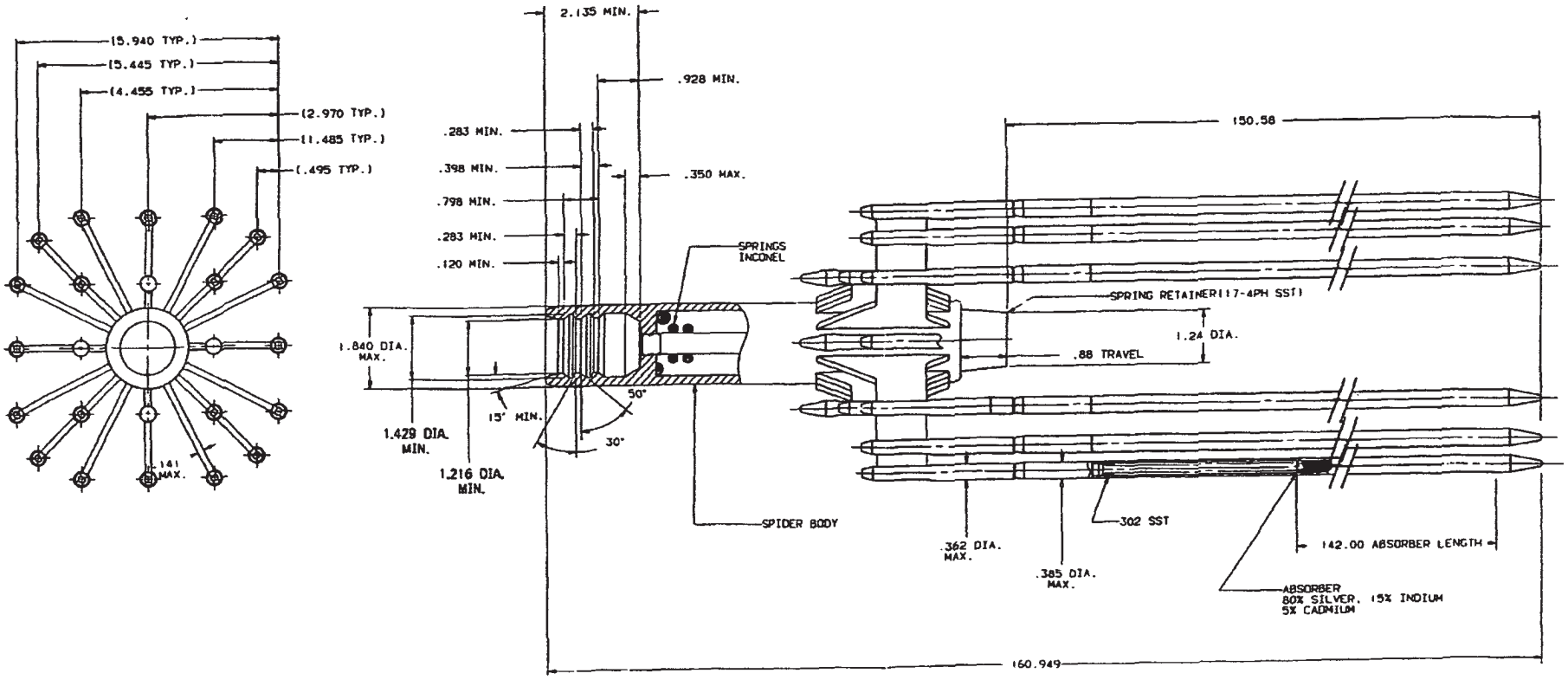

NOTES:

1. THE RCC ASSEMBLY IS MADE OF TYPE 304 SST EXCEPT AS INDICATED
2. ALL DIMENSIONS ARE NOMINAL UNLESS OTHERWISE NOTED.
3. THE OUTSIDE OF THE CONTROL ROD TUBES ARE **CHROME** PLATED.

BYRON/BRAIDWOOD STATION
UPDATED FINAL SAFETY ANALYSIS REPORT

FIGURE 4.2-9

ROD CLUSTER CONTROL ASSEMBLY OUTLINE

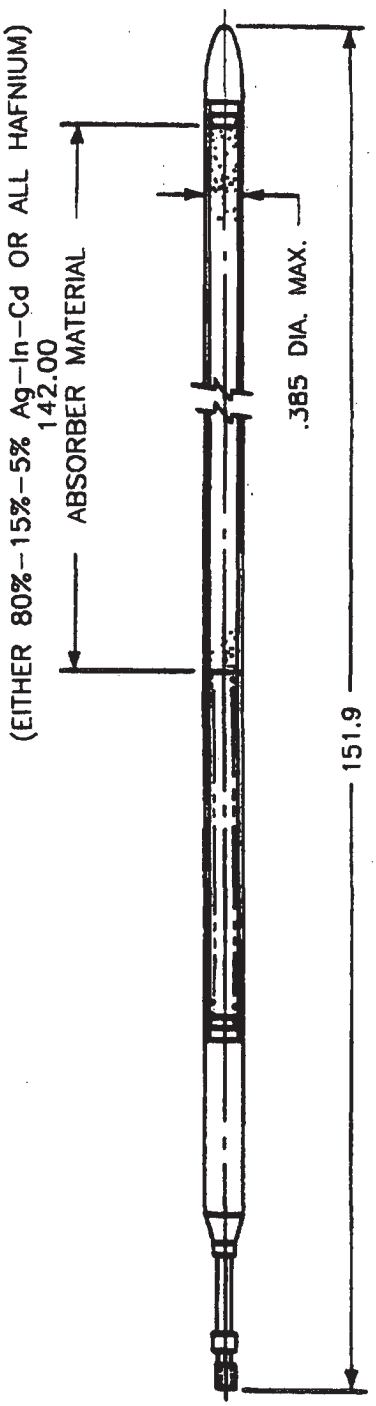

BYRON/BRAIDWOOD STATION
UPDATED FINAL SAFETY ANALYSIS REPORT

FIGURE 4.2-10

ABSORBER ROD DESIGN

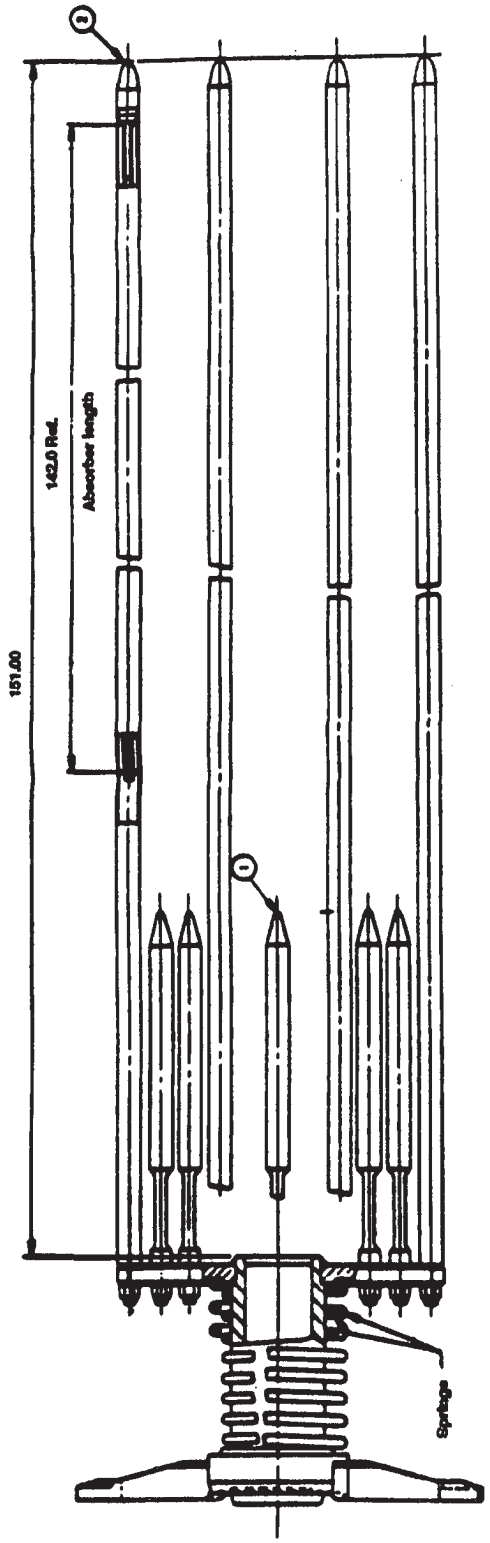

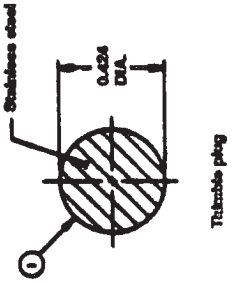

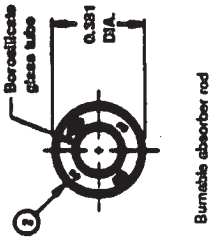

BYRON/BRAIDWOOD STATIONS
UPDATED FINAL SAFETY ANALYSIS REPORT

FIGURE 4.2-11

BURNABLE ABSORBER ASSEMBLY

REVISION 6
DECEMBER 1996

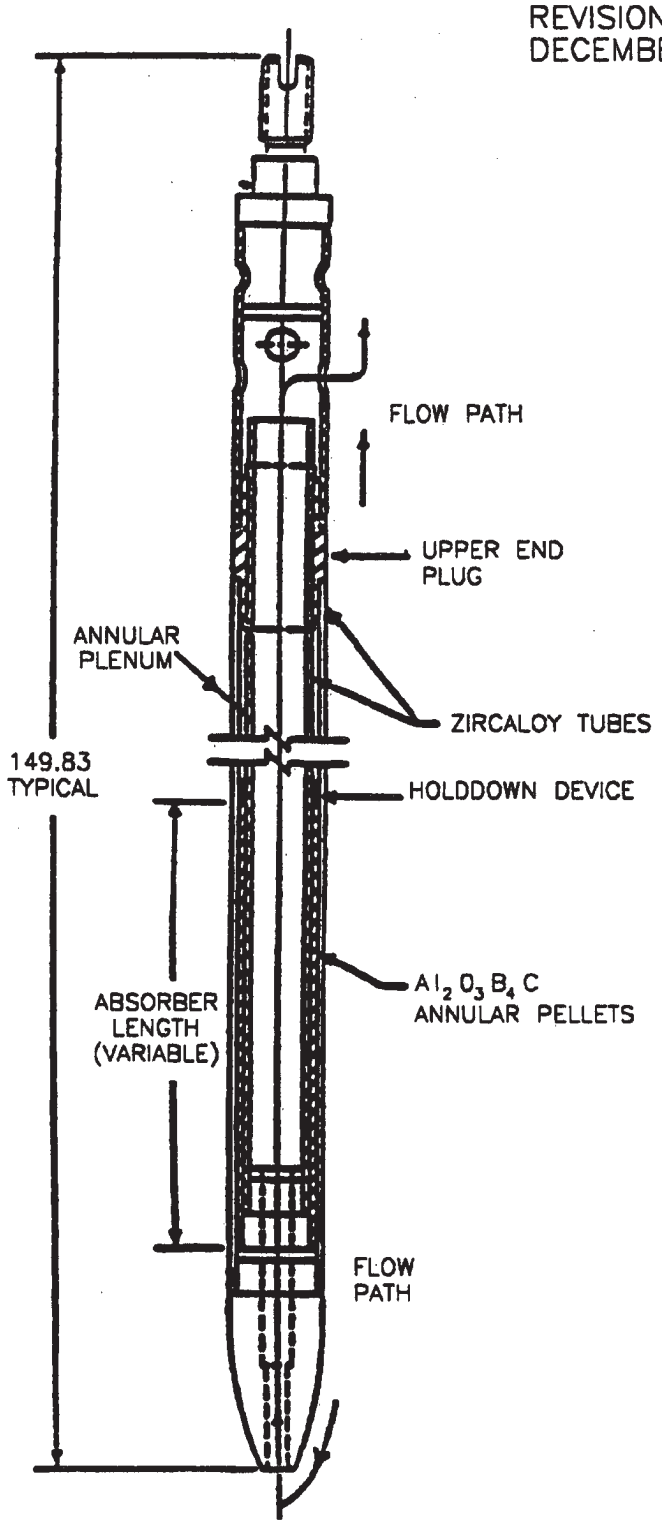

BYRON/BRAIDWOOD STATION
UPDATED FINAL SAFETY ANALYSIS REPORT

FIGURE 4.2–12

WET ANNULAR BURNABLE ABSORBER ROD

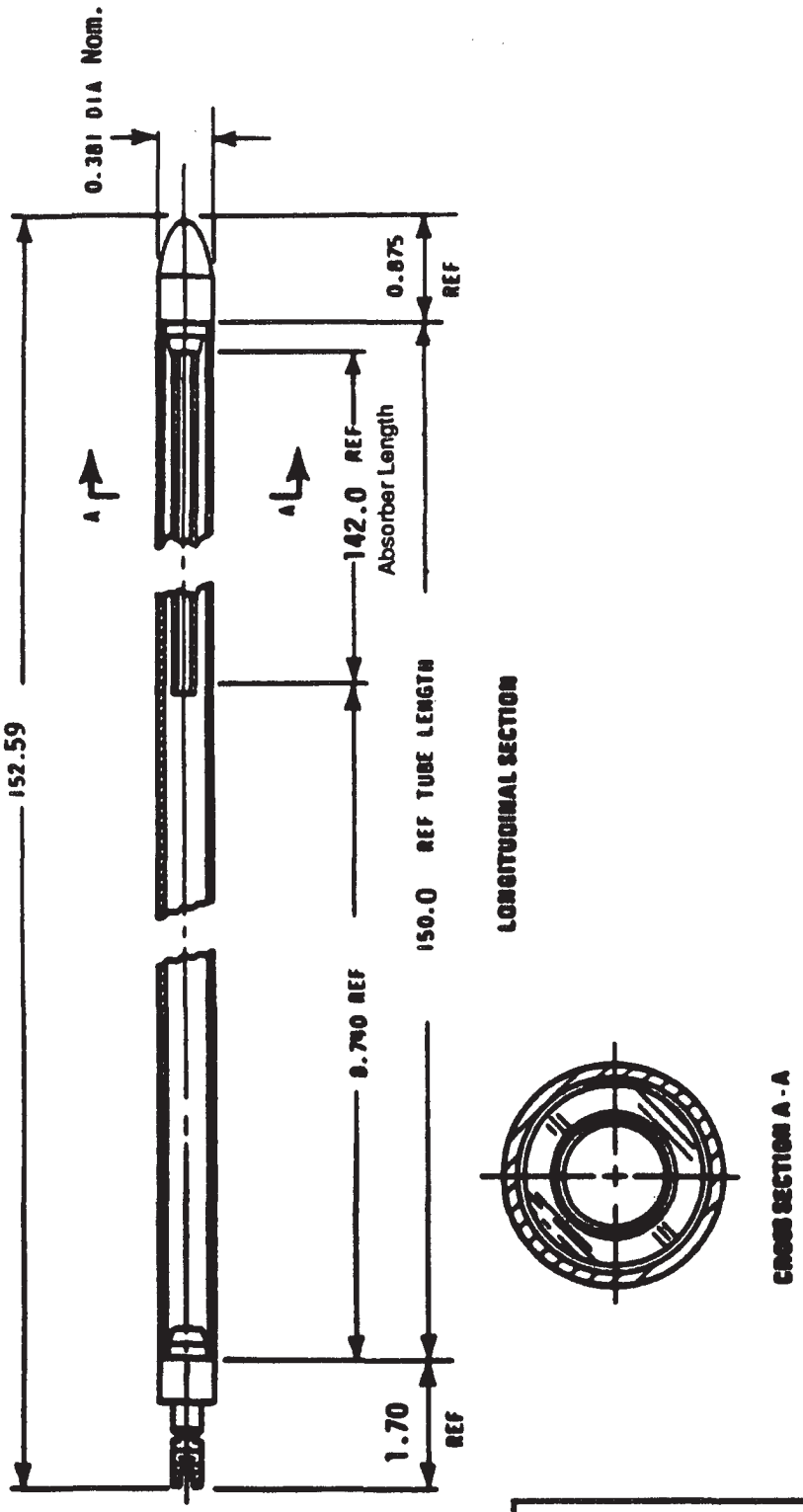

BYRON/BRAIDWOOD STATIONS
UPDATED FINAL SAFETY ANALYSIS REPORT

FIGURE 4.2-13

BURNABLE ABSORBER ROD SECTIONS

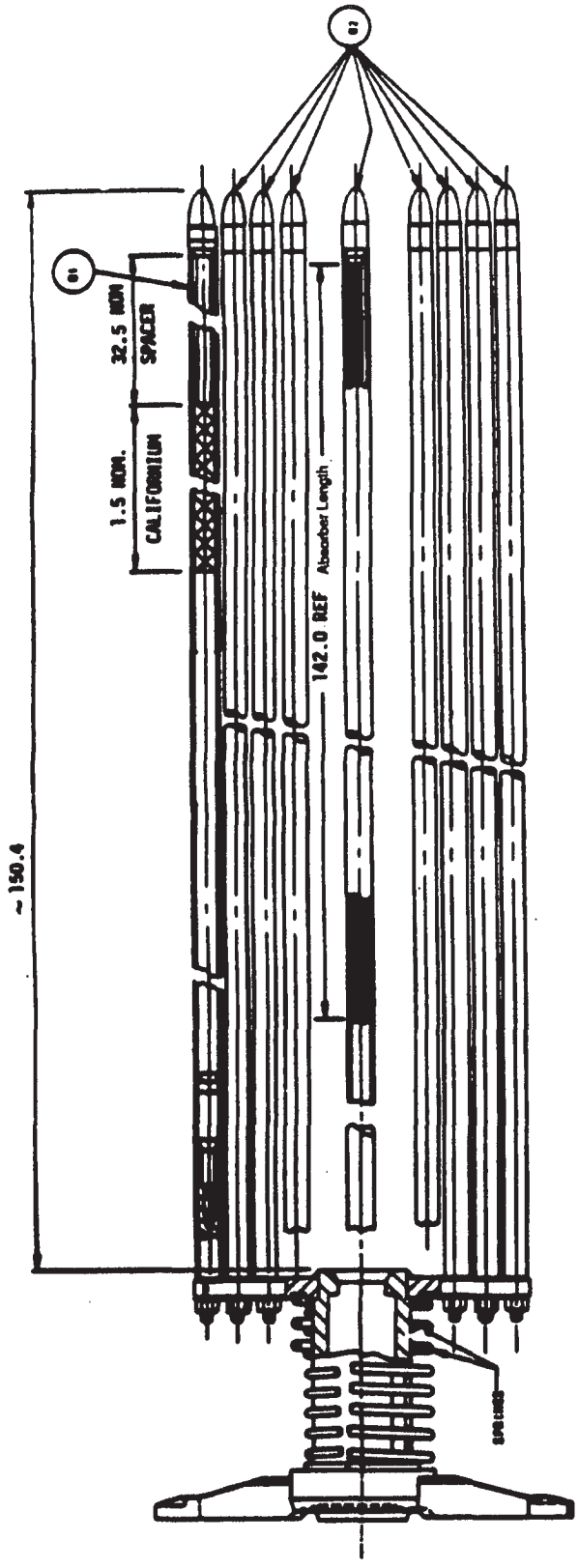

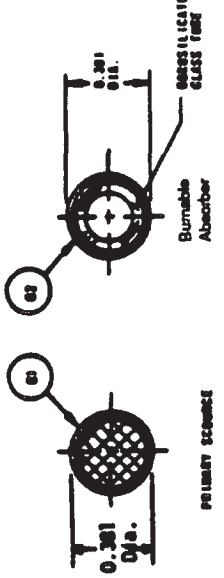

BYRON/BRAIDWOOD STATIONS
UPDATED FINAL SAFETY ANALYSIS REPORT

FIGURE 4.2-14

PRIMARY SOURCE ASSEMBLY

REVISION 6
DECEMBER 1996

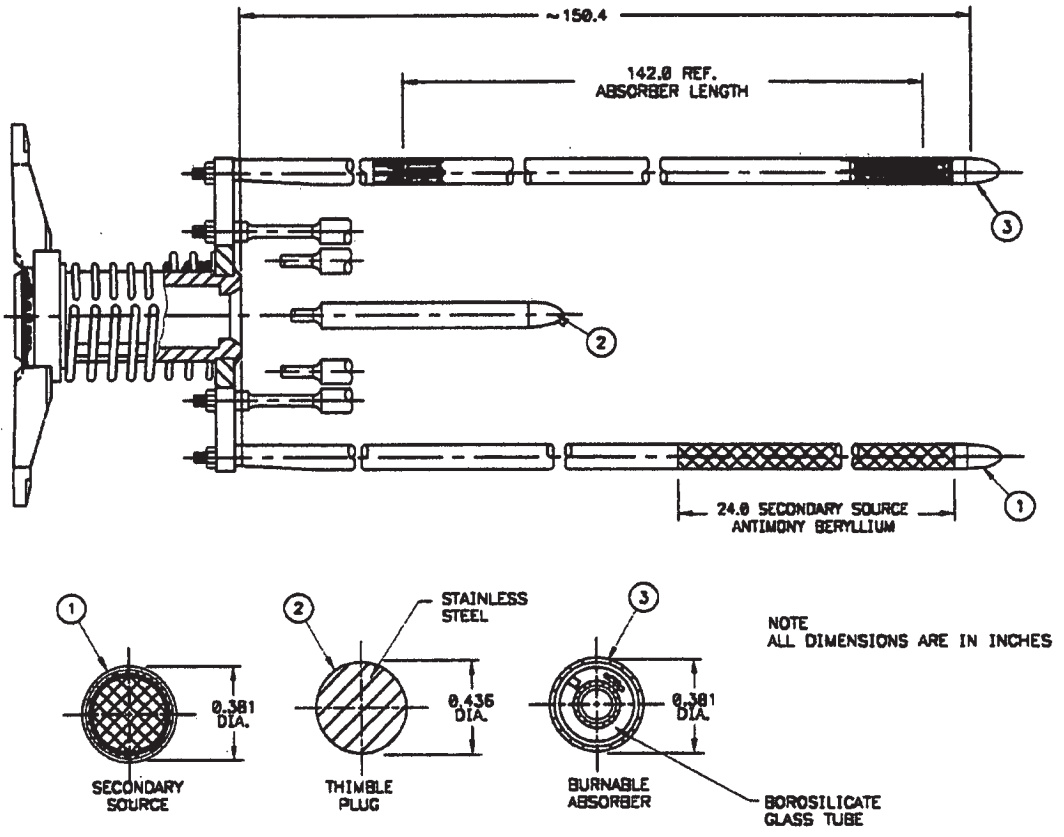

BYRON/BRAIDWOOD STATION
UPDATED FINAL SAFETY ANALYSIS REPORT

4.2-15

SECONDARY SOURCE ASSEMBLY
(FOUR SECONDARY SOURCE RODS)

REVISION 6
DECEMBER 1996

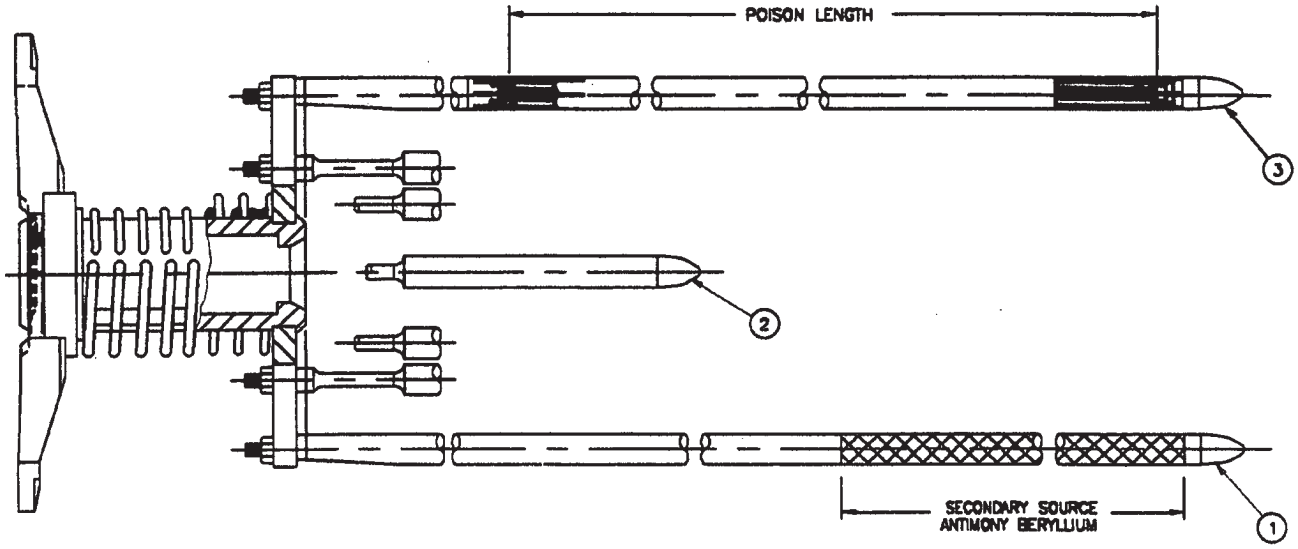

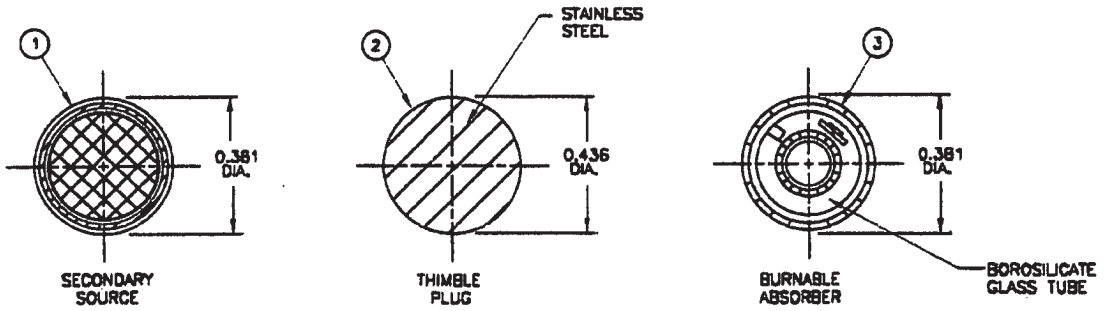

NOTE
ALL DIMENSIONS ARE IN INCHES

BYRON/BRAIDWOOD STATION
UPDATED FINAL SAFETY ANALYSIS REPORT

4.2-15A

SECONDARY SOURCE ASSEMBLY
(SIX SECONDARY SOURCE RODS)

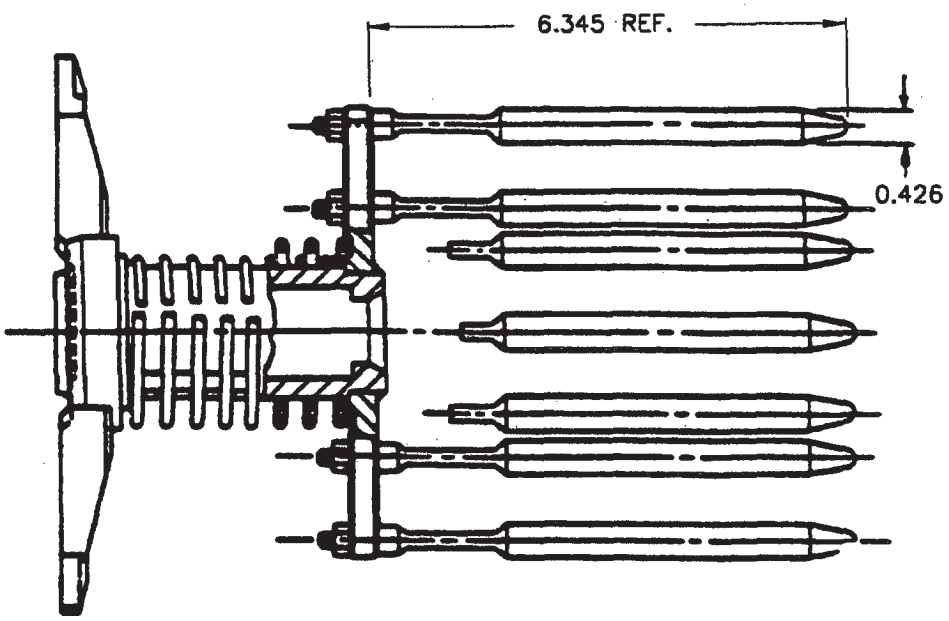

BYRON/BRAIDWOOD STATION
UPDATED FINAL SAFETY ANALYSIS REPORT

FIGURE 4.2-16

THIMBLE PLUG ASSEMBLY

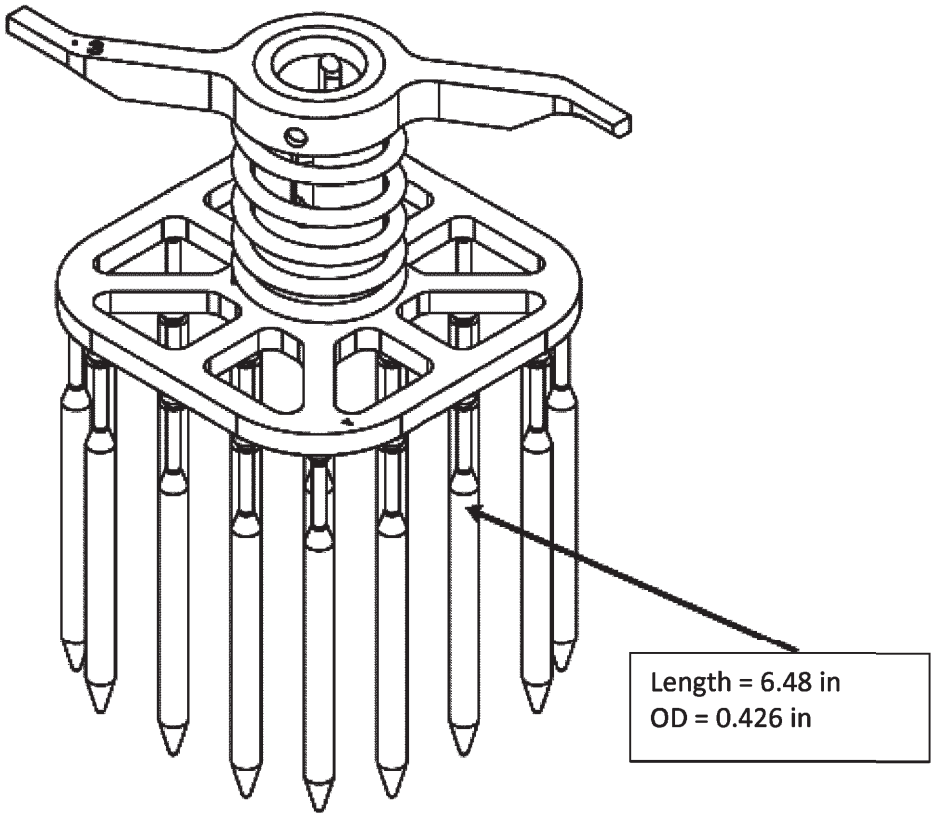

BYRON/BRAIDWOOD STATIONS
UPDATED FINAL SAFETY ANALYSIS REPORT

FIGURE 4.2–16A

ADDITIVELY MANUFACTURED
THIMBLE PLUG ASSEMBLY (AM–TPA)

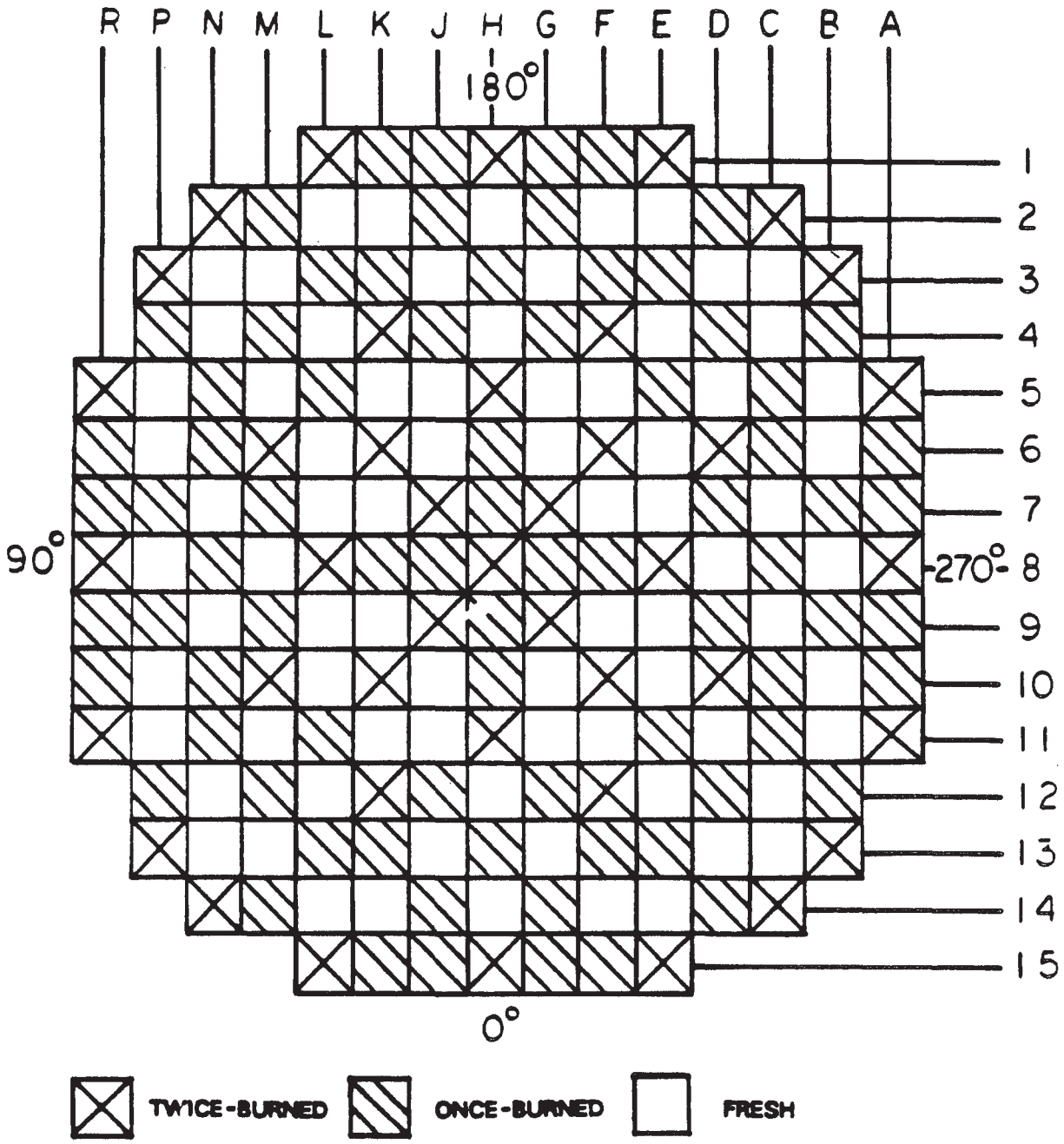

BYRON/BRAIDWOOD STATION
UPDATED FINAL SAFETY ANALYSIS REPORT

FIGURE 4.3-1

TYPICAL FUEL LOADING ARRANGEMENT

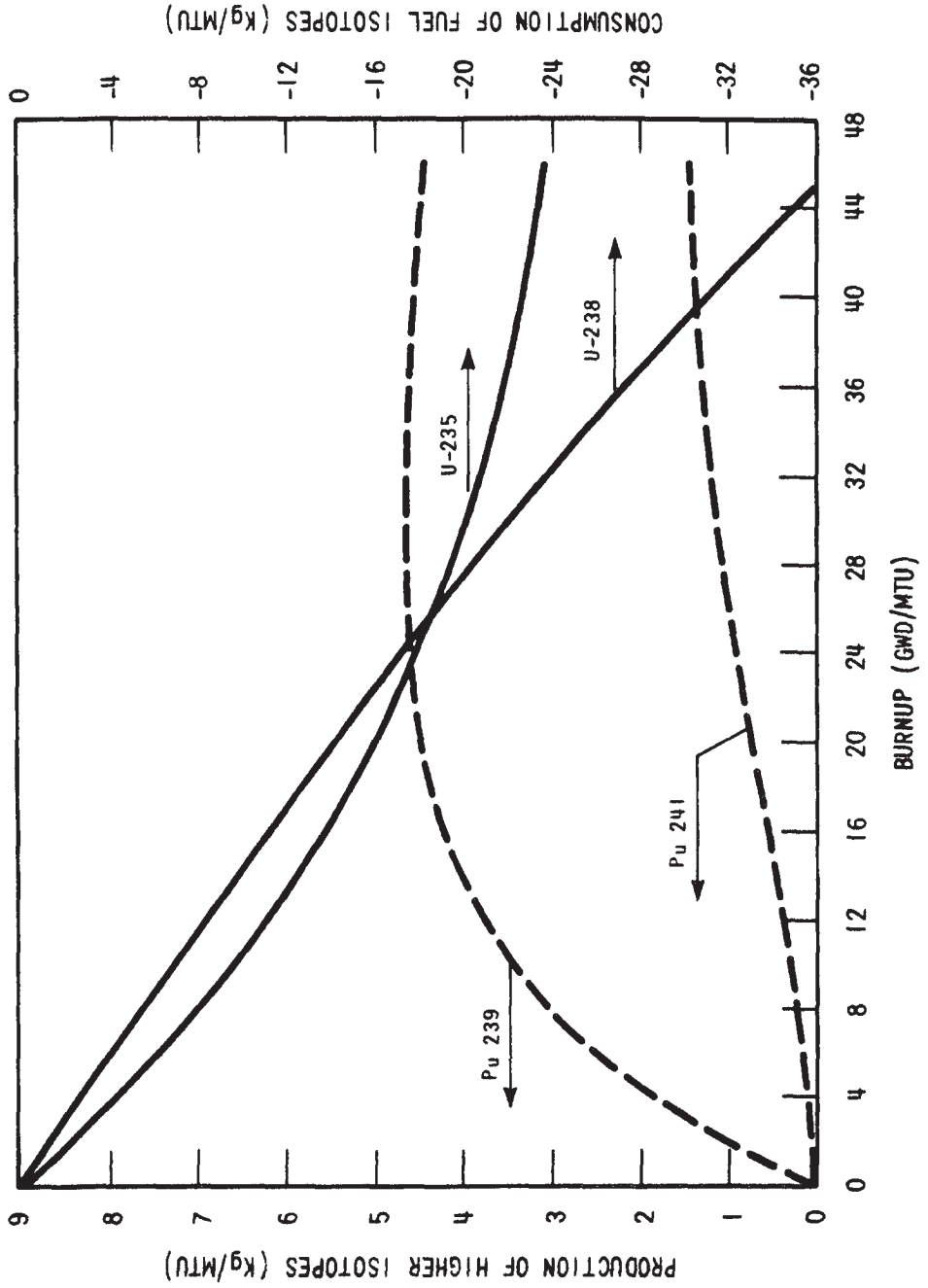

BYRON/BRAIDWOOD STATION
UPDATED FINAL SAFETY ANALYSIS REPORT

FIGURE 4.3-2

PRODUCTION AND CONSUMPTION OF
HIGHER ISOTOPES

REVISION 6
DECEMBER 1996

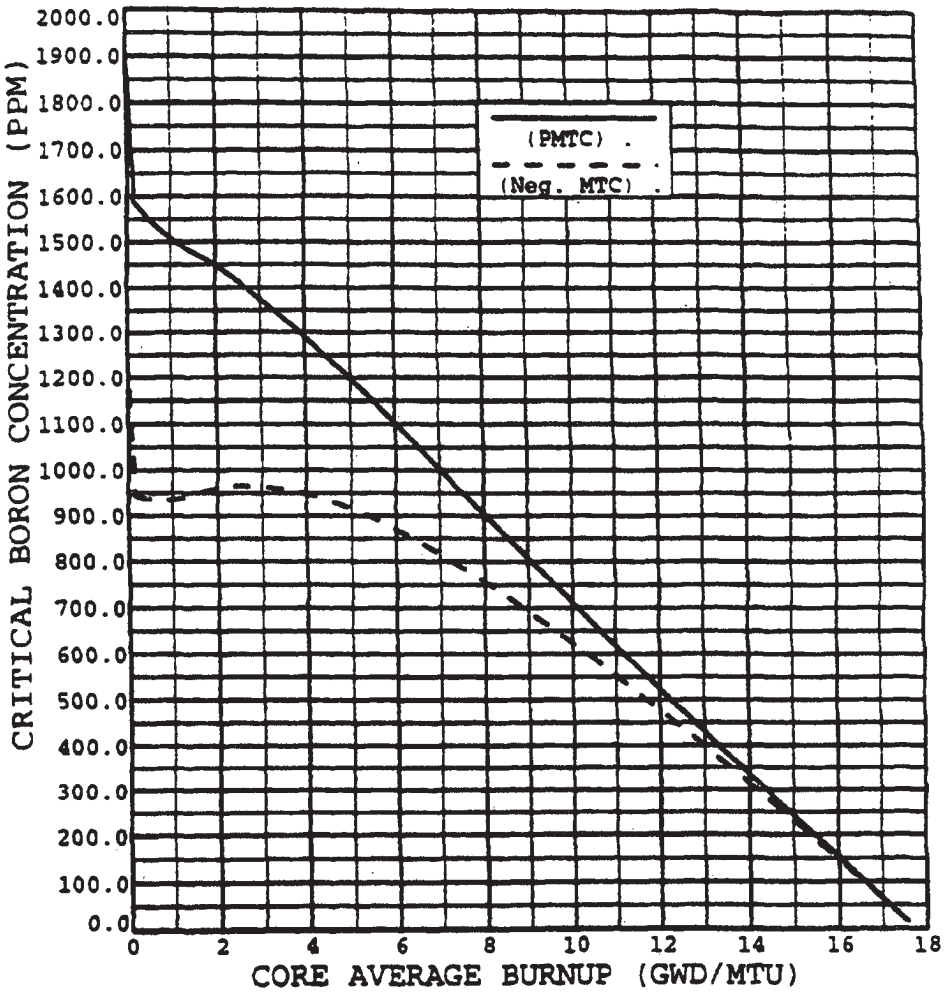

BYRON/BRAIDWOOD STATION
UPDATED FINAL SAFETY ANALYSIS REPORT

FIGURE 4.3-3

CRITICAL BORON CONCENTRATION VERSUS CYCLE BURNUP

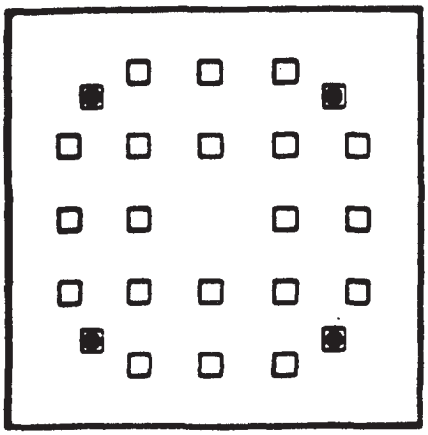

4 Fresh BA

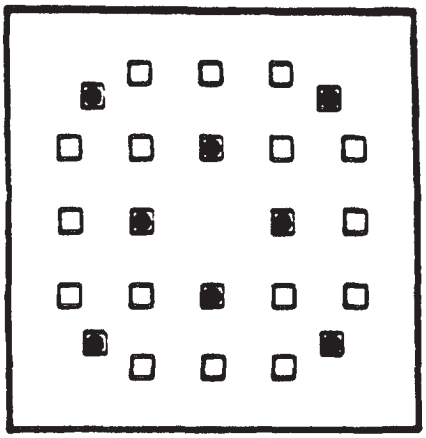

8 Fresh BA

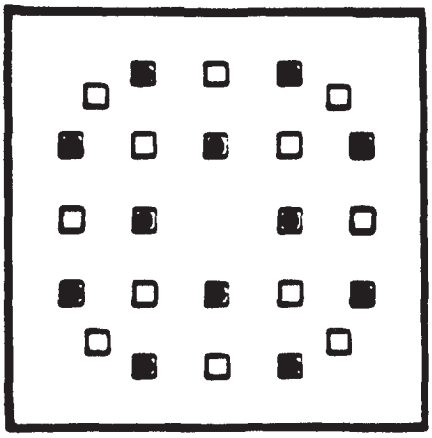

12 Fresh BA

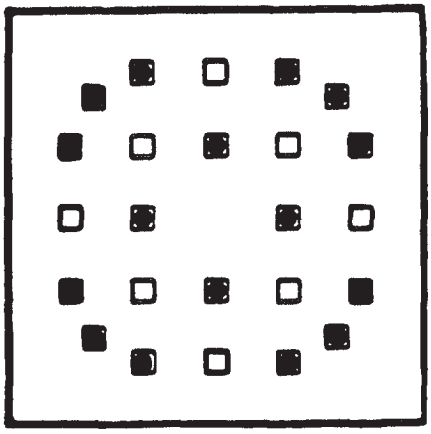

16 Fresh BA

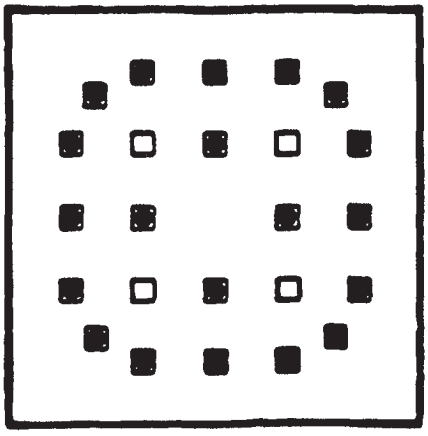

20 Fresh BA

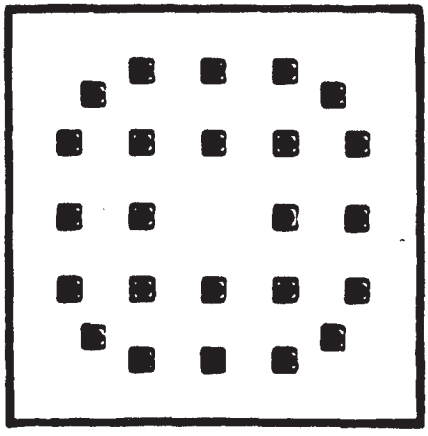

24 Fresh BA

BYRON/BRAIDWOOD STATIONS
UPDATED FINAL SAFETY ANALYSIS REPORT

FIGURE 4.3-4

TYPICAL DISCRETE BURNABLE ABSORBER ROD ARRANGEMENT WITHIN AN ASSEMBLY

Configurations for IFBA Rod Assemblies

REVISION 7
DECEMBER 1998

17X17 Default Burnable Absorber Patterns

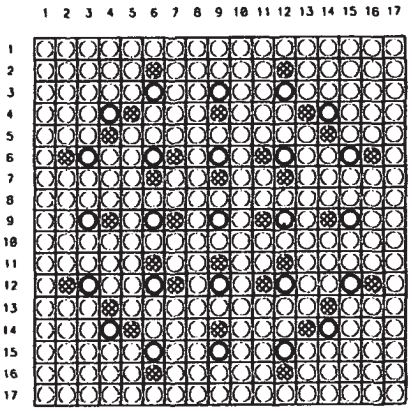

Figure Number 25 - 32 IFBAs

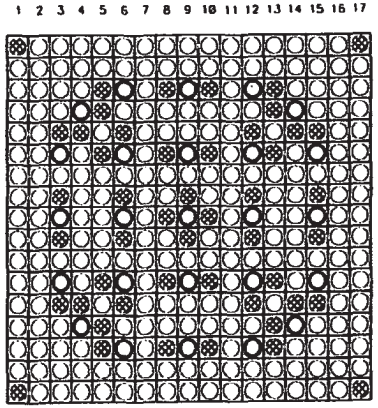

Figure Number 26 -- 48 IFBAs

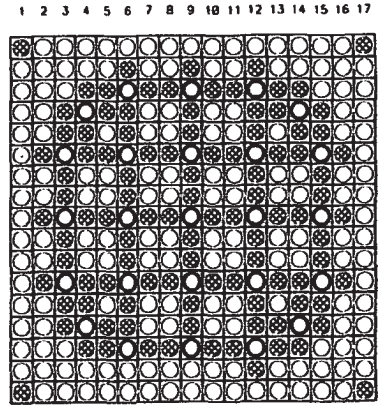

Figure Number 29 -- 104 IFBAs

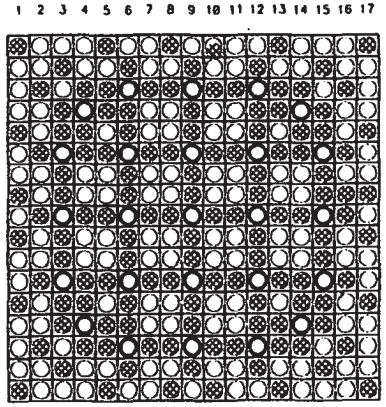

Figure Number 30 -- 128 IFBAs

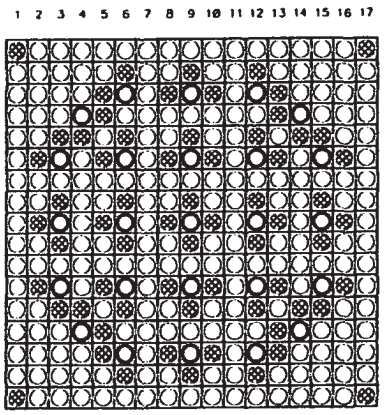

Figure Number 27 - 64 IFBAs

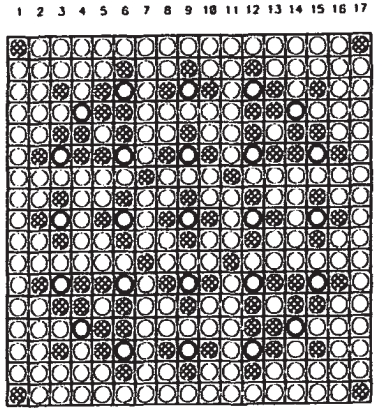

Figure Number 28 - 80 IFBAs

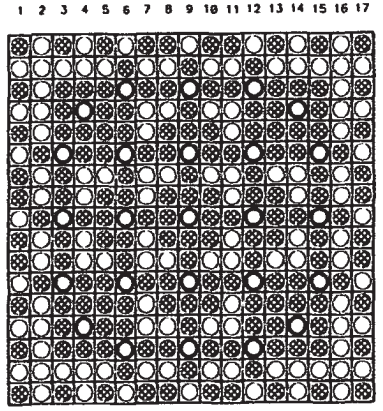

Figure Number 31 - 156 IFBAs

17x17 IFBA Patterns for Feed Assemblies:
Figure Numbers 17,25,26,27,28,29,30,31

Discontinued 17X17 IFBA Patterns:
Figure Numbers 18,19,20,21,22,23,24

BYRON/BRAIDWOOD STATIONS
UPDATED FINAL SAFETY ANALYSIS REPORT

FIGURE 4.3-5

INTEGRAL FUEL BURNABLE ABSORBER ROD ARRANGEMENT WITHIN AN ASSEMBLY

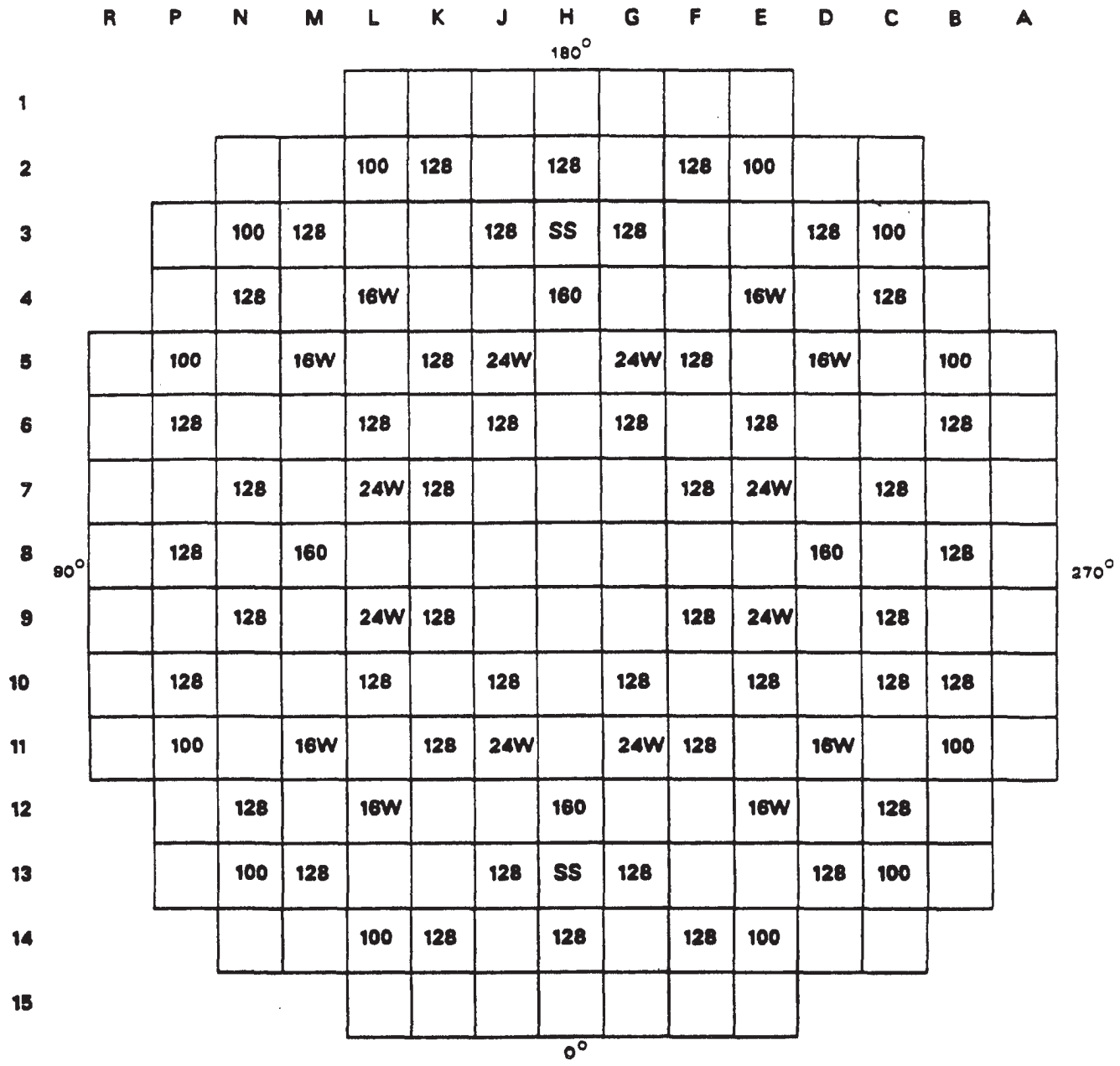

# BA	Number of Fresh Burnable Absorber Rods IFBA / WABA (W) or Secondary Sources (SS)

BYRON/BRAIDWOOD STATIONS
UPDATED FINAL SAFETY ANALYSIS REPORT

FIGURE 4.3-6

BURNABLE ABSORBER LOADING PATTERN
(TYPICAL)

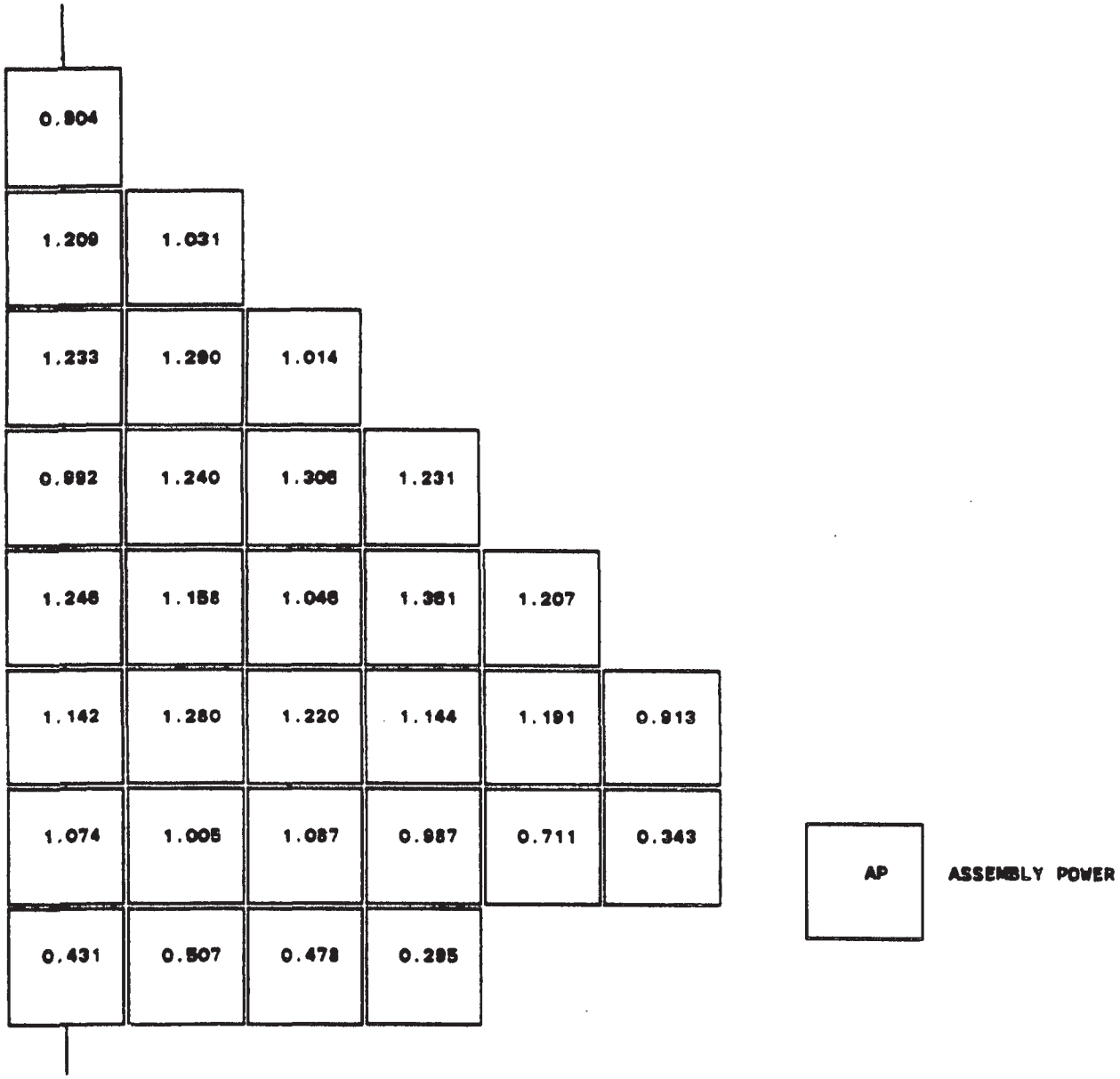

BYRON/BRAIDWOOD STATION
UPDATED FINAL SAFETY ANALYSIS REPORT

FIGURE 4.3-7

NORMALIZED POWER DENSITY DISTRIBUTION
NEAR BEGINNING OF LIFE, UNRODDED CORE,
HOT FULL POWER, EQUILIBRIUM XENON

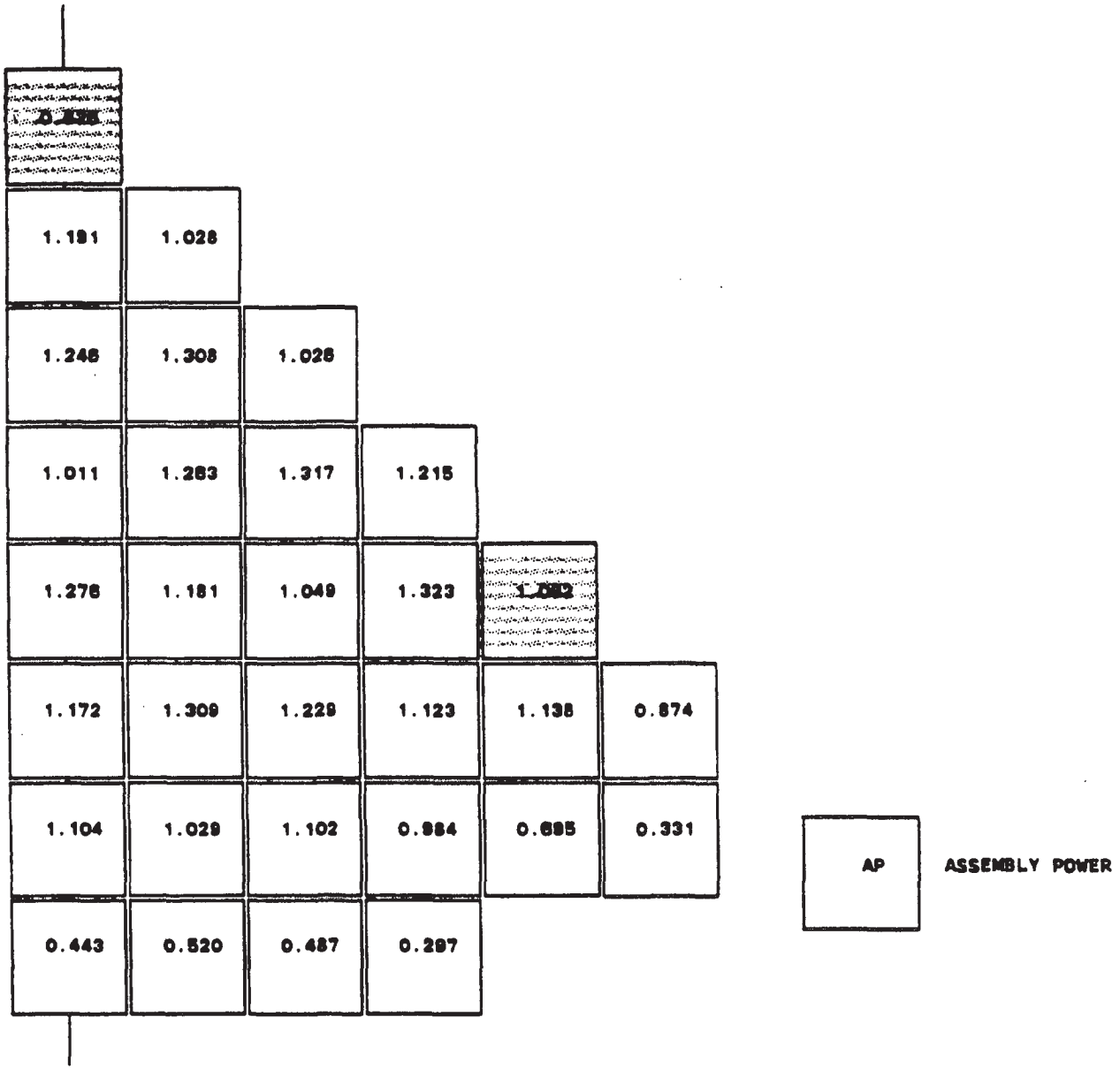

BYRON/BRAIDWOOD STATIONS
UPDATED FINAL SAFETY ANALYSIS REPORT

FIGURE 4.3-8

NORMALIZED POWER DENSITY DISTRIBUTION
NEAR BEGINNING OF LIFE, BANK-D AT INSERTION
LIMIT, HOT FULL POWER, EQUILIBRIUM XENON

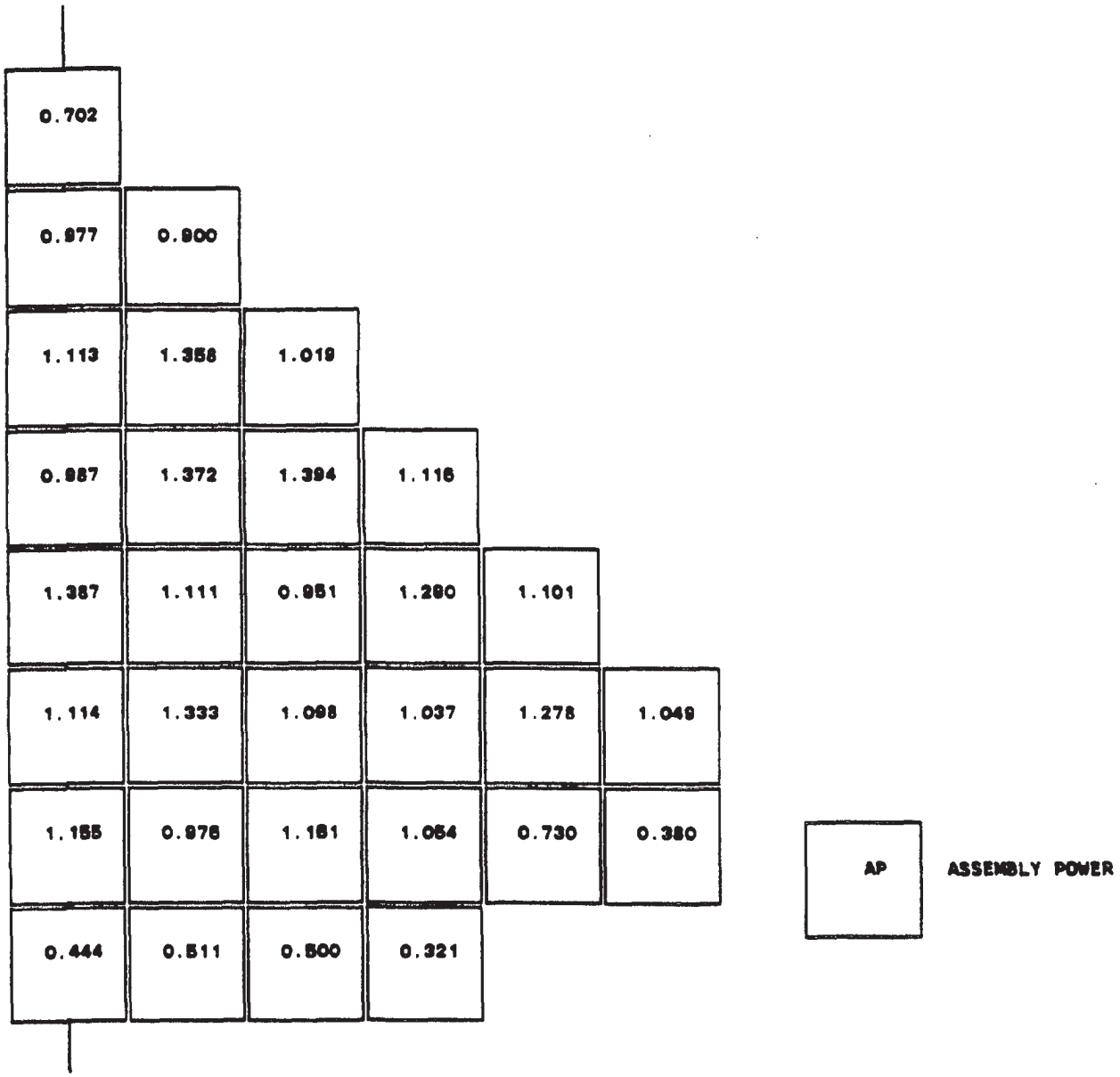

BYRON/BRAIDWOOD STATION
UPDATED FINAL SAFETY ANALYSIS REPORT

FIGURE 4.3-9

NORMALIZED POWER DENSITY DISTRIBUTION
NEAR MIDDLE OF LIFE, UNRODDED CORE,
HOT FULL POWER, EQUILIBRIUM XENON

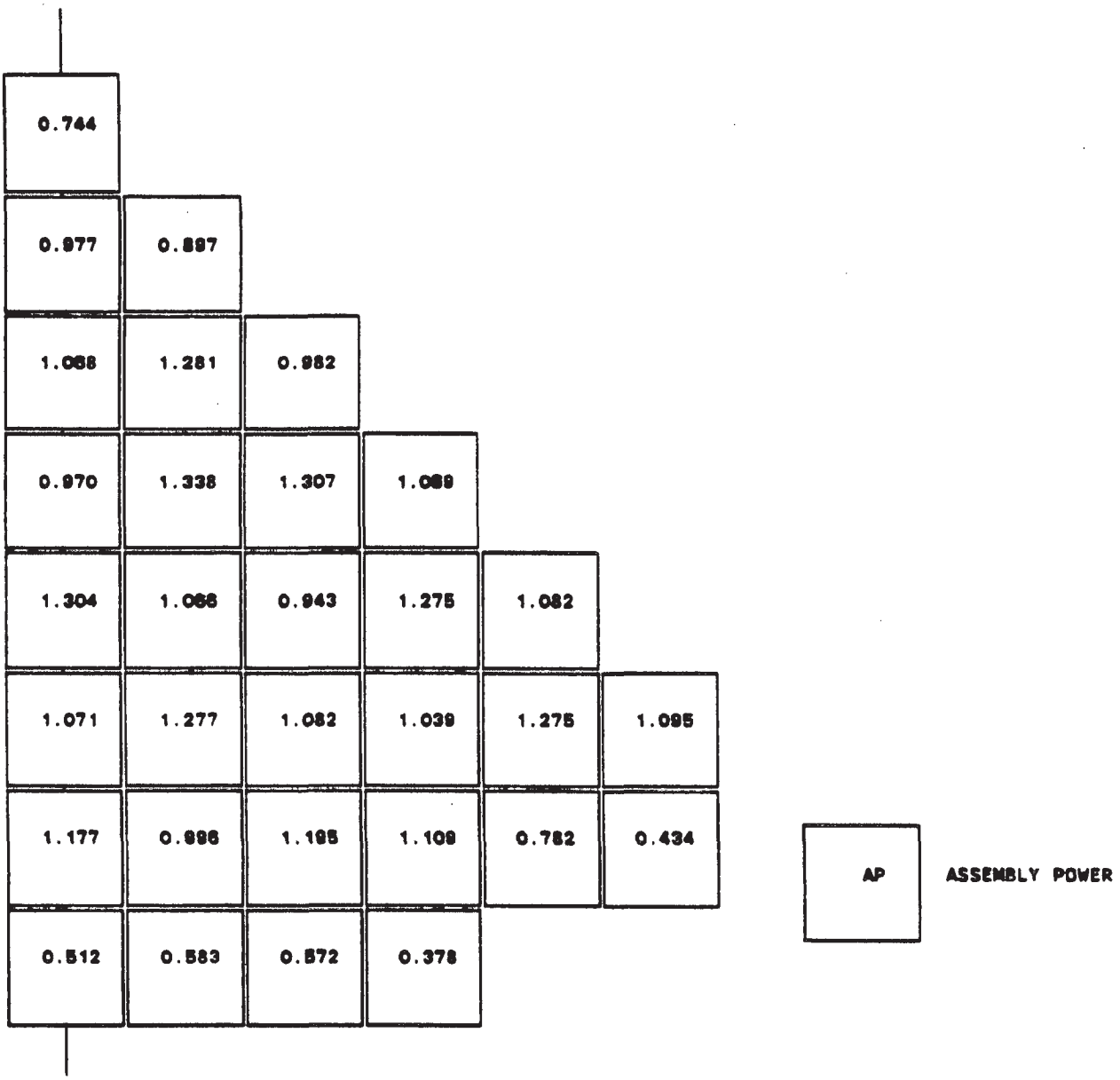

BYRON/BRAIDWOOD STATION
UPDATED FINAL SAFETY ANALYSIS REPORT

FIGURE 4.3-10

NORMALIZED POWER DENSITY DISTRIBUTION
NEAR END OF LIFE, UNRODDED CORE,
HOT FULL POWER, EQUILIBRIUM XENON

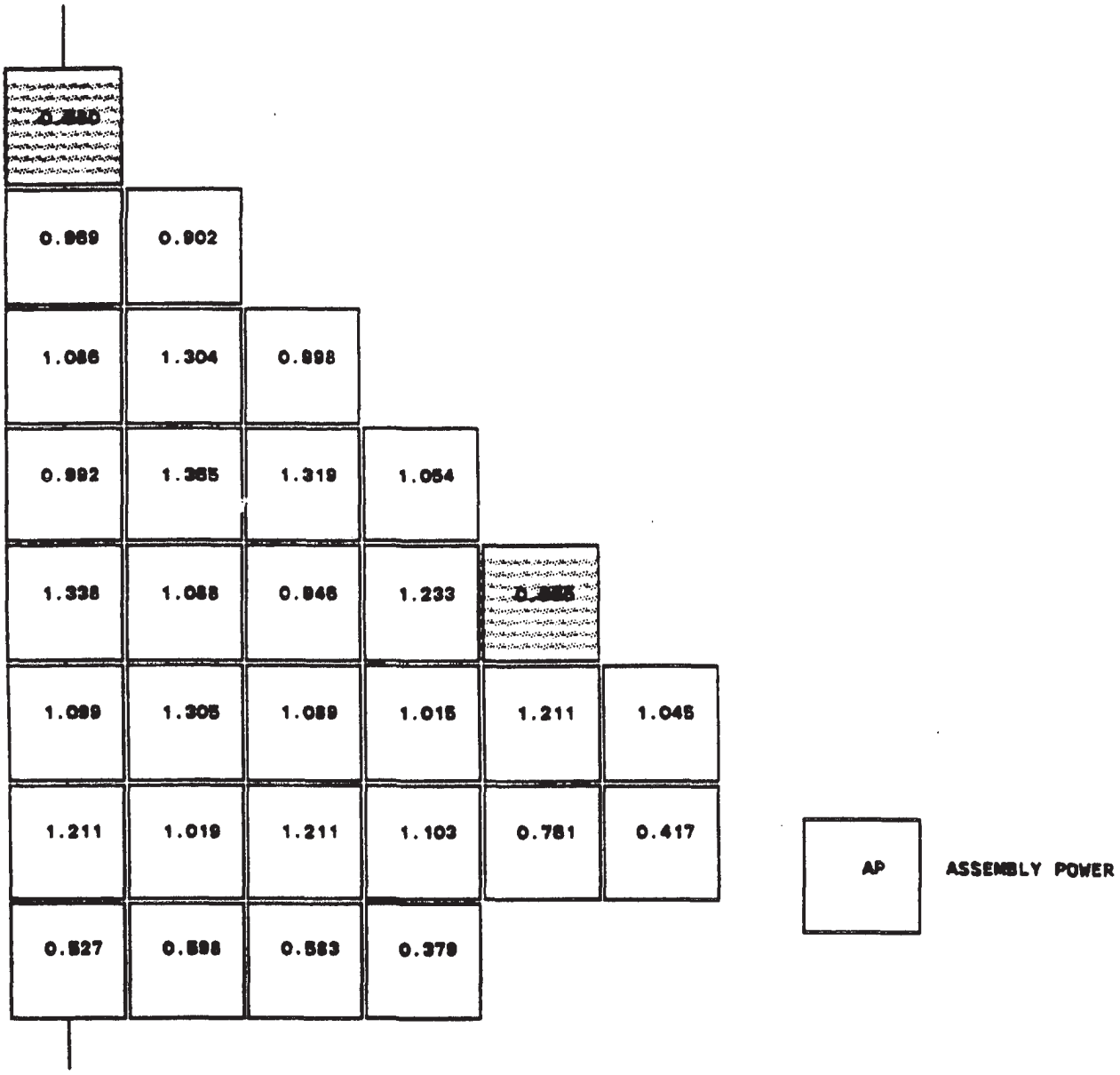

BYRON/BRAIDWOOD STATIONS
UPDATED FINAL SAFETY ANALYSIS REPORT

FIGURE 4.3-11

NORMALIZED POWER DENSITY DISTRIBUTION
NEAR END OF LIFE, BANK-D AT INSERTION LIMIT,
HOT FULL POWER, EQUILIBRIUM XENON

1.245	1.262	1.191	1.265	1.214	1.287	1.223	1.280	1.233	1.289	1.224	1.300	1.219	1.271	1.189	1.272	1.259
1.264	1.176	1.175	1.204	1.228	1.335	1.233	1.236	1.320	1.236	1.234	1.339	1.232	1.210	1.183	1.186	1.279
1.189	1.181	1.213	1.347	1.377	0.000	1.361	1.361	0.000	1.361	1.363	0.000	1.383	1.354	1.221	1.191	1.213
1.279	1.216	1.354	0.000	1.407	1.398	1.265	1.257	1.348	1.258	1.267	1.404	1.414	0.000	1.364	1.227	1.295
1.234	1.246	1.391	1.414	1.314	1.398	1.271	1.264	1.356	1.266	1.274	1.404	1.321	1.423	1.402	1.258	1.250
1.323	1.360	0.000	1.412	1.405	0.000	1.386	1.386	0.000	1.389	1.391	0.000	1.413	1.422	0.000	1.375	1.341
1.252	1.260	1.384	1.280	1.279	1.390	1.274	1.272	1.370	1.276	1.279	1.398	1.288	1.280	1.397	1.274	1.269
1.321	1.265	1.386	1.274	1.274	1.392	1.274	1.275	1.377	1.279	1.280	1.401	1.284	1.285	1.400	1.280	1.341
1.259	1.347	0.000	1.366	1.369	0.000	1.372	1.376	0.000	1.377	1.376	0.000	1.380	1.380	0.000	1.370	1.285
1.314	1.260	1.382	1.272	1.275	1.394	1.277	1.279	1.377	1.276	1.279	1.401	1.286	1.288	1.405	1.286	1.350
1.245	1.255	1.380	1.278	1.279	1.391	1.276	1.276	1.372	1.275	1.280	1.400	1.292	1.295	1.405	1.283	1.281
1.315	1.354	0.000	1.409	1.404	0.000	1.389	1.390	0.000	1.391	1.395	0.000	1.420	1.431	0.000	1.388	1.356
1.227	1.240	1.386	1.411	1.313	1.399	1.272	1.267	1.361	1.271	1.280	1.413	1.331	1.436	1.416	1.273	1.267
1.271	1.210	1.349	0.000	1.406	1.400	1.266	1.260	1.354	1.266	1.277	1.416	1.428	0.000	1.381	1.244	1.316
1.192	1.175	1.208	1.344	1.375	0.000	1.363	1.365	0.000	1.374	1.377	0.000	1.400	1.373	1.239	1.210	1.236
1.257	1.171	1.171	1.202	1.227	1.337	1.236	1.240	1.331	1.251	1.251	1.359	1.252	1.230	1.204	1.209	1.306
1.241	1.259	1.190	1.266	1.217	1.302	1.228	1.297	1.245	1.310	1.246	1.325	1.244	1.299	1.226	1.303	1.291

BYRON/BRAIDWOOD STATIONS
UPDATED FINAL SAFETY ANALYSIS REPORT

FIGURE 4.3-12
RODWISE POWER DISTRIBUTION IN A TYPICAL ASSEMBLY (ASSEMBLY F-11) NEAR BEGINNING OF LIFE, HOT FULL POWER, EQUILIBRIUM XENON, UNRODDED CORE

1.270	1.270	1.297	1.280	1.311	1.282	1.306	1.276	1.301	1.276	1.298	1.276	1.285	1.247	1.257	1.231	1.239
1.259	1.277	1.286	1.302	1.315	1.315	1.309	1.305	1.299	1.304	1.300	1.296	1.287	1.266	1.244	1.236	1.228
1.285	1.287	1.311	1.330	1.343	0.000	1.328	1.325	0.000	1.324	1.316	0.000	1.312	1.291	1.267	1.244	1.256
1.275	1.311	1.338	0.000	1.362	1.355	1.335	1.327	1.323	1.326	1.322	1.332	1.329	0.000	1.292	1.266	1.246
1.314	1.333	1.361	1.372	1.373	1.360	1.344	1.336	1.331	1.333	1.329	1.335	1.338	1.328	1.312	1.287	1.283
1.305	1.343	0.000	1.375	1.370	0.000	1.353	1.350	0.000	1.346	1.337	0.000	1.334	1.331	0.000	1.295	1.273
1.328	1.345	1.362	1.362	1.362	1.361	1.350	1.345	1.339	1.338	1.334	1.335	1.325	1.318	1.312	1.296	1.293
1.304	1.345	1.365	1.360	1.360	1.364	1.350	1.344	1.338	1.336	1.334	1.338	1.325	1.317	1.316	1.296	1.266
1.325	1.334	0.000	1.358	1.358	0.000	1.349	1.343	0.000	1.330	1.330	0.000	1.325	1.317	0.000	1.291	1.290
1.298	1.340	1.362	1.359	1.360	1.367	1.354	1.350	1.339	1.333	1.332	1.338	1.325	1.319	1.318	1.299	1.269
1.316	1.334	1.353	1.355	1.355	1.357	1.348	1.344	1.335	1.331	1.328	1.331	1.322	1.316	1.311	1.295	1.282
1.287	1.325	0.000	1.361	1.357	0.000	1.344	1.343	0.000	1.336	1.329	0.000	1.327	1.325	0.000	1.291	1.269
1.290	1.309	1.338	1.352	1.354	1.343	1.329	1.322	1.318	1.319	1.317	1.324	1.328	1.320	1.304	1.280	1.277
1.245	1.281	1.309	0.000	1.337	1.332	1.314	1.308	1.306	1.309	1.307	1.318	1.316	0.000	1.280	1.255	1.236
1.249	1.252	1.277	1.288	1.313	0.000	1.301	1.300	0.000	1.304	1.298	0.000	1.296	1.276	1.252	1.231	1.243
1.219	1.238	1.248	1.265	1.280	1.282	1.278	1.275	1.279	1.282	1.279	1.277	1.268	1.248	1.227	1.220	1.214
1.226	1.228	1.256	1.242	1.273	1.286	1.271	1.243	1.271	1.251	1.275	1.254	1.264	1.228	1.238	1.212	1.221

BYRON/BRAIDWOOD STATIONS
UPDATED FINAL SAFETY ANALYSIS REPORT

FIGURE 4.3-13

RODWISE POWER DISTRIBUTION IN A TYPICAL ASSEMBLY (ASSEMBLY F-11) NEAR END OF LIFE, HOT FULL POWER, EQUILIBRIUM XENON, UNRODDED CORE

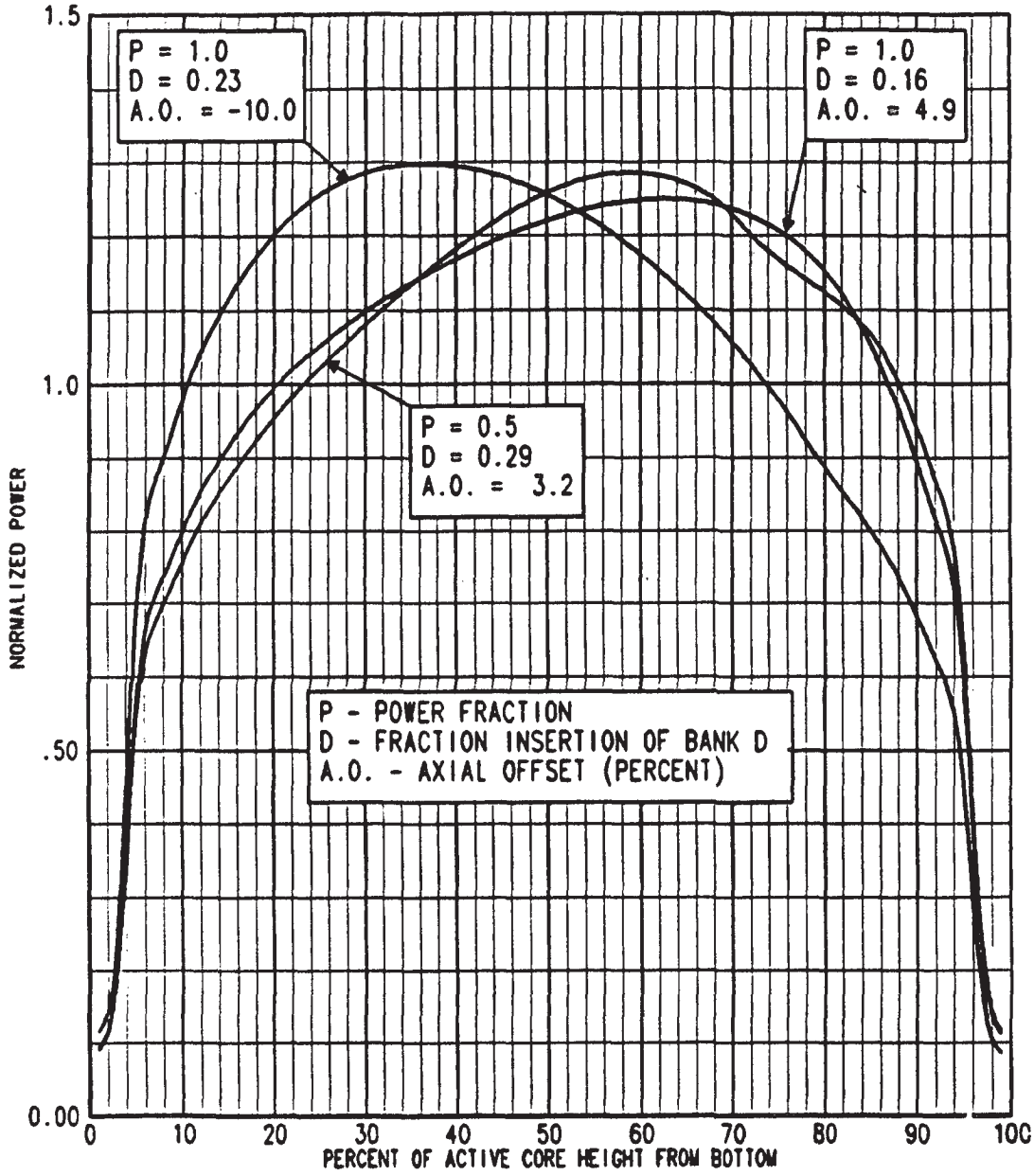

BYRON/BRAIDWOOD STATION
UPDATED FINAL SAFETY ANALYSIS REPORT

FIGURE 4.3-14

TYPICAL AXIAL POWER SHAPES OCCURRING AT BEGINNING OF LIFE

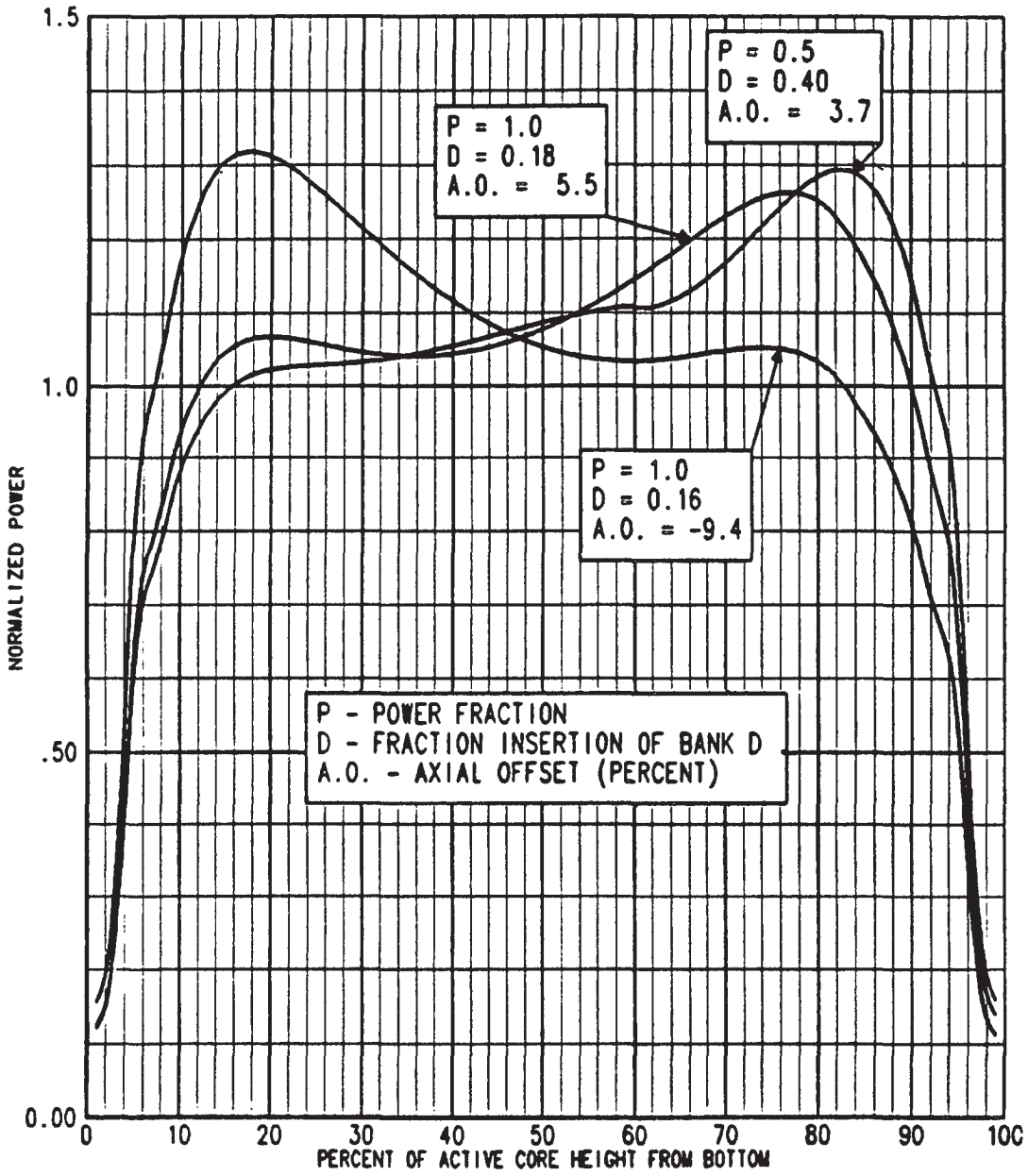

BYRON/BRAIDWOOD STATION
UPDATED FINAL SAFETY ANALYSIS REPORT

FIGURE 4.3-15

TYPICAL AXIAL POWER SHAPES OCCURRING AT MIDDLE OF LIFE

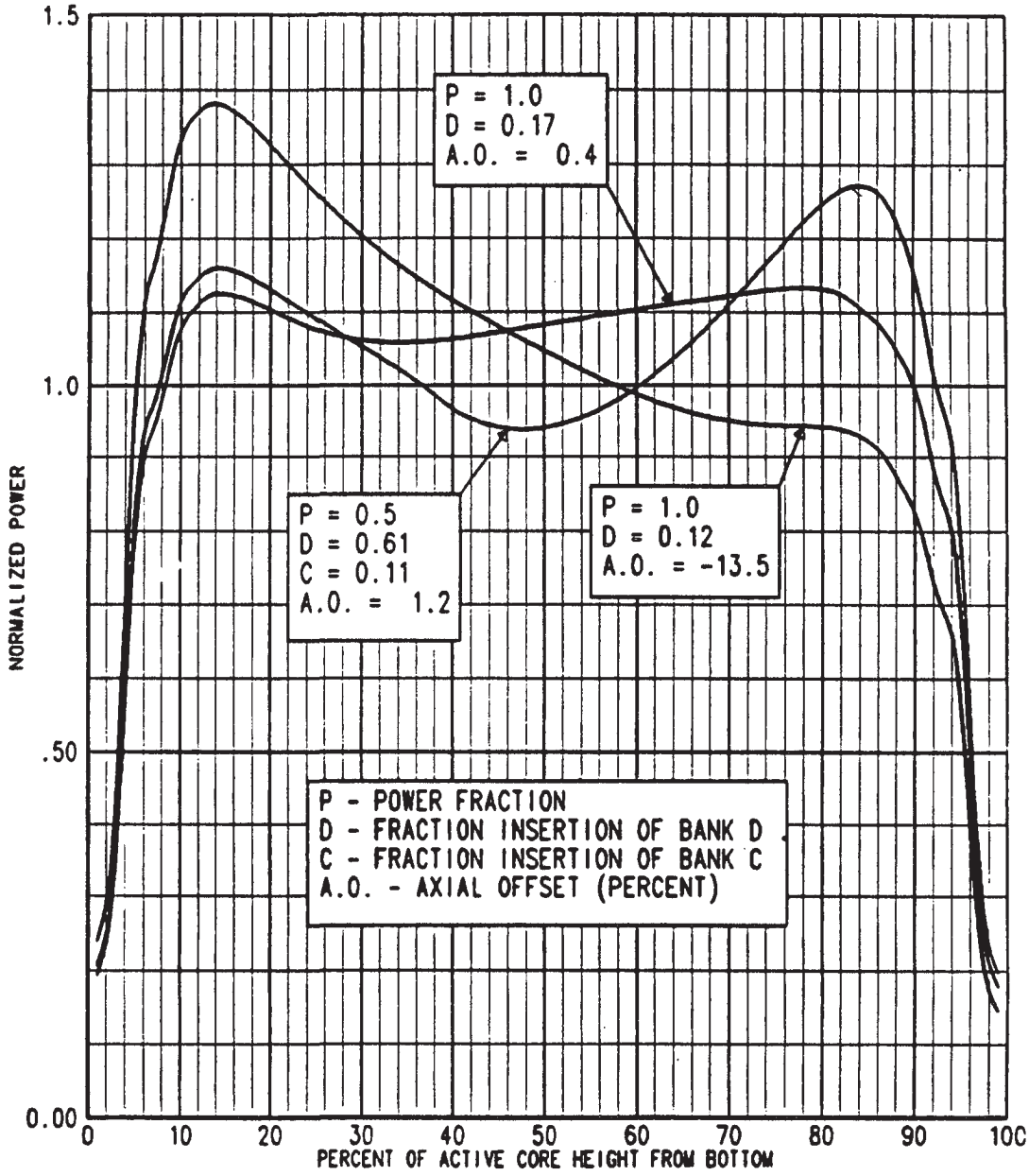

BYRON/BRAIDWOOD STATION
UPDATED FINAL SAFETY ANALYSIS REPORT

FIGURE 4.3-16

TYPICAL AXIAL POWER SHAPES OCCURRING AT END OF LIFE

Figures 4.3-17, 4.3-18, and 4.3-19
have been deleted intentionally.

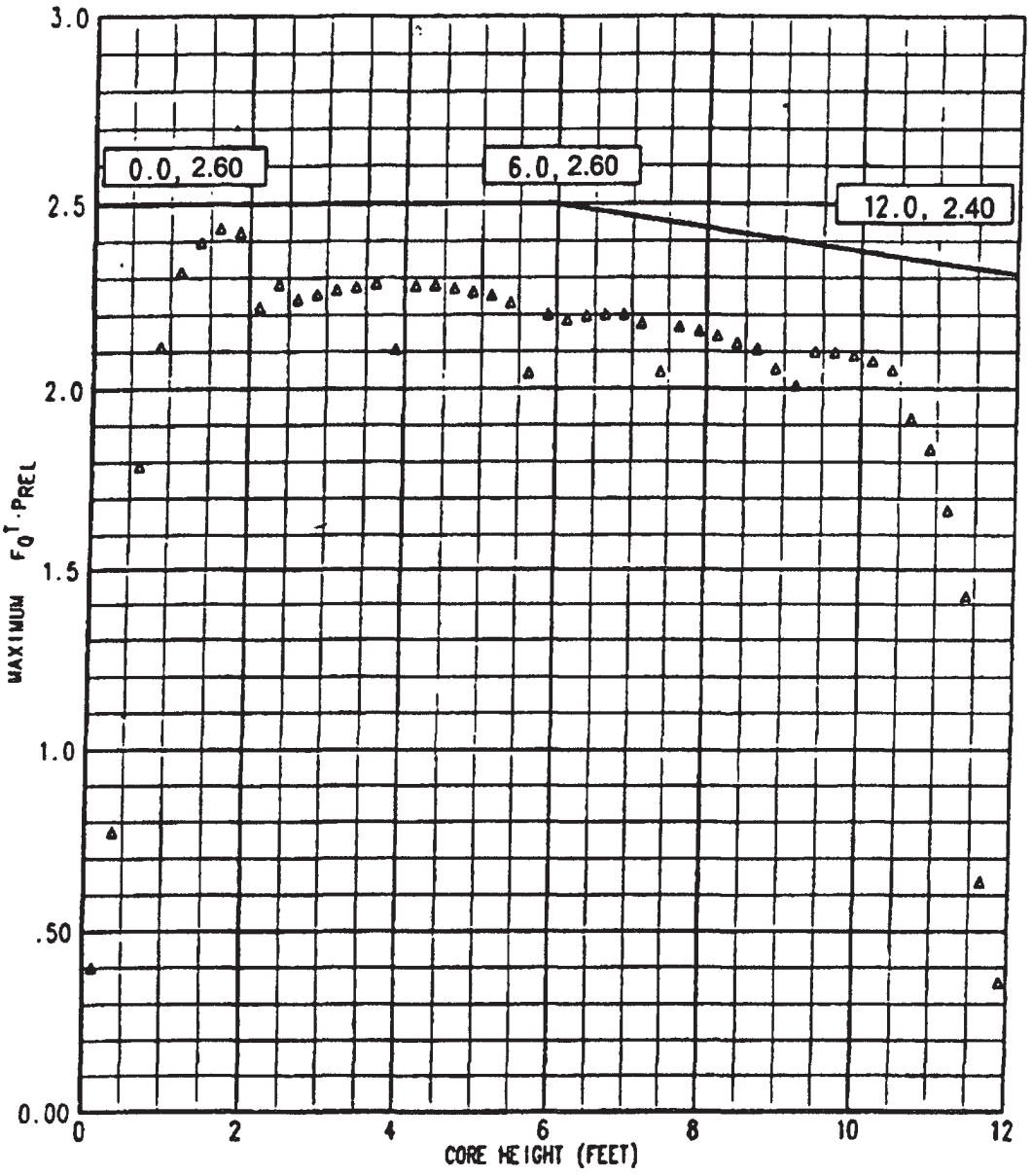

BYRON/BRAIDWOOD STATIONS
UPDATED FINAL SAFETY ANALYSIS REPORT

FIGURE 4.3-20

MAXIMUM F(Q) X POWER VERSUS AXIAL HEIGHT
DURING NORMAL CORE OPERATION

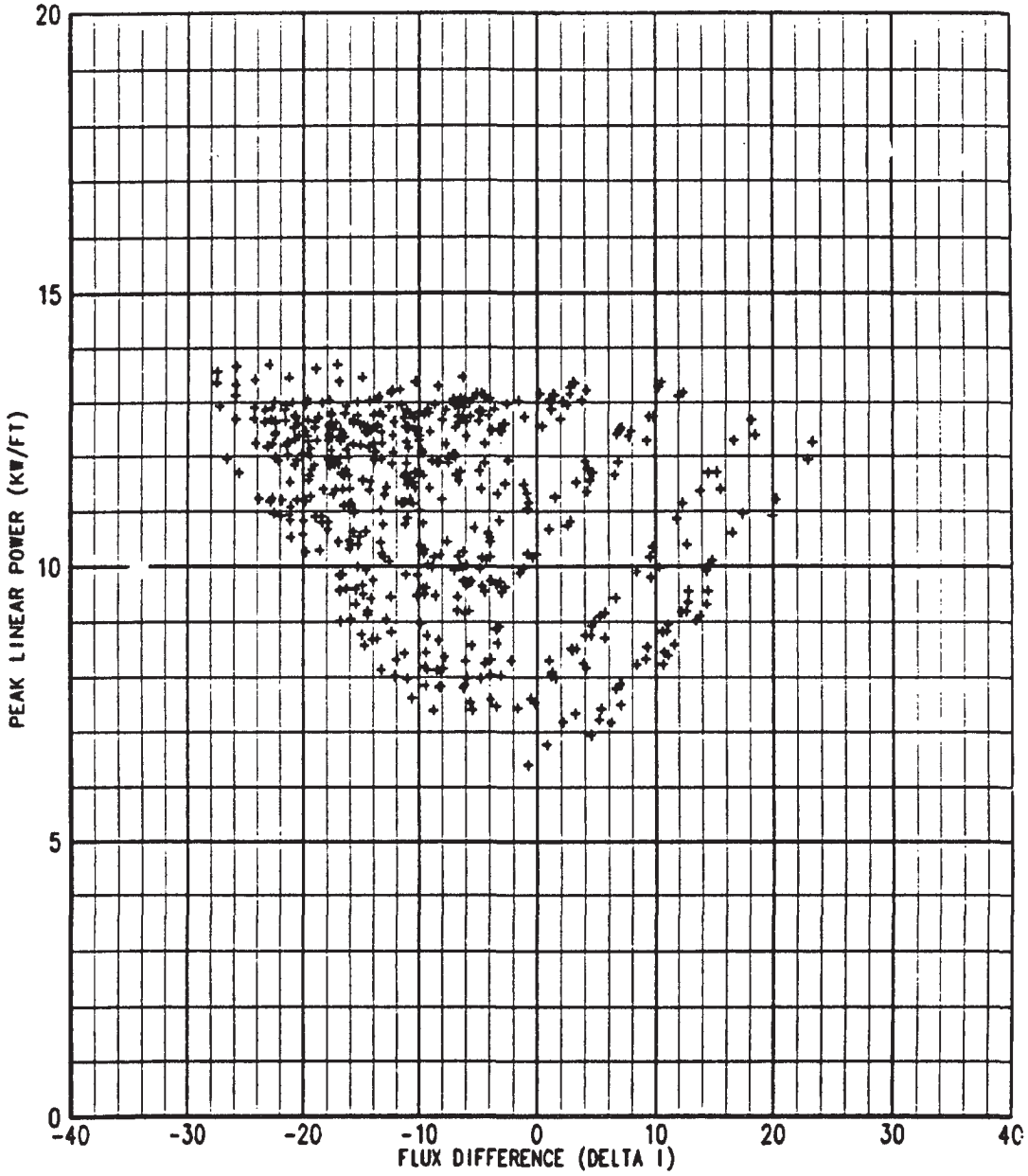

BYRON/BRAIDWOOD STATIONS
UPDATED FINAL SAFETY ANALYSIS REPORT

FIGURE 4.3-21

PEAK LINEAR POWER DURING CONTROL ROD MALFUNCTION OVERPOWER TRANSIENTS

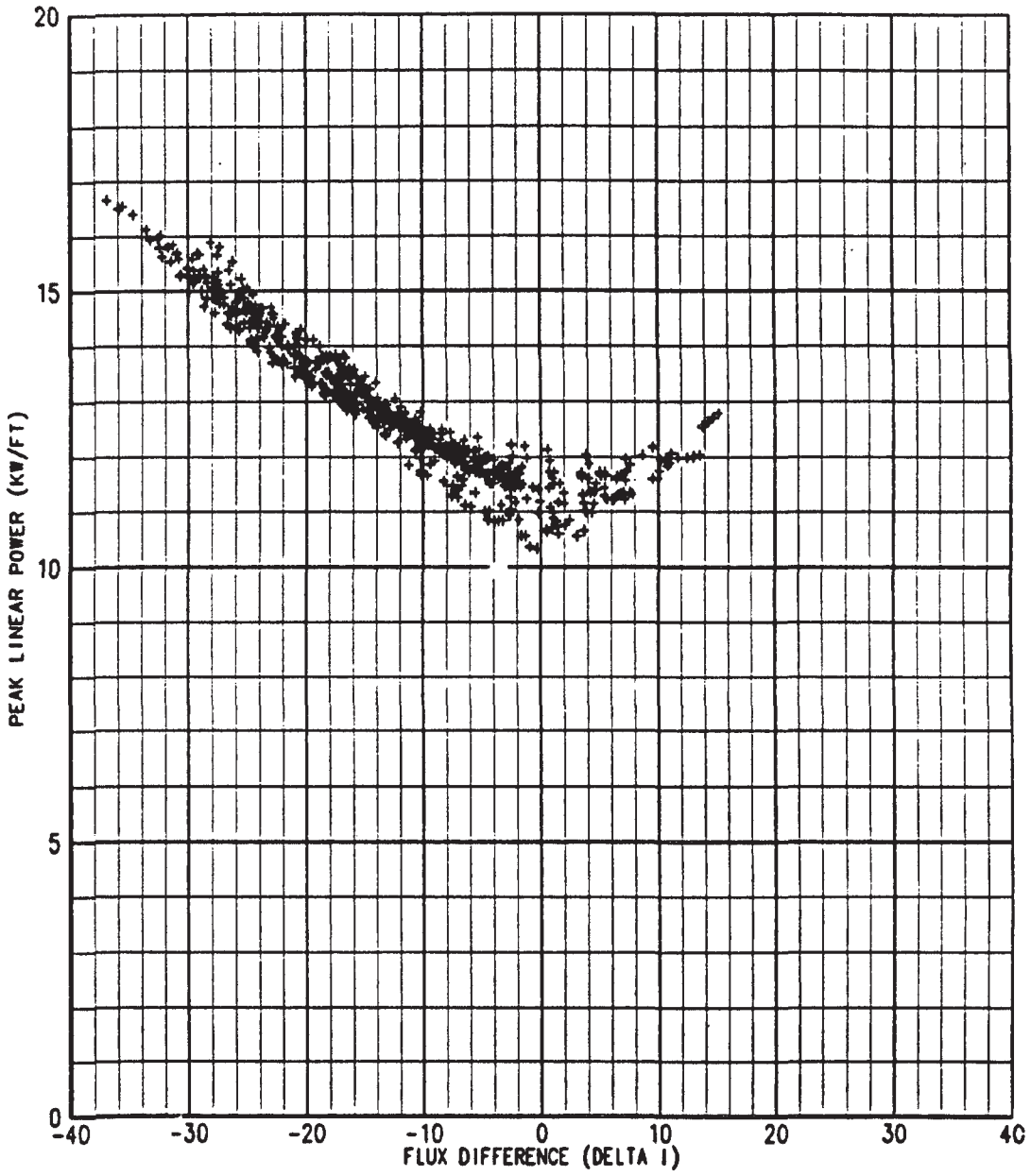

BYRON/BRAIDWOOD STATIONS
UPDATED FINAL SAFETY ANALYSIS REPORT

FIGURE 4.3-22

PEAK LINEAR POWER DURING
BORATION/DEBORATION OVERPOWER
TRANSIENTS

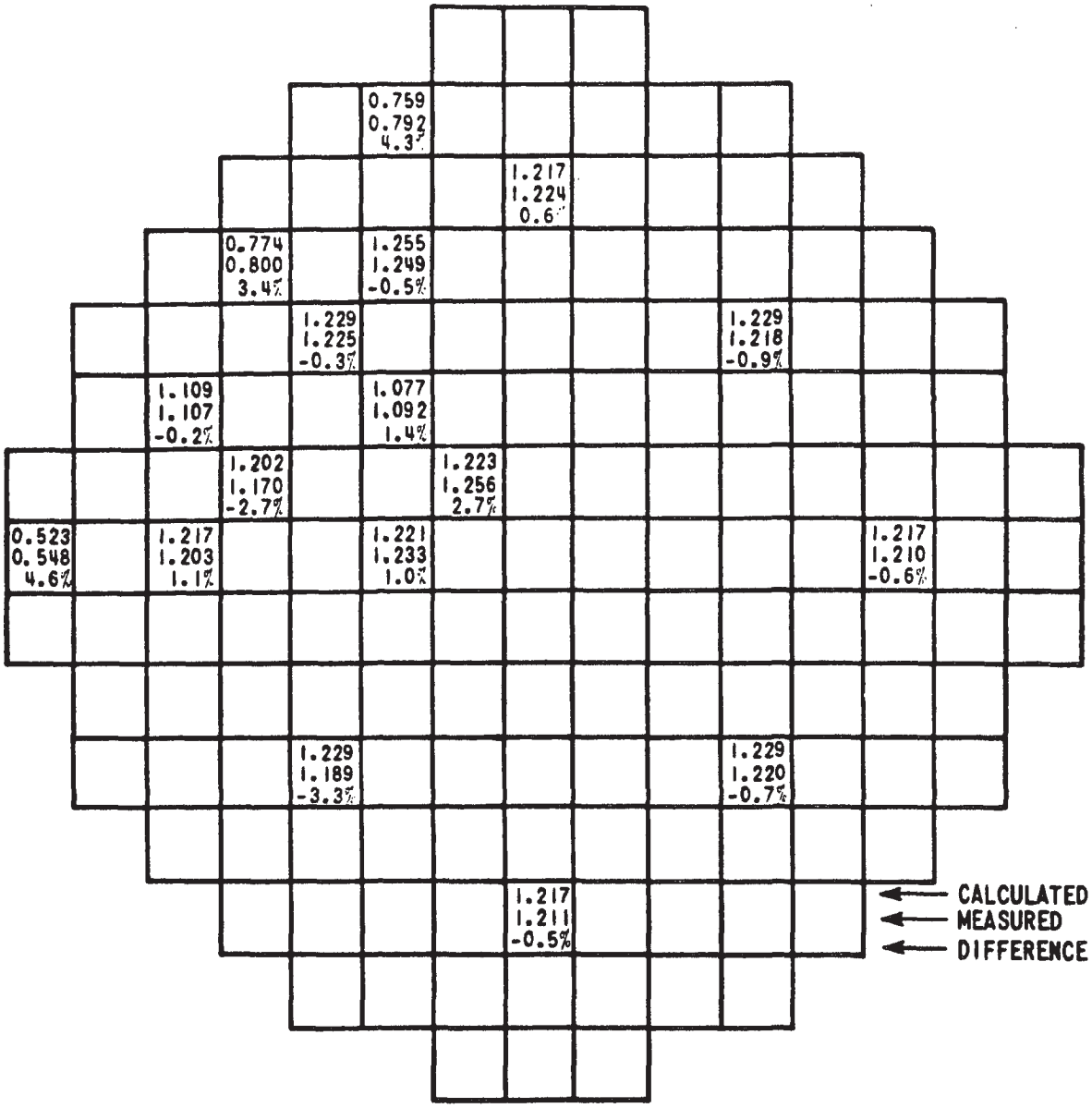

PEAKING FACTORS

$\bar{F}_Z$ = 1.5

$F^N_{\Delta H}$ = 1.357

F^N_Q = 2.07

BYRON/BRAIDWOOD STATIONS
UPDATED FINAL SAFETY ANALYSIS REPORT

FIGURE 4.3-23

TYPICAL COMPARISON BETWEEN CALCULATED AND MEASURED RELATIVE FUEL ASSEMBLY POWER DISTRIBUTION

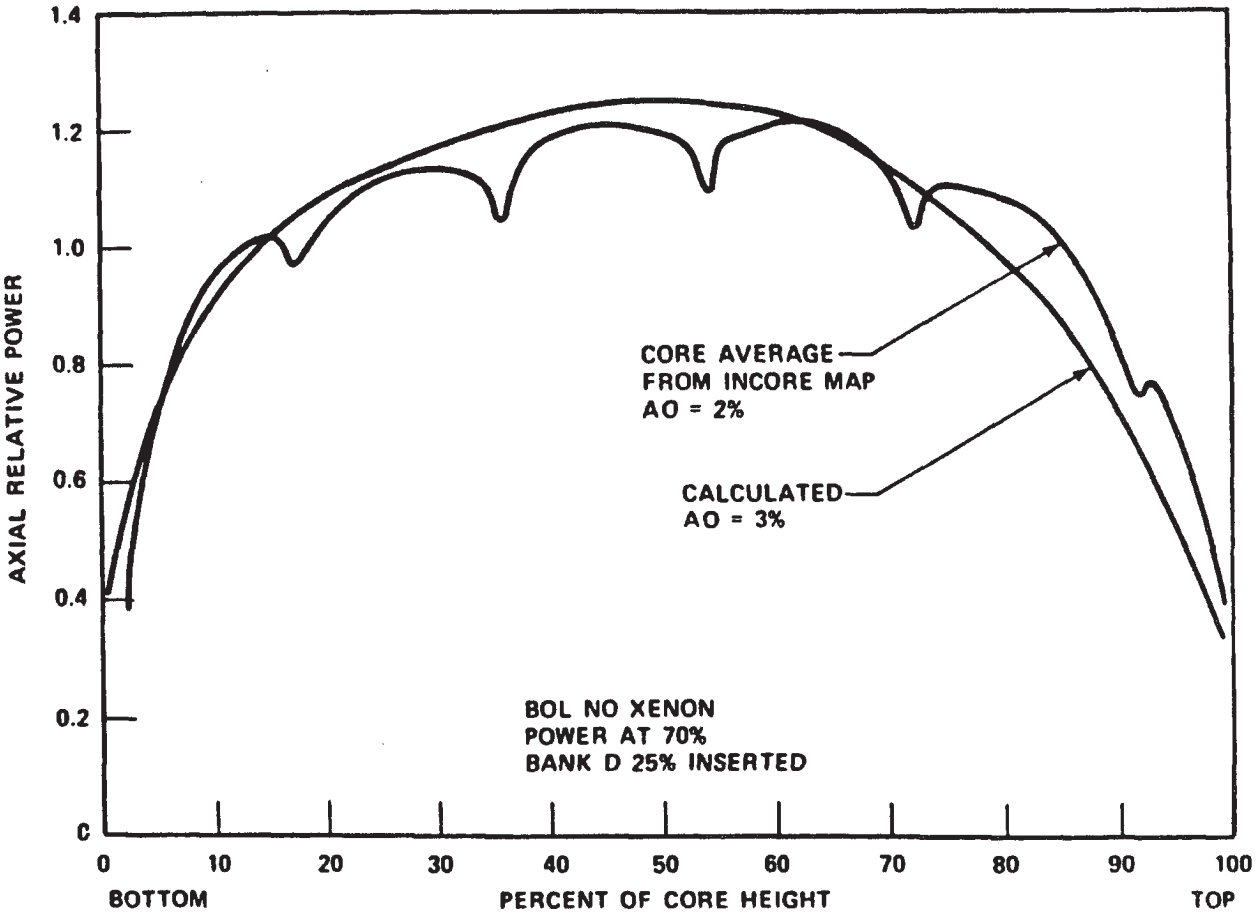

BYRON/BRAIDWOOD STATIONS
UPDATED FINAL SAFETY ANALYSIS REPORT

FIGURE 4.3-24

COMPARISON OF CALCULATED AND MEASURED AXIAL SHAPE

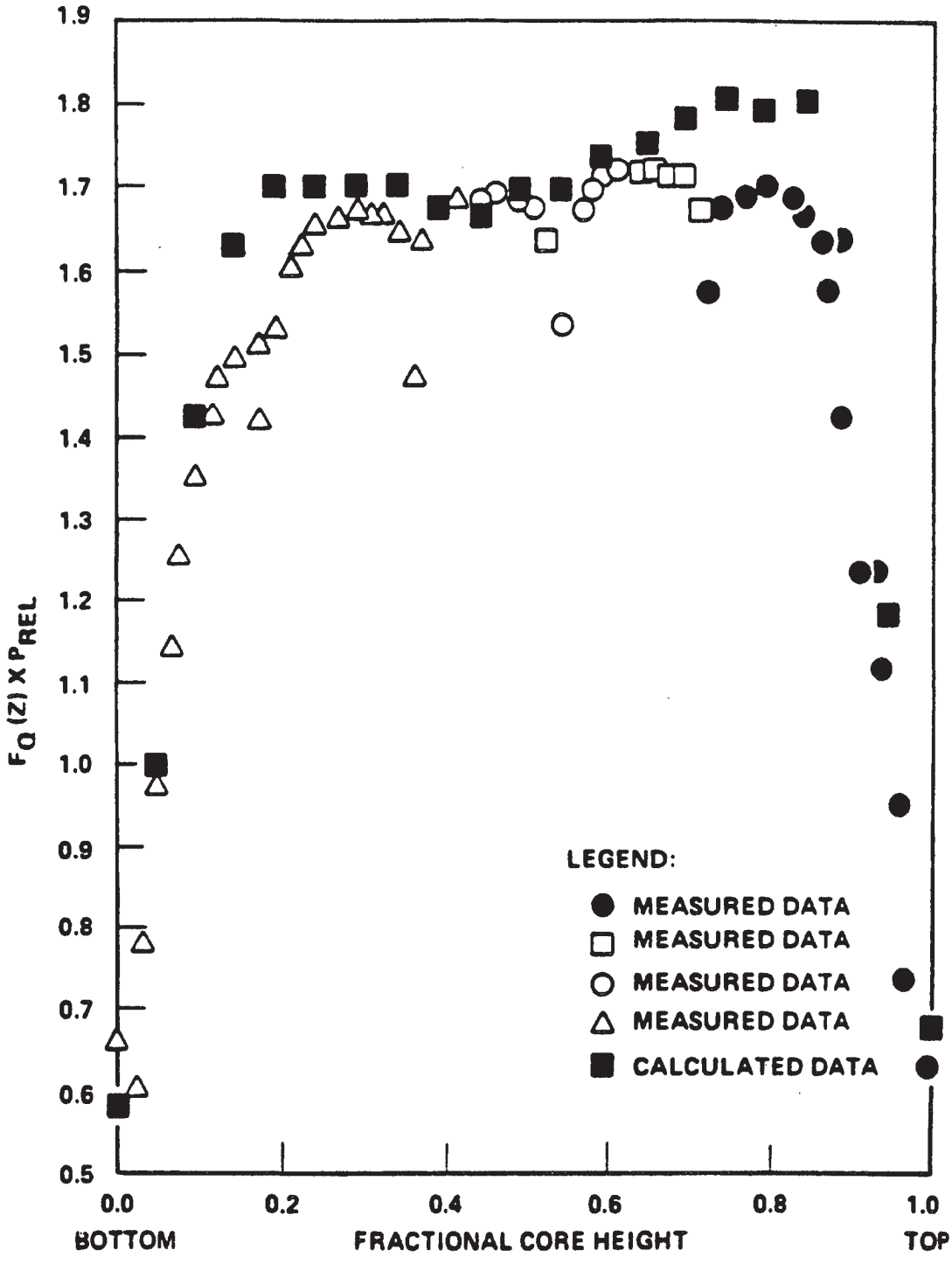

BYRON/BRAIDWOOD STATIONS
UPDATED FINAL SAFETY ANALYSIS REPORT

FIGURE 4.3-25

COMPARISON OF CALCULATED AND MEASURED PEAKING FACTORS, $[F_Q \times P_{REL}]_{MAX}$ ENVELOPE AS A FUNCTION OF CORE HEIGHT

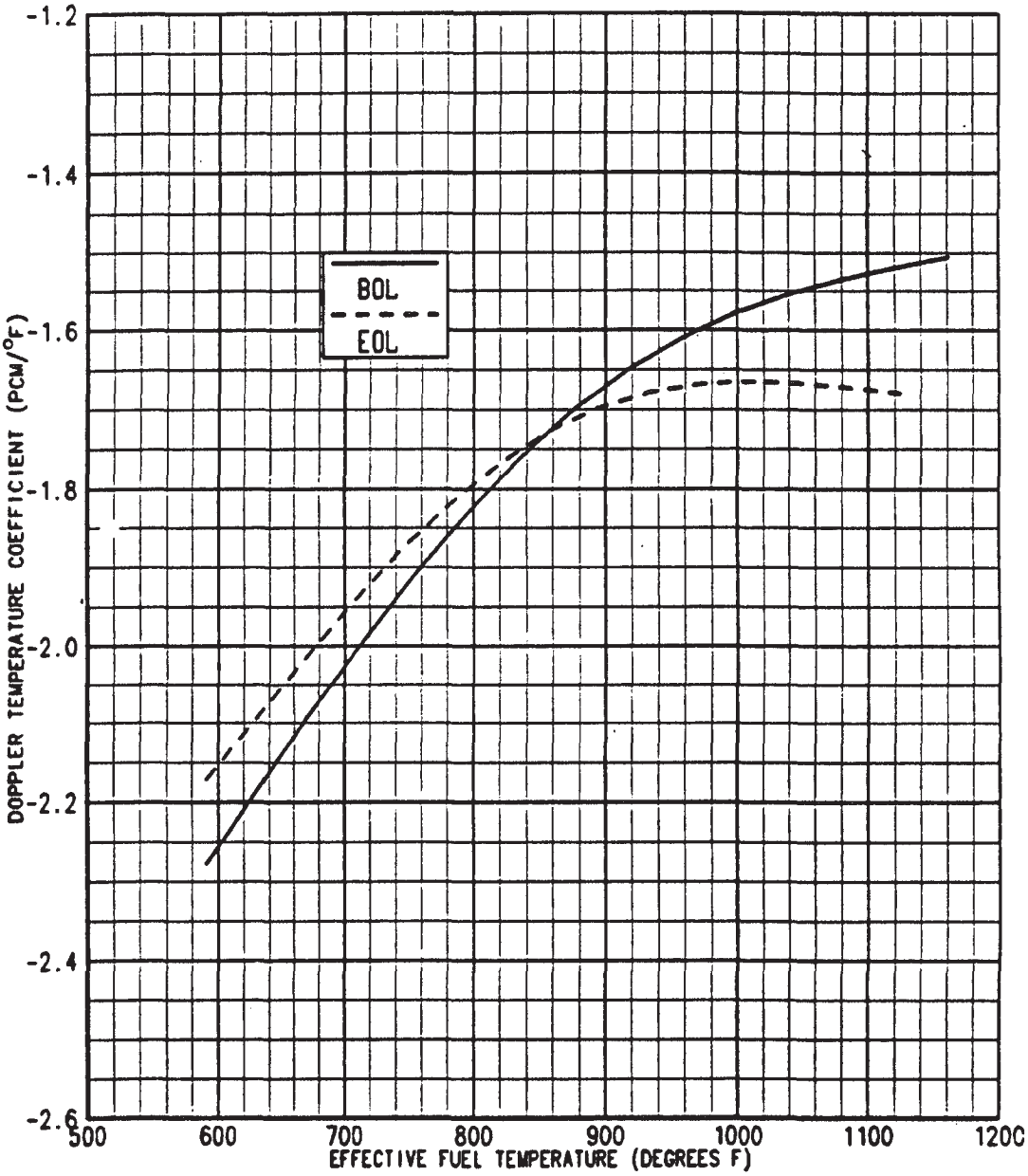

BYRON/BRAIDWOOD STATIONS
UPDATED FINAL SAFETY ANALYSIS REPORT

FIGURE 4.3-26

DOPPLER TEMPERATURE COEFFICIENT AT BOL AND EOL

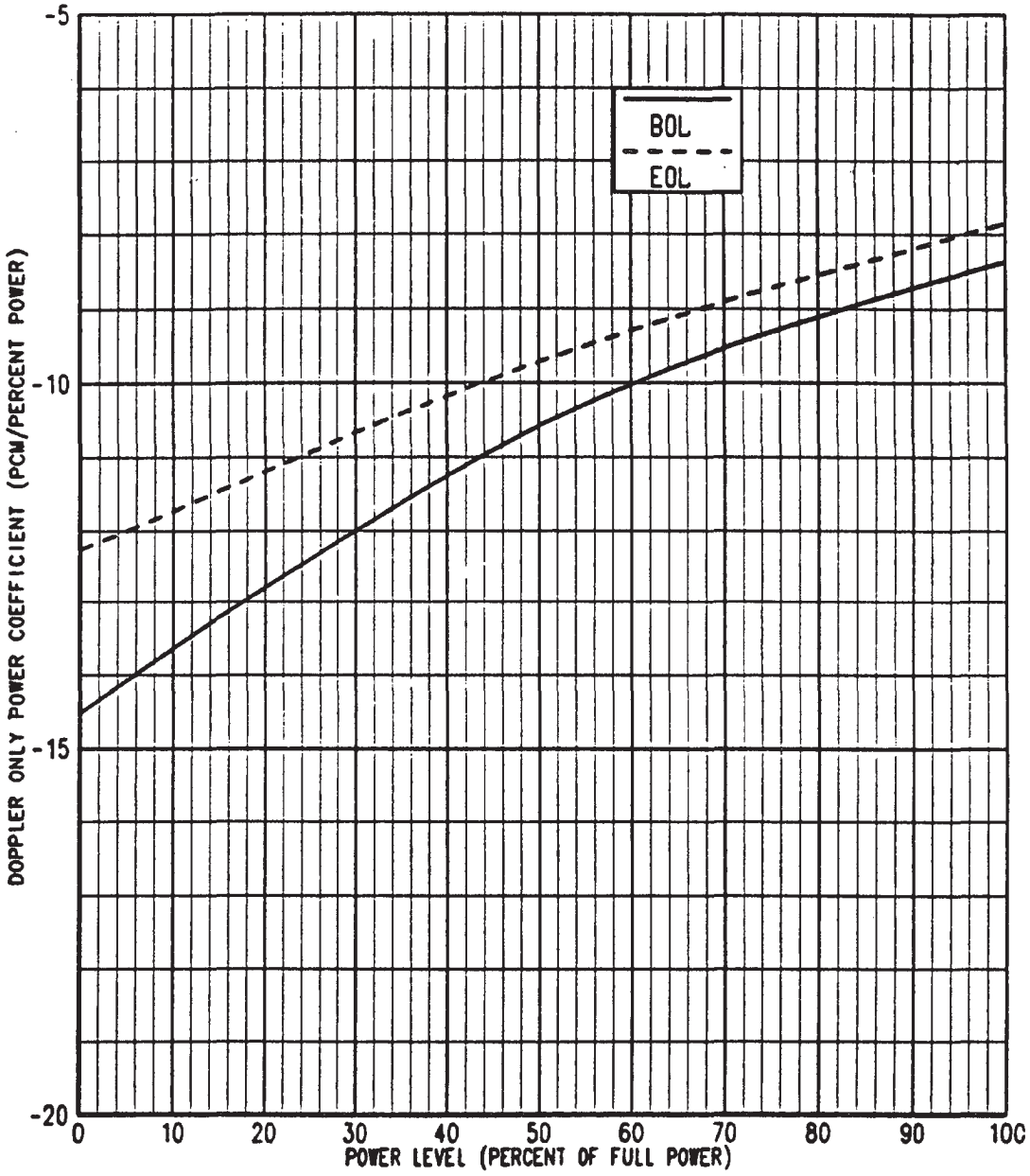

BYRON/BRAIDWOOD STATIONS
UPDATED FINAL SAFETY ANALYSIS REPORT

FIGURE 4.3-27

DOPPLER ONLY POWER COEFFICIENT
BOL AND EOL

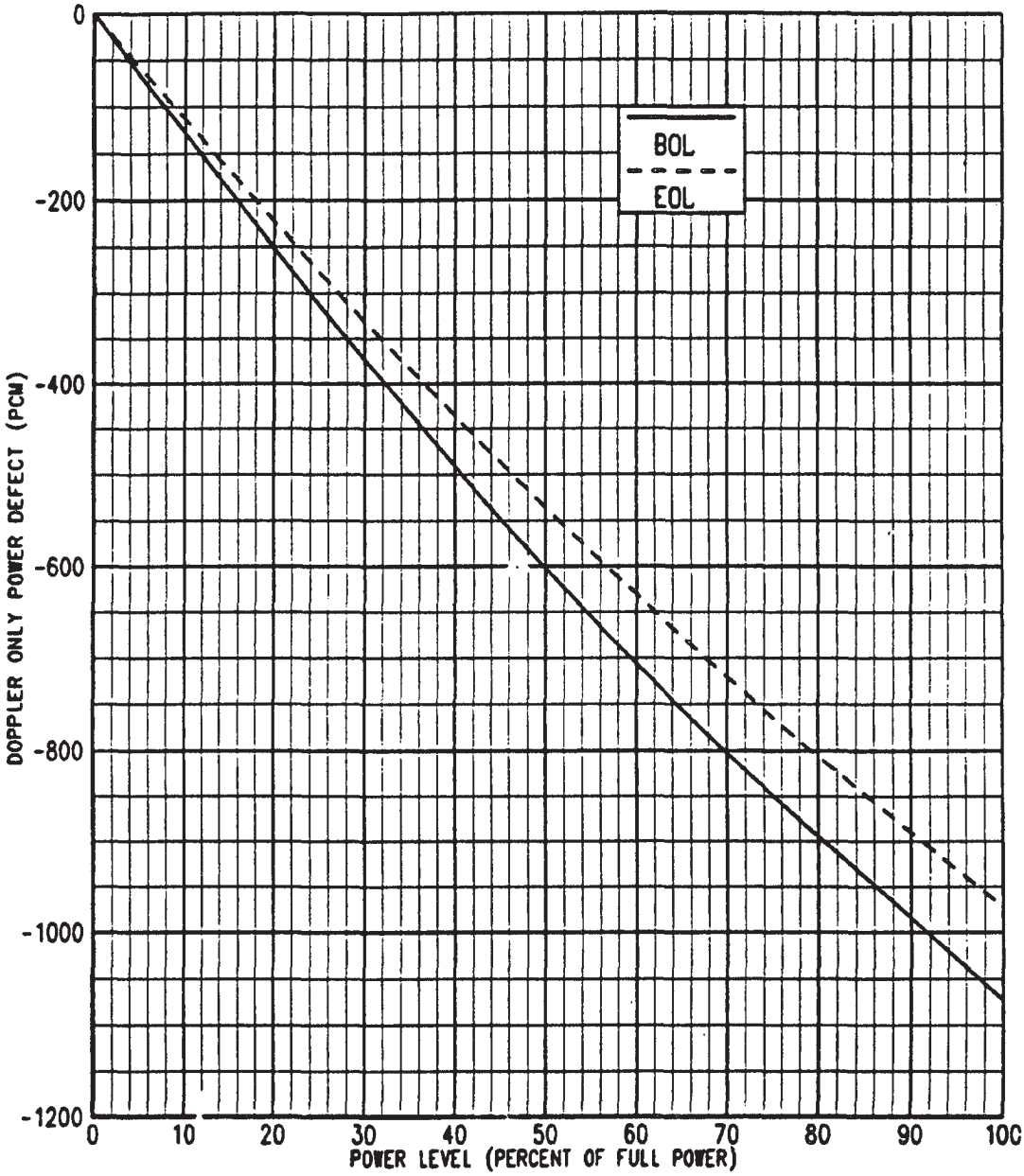

BYRON/BRAIDWOOD STATIONS
UPDATED FINAL SAFETY ANALYSIS REPORT

FIGURE 4.3-28

DOPPLER ONLY POWER DEFECT
BOL AND EOL

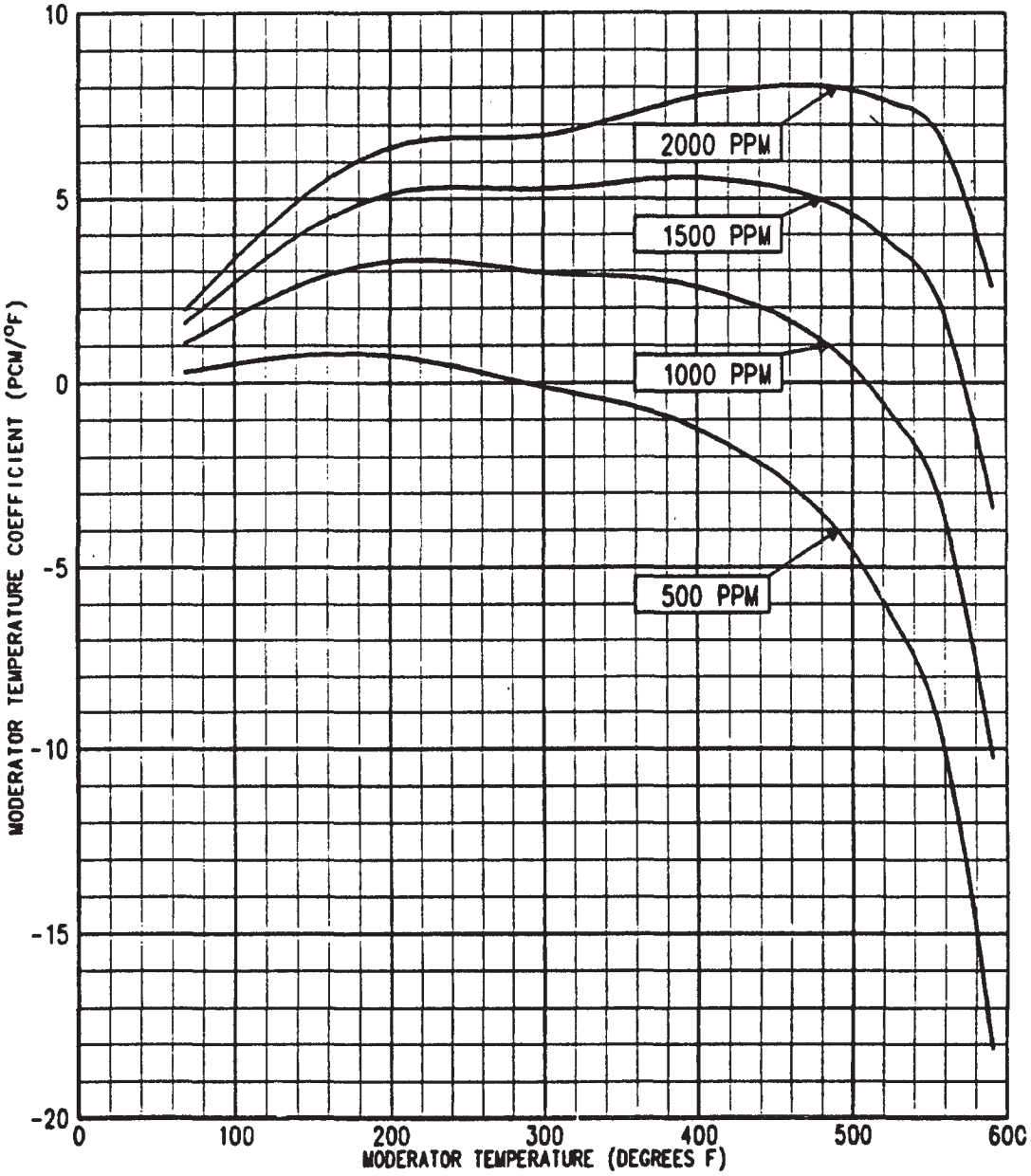

BYRON/BRAIDWOOD STATIONS
UPDATED FINAL SAFETY ANALYSIS REPORT

FIGURE 4.3-29

MODERATOR TEMPERATURE COEFFICIENT
BOL, ALL RODS OUT

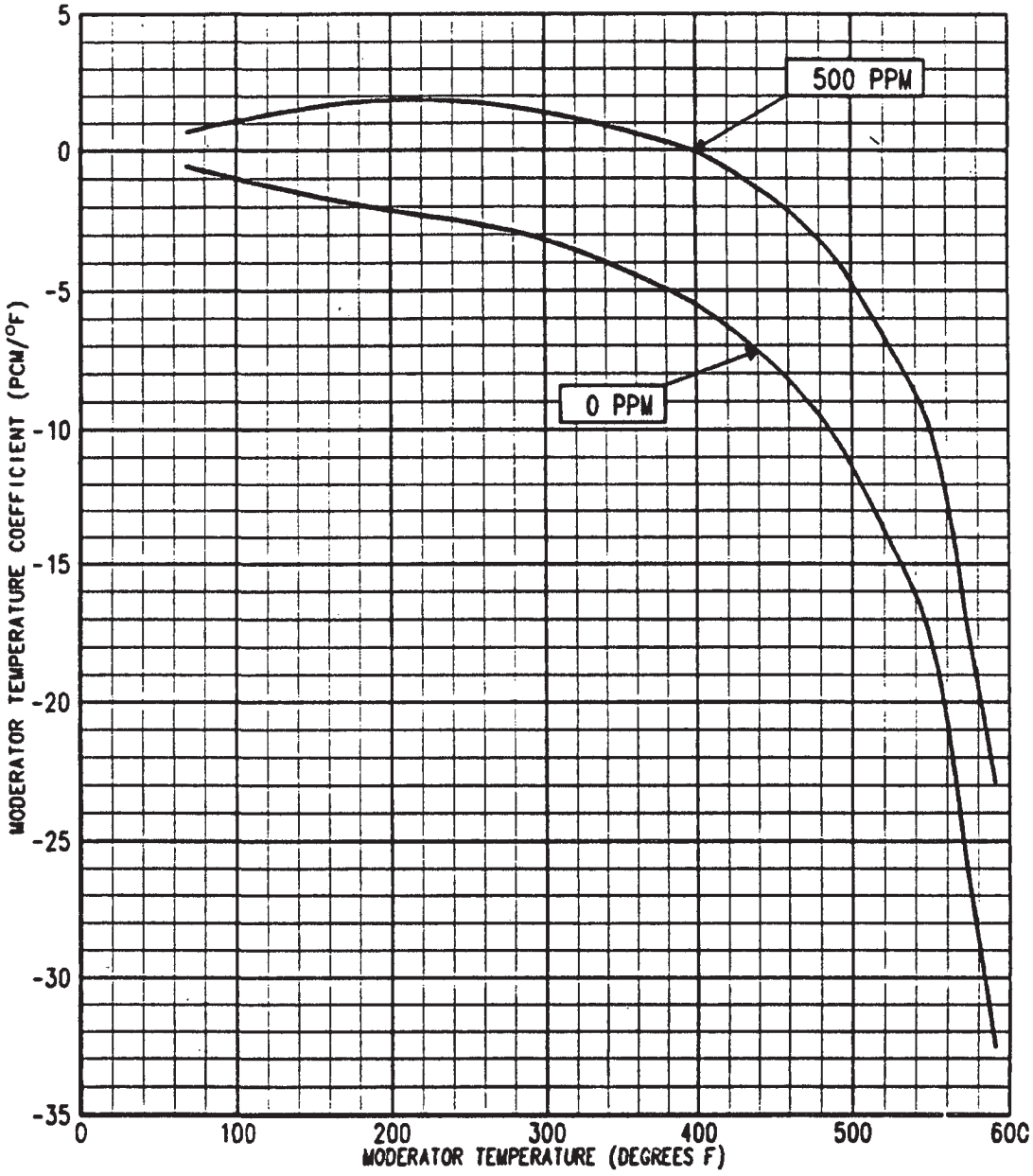

BYRON/BRAIDWOOD STATIONS
UPDATED FINAL SAFETY ANALYSIS REPORT

FIGURE 4.3-30

MODERATOR TEMPERATURE COEFFICIENT
EOL, ALL RODS OUT

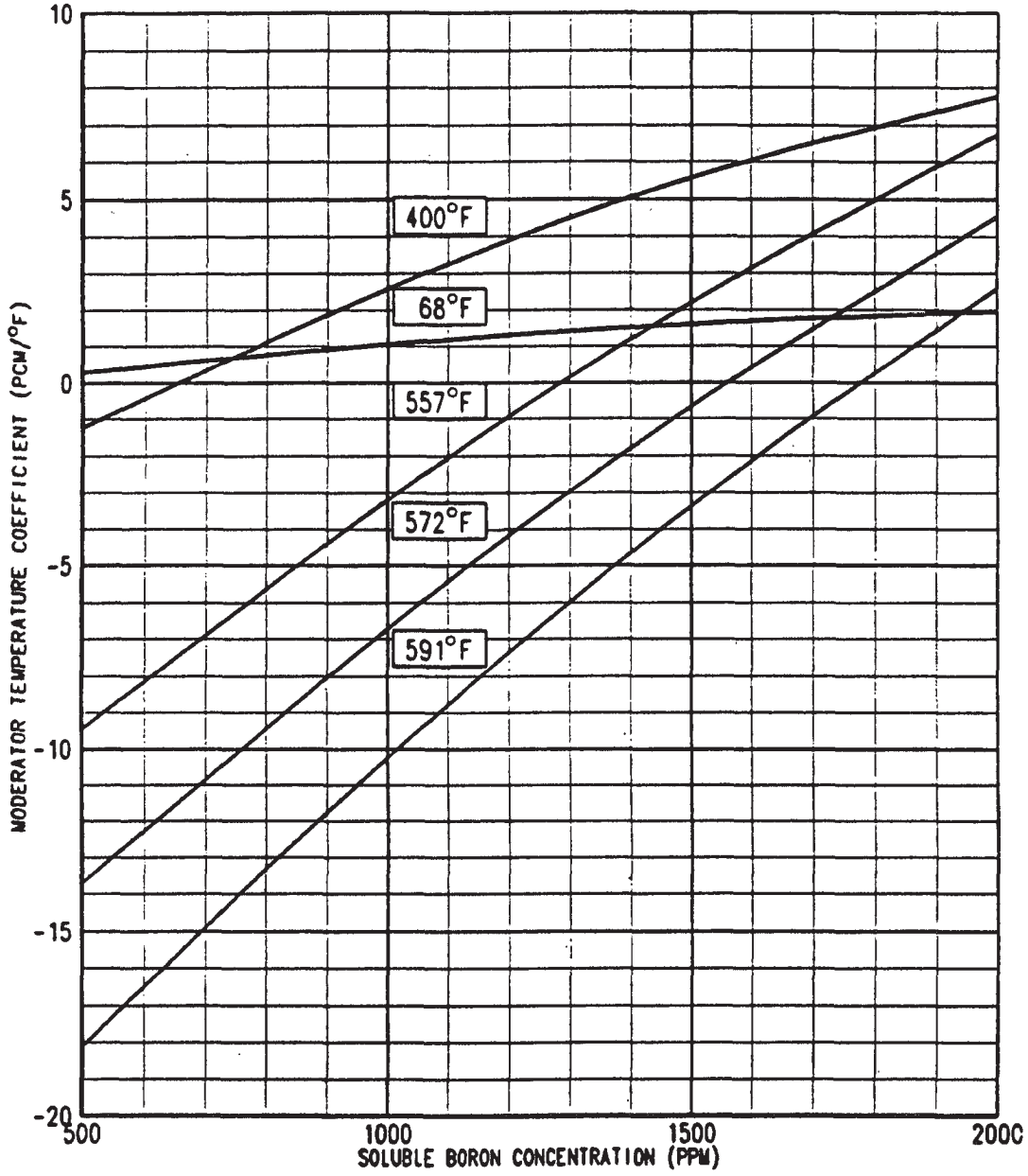

BYRON/BRAIDWOOD STATIONS
UPDATED FINAL SAFETY ANALYSIS REPORT

FIGURE 4.3-31

MODERATOR TEMPERATURE COEFFICIENT AS A FUNCTION OF BORON CONCENTRATION BOL, ALL RODS OUT

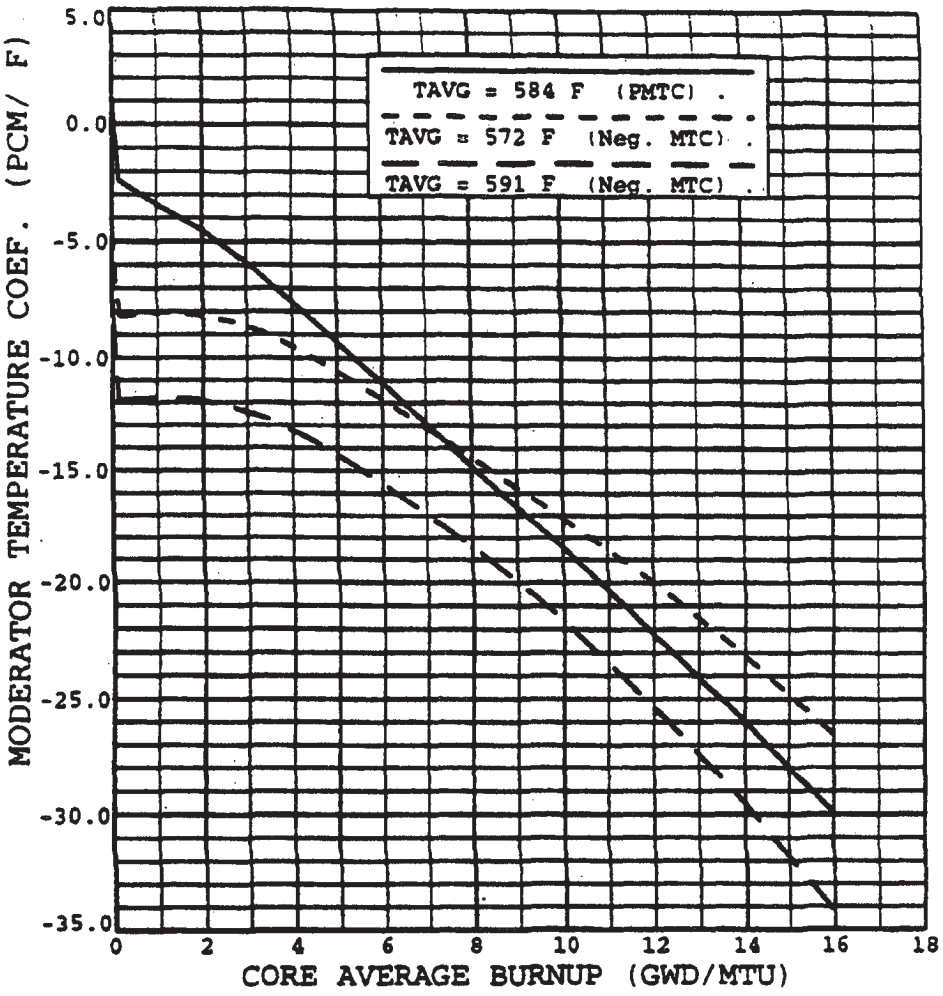

BYRON/BRAIDWOOD STATION
UPDATED FINAL SAFETY ANALYSIS REPORT

FIGURE 4.3-32

HOT FULL POWER
MODERATOR TEMPERATURE COEFFICIENT
VERSUS CRITICAL BORON CONCENTRATION

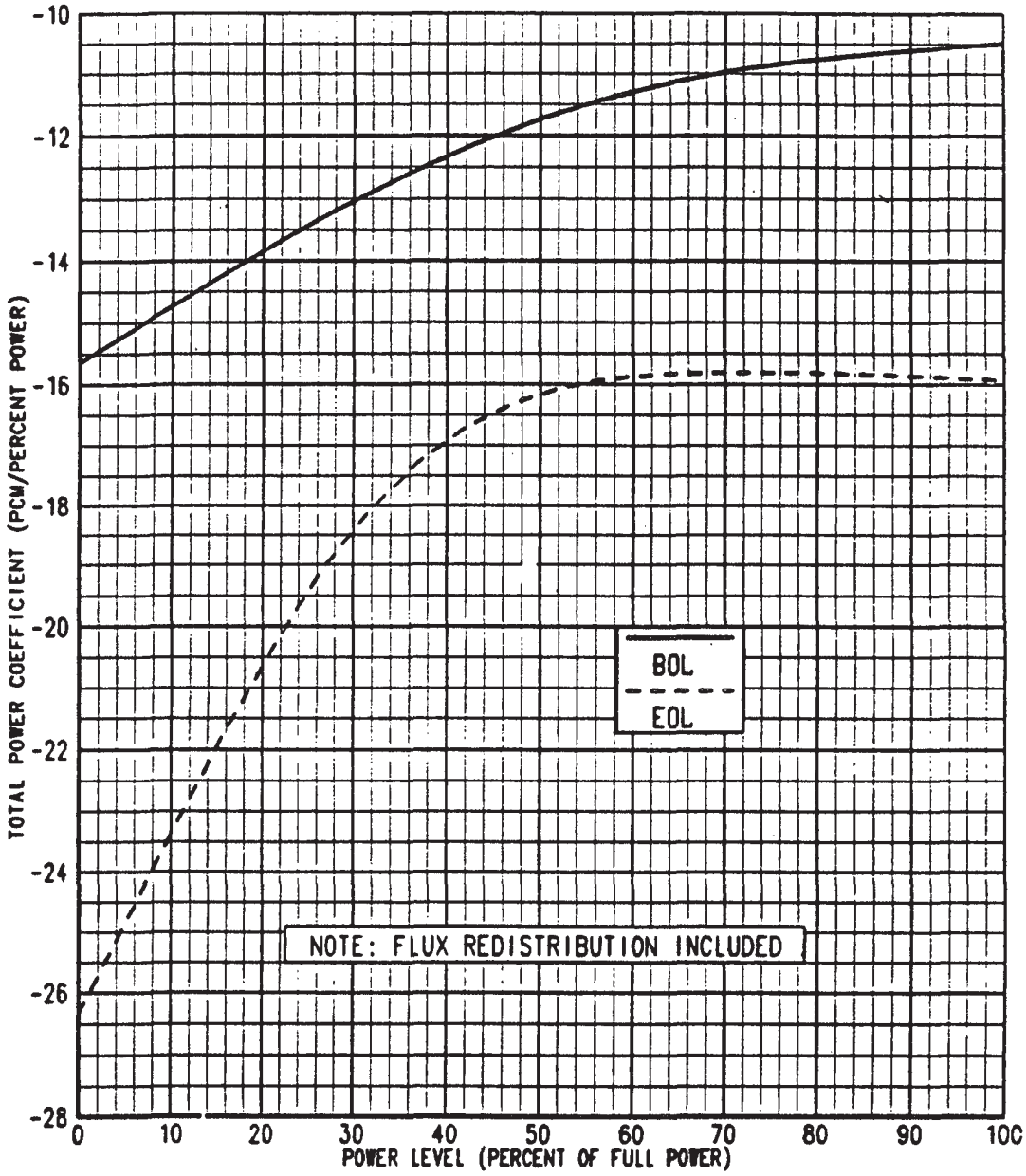

BYRON/BRAIDWOOD STATIONS
UPDATED FINAL SAFETY ANALYSIS REPORT

FIGURE 4.3-33

TOTAL POWER COEFFICIENT
BOL AND EOL

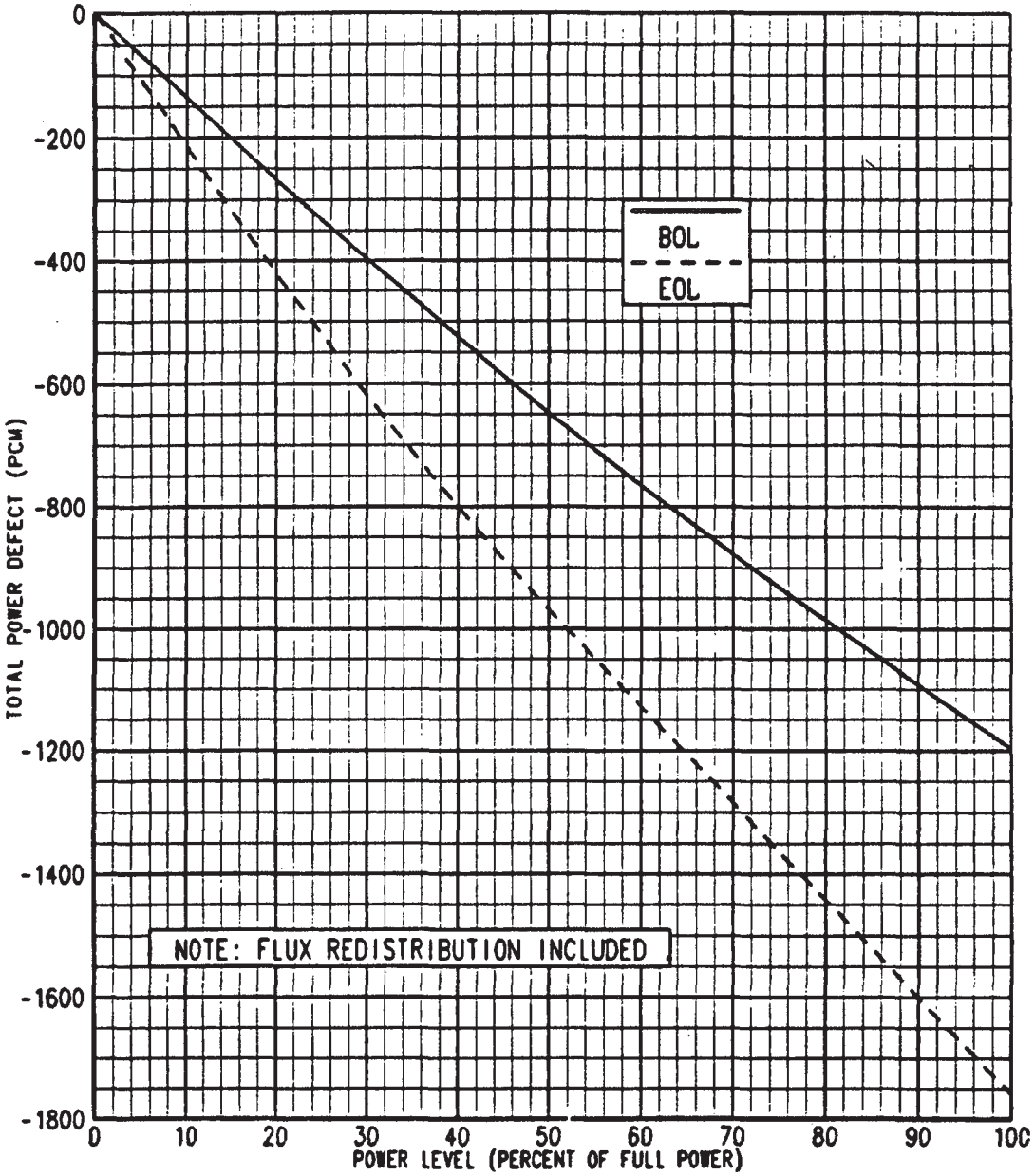

BYRON/BRAIDWOOD STATIONS
UPDATED FINAL SAFETY ANALYSIS REPORT

FIGURE 4.3-34

TOTAL POWER DEFECT BOL AND EOL

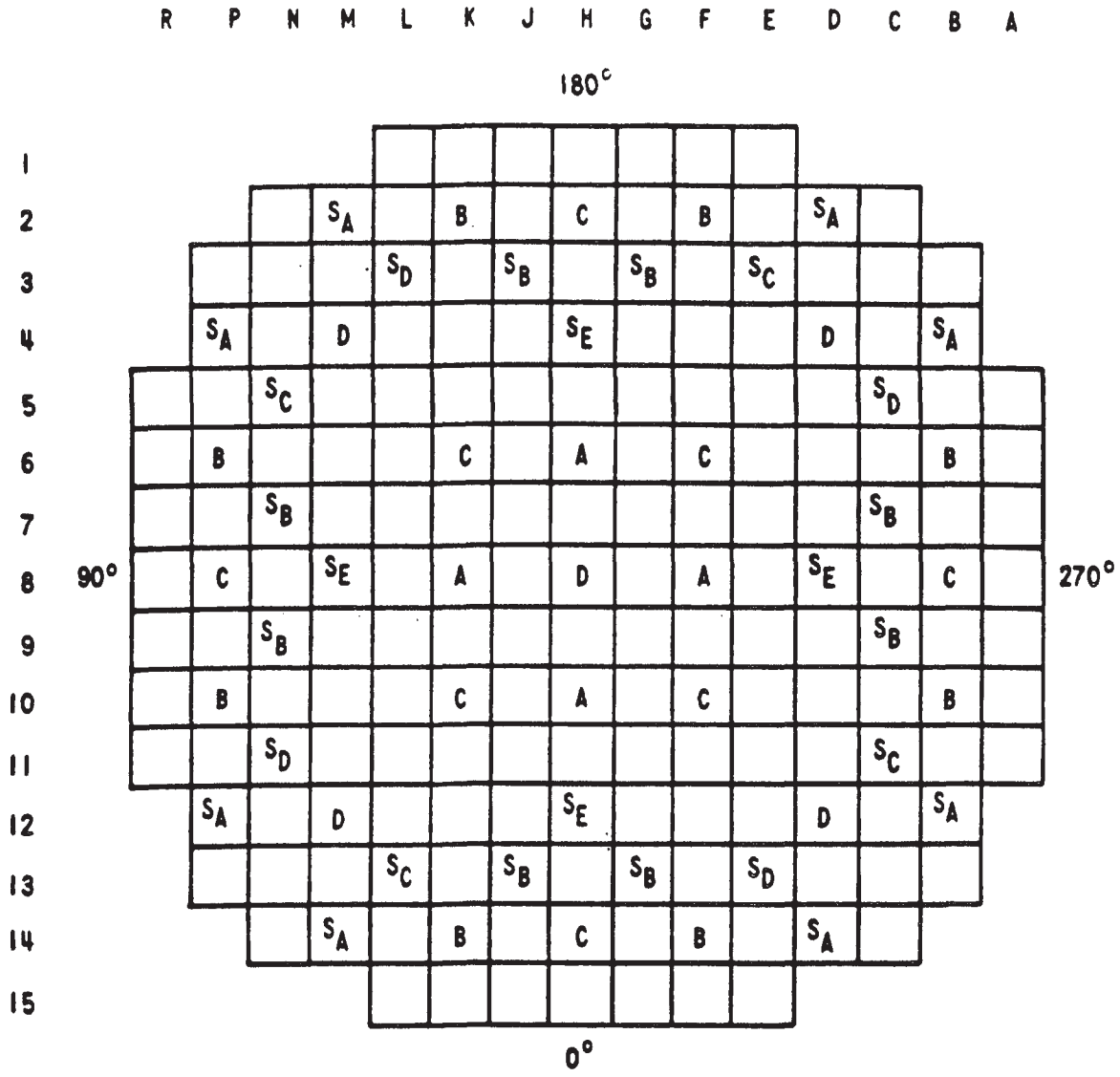

CONTROL BANK	NUMBER OF RODS
A	4
B	8
C	8
D	5
TOTAL	25

SHUTDOWN BANK	NUMBER OF RODS
SA	8
SB	8
SC	4
SD	4
SE	4
TOTAL	28

BYRON/BRAIDWOOD STATIONS
UPDATED FINAL SAFETY ANALYSIS REPORT

FIGURE 4.3-35

ROD CLUSTER CONTROL ASSEMBLY PATTERN

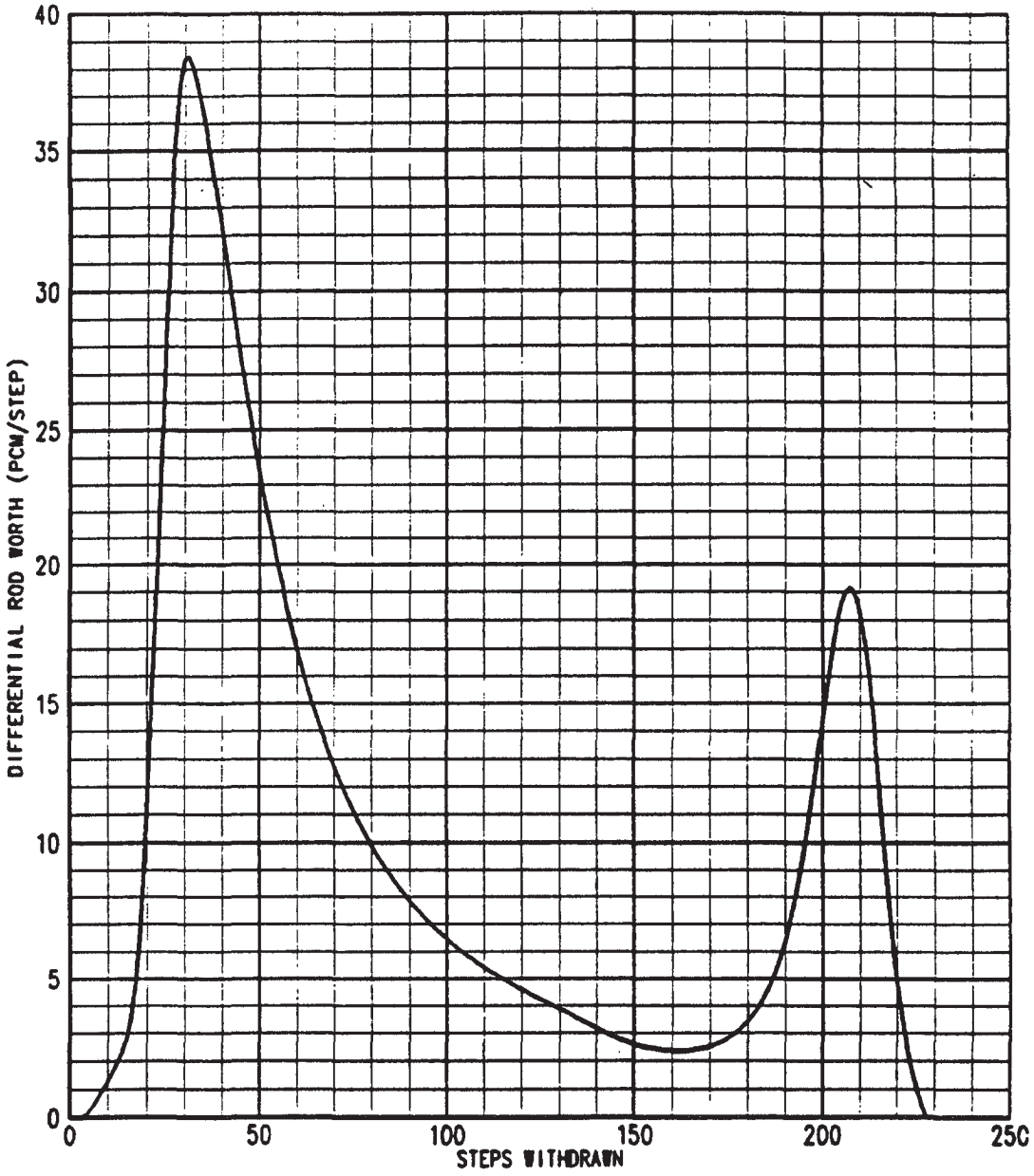

BYRON/BRAIDWOOD STATIONS
UPDATED FINAL SAFETY ANALYSIS REPORT

FIGURE 4.3-36

ACCIDENTAL SIMULTANEOUS WITHDRAWAL OF TWO CONTROL BANKS, EOL, HOT ZERO POWER, BANKS C AND B MOVING IN SAME PLANE

Figures 4.3-37 through 4.3-38 have been deleted intentionally.

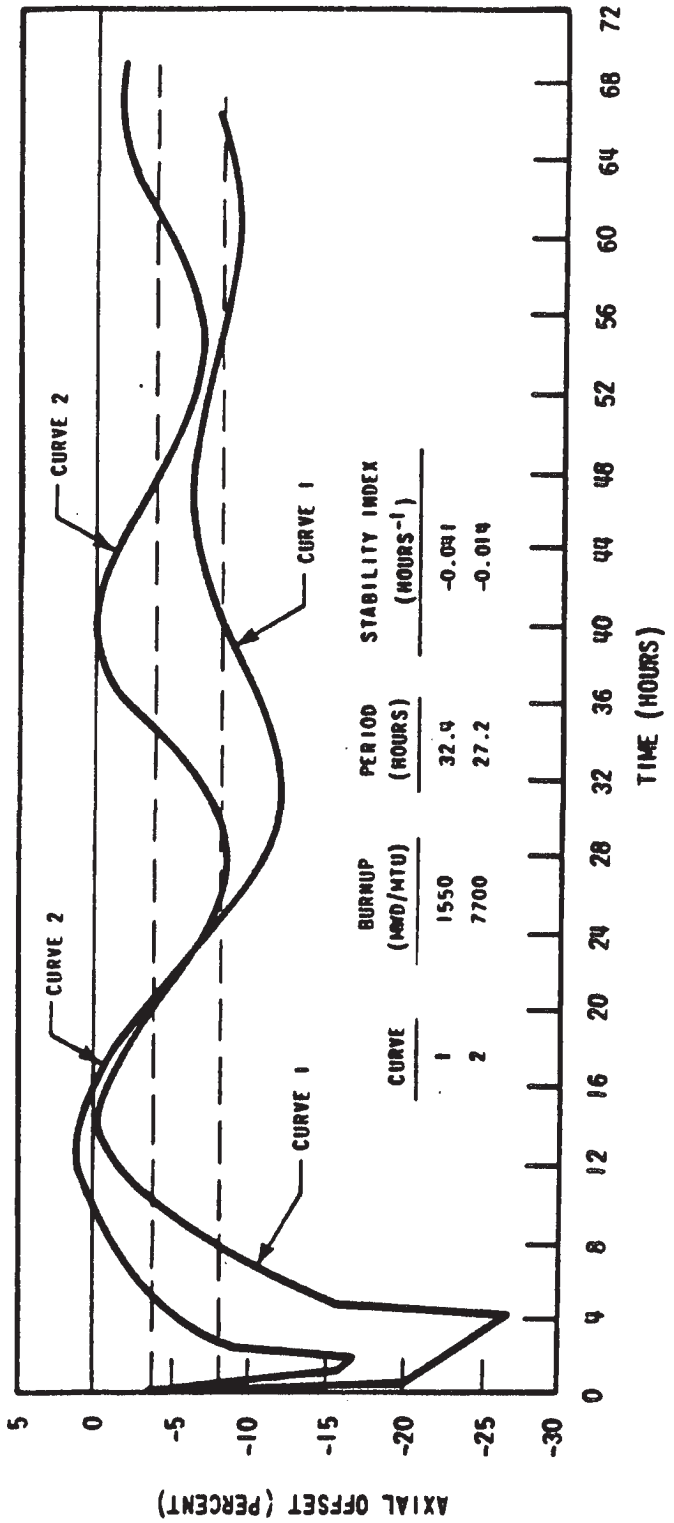

BYRON/BRAIDWOOD STATIONS
UPDATED FINAL SAFETY ANALYSIS REPORT

FIGURE 4.3-39

AXIAL OFFSET VERSUS TIME PWR CORE WITH A 12-FOOT HEIGHT AND 121 ASSEMBLIES

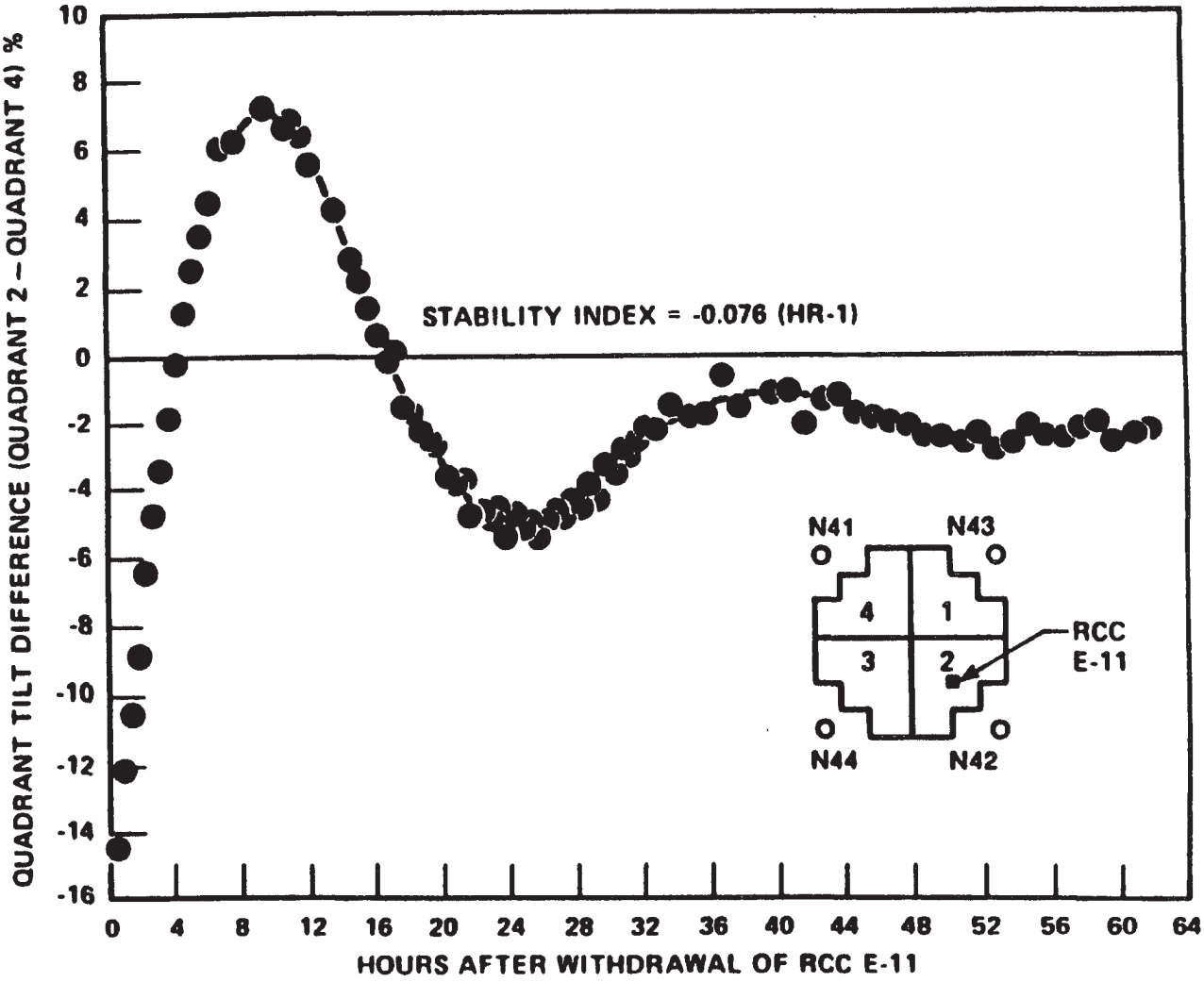

BYRON/BRAIDWOOD STATIONS
UPDATED FINAL SAFETY ANALYSIS REPORT

FIGURE 4.3-40

XY XENON TEST THERMOCOUPLE RESPONSE
QUADRANT TILT DIFFERENCE VERSUS TIME

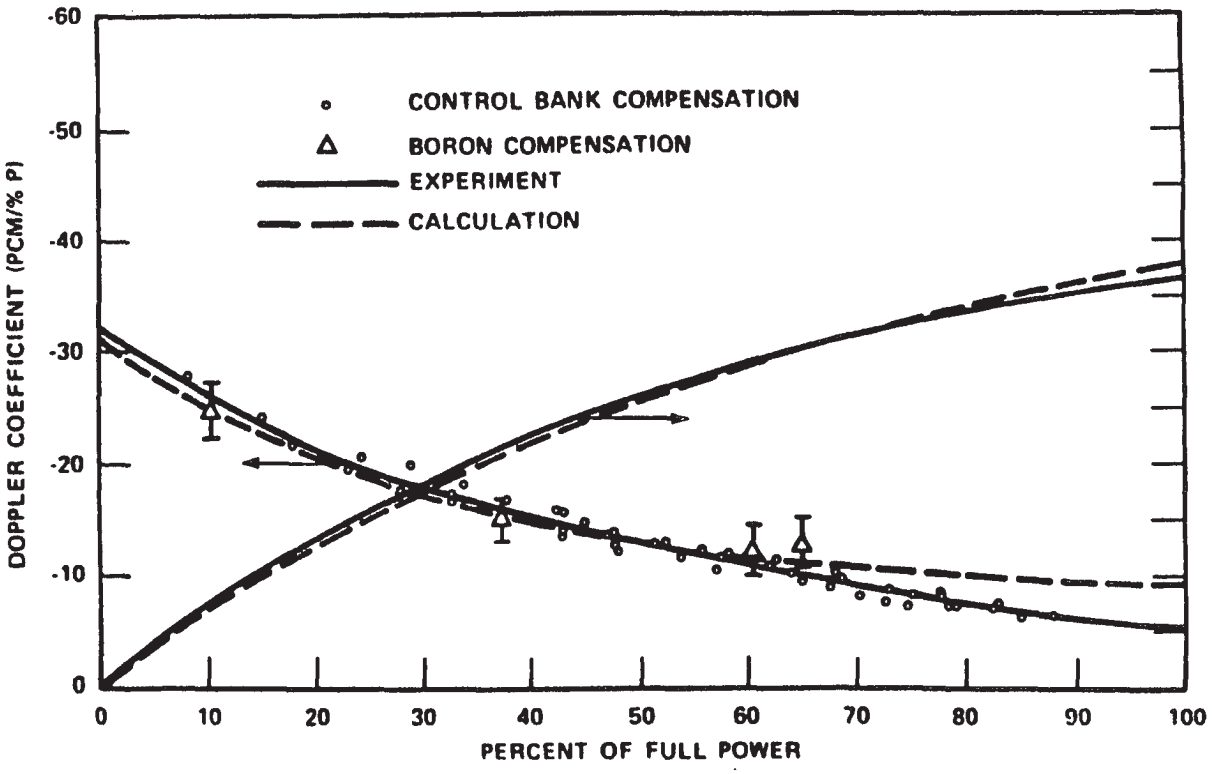

BYRON/BRAIDWOOD STATIONS
UPDATED FINAL SAFETY ANALYSIS REPORT

FIGURE 4.3-41

CALCULATED AND MEASURED DOPPLER DEFECT AND COEFFICIENTS AT BOL, 2-LOOP PLANT, 121 ASSEMBLIES, 12-FOOT CORE

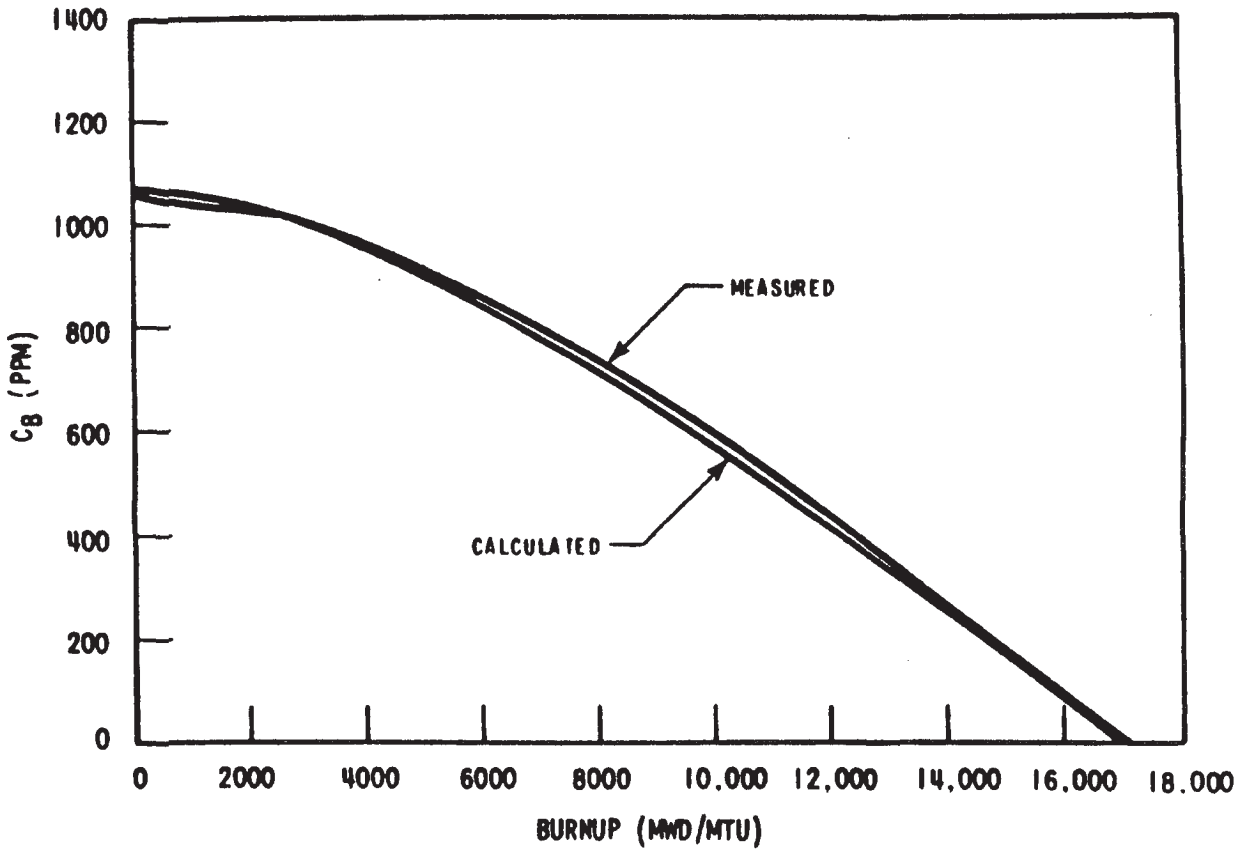

BYRON/BRAIDWOOD STATIONS
UPDATED FINAL SAFETY ANALYSIS REPORT

FIGURE 4.3-42

COMPARISON OF CALCULATED AND MEASURED BORON CONCENTRATION FOR 2-LOOP PLANT, 121 ASSEMBLIES, 12-FOOT CORE

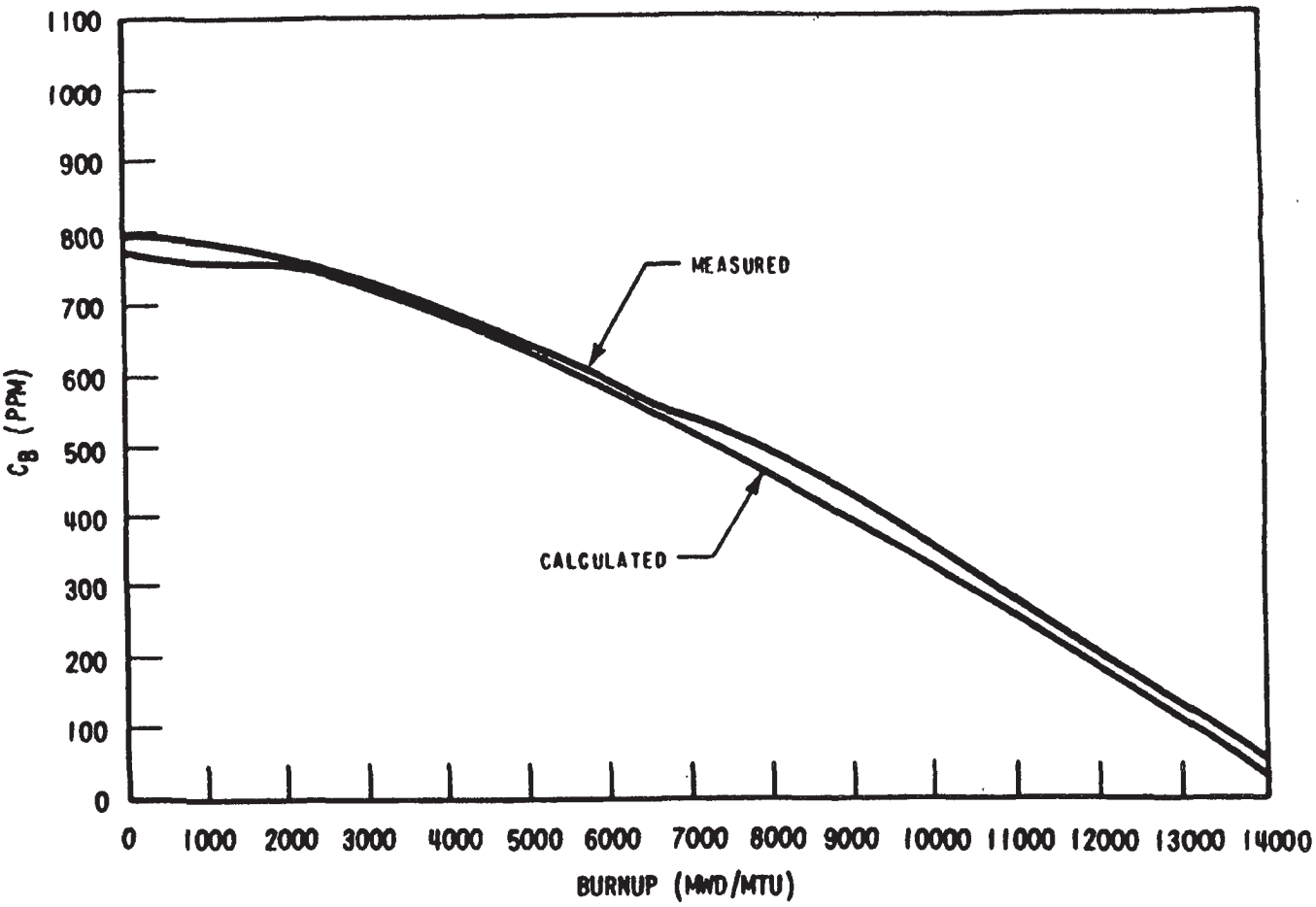

BYRON/BRAIDWOOD STATIONS
UPDATED FINAL SAFETY ANALYSIS REPORT

FIGURE 4.3-43

COMPARISON OF CALCULATED AND MEASURED
C_B 3-LOOP PLANT, 157 ASSEMBLIES,
12-FOOT CORE

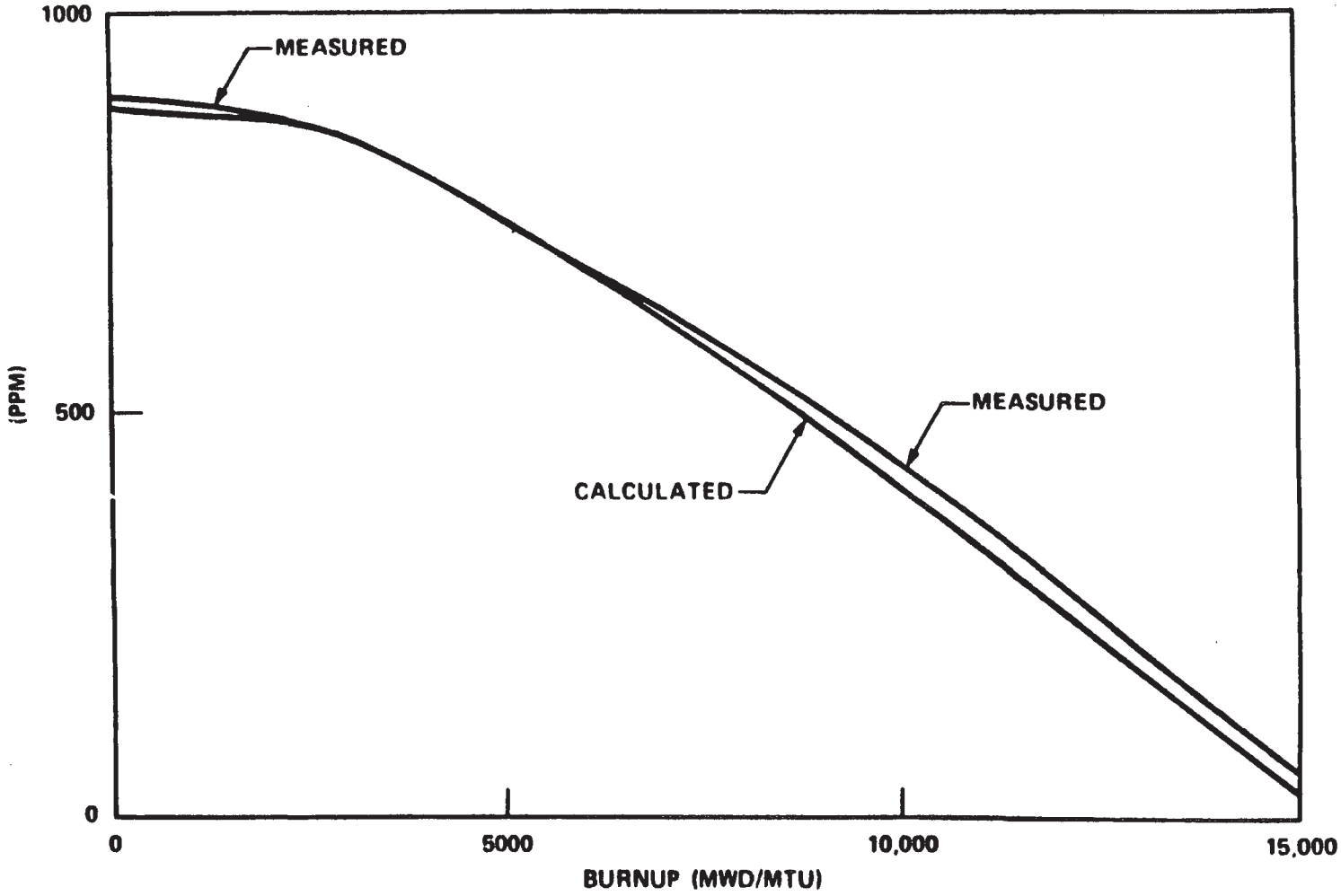

BYRON/BRAIDWOOD STATIONS
UPDATED FINAL SAFETY ANALYSIS REPORT

FIGURE 4.3-44

COMPARISON OF CALCULATED AND MEASURED
C_B 4-LOOP PLANT, 193 ASSEMBLIES,
12-FOOT CORE

Figure 4.4-1 has been deleted intentionally.

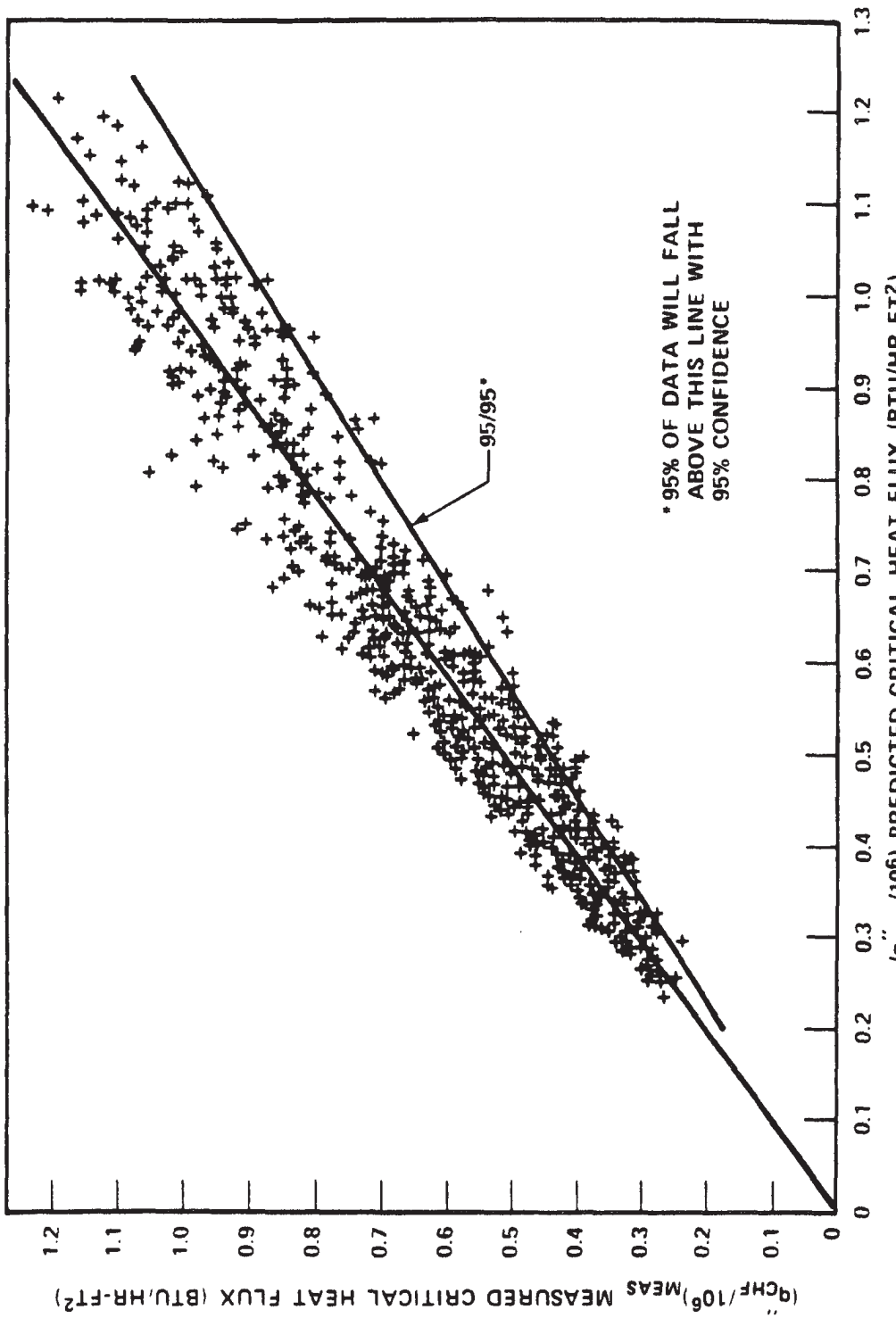

BYRON/BRAIDWOOD STATIONS
UPDATED FINAL SAFETY ANALYSIS REPORT

FIGURE 4.4-2

MEASURED VERSUS PREDICTED CRITICAL HEAT FLUX WRB-1 CORRELATION

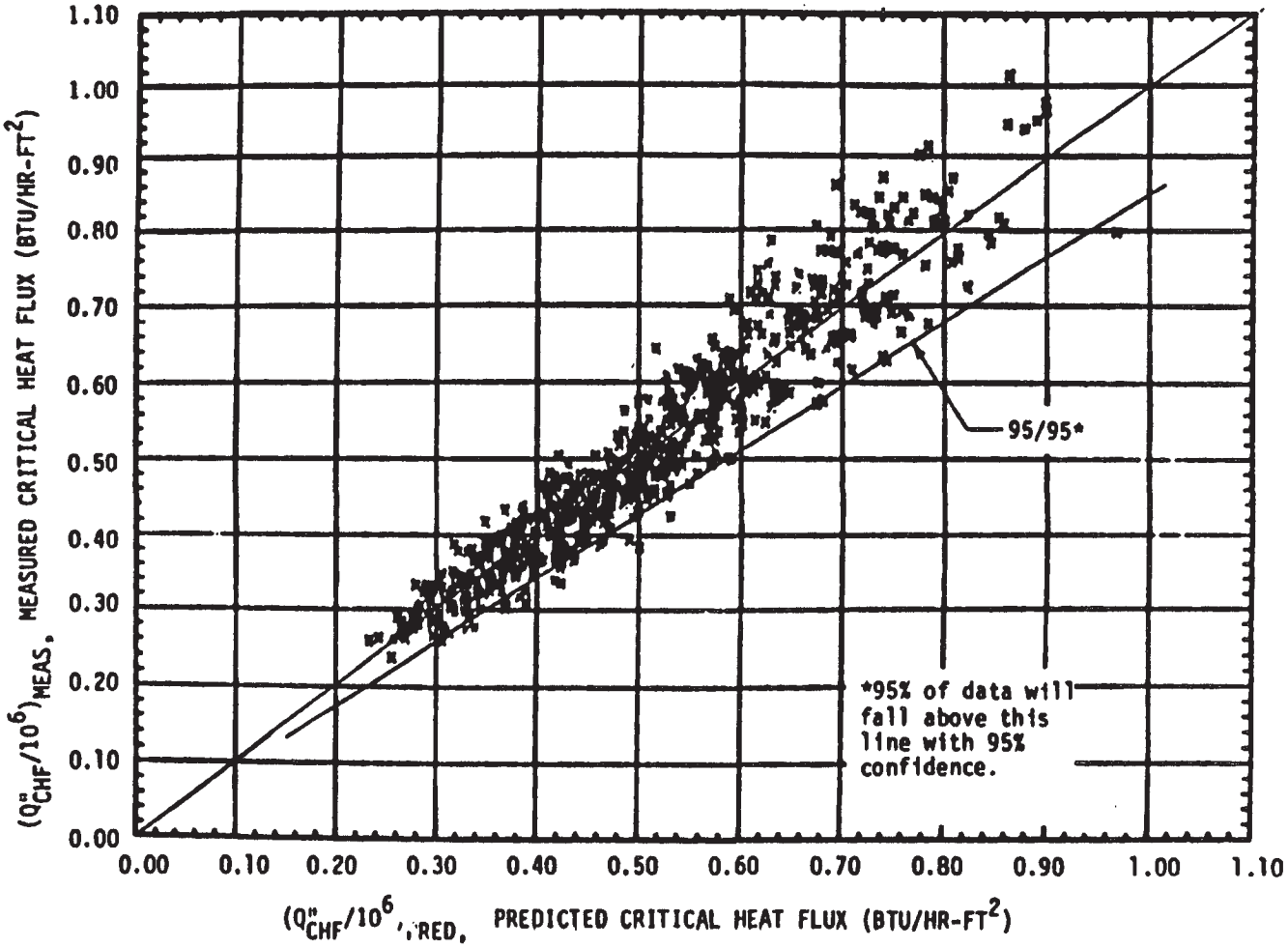

BYRON/BRAIDWOOD STATIONS
UPDATED FINAL SAFETY ANALYSIS REPORT

FIGURE 4.4-2a

MEASURED VERSUS PREDICTED CRITICAL HEAT FLUX WRB-2 CORRELATION

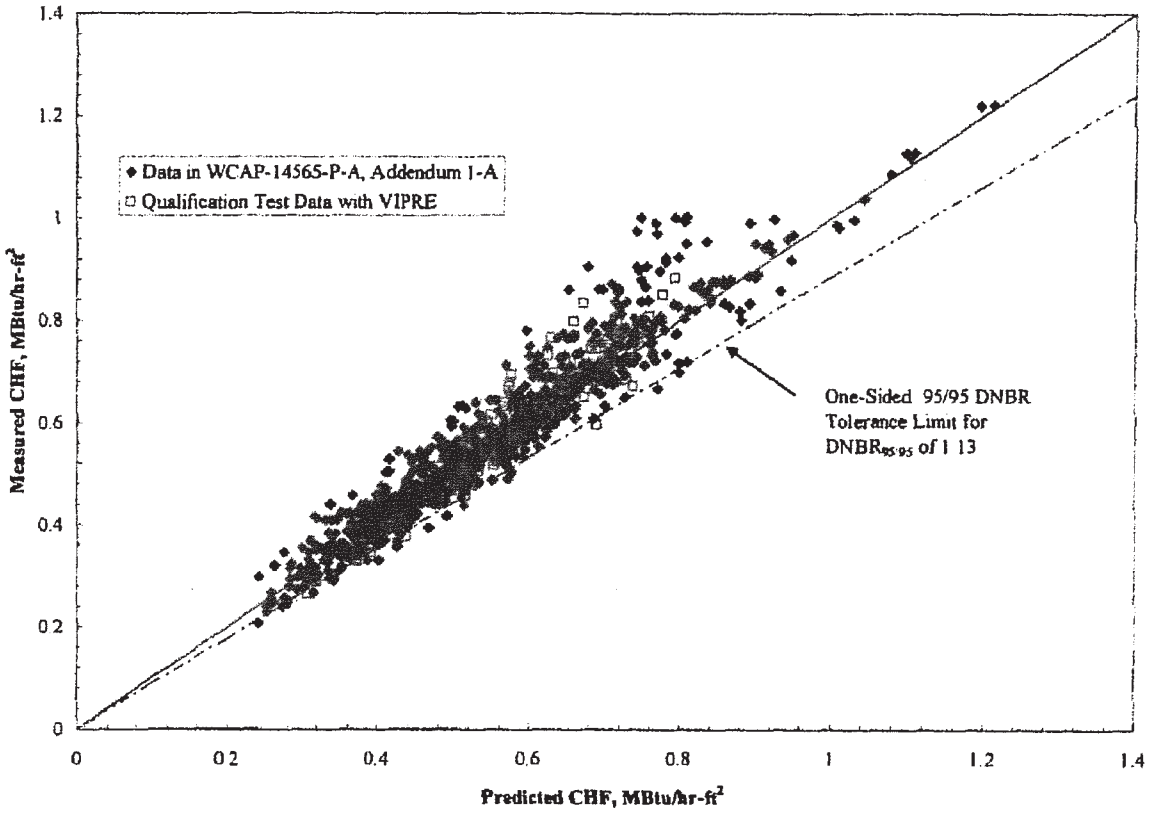

BYRON/BRAIDWOOD STATIONS
UPDATED FINAL SAFETY ANALYSIS REPORT

FIGURE 4.4-2b

MEASURED VERSUS PREDICTED
CRITICAL HEAT FLUX
ABB-NV CORRELATION

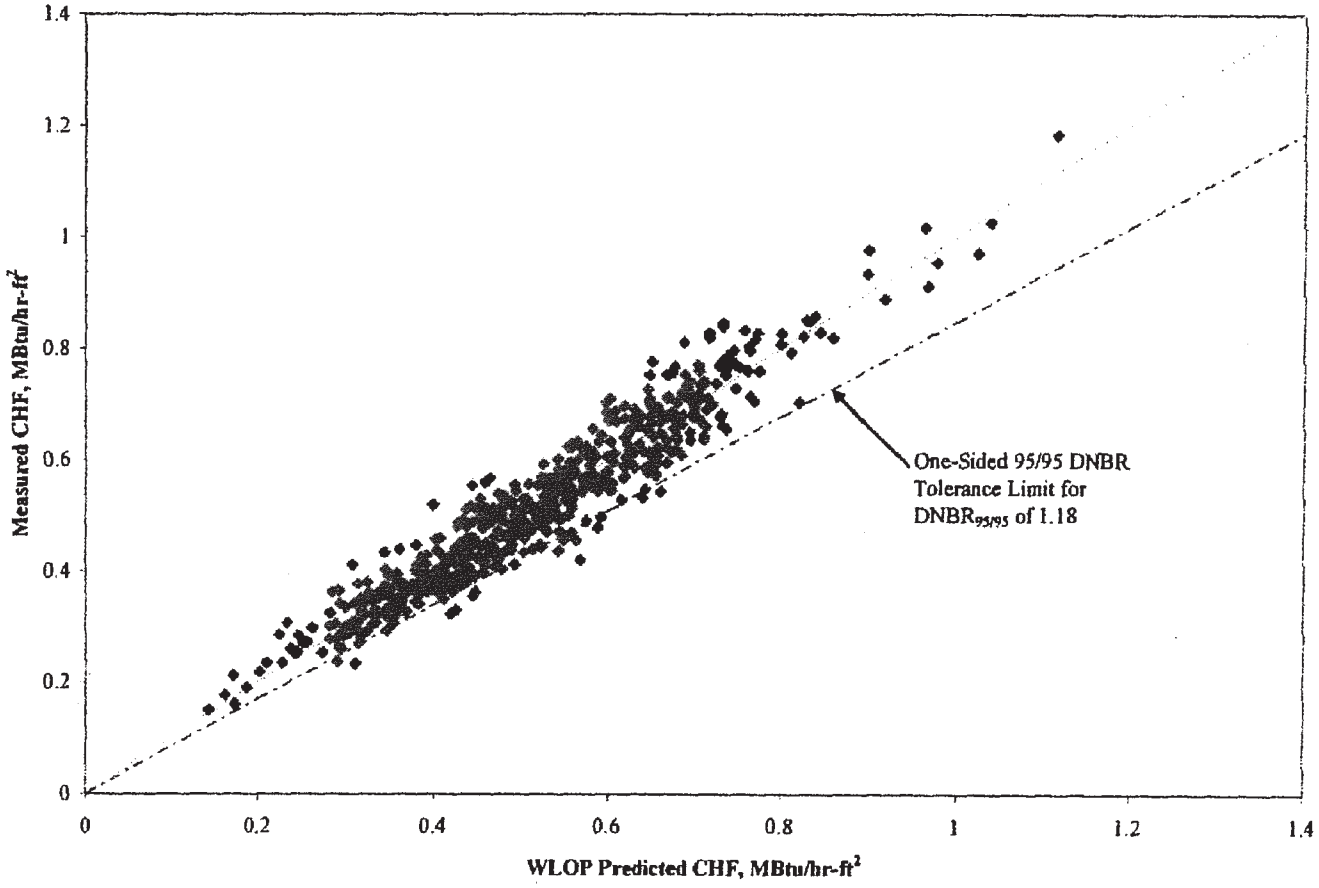

BYRON/BRAIDWOOD STATIONS
UPDATED FINAL SAFETY ANALYSIS REPORT

FIGURE 4.4-2c

MEASURED VERSUS PREDICTED
CRITICAL HEAT FLUX
WLOP CORRELATION

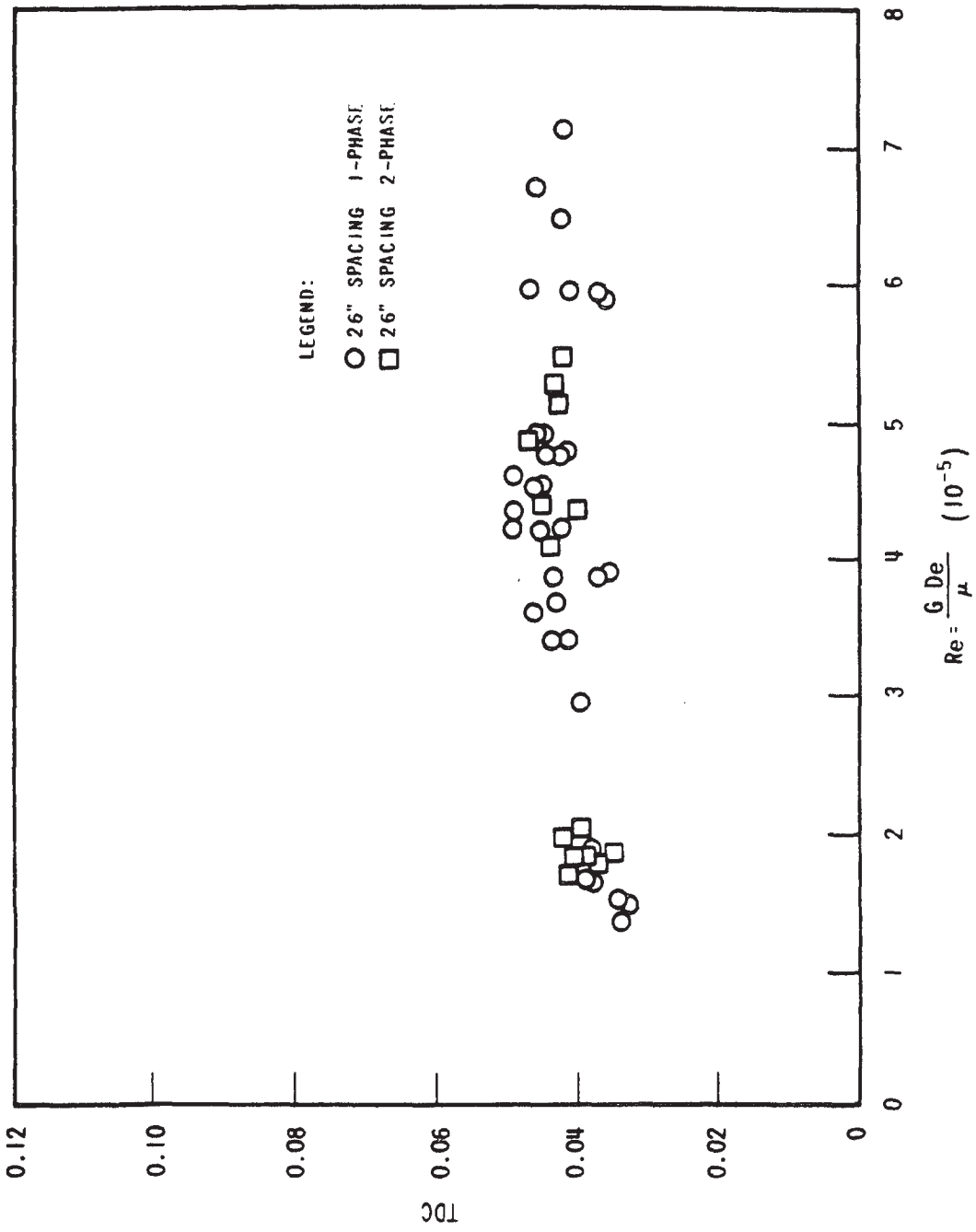

BYRON/BRAIDWOOD STATIONS
UPDATED FINAL SAFETY ANALYSIS REPORT

FIGURE 4.4-3

TDC VERSUS REYNOLDS NUMBER
FOR 26" GRID SPACING

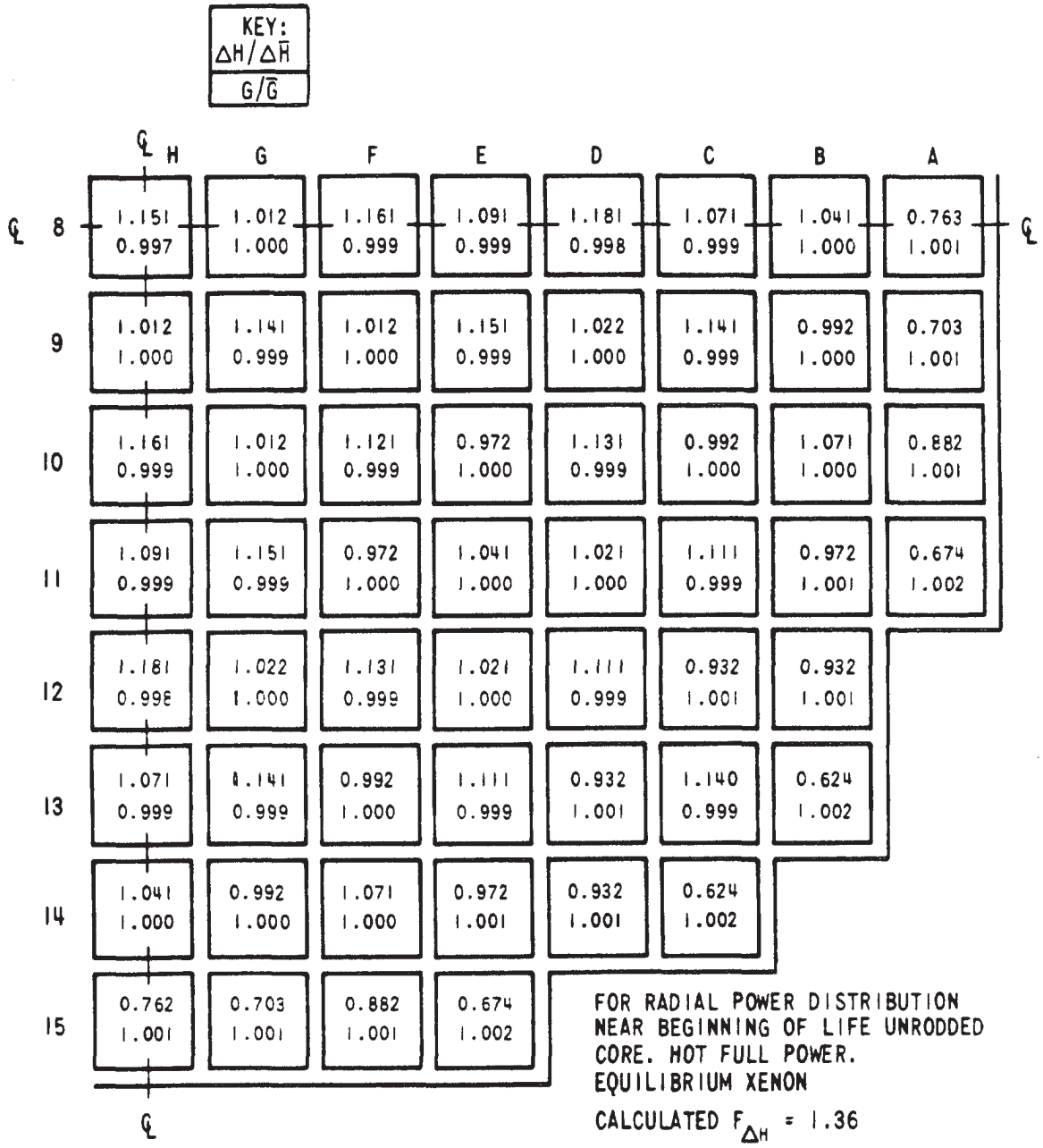

BYRON/BRAIDWOOD STATIONS
UPDATED FINAL SAFETY ANALYSIS REPORT

FIGURE 4.4-4

NORMALIZED RADIAL FLOW AND ENTHALPY RISE DISTRIBUTION AT 4 FT ELEVATION

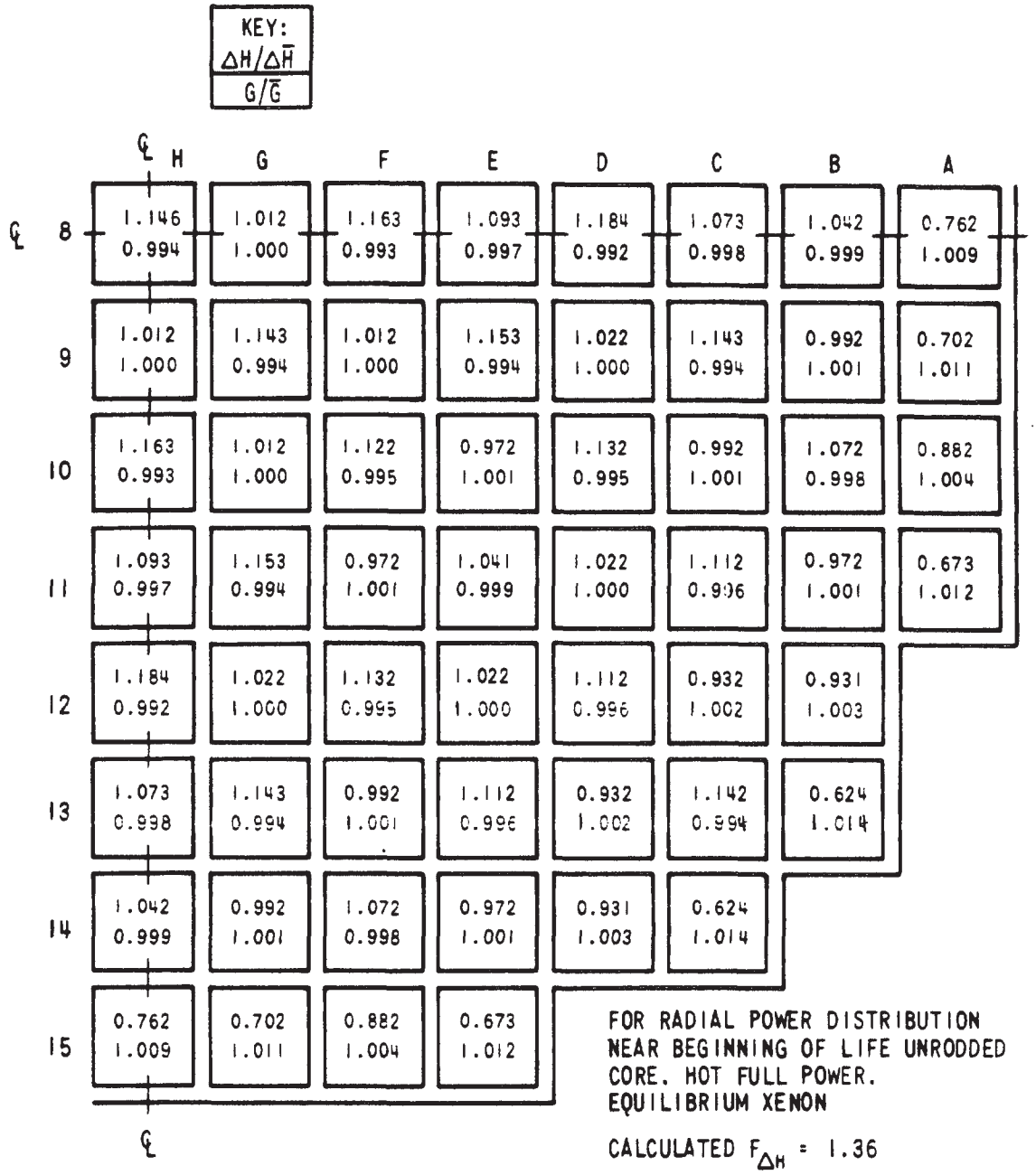

FOR RADIAL POWER DISTRIBUTION NEAR BEGINNING OF LIFE UNRODDED CORE. HOT FULL POWER. EQUILIBRIUM XENON

CALCULATED $F_{\Delta H}$ = 1.36

BYRON/BRAIDWOOD STATIONS
UPDATED FINAL SAFETY ANALYSIS REPORT

FIGURE 4.4-5

NORMALIZED RADIAL FLOW AND ENTHALPY RISE DISTRIBUTION AT 8 FT ELEVATION

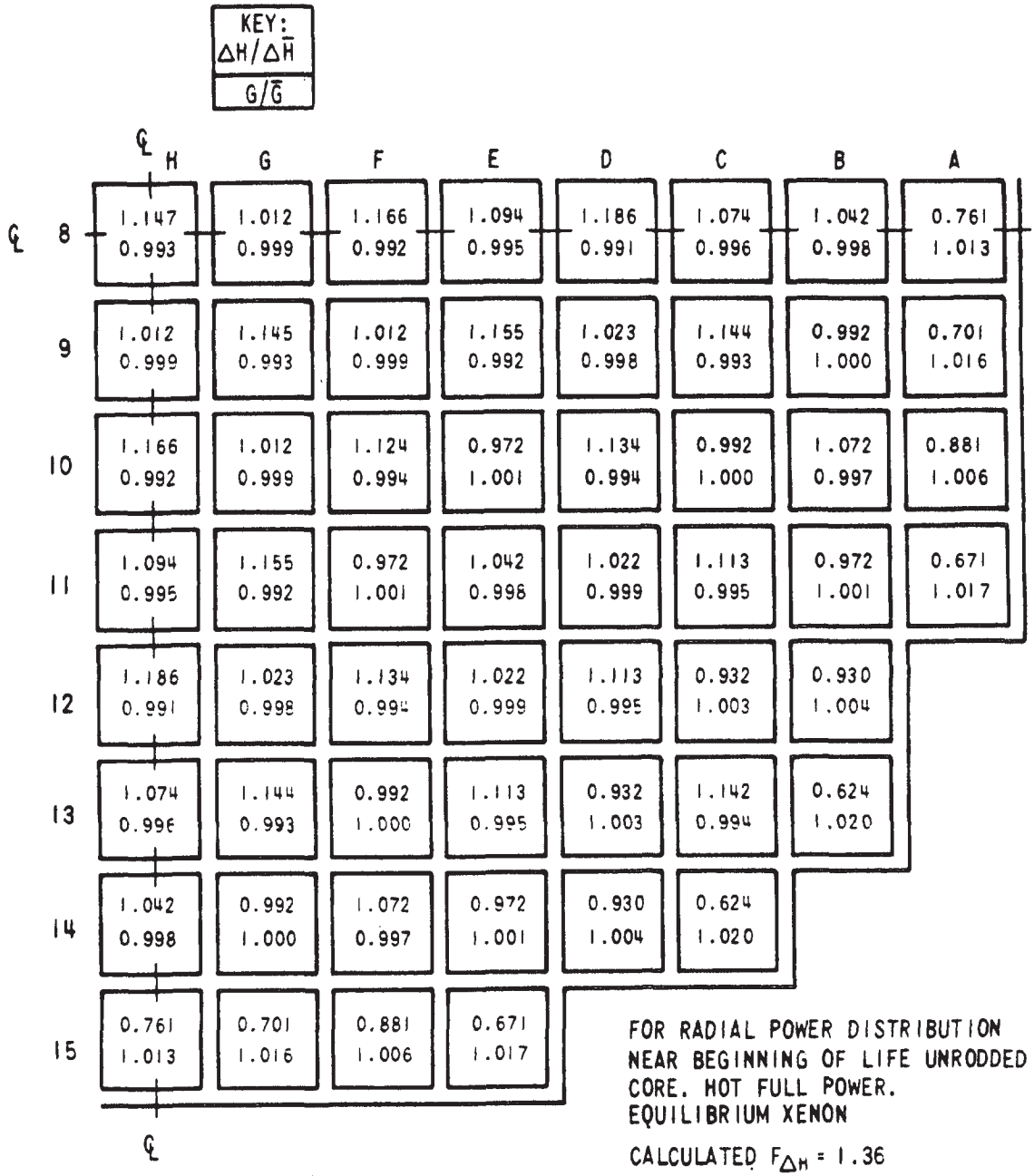

FOR RADIAL POWER DISTRIBUTION NEAR BEGINNING OF LIFE UNRODDED CORE. HOT FULL POWER. EQUILIBRIUM XENON

CALCULATED $F_{\Delta H} = 1.36$

BYRON/BRAIDWOOD STATIONS
UPDATED FINAL SAFETY ANALYSIS REPORT

FIGURE 4.4-6

NORMALIZED RADIAL FLOW AND ENTHALPY RISE DISTRIBUTION AT 12 FT ELEVATION

Figure 4.4-7 has been deleted intentionally.

BYRON/BRAIDWOOD STATIONS
UPDATED FINAL SAFETY ANALYSIS REPORT

FIGURE 4.4-8

THERMAL CONDUCTIVITY OF UO_2
(DATA CORRELATED TO 95%
THEORETICAL DENSITY)

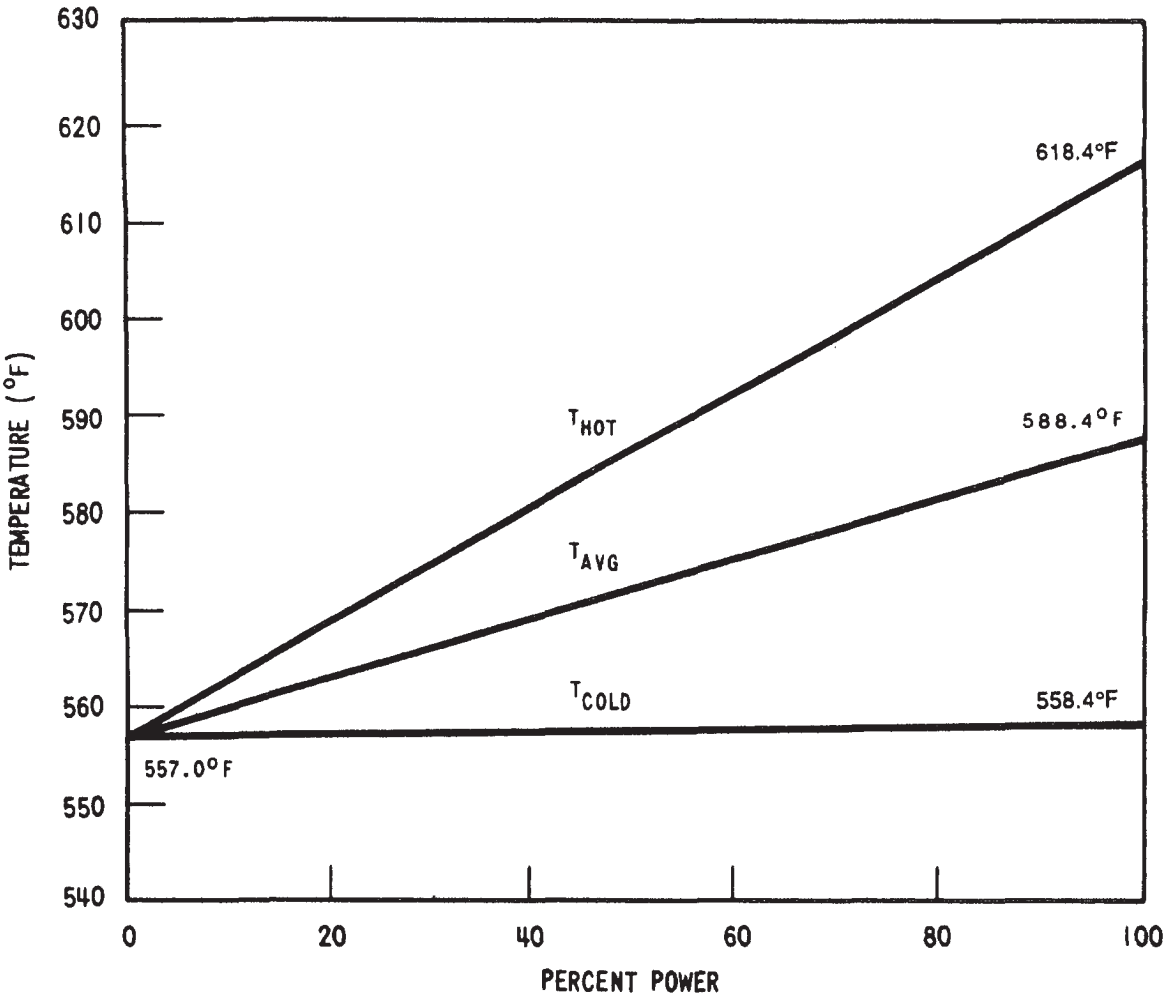

BYRON/BRAIDWOOD STATIONS
UPDATED FINAL SAFETY ANALYSIS REPORT

FIGURE 4.4-9

REACTOR COOLANT SYSTEM TEMPERATURE
PERCENT POWER MAP

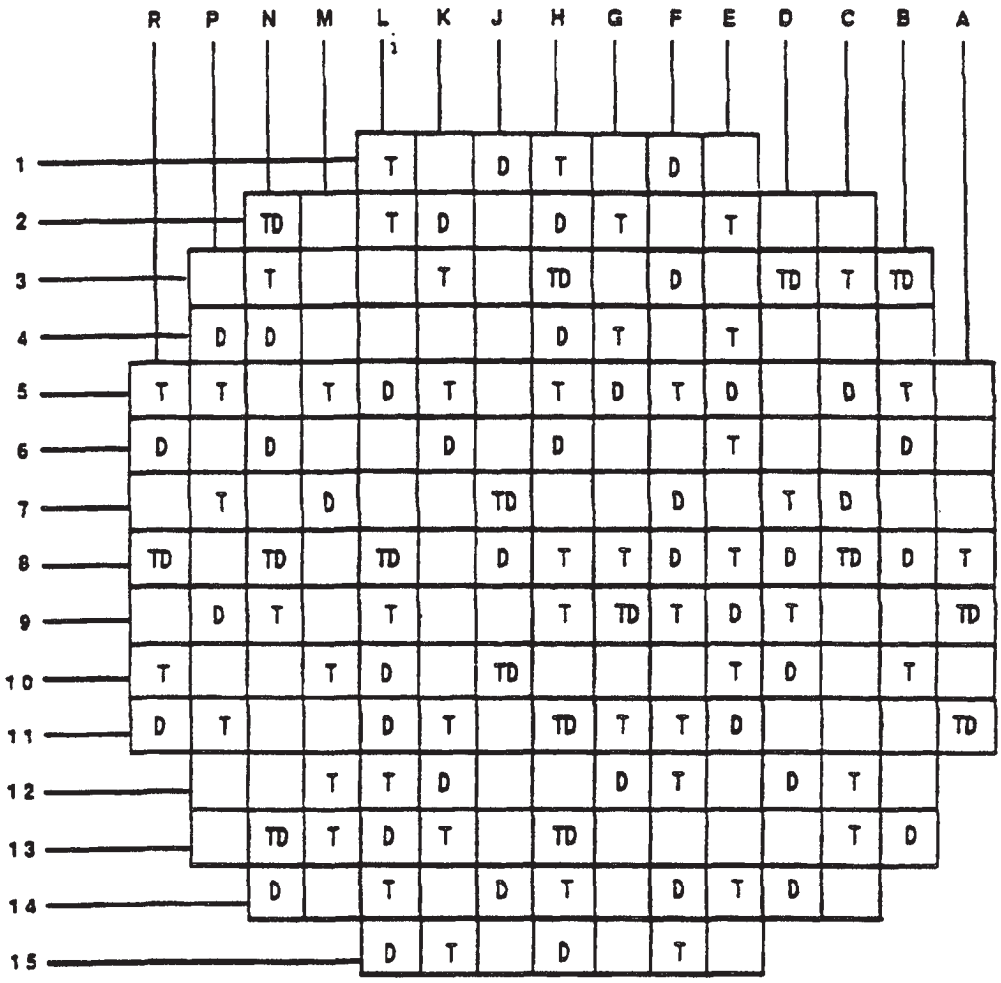

T = THERMOCOUPLE (65)

D = MOVABLE INCORE DETECTOR (58 LOCATIONS)

Note: For Braidwood Unit 1, thermocouple location M10 is K10

BYRON/BRAIDWOOD STATIONS
UPDATED FINAL SAFETY ANALYSIS REPORT

FIGURE 4.4-10

DISTRIBUTION OF INCORE INSTRUMENTATION

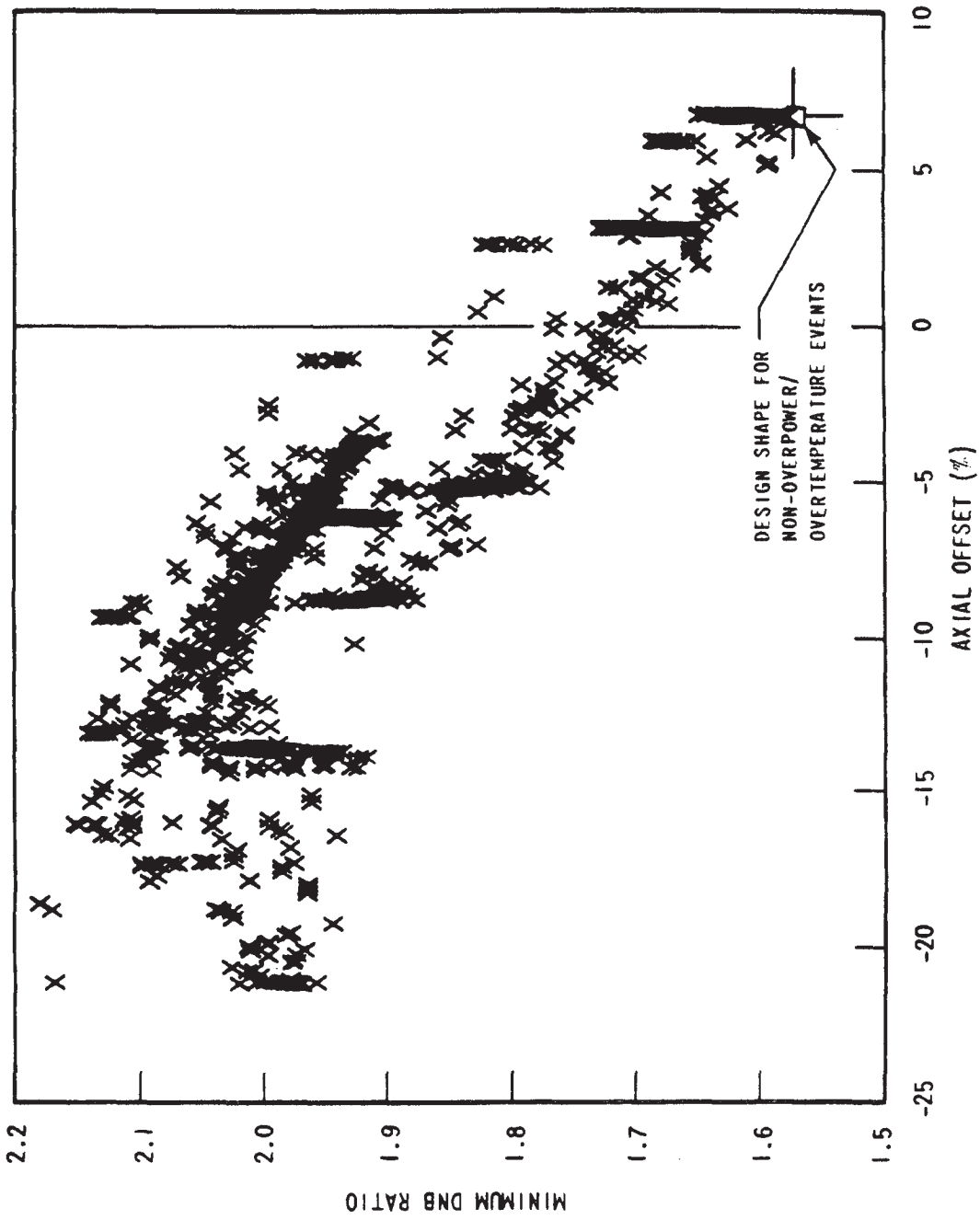

BYRON/BRAIDWOOD STATIONS
UPDATED FINAL SAFETY ANALYSIS REPORT

FIGURE 4.4-11

100 PERCENT POWER SHAPES EVALUATED AT CONDITIONS REPRESENTATIVE OF LOSS OF FLOW

ALL SHAPES EVALUATED WITH $F^{N}_{\Delta H} = 1.49$